

# Up-scaling of the Ultrasonic Welding Process for Joining Carbon Fibre PEEK Composites - A Clean Sky Eco-Design Specific Case

MSc Thesis by F.M. Agricola

Delft University of Technology  
Faculty of Aerospace Engineering



Clean Sky

**n|w**

Fachhochschule  
Nordwestschweiz

Design and Production of Composite Structures





- deceleration of chopped material  
→ carrier

14.05  
14.43

- lap shear → error bars → variation in measurement  
or strength error

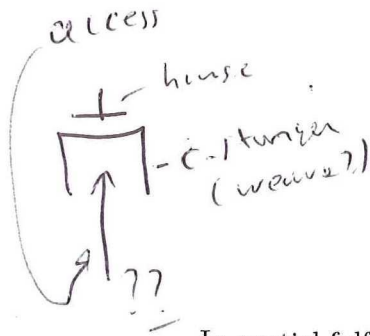
- welding energy: how is it measured  
→ what is it → how does this  
relate to weld quality

EST

# Up-scaling of the Ultrasonic Welding Process for Joining Carbon Fibre PEEK Composites – A Clean Sky Eco-Design Specific Case

$W_s = I$   
→ why

*A first investigation into identifying challenges for up-scaling, proposing and testing new ultrasonic welding concepts and utilization of the best concept in the design of a sequential welding procedure for a practical application.*



MASTER OF SCIENCE THESIS

BY

F.M. AGRICOLA

Weld left / right  
different  
why not  
1 → 2 → 1  
if  
re-weld  
Tissue??  
Epineur vagen

In partial fulfilment of the requirements for the degree of Master of Science  
in Aerospace Engineering  
at Delft University of Technology

TO BE DEFENDED PUBLICLY ON TUESDAY MARCH 18, 2014 AT 2.00 PM

|             |                              |                                |
|-------------|------------------------------|--------------------------------|
| Chair:      | Prof.dr.ir. R. Benedictus    | Delft University of Technology |
| Supervisor: | Dr.ir. I. Fernandez Villegas | Delft University of Technology |
|             | Dr.-Ing. N. Eguémann         | FHNW, Switzerland              |
|             | ir. W.J.C Verhagen           | Delft University of Technology |

Delft University of Technology - Faculty of Aerospace Engineering  
Design and Production of Composite Structures

“It was not the lack of stones that ended the Stone Age”

- **Ahmed Zaki Yamani** (Saudi Arabian politician, Minister of oil and mineral Resources 1962 – 1986)



DELFT UNIVERSITY OF TECHNOLOGY  
DEPARTMENT OF  
AEROSPACE STRUCTURES AND MATERIALS  
DESIGN AND PRODUCTION OF COMPOSITE STRUCTURES

The undersigned hereby certify that they have read and recommended to the Faculty of Aerospace Engineering for acceptance a thesis entitled **“Up-scaling of the Ultrasonic Welding Process for Joining Carbon Fibre PEEK Composites – A Clean Sky Eco-Design Specific Case”** by **F.M. Agricola** in partial fulfilment of the requirements for the degree of Master of Science.

Dated: March 18, 2014

Chair:

---

Prof.dr.ir. R. Benedictus

Supervisor:

---

Dr.ir. I. Fernandez Villegas

Reader (external, FHNW):

---

Dr.-Ing. N. Eguémann

Reader:

---

ir. W.J.C Verhagen





## Abstract

The aerospace industry is looking to reduce their environmental impact through projects like the Clean Sky Joint Technology Initiative. Two measures to help achieve this goal are to reduce the aircraft weight so the emissions during flight decrease and to increase the manufacturing efficiency. Composites often offer lighter solutions and new manufacturing possibilities. Especially thermoplastic composites, which have the ability to melt and fuse, offer many interesting possibilities in manufacturing and structural integration. Ultrasonic welding (USW) is a fusion bonding process which utilizes the ability of thermoplastic composites to form a fusion bond. USW has extremely short process cycles, does not introduce any foreign materials regardless of the composition of the samples to be welded, is energy efficient and has the ability to be on-line monitored, providing joint quality information during welding. With USW it is possible to create fast, clean and consistent welds in lap shear samples. However the step to up-scaling of the process has yet to be made. If found possible, USW might contribute to clean joints with strongly reduced processing times and therefore reduce the environmental impact.

This research investigates the up-scaling of USW using sequential welding for the attachment of recycled chopped carbon fibre PEEK hinges to continuous carbon fibre PEEK plates. This is done for the Clean Sky Eco-Design Integrated Technology Demonstrator. Several steps were taken to up-scale the process from lap shear sample welding to this specific Clean Sky case.

In this research first baseline data was collected by conventional welds as reference for the subsequent experiments. It was found that the chopped fibre material could not be welded properly if used as the top sample, close to the sonotrode. This would result in deconsolidation of the material. Continuous fibre material was therefore used as top sample. It was also found that for up-scaling using spot welding, restrictions made it impossible to weld using the well-established travel controlled process. Instead the energy controlled process was used and investigated.

To use the energy controlled process in a new setup, the influence of different factors on the energy dissipation during welding was investigated. The results found however did not provide enough information for accurate predictions and still need further research to be conclusive. Experiments still provide the best insight in the welding energy needed.

Two new concepts and several practicalities were proposed and investigated. Experiments with the energy controlled zero travel spot welding of a larger overlap proved unsuccessful. The stiffness of the composite material caused welding of unintended parts of the overlap, introducing lots of scatter in the results. For another experiment with dedicated area sized energy director welding, this did not pose a problem and resulted in more consistent data and higher average strength. Combined with pre-attached energy directors and the rectangular sonotrode, this process was deemed to provide good welding conditions for up-scaling.

All the conclusions were used to up-scale the process and design a sequential USW procedure for the Clean Sky case. This research presents the successful result of this newly proposed welding procedure, showing welds which were stronger than the hinges. Now that the concept is proven to work, several suggestions for optimizing the process are presented as well.





## Acknowledgements

A little more than nine months ago I walked into the office of dr.ir Irene Fernandez Villegas. She told me about the Clean Sky project and the hinge attachment for which ultrasonic welding might be useful. I was, and still am, intrigued with the subject and decided to make this my graduation project. This thesis entails all the results I achieved for this challenging research and is the final step in my studies at the Faculty of Aerospace Engineering. During my research I received input and support from many people which I like to thank here.

First and most of all, I would like to thank my supervisor dr.ir. Irene Fernandez Villegas. Her advice, feedback and pragmatic mind-set was of great value during my research. Her optimistic view helped navigate me through the many different experiments and motivated me to continue whenever I got stuck.

I conducted part of my research at the University of Applied Sciences in Northwestern Switzerland, FHNW. I like to thank Nicolas Eguémann, Maxime Roux and Lian Giger for sharing their visions, providing input for my research and helping with the production of the hinges and other samples. I am truly grateful to have had the opportunity to work as a student at their facilities for one month.

Furthermore I would like to thank all the experts of the Delft Aerospace Structures and Materials Laboratory who helped me with my many questions and ‘creative’ ideas regarding the equipment. Fred Bosch, Bart Wiegant, Bob de Vogel, Berthil Grashof, Frans Oostrum, Ed Roessen, Cees Paalvast and Johan Boender. Many thanks for your patience and time. I also like to thank Rudolf Dasbach of Aeson, an industry expert in the field of ultrasonic welding, who was always eager to share his thoughts on problems I encountered during my experiments and helped me to better understand the workings of the machine and the process related to them.

Finally I would like to thank all my fellow students who discussed the project with me, and allowed me to relax in lunch and coffee breaks during the many hours at the faculty. Special thanks to Crispijn Huijts for reading parts of my final thesis and providing valuable feedback which is included in this final version. And last but certainly not least, I would like to thank my girlfriend Suzanne Vromen for proofreading my entire thesis and providing feedback and support throughout the entire process. You kept me motivated and always succeeded in putting a smile on my face.

Matthijs Agricola  
March 18, 2014





## Contents

|  |       |
|--|-------|
| Abstract.....  | i     |
| Acknowledgements .....   | iii   |
| List of Figures .....  | viii  |
| List of Tables .....   | xv    |
| Abbreviations .....  | xix   |
| Symbols .....  | xix   |
| <br>I – Research Design.....   | <br>1 |
| 1 Introduction .....   | 3     |
| 1.1 Motivation.....  | 3     |
| 1.2 Background information .....   | 6     |
| 1.2.1 Thermoplastic composite materials, production and recycling.....                 | 6     |
| 1.2.2 Ultrasonic welding of thermoplastic composites .....                             | 9     |
| 1.3 Research goals .....   | 20    |
| 1.4 Outline .....  | 20    |
| 2 Experimental Procedure .....   | 21    |
| 2.1 Materials and manufacturing.....   | 21    |
| 2.1.1 Toho Tenax continuous fibre weave and chopped fibre PEEK composite.....          | 21    |
| 2.1.2 Ten Cate continuous carbon fibre weave PEEK composite.....                       | 23    |
| 2.1.3 Energy directors .....   | 25    |
| 2.2 Ultrasonic welding.....  | 27    |
| 2.2.1 Ultrasonic welding machine – AESON Dynamic 3000 and ACU .....                    | 27    |
| 2.2.2 Machine settings.....  | 27    |
| 2.2.3 Samples and ED attachment.....   | 28    |
| 2.2.4 Sonotrodes .....   | 28    |
| 2.3 Welding jig configurations.....  | 30    |
| 2.3.1 9109 jig .....   | 31    |
| 2.3.2 9110 jig .....   | 33    |
| 2.4 Universal testing machine – Zwick 250kN .....                                      | 34    |
| 2.5 Optical microscopy and C-scan equipment and procedures .....                       | 35    |
| 2.6 Experiment description .....   | 37    |
| 2.6.1 Standard welding process for baseline creation and parameter determination ..... | 38    |

|            |  |            |
|------------|--|------------|
| 2.6.2      | Investigating new concepts for up-scaling using spot welding .....   | 39         |
| <b>II</b>  | <b>– Experiments, Results and Discussion .....</b>   | <b>41</b>  |
| <b>3</b>   | <b>Baseline Results and Determined Welding Parameters.....</b>   | <b>43</b>  |
| 3.1        | Basic USW-machine control parameters.....  | 43         |
| 3.2        | Dissimilar materials.....  | 47         |
| 3.3        | Practical Limitations for Up-Scaling and Welding Dissimilar Materials.....   | 52         |
| <b>4</b>   | <b>Energy Determination .....</b>  | <b>55</b>  |
| 4.1        | Energy determination experiments.....  | 55         |
| 4.2        | Area influence .....   | 56         |
| 4.3        | Jig influence .....  | 61         |
| 4.4        | Material influence.....  | 63         |
| 4.5        | Discussion on Energy Determination.....  | 66         |
| <b>5</b>   | <b>New Concepts: Zero Travel Spot Welding, Dedicated Area Sized ED<br/>Welding and Process Practicalities.....</b> | <b>67</b>  |
| 5.1        | Experiment design for spot welding of a larger overlap .....   | 67         |
| 5.2        | Thin energy directing surfaces .....   | 71         |
| 5.3        | Spot welding in a larger overlap area with zero (low) travel using energy as the<br>controlling parameter.....     | 72         |
| 5.4        | Experiment design for area sized energy director welding .....   | 80         |
| 5.5        | Dedicated area sized energy director spot welding.....   | 81         |
| 5.6        | Pre-Attached Energy Directors.....   | 91         |
| <b>6</b>   | <b>Sequential Spot Welding of the Clean Sky Hinge.....</b>   | <b>95</b>  |
| 6.1        | Sonotrode Selection and Spot Welding Strategy .....  | 95         |
| 6.2        | New Jig Design for Sequential Spot Welding of the Clean Sky Hinges .....   | 97         |
| 6.2.1      | Jig Design and Manufacturing .....   | 97         |
| 6.2.2      | Elaboration on the Design Choices .....  | 100        |
| 6.2.3      | Discussion on the operations of the new jig.....   | 100        |
| 6.3        | Tension strength test setup for the welded hinges.....   | 101        |
| 6.4        | Ultrasonic sequential spot welding of chopped fibre hinges to continuous fibre plates.....                         | 102        |
| <b>III</b> | <b>– Conclusions and Recommendations .....</b>   | <b>113</b> |
| <b>7</b>   | <b>Conclusions .....</b>   | <b>115</b> |
| <b>8</b>   | <b>Future Research Recommendations.....</b>  | <b>119</b> |



|   |            |
|---|------------|
| <b>Appendices .....</b>   | <b>121</b> |
| A. Drawings of the New Jig Design.....  | 123        |
| B. Relevant Welding and LSS Parameters of All Welded Samples.....   | 127        |
| C. Welding and LSS Curves for 300 [N] and 1000 [N] Travel Controlled Welding of Continuous Weave CF/PEEK Toho Tenax Material Using a 2 Layer PEEK Toho Tenax ED ..... | 131        |
| D. Welding and LSS Curves for 300 [N] Travel Controlled Welding of chopped to chopped CF/PEEK Toho Tenax Material Using a 2 Layer PEEK Toho Tenax ED .....            | 139        |
| E. Welding and LSS Curves for 300 [N] Travel Controlled Welding of continuous weave to chopped CF/PEEK Toho Tenax Material Using a 2 Layer PEEK Toho Tenax ED .....   | 143        |
| F. Welding and LSS Curves for 500 [N] Travel Controlled Energy Determination Welds and Energy Controlled Spot Welding of s Larger Overlap .....                       | 149        |
| G. Welding and LSS Curves for 500 [N] Energy Controlled Spot Welds Using Dedicated ED Area Sizing .....   | 157        |
| H. Welding and LSS Curves for 500 [N] Energy Controlled Spot Welds Using Dedicated ED Area Sizing For Weave (90 [°] Ten Cate) – Chopped Material .....                | 163        |
| I. Welding and LSS Curves for Pre-attached ED Welding .....   | 169        |
| J. Welding Curves for Hinge Welding.....  | 171        |
| <b>Bibliography .....</b>   | <b>181</b> |

## List of Figures

|   |    |
|---|----|
| Figure 1-1   Schematic overview of the Clean Sky JTI Eco-Design ITD F1 – Thermoplastic Composite Airframe Panel [8] .....   | 5  |
| Figure 1-2   Schematic view of the TPC helicopter door hinge (left) and actual view of the door hinge produced of recycled CF/PEEK (right) by FHWN [8], [9] .....   | 5  |
| Figure 1-3   Schematic view of continuous and discontinuous fibre configurations used in composites [14].....   | 7  |
| Figure 1-4   Thermoplastic composite processing techniques for continuous and discontinuous fibres [16] .....   | 8  |
| Figure 1-5   Overview of recycling processes for thermoplastic composites [19].....   | 8  |
| Figure 1-6   Schematic view of an ultrasonic welding machine showing amplification steps [6], [20] .....  | 10 |
| Figure 1-7   Typical output of the USW process, showing travel, force and dissipated power as well as displaying other welding information, as produced by the AcuCapture software coupled to the ACU of the Rinco Dynamic 3000 USW machine used by the faculty of Aerospace Engineering DASML. Showing the, I) initial (built-up) phase, II) vibration phase, III) solidification phase..... | 11 |
| Figure 1-8   Typical evolution of the power dissipation and displacement curves for the different welding steps during the vibration (welding) phase of the USW process. The displacement of the sonotrode is relative to its position at the beginning of the phase and positive values indicate downward displacement. [22].....  | 12 |
| Figure 1-9   Influence of the amplitude of vibration ( $A_1 = 51.8$ [μm], $A_9 = 86.2$ [μm]) on the power curves for a low welding force (300 [N], top) and a high welding force (1500 [N], bottom) [22]. Depicting less change considering duration of stage 3 in the 1500 [N] welds with varying amplitude compared to the 300 [N] welds. ....  | 14 |
| Figure 1-10   Schematic overview of an USW system (A) and the corresponding lumped parameter model (B) as described by A. Benatar and T. G. Gutowski. [24] The masses $m_7$ , $m_8$ , $m_n$ describe the triangular ED used in this parameter model, were the other masses represent all the other separate parts in the welding column for this setup. ....                                  | 16 |
| Figure 1-11   Healing of a polymer interface (ED-joining parts) showing: a) two distinct interfaces; b) intimate contact; and c) inter-diffusion of the polymer chains [6].....   | 18 |
| Figure 1-12   Polymer chain movement from its initial to its final position as described in the reptation theory [6].....   | 19 |
| Figure 1-13   Tension load case for the Clean Sky hinge.....  | 20 |

|  |    |
|--|----|
| Figure 2-1   Dimensions in [mm] for one sample used in the creation of lap shear samples following the ASTM D1002 standard.....  | 21 |
| Figure 2-2   Newly produced hinge, without holes in the bottom plate, using Toho Tenax CF/PEEK chopped fibre material .....  | 23 |
| Figure 2-3   DASML – A) Automatic sheet cutting machine, B) Ultrasonic hand plunge welder.....   | 23 |
| Figure 2-4   DASML – Heated flat plate press (JoosPress) 1000 [kN], 450 [°C], 600 x 600 [mm].....  | 24 |
| Figure 2-5   Temperature and pressure curves from the JoosPress for the manufacturing of a 8 layer prepreg weave CF/PEEK Ten Cate laminate.....  | 24 |
| Figure 2-6   Temperature and pressure curves from the JoosPress for the manufacturing of energy directors of Toho Tenax Vestakeep® PEEK film / Ten Cate Victrex® PEEK film.....  | 25 |
| Figure 2-7   PEEK film and the attachment to a chopped fibre composite plate using the film stacking process (temperature just below $T_m$ and 0.9[MPa] pressure).....   | 26 |
| Figure 2-8   Chopped fibre hinge with extra layer PEEK attached using the same film stacking process.....  | 26 |
| Figure 2-9   Rinco Dynamic 3000 ultrasonic welder equipped with an Advanced Control Unit....   | 27 |
| Figure 2-10   A typical power and travel curve for the USW process, showing the welding energy as the highlighted area under the power curve.....  | 28 |
| Figure 2-11   Three different sonotrodes used in this research and their specifications, note that the maximum peak-to-peak amplitude shown, is valid for the combination with the AESON Dynamic 3000 and the 1:2 booster .....                      | 29 |
| Figure 2-12   Front view USW machine, highlighted bolt is used to loosen the complete welding train.....   | 30 |
| Figure 2-13   Baseplate of the USW-machine showing the bolt holes and T-slots.....   | 31 |
| Figure 2-14   Dimensions in [mm] following the ASTM D1002 standard for a lap shear sample showing the sample size and the ½ inch overlap .....   | 31 |
| Figure 2-15   Detailed overview of the 9109 and 9110 jig variations .....  | 32 |
| Figure 2-16   Two different bottom plates for the: A) 9109 jig (steel bottom plate), B) 9110 jig (aluminium bottom plate), showing the clamping block of the bottom sample and the 4 poles on jig 9110 which are interchangeable with jig 9109 ..... | 33 |

|   |    |
|---|----|
| Figure 2-17   Zwick 250 kN universal testing machine used for static lap shear strength determination.....  | 34 |
| Figure 2-18   Schematic view of the offset displacement between the top and lower grip of the Zwick 250 kN universal testing machine, allowing to align the load direction with the centre weld line to minimize bending during static the lap shear strength test.....   | 35 |
| Figure 2-19   Zeiss Discovery.V8 SteREO optical microscope, equipped with an Zeiss AxioCam ERc5s digital camera and external (cold) light source available at the DASML.....  | 36 |
| Figure 2-20   C-scan equipment available in the DASML used for non-destructive testing of the used composite materials and analysis of the hinge weld quality.....  | 37 |
| Figure 2-21   Schematic roadmap of experimental approach towards up-scaling of the USW process .....  | 37 |
| Figure 3-1   Power and relative travel curves for a melting on setting of 100% travel, used for the determination of the ideal welding on setting for a 300 [N] and a 1000 [N] welding force, welding Toho Tenax CF/PEEK continuous weave standard size lap shear samples using 2 layer (0.23 [mm]) Toho Tenax ED (showing sample #01 and #10, appendix B).....   | 44 |
| Figure 3-2   Average values and range of values for the maximum power (maximum level reached during the weld as percentage of the total USW machine capacity), welding time, energy dissipated and LSS, for optimal welding conditions using 300 [N] and 1000 [N] welding force for a standard ASTM D1002 12.7 [mm] (Ø 40 [mm] sonotrode) overlap (samples #04-09, 300 [N], #11-15 1000 [N], appendix B)..... | 45 |
| Figure 3-3   Fracture surfaces of Toho Tenax material, 12.7 [mm] overlap, welded with the Ø 40 [mm] cylindrical sonotrode and a welding force of A) 300 [N] (#4 appendix B), B) 1000 [N] (#12 appendix B) using optimum welding conditions.....   | 46 |
| Figure 3-4   Sample A (#09, appendix B) cross section of a Toho Tenax weave – weave weld using 300 [N] welding force, Sample B (#17, appendix B) cross section of a Toho Tenax weave – weave weld using 1000 [N] welding force, 1.25x magnified.....  | 46 |
| Figure 3-5   Inconsistent welding curves for USW of chopped to chopped Toho Tenax CF/PEEK, for melting on 100 [%] travel using 300 [N] welding force , 12.7 [mm] overlap and the Ø 40 [mm] sonotrode (samples #45,#46, appendix B).....   | 47 |
| Figure 3-6   Melting on 100% travel chopped to chopped fibre welded sample, showing extensive deconsolidation mostly in the top sample, showing samples #45 and #46 (appendix B).....   | 48 |
| Figure 3-7   Surface damage as a result of an energy controlled welding experiment, delivering 500 [Ws] of energy with the Ø 10 [mm] cylindrical sonotrode, using a 300 [N] welding force, sample #94 (appendix B) .....  | 49 |

|   |    |
|---|----|
| Figure 3-8   Welding of sample #50 (appendix B) for continuous weave to chopped Toho Tenax CF/PEEK material, using melting on 80 [%] travel, 12.7 [mm] overlap, 300 [N] welding force and the Ø 40 [mm] sonotrode .....   | 50 |
| Figure 3-9   Sample #55 (appendix B) section of a continuous weave (top sample) to a chopped fibre (bottom sample) weld, 1.25x magnified .....  | 50 |
| Figure 3-10   Welding surfaces of weave to chopped material welded samples #52 (left) and #53 (right) (appendix B), highlighting the poorly welded area of the overlap for sample #52....   | 52 |
| Figure 3-11   Schematic view of the practical limitation of the travel controlled USW process: The colder ED surrounding the affected area by the sonotrode does not melt and therefore prohibits travel by the sonotrode .....   | 53 |
| Figure 4-1   Welding curves for different overlaps (A1 = 12.7 [mm], A2 = 19.05 [mm], A3 = 25.4 [mm]) comparing Ten Cate and Toho Tenax material to the baseline, with the red arrow highlighting the increasing negative travel for welding of larger overlaps .....                      | 57 |
| Figure 4-2   Fracture surfaces of the samples poorly welded with 300 [N] for A) 19.05 [mm] overlap (#29 appendix B) and B) 25.4 [mm] overlap (#41 appendix B) .....   | 59 |
| Figure 4-3   (Irregular) Welding curves for sample #68 and #69 (appendix B), experiment with 450 [N] (0.93 [MPa]) and 600 [N] (1.24 [MPa]) welding force, 19.05 [mm] overlap, reaching the power limits of the USW machine for 100 [%] travel.....  | 60 |
| Figure 4-4   Welding curves for identical welding conditions using the 9109 (left) and the 9110 jig (right).....  | 61 |
| Figure 4-5   Average and range values for several welding outcome parameters comparing identical welded samples for the 9109 and 9110 jig .....   | 62 |
| Figure 4-6   Average energy levels for identical welds (optimal conditions for 300 [N], 12.7 [mm] overlap using the 40[mm] sonotrode) in different materials for the 9109 jig (left) and 9110 jig (right).....  | 64 |
| Figure 4-7   2.5x magnification of a Toho Tenax welded sample showing the two layer ED separation at the edge (left) and a Ten Cate welded sample showing the 5 layer ED separation at the edge (right).....  | 65 |
| Figure 4-8   Sample of a delaminated corner due to water jet cutting of the Ten Cate material.....  | 65 |
| Figure 4-9   Colour and black & white C-scan images of the edges of the laminate plates: A) Ten Cate material, B) Toho Tenax material, the dark/red colour indicates poorly consolidated material. The colours are used for relative comparison, not for absolute attenuation values..... | 66 |



|  |    |
|--|----|
| Figure 5-1   Schematic view of the initial experiment to determine the possibility of energy controlled zero travel welding using the 9109 jig .....   | 67 |
| Figure 5-2   Schematic view of the setup using the 9110 jig for: A) Energy determination 14.9 [mm] overlap using travel as the controlling parameter, B) Spot welding of a larger overlap using energy as the controlling parameter.....   | 68 |
| Figure 5-3   Welding curve for the welding of a 14.9 [mm] overlap 100 [%] travel weld using the rectangular sonotrode, a welding force of 500 [N] and the 9110 jig, showing an optimum around 0.048 [mm] – 20 [%] travel (showing sample #79, appendix B) and a comparison to the baseline welding curves for 300 [N] and 1000 [N] .....         | 69 |
| Figure 5-4   Average values and range of values for the maximum power, welding time, energy dissipated and LSS, for optimal welding conditions using 300 [N] and 1000 [N] welding force for a standard 12.7 [mm] (cylindrical Ø 40 [mm] sonotrode, 9109 jig) overlap and 500 [N] for a 14.9 [mm] (rectangular sonotrode, 9110 jig) overlap ..... | 70 |
| Figure 5-5   Welding curves for 1 layer (thin, 0.12 [mm]) ED welds using melting on 100 [%] travel for 300 [N] and 1000 [N] using the 9109 jig, showing samples #20, #21 (appendix B) compared to the 100 [%] travel baseline (1000 [N]) welded sample with a 2 layer, 0.23 [mm] ED (sample #10).....  | 71 |
| Figure 5-6   Experiment for zero travel energy controlled welding of a larger overlap with, A) the large ED placement, B) the welding setup and C) the fracture surfaces, showing sample #19 (appendix B).....   | 73 |
| Figure 5-7   Power and travel curves of samples #18 and #19 (appendix B) for the energy controlled zero travel welding of a larger overlap.....  | 74 |
| Figure 5-8   Welding curves for the travel controlled process for energy determination and the energy controlled process for the zero travel welding of a spot in a larger overlap, showing sample #82, travel welded, and #90, energy spot welded, (appendix B) .....   | 76 |
| Figure 5-9   Stress – strain curves depicting the LSS for regular travel controlled welded samples (used for energy determination) and the energy controlled zero travel spot welds of a larger overlap .....  | 76 |
| Figure 5-10   Difference in average values for welding parameters comparing the regular travel controlled welds with energy controlled spot welds .....  | 77 |
| Figure 5-11   Relative compression due to the applied force of the rectangular sonotrode for Toho Tenax samples with a 2 layer (0.24 [mm]) ED, highlighting the compression related to a force of 1000 [N].....  | 78 |
| Figure 5-12   Fracture surfaces for energy controlled zero travel spot welds in a larger overlap showing sample A-E (#88 - #92, appendix B), where X shows the area of the overlap   |    |

|  |    |
|--|----|
| directly affected by the sonotrode (14.9 [mm]) and Y the remainder of the total overlap (10.5 [mm]) .....  | 79 |
| Figure 5-13   1.25x enlarged image of the cross-section of sample #87 (appendix B) zero travel welded using energy as controlling parameter, showing the edge effect and bubble forming in the centre of the weld .....  | 80 |
| Figure 5-14   Dedicated ED size welding showing ED attachment to the jig on the left and a schematic view on the right.....  | 81 |
| Figure 5-15   Welding curves for the welding of dedicated area sized ED welds of samples #100 - #106 (appendix B).....   | 82 |
| Figure 5-16   Comparison of two different dedicated area sized ED welding curves (power & travel) with the travel controlled welding curves and the welding curves for the spot welding of the large overlap. All for Ten Cate samples and 5 layer (0.25 [mm]) ED, welded with the rectangular sonotrode, in the 9110 jig using a welding force of 500 [N] ..... | 83 |
| Figure 5-17   Average and range values, comparing the regular travel controlled welds and the energy controlled spot welds of the larger overlap with the dedicated area sized ED welds ...  | 84 |
| Figure 5-18   Fracture surfaces of the dedicated area sized ED welded samples A – E: #101 – #105 (appendix B).....   | 85 |
| Figure 5-19   Welding curves for sample #108 (appendix B), experiments for the dedicated area sized ED welding using travel with 1000 [N] welding force, 50% travel, the rectangular sonotrode and jig 9110 for Ten Cate samples with a 90 [°] apparent fibre direction .....  | 86 |
| Figure 5-20   Overlap for the #109 (appendix B) welded sample, showing surface damage and ED squeeze out on all sides.....   | 87 |
| Figure 5-21   Welding curves for the welding of a small ED with a larger sonotrode using the 9110 jig, 90 [°] Ten Cate weave and 5-layer (0.25 [mm] ED), with a welding force of 500 [N] and 100 [%] travel and 1000 [N] and 30 [%] travel (samples #119 and #121, appendix B).....  | 88 |
| Figure 5-22   Typical fracture surface for the welding of weave (Ten Cate 90 [°]) to chopped fibres using the dedicated area sized ED welding (sample #117, appendix B).....   | 89 |
| Figure 5-23   Welding curves comparing a weave – chopped weld to a weave – weave weld for the welding of a dedicated area sized ED .....   | 89 |
| Figure 5-24   Welding curves for the welding of weave (Ten Cate 90 [°]) to chopped fibre using the dedicated area sized EDs for samples #112 – #118, appendix B .....  | 90 |
| Figure 5-25   Ten Cate 90 [°] sample with Ten Cate 5 layer (0.25 [mm]) ED pre-attached to it with four plunge welds, clamped in the 9110 jig .....   | 91 |

|   |     |
|---|-----|
| Figure 5-26   Welding curves for the samples with the (regular) taped ED (Toho Tenax 0 [°] weave samples, and Toho Tenax 0.24 [mm] ED) and the plunge welded pre-attached ED (Ten Cate 90 [°] weave samples and Ten Cate 0.25 [mm] ED welded with a 500 [N] welding force, the rectangular sonotrode for a 14.9 [mm] overlap and the 9110 jig. .... | 92  |
| Figure 5-27   Fracture surfaces of sample #125 (appendix B), welded with pre-attached ED .....  | 93  |
| Figure 6-1   Tension load case for the Clean Sky hinge.....   | 96  |
| Figure 6-2   ED alignment aid for plunge welding EDs to larger plates for hinge welding with square holes identical to the ED dimensions an rounded corners for accessibility of the USW hand plunge welder. The edges are covered with Kapton tape against possible overheating. ....  | 96  |
| Figure 6-3   Schematic view of the sequential spot weld configuration used showing plate dimensions (manufacturing process is described in section 2.1.2) .....   | 97  |
| Figure 6-4   New jig designed for welding of (chopped fibre) Clean Sky ITD hinges .....   | 98  |
| Figure 6-5   Detailed overview of the new jig for hinge welding.....  | 99  |
| Figure 6-6   New jig design with Kapton tape on the DE-STA-CO dampening pods and extra silicone rubber supporting material (the blue stack down in the middle of the jig) for the protruding plates .....   | 101 |
| Figure 6-7   Setup of the Zwick 250 kN universal testing machine for hinge tension testing showing: A) custom made aluminium cylinder for fitting the hinge to the frame, B) 90 [°] rotated frame .....   | 102 |
| Figure 6-8   Experiments for the energy determination for hinge welding, welding one hinge per setting with two sequential spot welds, showing hinge 1 (1200 [Ws]), 2 (1400 [Ws]), 4 (1800 [Ws]) and 3-2 (2000 [Ws]).....   | 104 |
| Figure 6-9   Tension test using the Zwick universel testing machine to test the hinge weld strength, showing clear sings of induced peel forces .....   | 105 |
| Figure 6-10   Fracture surfaces for the 1800 [Ws] energy welded hinge and the 2000 [Ws] welded hinge, showing that a larger part of the two EDs melted for 2000 [Ws], providing better attachment of the hinge.....   | 106 |
| Figure 6-11   Typical welding curves for the first and second spot weld for hinge welding, showing a large positive (downward motion of the sonotrode) travel at the beginning of the first weld and more hammering (negative travel) for the second weld.....  | 106 |
| Figure 6-12   Zwick strain curves for the welded hinges 4 (1800 [Ws]), 3-2, 7, 9 and 11 (2000 [Ws]) compared to the Eurocopter load case, hinge 4 failed in the weld, for the other welds the hinge failed .....  | 108 |
| Figure 6-13   Broken hinge as result of the Zwick strength test of the weld.....  | 108 |

Figure 6-14 | C-scan for 2000 [Ws] energy welded hinges 5-11, showing the cross-section that was investigated with microscopy, first and second spot welds for all hinges are, L=Left, R=Right: 5 (1: L, 2: R), 6 (1: R, 2: L), 7 (1: L, 2: R), 8 (1: R, 2: L), 9 (1: L, 2: R), 10 (1: R, 2: L), 11 (1: L, 2: R), showing that the first weld generally is of worse quality indicated by the red area. The colours are used for relative comparison, not for absolute attenuation values. .... 109

Figure 6-15 | Cross-section depicted in the C-scan, top two pictures showing the untreated cross-section, bottom four (mirrored) pictures show the embedded cross-section (1x and 8x magnification) showing more air in the first spot weld on the right side for hinge 6..... 110

Figure 6-16 | Fracture surfaces of welded hinges 8 (left), 9 (middle) and a one side welded hinge (right), first and second spot welds for the hinges are, L=Left, R=Right: 8 (1: R, 2: L), 9 (1: L, 2: R) and only the left one for the last hinge..... 110

## List of Tables

Table 1-1 | List of high performance thermoplastic matrix materials and their properties, note that this table only provides an indication since there are many variants within one polymer type (depending on manufacturer, process, chain length etc.), providing different values for  $T_g$ ,  $T_m$  and  $T_{max.serv.}$  [12], [2], [10], [13] ..... 6

Table 1-2 | List of commonly used fibre materials and their strength and stiffness properties [14], [15] ..... 7

Table 3-1 | Overview of the materials used (TT = Toho Tenax), sonotrodes used and input settings for the USW machine for the welding of the baseline samples for a standard 12.7 [mm] overlap using the 9109 jig and Toho Tenax 2 layer (0.23 [mm]) ED, comparing a 300 [N] and 1000 [N] welding force ..... 43

Table 3-2 | Average values and their  $c_v$  for the maximum power (maximum level reached during the weld as percentage of the total USW machine capacity), welding time, energy dissipated and LSS, for optimal welding conditions using 300 [N] and 1000 [N] welding force for a standard ASTM D1002 12.7 [mm] ( $\varnothing$  40 [mm] sonotrode) overlap (samples #04-09, 300 [N], #11-15 1000 [N], appendix B)..... 45

Table 3-3 | Overview of the materials used (TT = Toho Tenax), sonotrodes used and input settings for the USW machine for the welding of the baseline chopped fibre samples for a standard 12.7 [mm] overlap using the 9109 jig and 2 layer (0.23 [mm]) Toho Tenax EDs ..... 47

Table 3-4 | Overview of the material used (TT = Toho Tenax), sonotrode used and input settings for the USW machine for the experiment of the energy controlled welding using a small sonotrode in the 9110 jig with an 2 layer (0.23 [mm]) Toho Tenax ED of a chopped fibre sample ..... 48



|   |    |
|---|----|
| Table 3-5   Overview of the materials used (TT = Toho Tenax), sonotrode used and input settings for the USW machine for the welding of the weave - chopped baseline samples for a standard 12.7 [mm] overlap using the 9109 jig and 2 layer (0.23 [mm]) Toho Tenax ED.....  | 49 |
| Table 3-6   Average values and their $c_v$ for the maximum power, welding time, energy dissipated and LSS, for welding weave to chopped fibre samples using 300 [N], 12.7 [mm] ( $\varnothing$ 40 [mm] sonotrode), all samples and excluding sample #52 (from #51-52, appendix B) compared to the values for the weave to weave welds .....   | 51 |
| Table 4-1   Overview of the material used (TC = Ten Cate), sonotrodes used and the welding parameters for the welding of the samples for a 12.7 [mm], a 19.05 [mm] and a 25.4 [mm] overlap using the 9110 jig and 5 layer (0.25 [mm]) Ten Cate ED .....   | 57 |
| Table 4-2   LSS and energy data for different overlap (A1 = 12.7 [mm], A2 = 19.05 [mm], A3 = 25.4 [mm]) welds comparing Ten Cate (with 5 layer, 0.25 [mm] ED) and Toho Tenax (with 2 layer, 0.23 [mm] ED) material (welded with the 9110 jig) with the baseline data (welded with the 9109 jig). *travel input used could not be determined with the established method and was estimated .....   | 58 |
| Table 4-3   Overview of the material used (TT = Toho Tenax), sonotrode used and the welding parameters for the welding of identical weave – weave samples for the 9109 jig and the 9110 jig using 2 layer (0.24 [mm]) Toho Tenax EDs .....  | 61 |
| Table 4-4   Average and $c_v$ values for several welding outcome parameters comparing identical welded samples the 9109 and 9110 jig .....  | 62 |
| Table 4-5   Overview of the materials (TT = Toho Tenax weave thickness = 1.85 [mm] chopped thickness = 3.86 [mm], TC = Ten Cate weave thickness = 1.82 [mm]), jigs used and the welding parameters for the welding of different materials using the 9109 jig and the 9110 jig and using Toho Tenax 2 layer (0.24 [mm]) ED for the TT and Ten Cate 5 layer (0.25 [mm]) ED for the TC samples ..... | 63 |
| Table 4-6   $c_v$ for identical welds (optimal conditions for 300 [N], 12.7 [mm] overlap using the 40[mm] sonotrode) in different materials for the 9109 and 9110 jig (not all samples were lap shear tested or the test failed, *1 = 3 samples, *2 = 4 samples) .....  | 64 |
| Table 5-1   Overview of the material used (TT = Toho Tenax), sonotrode used and the welding parameters for the welding experiments with a higher welding force using TT 2 layer, 0.24 [mm], EDs and the 9110 jig .....  | 69 |
| Table 5-2   Average values and $c_v$ for the maximum power, welding time, energy dissipated and LSS, for optimal welding conditions using 300 [N] and 1000 [N] welding force for a standard 12.7 [mm] (cylindrical $\varnothing$ 40 [mm] sonotrode, 9109 jig) overlap and 500 [N] for a 14.9 [mm] (rectangular sonotrode, 9110 jig) overlap.....  | 70 |
| Table 5-3   Overview of the materials used (TT = Toho Tenax), sonotrode used and the welding parameters for the welding of samples using 1 layer ED (0.12 [mm]) in the 9109 jig.....  | 71 |



|   |    |
|---|----|
| Table 5-4   Overview of the material used (TT = Toho Tenax), sonotrode used and input settings for the USW machine for the zero travel welding using the 9109 jig using 0.24 [mm] Toho Tenax EDs.....   | 72 |
| Table 5-5   Overview of the materials used (TT = Toho Tenax), sonotrode used and the welding parameters for the welding experiments for the energy determination needed for the energy controlled spot welding using TT 2 layer, 0.24 [mm], EDs and the 9110 jig.....   | 74 |
| Table 5-6   Average values and $c_v$ for the maximum power, welding time, energy dissipated and LSS, for optimal welding conditions using a 500 [N] welding force for a 14.9 [mm] (rectangular sonotrode) overlap .....   | 75 |
| Table 5-7   Overview of the materials used (TT = Toho Tenax), sonotrode used and the welding parameters for the welding experiments for the energy welded spot in the middle of a larger overlap, using TT 2 layer, 0.24 [mm], EDs and the 9110 jig.....  | 75 |
| Table 5-8   Average values and their $c_v$ for welding parameters comparing the regular travel controlled welds with energy controlled spot welds .....   | 77 |
| Table 5-9   Overview of the materials used (TC = Ten Cate), sonotrode used and the welding parameters for the welding experiments for the energy welded dedicated area sized ED, using TC 5 layer, 0.25 [mm], EDs and the 9110 jig .....  | 82 |
| Table 5-10   Average values and their $c_v$ for welding parameters comparing the regular travel controlled welds and the energy controlled spot welds of the larger overlap with the dedicated area sized ED welds .....  | 84 |
| Table 5-11   Overview of the materials used (TC = Ten Cate 90 [°]), sonotrode used and the welding parameters for the welding experiments for the travel welded dedicated area sized ED, using TC 5 layer, 0.25 [mm], EDs and the 9110 jig .....  | 85 |
| Table 5-12   Overview of the materials used (TC = Ten Cate 90 [°], TT = Toho Tenax), sonotrode used and the welding parameters for the welding experiments for the travel welded dedicated area sized ED, using TC 5 layer, 0.25 [mm], EDs and the 9110 jig.....  | 88 |
| Table 5-13   Average values and $c_v$ for the welding distance, maximum power, welding time and LSS, for the dedicated area sized ED welding using a 500 [N] welding force, the rectangular sonotrode and the 9110 jig and welding energy of 855 [Ws]. Presenting the results for the weave to chopped welded samples compared to the weave to weave welded samples. .... | 90 |
| Table 5-14   Overview of the materials used (TC = Ten Cate 90 [°]), sonotrode used and the welding parameters for the welding experiments welding a 14.9 [mm] overlap with pre-attach ED, using TC 5 layer, 0.25 [mm], EDs and the 9110 jig .....   | 92 |
| Table 5-15   Average values and $c_v$ (if applicable) for the maximum power, welding time, energy dissipated and LSS, for optimal welding conditions using a 500 [N] welding force, the   |    |

rectangular sonotrode for a 14.9 [mm] overlap and the 9110 jig, comparing the samples with the (regular) taped ED (Toho Tenax 0 [°] weave samples, and Toho Tenax 0.24 [mm] ED) and the plunge welded pre-attached ED (Ten Cate 90 [°] weave samples and Ten Cate 0.25 [mm] ED)..... 93

Table 6-1 | Overview of the materials used (TC = Ten Cate, hinge is produced from chopped fibre Toho Tenax material), sonotrode used and the welding parameters for the welding experiments sequentially welding a plate with two pre-attached ED to the hinge, using TT 2 layer, 0.24 [mm], EDs and the 9110 jig ..... 103

Table 6-2 | Overview of the materials used (TC = Ten Cate, hinge is produced from chopped fibre Toho Tenax material), sonotrode used and the welding parameters for the energy determination for hinge welding, using TT 2 layer, 0.24 [mm], EDs and the 9110 jig..... 104

## Abbreviations

|      |  |
|------|--|
| ACU  | Advanced Control Unit  |
| ASTM | American Society for Testing and Materials   |
| CF   | Carbon Fibre   |
| CFRP | Carbon Fibre Reinforced Plastics   |
| DEMO | Dienst Elektronische en Mechanische Ontwikkeling   |
| DUT  | Delft University of Technology   |
| ED   | Energy Director  |
| FHNW | (Fachhochschule Norwestschweiz)<br>University of Applied Sciences Northwestern Switzerland             |
| FRP  | Fibre Reinforced Plastics  |
| ITD  | Integrated Technology Demonstrator   |
| JTI  | Joint Technology Initiative  |
| LSS  | Lap Shear Strength   |
| NLR  | (Nationaal Luchtvaart- en Ruimtevaartlaboratorium)<br>National Aerospace Laboratory of the Netherlands |
| TPC  | Thermoplastic Composite  |
| TSC  | Thermoset Composite  |
| UD   | Unidirectional   |
| USW  | Ultrasonic Welding   |

## Symbols

|                           |  |
|---------------------------|--|
| $\alpha_h$                | Empirical hammering correction factor  |
| $\epsilon_0$              | Cyclic amplitude of strain   |
| $\eta_{\text{hammering}}$ | Hammering efficiency factor  |
| $\mu$                     | Mean of the considered set   |
| $\sigma$                  | Standard deviation of the considered set   |
| $\omega$                  | Frequency of vibration   |
| $c_v$                     | Coefficient of variation of the considered set                                   |
| $E''$                     | Frequency and temperature dependent loss modulus                                 |
| $E_{\text{hammering}}$    | Energy that is lost through impact at the surface of the top sample              |
| $E_{\text{jig}}$          | Energy loss due to jig properties  |
| $E_{\text{loss}}$         | Total energy losses  |
| $E_{\text{machine}}$      | Energy loss of the machine, sonotrode and baseplate configuration                |
| $E_{\text{materials}}$    | Energy loss in the ED and TPC material (due to composition, geometry or defects) |
| $E_{\text{tot}}$          | Total energy delivered   |
| $E_{\text{weld}}$         | Energy needed for the weld   |
| $F_{\text{max}}$          | Maximum force  |
| $\dot{Q}_{\text{avg}}$    | Average viscoelastic heating rate  |



# I – Research Design





# 1 Introduction

---

## 1.1 Motivation

The aerospace industry is paying increasing attention to the environmental impact of air transportation, which is linked for a large part to the aircraft weight. The CO<sub>2</sub> emissions of this industry are expected to increase by 50 [%] in 2050 if no action is taken (although this is only from 2 [%] to 3 [%] of the total man-made CO<sub>2</sub> emissions) [1]. Lighter and more efficient structures and materials, shorter and more efficient production processes (and less energy consuming as a result), can help their bit in reducing the environmental impact. Projects like the Clean Sky Joint Technology Initiative (JTI), a public private partnership between the European Commission and the Aeronautical industry, are working on reducing the environmental impact of aviation. Several new concepts are demonstrated by the production of Integrated Technology Demonstrators (ITD). The faculty of Aerospace Engineering of Delft University of Technology is one of the organizations involved in the eco-design airframe ITD, which, among other technologies, is making use of thermoplastic composites (TPCs) and innovative design and production methods.

In general the use of composites in (the aerospace) industry is continuously increasing due to the many advantages composites have over conventional materials. Composites have the ability to be tailored to meet specific design needs. They combine different materials and therefore different material properties (high strength of the fibres, low density of the polymer). This results in, if used properly, lighter solutions for the same structural purpose. Additionally, these composite solutions often offer better fatigue and environmental resistance. Although thermosetting composites (TSCs) are currently more common, TPCs (using new thermoplastic resins with similar engineering properties as commonly used thermosetting resins) are gaining ground because they offer several advantages. The most important advantages are, their cost effectiveness in manufacturing (due to short production times and their joining possibilities), high impact strength and fracture resistance. Even though higher temperature and pressure are needed in the production of TPCs, other advantages are unlimited shelf-life, post formability, ease of repair and ease of handling [2].

To profit from all the advantages composites offer, ideally completely integrated structures are preferred. The higher temperature and pressure required in TPC processing and the higher viscosity of the thermoplastic resin (500 – 5000 [Pa · s] for thermoplastic resins compared to 100 [Pa · s] for thermosets [3]), can make the manufacturing of more complex shapes difficult and costly. This can limit the level of integration and calls for other (cheaper) integration techniques [4]. Conventional integration techniques like mechanical fastening or adhesive bonding are labour intensive and costly. Additionally, the use of mechanical fastening also results in problems with stress concentrations. TPC composites however offer the possibility to be fusion bonded, which potentially increases the cost effectiveness of manufacturing even more. For fusion bonding techniques there is hardly need for surface treatment of the samples and they have the potential to offer rapid, reliable and cost effective integration [4].

Several fusion bonding techniques for TPC exist today, of which ultrasonic welding (USW) has the highest potential for the very fast welding of small surfaces and is therefore the focus of this research. USW is a high-frequency low-amplitude process which has several main advantages compared to other processes. It has an extremely short process time (1-5 [s] total cycle) and is therefore energy-efficient, it does not require any foreign materials regardless of the structure of the TPC, on-line monitoring of the welding process is possible with modern USW machines providing indirect feedback on the weld quality and is therefore well suited for automation [5], [6]. The current practice produces fast, clean and consistent high quality welds in single lap shear samples. However, except for a successful experiment of Benatar [7] with the sequential welding for single and double lap shear specimen, virtually no research has been done in the up-scaling of the process towards a practical application [4].

This thesis will present a first investigation into identifying challenges for up-scaling. To this end, new ultrasonic welding concepts are proposed and tested. Based on the results of these new concepts, a sequential USW procedure for the welding of chopped fibre hinges to continuous fibre frames in the Clean-Sky Eco-Design ITD is developed.

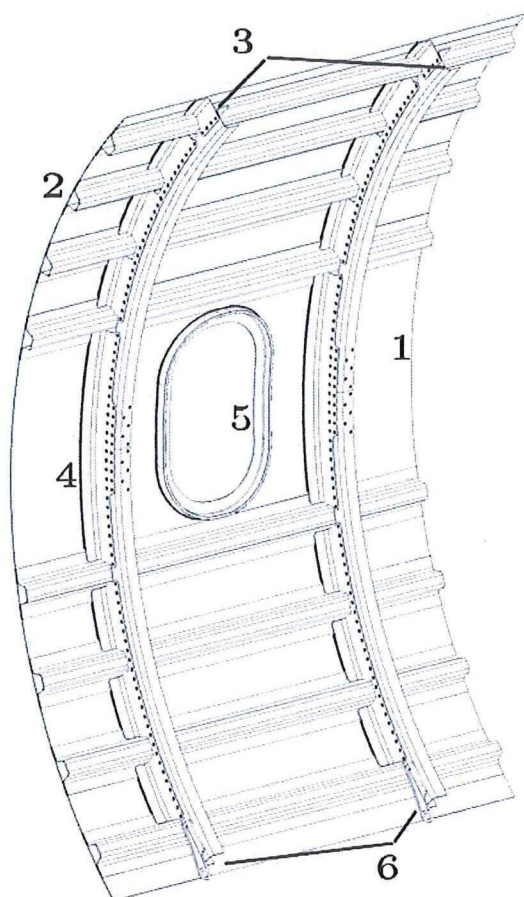
### ***A Clean-Sky Eco-Design specific case***

For the eco-design ITDs built in the Clean Sky Joint Technology Initiative (JTI) (the ITD F1) considered in this research, USW can play an important role. The eco-design ITD is a skin panel reinforced with frames and stringers, has one window cut-out and has two hinges as can be seen in Figure 1-1. The ITD is used to research and demonstrate several cutting edge technologies which could help increase structural efficiency, optimize production and reduce environmental footprint. The faculty of Aerospace Engineering of Delft University of Technology is coordinating the activities for the design and manufacturing of the F1 eco-design ITD. Other organisations involved are Fokker Aerostructures, Nationaal Luchtvaart- en Ruimtevaartlaboratorium (NLR), Eurocopter and the Fachhochschule Nordwestschweiz (FHNW) [8]. Some of the technologies demonstrated are advanced laser assisted fibre placement, consolidation of the skin panel using out-of-autoclave infrared heating, stiffener integration on the skin using induction welding, co-consolidation of the window frame to the skin, microwave in-situ consolidation and recycling of TPCs. For this last technology FHNW designed and produced helicopter door hinges from recycled and chopped fibre TPCs (PEEK matrix).

The door hinges are designed to replace similar steel hinges and are compression moulded. The new design offers a weight reduction from 134 [g] (steel) to 22 [g] (recycled/chopped CF/PEEK) and is one-step recyclable (which means the material goes from the original hinge to recycling and the recycled material can directly be used for production again, only needing one step). The hinges made from recycled TPCs (produced using high voltage fragmentation) only show a 17 [%] decrease of mechanical properties compared to the first generation hinges, which is promising [9]. A schematic view and a produced hinge can be seen in Figure 1-2.

This hinge will be attached to the edge of the C-frames (manufactured using CF/PEEK-UD), for which USW can be very promising, making this an interesting application for research into up-scaling of the process. USW can make the structure more efficient (no cut-outs, stress concentrations, fasteners, foreign material, short cycle time <5 [s]), saving weight, energy, time and improving recyclability [8]. This covers many of the goals set by the Clean Sky project [1].





- 1) Skin
- 2) Hat Stiffeners
- 3) C-Frames
- 4) Clips
- 5) Window Frame
- 6) Hinges



[www.cleansky.eu](http://www.cleansky.eu) CLEANSKY

Figure 1-1 | Schematic overview of the Clean Sky JTI Eco-Design ITD F1 – Thermoplastic Composite Airframe Panel [8]

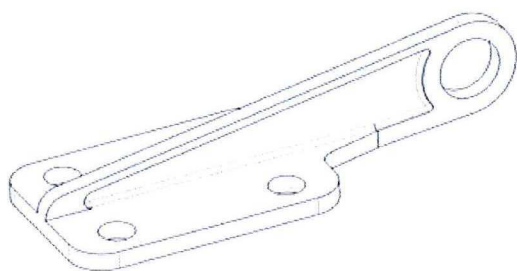


Figure 1-2 | Schematic view of the TPC helicopter door hinge (left) and actual view of the door hinge produced of recycled CF/PEEK (right) by FHWN [8], [9]

## 1.2 Background information

### 1.2.1 Thermoplastic composite materials, production and recycling

Many of the high performance technical applications of recent years ask for special material properties that are difficult to achieve by metal alloys, especially in aerospace, underwater and transport applications. A composite material is generally considered to be made from two or more constituent materials with significantly different properties, which combined provide a material with better overall properties [10].

In TPC materials a thermoplastic polymer is used as matrix material. A thermoplastic polymer, is a linear or branched polymer and will soften when heated and harden when cooled, which offers advantages compared to thermosetting polymer (a thermosetting polymer is a network polymer, once produced they become permanently rigid and do not soften upon heating). The process for thermoplastics is reversible, which makes it amongst other things suitable for fusion bonding (since two separate parts can be molten together) and offers more flexibility in (post-) processing. Although the processing temperature for thermoplastics is generally higher compared to thermosets, another advantage is the strongly reduced processing time [10].

#### **Aerospace grade TPC matrix and fibre materials**

In the production of TPCs several matrix materials and fibres can be selected. The combinations are numerous and are driven by criteria like the mechanical properties required, the operation environment of the material and the costs. Table 1-1 contains some of the aerospace grade high performance thermoplastic polymer resins showing their structure (amorphous: no crystallisation, or semi-crystalline: both with an amorphous and a crystalline region), their  $T_g$  (glass transition temperature: where an amorphous polymer, or the amorphous phase of a semi-crystalline polymer, transforms abruptly from a rigid glass state to a soft rubbery state), their  $T_m$  (melting temperature; note that amorphous polymers do not have a melting temperature since they don't possess ordered phases, with increasing temperature the polymer just becomes more viscous) and their  $T_{max.serv.}$  (maximum service temperature, the temperature at which the polymer can be used for an extensive time without significant problems) [11], [12].

Table 1-1 | List of high performance thermoplastic matrix materials and their properties, note that this table only provides an indication since there are many variants within one polymer type (depending on manufacturer, process, chain length etc.), providing different values for  $T_g$ ,  $T_m$  and  $T_{max.serv.}$  [12], [2], [10], [13]

| Polymer                        | Structure        | $T_g$ [°C] | $T_m$ [°C] | $T_{max.serv.}$ [°C] |
|--------------------------------|------------------|------------|------------|----------------------|
| PPS – PolyPhenylene Sulfide    | Semi-crystalline | 81 – 97    | 285 – 290  | 200 – 260            |
| PEI – Polyether Imide          | Amorphous        | 215 – 217  | -          | 161 – 179            |
| PEKK – PolyEtherKeytoneKeytone | Semi-crystalline | 153 – 170  | 347 – 373  | 250 – 260            |
| PEEK –PolyEtherEtherKeytone    | Semi-crystalline | 143 – 157  | 322 – 346  | 239 – 260            |

For composites most of the structural strength and stiffness can usually be attributed to the fibres embedded in the polymer matrix. Table 1-2 provides general information on strength and stiffness properties of commonly used fibres in (thermoplastic) composites.



Table 1-2 | List of commonly used fibre materials and their strength and stiffness properties [14], [15]

| Fibre type       | Tensile Strength [GPa] | Elastic Modulus [GPa] |
|------------------|------------------------|-----------------------|
| Glass (S-glass)  | 4.48                   | 85.6                  |
| Carbon (IM-7)    | 5.17                   | 290                   |
| Graphite (GY-70) | 1.73                   | 517                   |
| Boron            | 3.66                   | 4.14                  |

The variation of thermoplastic matrix material combined with the various different fibre materials gives the designer freedom to produce efficient composite structures, suited for each individual application (light weight, cheap, recyclable, etc.). Next to the material choice the designer can also vary the properties of the composite with the fibre length, stacking sequence and production process. The fibre length can basically be divided in two groups, continuous and discontinuous fibres (Figure 1-3). Looking at Figure 1-3, laminates consisting of continuous fibres in a polymer matrix, like unidirectional (UD) fibres, are more difficult to manufacture but result in higher strength/stiffness, where discontinuous fibres, like chopped fibres, are relatively easy to produce but have far lower mechanical properties [2].

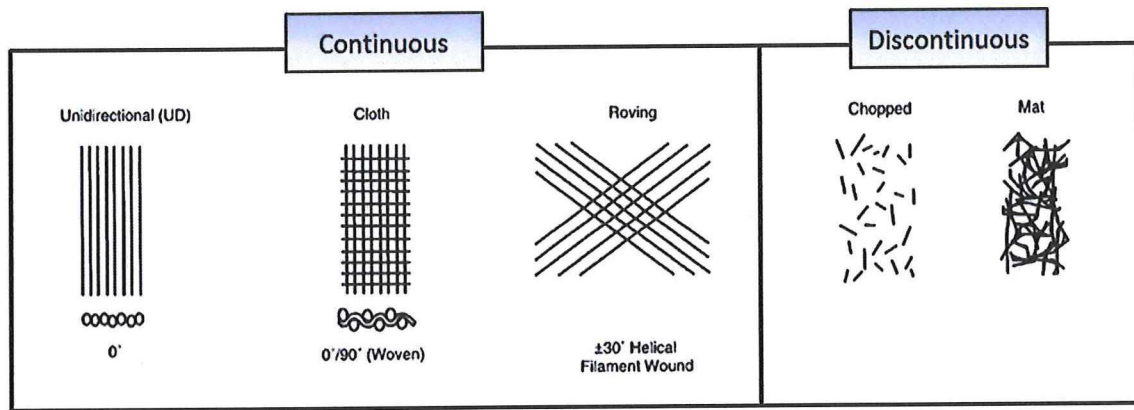


Figure 1-3 | Schematic view of continuous and discontinuous fibre configurations used in composites [14]

The materials used for the structural parts of the Clean Sky ITD that are of special interest for this research are the frames and the hinges. The frames are produced of UD continuous carbon fibres in a PEEK matrix, whereas the hinges are made from chopped fibres (either virgin or recycled) also embedded in a PEEK matrix.

### Production processes for TPCs

Figure 1-4 shows for both continuous and discontinuous fibres several common processes which are currently used for the production of TPCs.

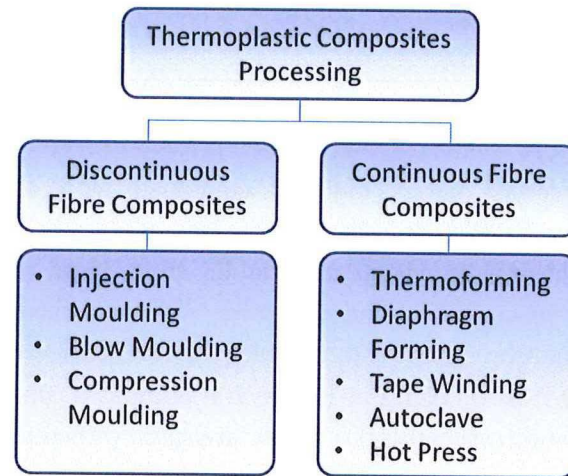


Figure 1-4 | Thermoplastic composite processing techniques for continuous and discontinuous fibres [16]

Due to the virtually unlimited variation in shape, fibres and resin material, for most processes several heating and pressure profiles are available depending on the configuration and material selection (due to different melting temperatures, viscosity, etc.).

### Recycling processes for TPCs

The need for feasible recycling processes for TPCs is increasing, due to the increasing production and waste stream (12 [%] growth per year) [17], strict regulations (making landfilling more expensive) [18] and relatively high cost of virgin material (up to 45[€/kg]) [17]. Common recycling processes for TPCs can be classified in three main methods, as shown in Figure 1-5.

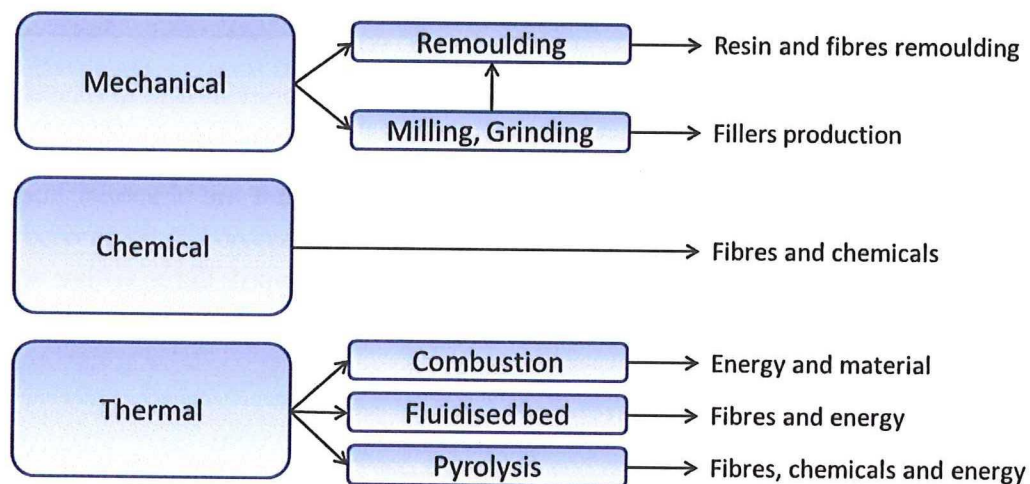


Figure 1-5 | Overview of recycling processes for thermoplastic composites [19]

Most of these processes have significant drawbacks and / or are energy intensive and costly. Although sometimes the mechanical properties of the fibres are sufficient, the whole process is not deemed (financially) feasible.



A new technique showing promising results is electro dynamical fragmentation, or high voltage fragmentation. In this process the chopped fibre TPC is placed in a tank filled with liquid (water) and is shredded by high voltage discharges between an anode and cathode in the tank. These discharges form an electric arc (plasma channel) which produces a shockwave and shreds the material. An advantage of this process is that it is already industrialized for the mining industry. Tests by FHNW [18] with chopped fibre samples show that most of the recycled fragments, although similar in composition as in mechanical recycling (fibre chunks / fibrous material with resin still attached to the fibres), do not contain broken or damaged fibres. This is due to the fact that the discharges mainly affect the matrix material which has a lower mechanical strength than the fibres. This is a major advantage compared to mechanical shredding. Also there is practically no wear on the equipment (only the anode and cathode have to be replaced after a long time), and there are no issues with small dust particles. There are no dust particles due to the fact that the process takes place in water (or another liquid). A downside is that the retrieved fragments need to be dried. Finally the fibre length of the recycled material can be reasonable controlled by the length of the recycling process (longer time, smaller parts). Initial experiments performed by the FHNW institute of polymer engineering show promising results in using this technique for the recycling of chopped PEEK/Carbon TPC [18].

### ***1.2.2 Ultrasonic welding of thermoplastic composites***

Although commonly used in the plastic industry, USW is still in the early stages for the welding of TPCs. This section will provide in depth background knowledge on the current understanding and possibilities of the USW process.

#### ***Recent developments and process setup***

USW uses ultrasonic low-amplitude high-frequency vibrations perpendicular to the contact area to generate heat at the interfaces. At the interfaces of the samples to be welded, an extra layer of polymer is applied called the energy director (ED). As a result of the generated heat the ED melts, which eventually welds the parts together. A schematic overview of the common setup used in USW can be found in Figure 1-6. The pneumatic piston is used to move the ultrasonic train (converter, booster and sonotrode) to the specimen and apply pressure. As explained in [20], the electric power (typically 60 [Hz] in Europe) is converted to high frequency mechanical vibrations (20-40 [kHz]) by the converter. The sonotrode or horn is used to transfer these vibrations to the parts that need to be welded, and the shape of the horn (its mass distribution with respect to the nodal plane) determines its amplification. Often a booster is used in between the converter and the horn to vary the amplitude of vibration without the need of reshaping the horn. The horn and booster together provide the total amplification ratio of the welding setup as can be seen in Figure 1-6.

Another important part in the setup is the welding fixture. The fixture should be designed in such a way that it can clamp the parts to be welded, it perfectly aligns them and makes sure that they do not shift horizontally under the applied vibration. Looking at the schematic overview in Figure 1-6, it can be seen that during the process some vertical travel should be allowed to cope with the melting (and flow) of the ED, preferably in such a way that it minimizes bending of the top part.

The maximum area that can be welded by this setup in one shot is limited by the shape of the sonotrode and (more importantly) by the maximum welding power of the machine. This means that for larger areas sequential welding (the use of multiple spot welds to connect two parts) can be used, which most likely would be the technique used for the hinge attachment of the Clean Sky ITD. During sequential welding the first weld will present some constraints to the two parts (by connecting them at one spot). This might cause problems as some of the vibration within the top part can result in heating in other (not yet welded) points in the overlap, which can result in overheating and / or delamination of these points [7]. Some preliminary analysis discussed by H.M. Lu and A. Benatar [7] shows that such issues might be controlled with the use of dampers on both sides of the horn. This reduced the vibration substantially elsewhere in the specimen while not significantly affecting the vibration under the sonotrode. The research on that topic, however, is very limited. Another option might be to use continuous welding. However, considering that the size of the specific application (or other general structural parts, like clips and brackets) is relatively small, spot welding is deemed more suitable. Also virtually no research on continuous USW of TPCs has been performed so far.

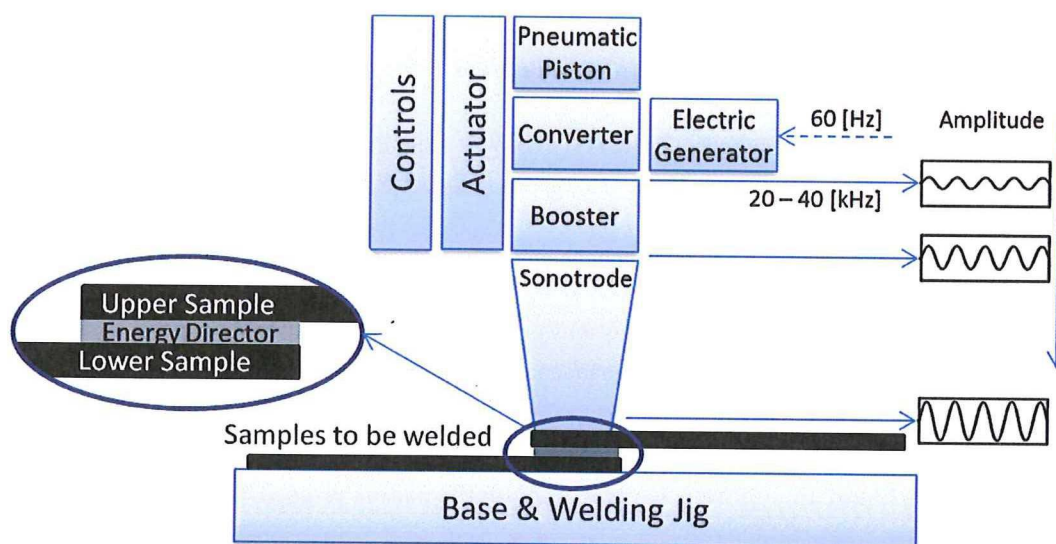


Figure 1-6 | Schematic view of an ultrasonic welding machine showing amplification steps [6], [20]

Another development in USW of TPCs concerns the EDs used. Formerly the EDs used in USW were manufactured like V-shaped protrusions. These protrusions heat up preferentially as a result of higher cyclic strains and concentrate the heat generation at the interface between the parts. Recent research by I. F. Villegas, however, has shown that the need of such complex EDs is not necessary for the welding of TPC [20], [5], [21]. One simple flat layer of ED material (which is basically the thermoplastic matrix material), will suffice in obtaining the desired weld. Instead of attaching / moulding V-shaped protrusions to the specimen, the flat ED can simply be taped to one of the parts. The lack of need for V-shaped protrusions can be attributed to the fact that the stiffness of the simple, one-layer, ED is already much lower than the stiffness of the parts to be welded, due to their lack of reinforcement. Therefore the flat layer will already experience higher cyclic strains. For the Clean Sky project however, the hinges are produced using chopped fibres which have a different stiffness than the UD carbon fibre reinforced TPCs used in the specimens



created by I.F. Villegas. Welding these to the frames, which are produced using continuous UD fibres, might result in the need for more complex EDs.

### Process monitoring and the effect of process parameters

With modern USW machines, it is possible to monitor the joint quality by measuring the dynamic mechanical impedance of the parts during welding, which is done by indirectly measuring the power dissipation [4], [5]. The USW machine available in the DASML, is controlled by a microprocessor unit, the Advanced Control Unit (ACU), which provides the dissipated power as output (next to usually the force and the displacement during the welding process), which is recorded by the computer software AcuCapture and can be easily exported and analysed in software like Microsoft Excel. Figure 1-7 shows an output of a typical weld. In the graph shown in Figure 1-7, three phases of the complete USW process can be distinguished. The initial phase, I, where the sonotrode travels to the samples and builds up to the welding force, the vibration phase, II, where the actual welding is done, and the solidification phase, III, in which (usually) the pressure is increased quickly and is kept constant for several seconds as the melt solidifies.

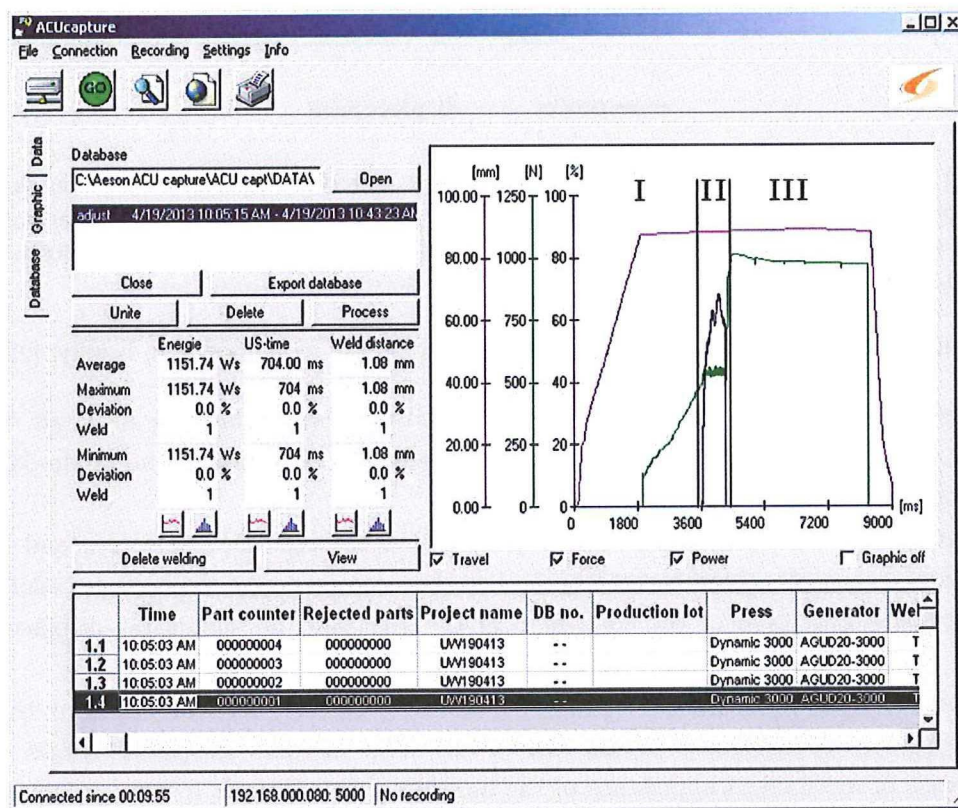


Figure 1-7 | Typical output of the USW process, showing travel, force and dissipated power as well as displaying other welding information, as produced by the AcuCapture software coupled to the ACU of the Rinco Dynamic 3000 USW machine used by the faculty of Aerospace Engineering DASML. Showing the, I) initial (built-up) phase, II) vibration phase, III) solidification phase

Using the power dissipation and the displacement curve, different (although coupled) steps in the vibration phase (II) of the USW process can be identified, which is clarified in Figure 1-8 from the research of I.F. Villegas [22]. Note that the displacement curve starts at 0 [mm] at the beginning of the process (Figure 1-8), and is corrected for the travel in phase I of the USW (by



subtracting the already travelled distance of the sonotrode in phase I from the other values in this phase) showing only the relative travel during this phase.

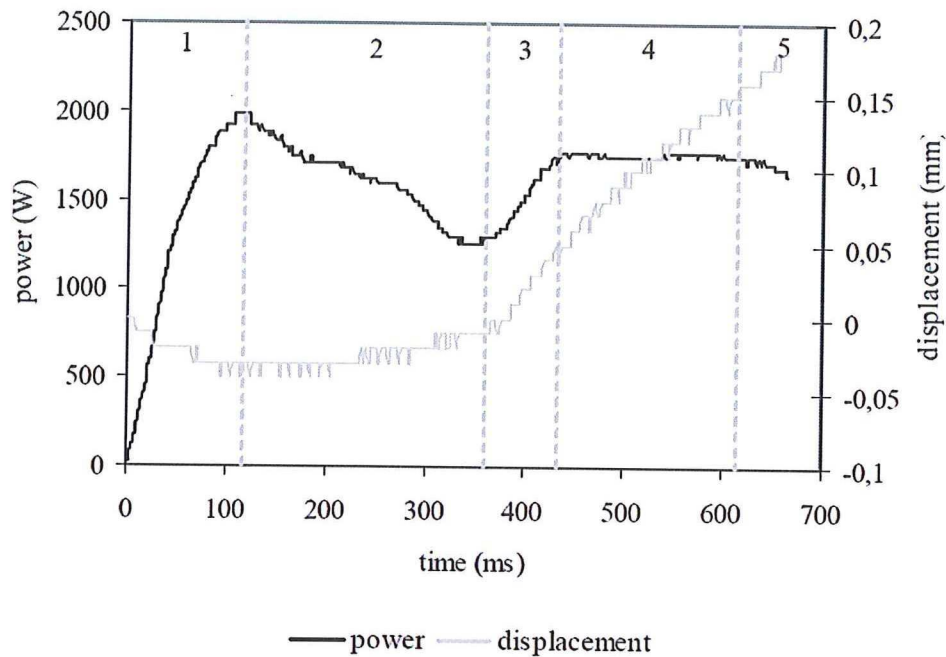


Figure 1-8 | Typical evolution of the power dissipation and displacement curves for the different welding steps during the vibration (welding) phase of the USW process. The displacement of the sonotrode is relative to its position at the beginning of the phase and positive values indicate downward displacement. [22]

The different steps that can be distinguished in Figure 1-8 are explained here briefly: [22]

1. Stage 1: Beginning of the process, characterized by a strong increase in power dissipation and a slightly negative (upward) displacement of the sonotrode to accommodate for the vibration at the start of the process.
2. Stage 2: The ED continues to heat up and melt through the nucleation and growth of random hot spots, characterized by a slow decrease in power dissipation (related to the progressive reduction of the solid area of the ED) and no significant displacement (no flow of the ED).
3. Stage 3: Beginning of the squeeze flow of the ED, this can be clearly seen by the positive (downward) displacement of the sonotrode. The increase in power comes from the increase of mechanical impedance of the interface when all melt fronts (growth of the hot spots) meet.
4. Stage 4: Approximately constant power dissipation in this phase, is believed to come from two counteracting effects which are the flow of the ED (causing power increase) and the beginning of melting the matrix in the composite parts (causing power decline). This can be seen by the flat power curve in this area, referred to as the power plateau.
5. Stage 5: At this stage the ED is completely squeezed out (practically no existence of resin at the weld line) and the power dissipation drops again. In this phase the matrix of the composite parts continues to melt and squeeze flow starts, squeezing out the matrix resin along with the reinforcing fibres.

The best quality weld is obtained if flow of the ED reaches the point where the melting of the composite matrix starts (in the power plateau) [5]. This area can be identified using the feedback of the USW machine, which makes it easy to identify the optimum welding conditions for various types of welding setups and materials [5], [22].

In the USW process there are various parameters that can be directly controlled (settings on the USW machine), like amplitude of vibration, welding (trigger) force, build-up rate for the welding force, travel of the sonotrode and the solidification force. Research done at the Aerospace Engineering faculty of Delft University of Technology by several authors ([22], [21]) describes the effect of these parameters on the mechanical quality of the welds, the vibration time, the maximum required power and the welding energy.

The experiments were done using CF/PEI TPC material, and the results indicated that none of the parameters had a significant effect on the mechanical quality of the welds [21], meaning that the processing window for this material is broad. This is due to the fact that PEI is an amorphous polymer, which allows for a relatively broad processing temperature range with no sudden phase changes [21]. The research also indicated that the build-up rate and the solidification force were never the first or second significant influencing factor of the process. The two most important parameters affecting the maximum dissipated power were 1) amplitude of vibration and 2) welding force, increasing those two parameters leads to an increase in the maximum power. For the vibration time these were found to be 1) welding force and 2) amplitude of vibration, increasing those two parameters leads to a reduction in vibration time. Influencing the welding energy, 1) travel of the sonotrode and 2) welding force were found to be the most significant parameters. Here increasing those parameters leads to an increase in welding energy [22].

Looking in more detail at the effect of the amplitude of vibration and the welding force on the different stages of the power curve displayed in Figure 1-8, several conclusions can be found in literature [22]. In the first stage, changing the amplitude has more effect than changing the welding force, although increasing them means an increase in the power peak in both cases. That changing the amplitude has (slightly) more effect in this stage can be attributed to the fact that the amplitude affects both the viscoelastic and the interfacial friction and the welding force only the interfacial friction. [22]

In the second stage changing the welding force has far more effect on the duration of this stage than changing the amplitude of vibration. This stage consists of the initiation and growth of hot spots. Increasing the amplitude (mainly) increases the growth rate of the hot spots, while increasing the welding force increases the amount of initiation sites for the hot spots. The latter has more effect on the duration of this stage and causes faster heat generation. The faster heat generation results in a continuous power drop instead of a step-like drop seen for lower welding forces. [22]

It is not stated in literature which affects the third stage more, but looking at the graphs shown in Figure 1-9 from the research of I.F. Villegas [22] it can be seen that for a higher (1500 [N]) welding force the difference in amplitude has less influence on the duration of this stage than if the welding process is performed with a low (300 [N]) welding force. Since flow already starts at

this stage, and squeeze flow rates are higher for a higher force, the welding force might be the most important factor.

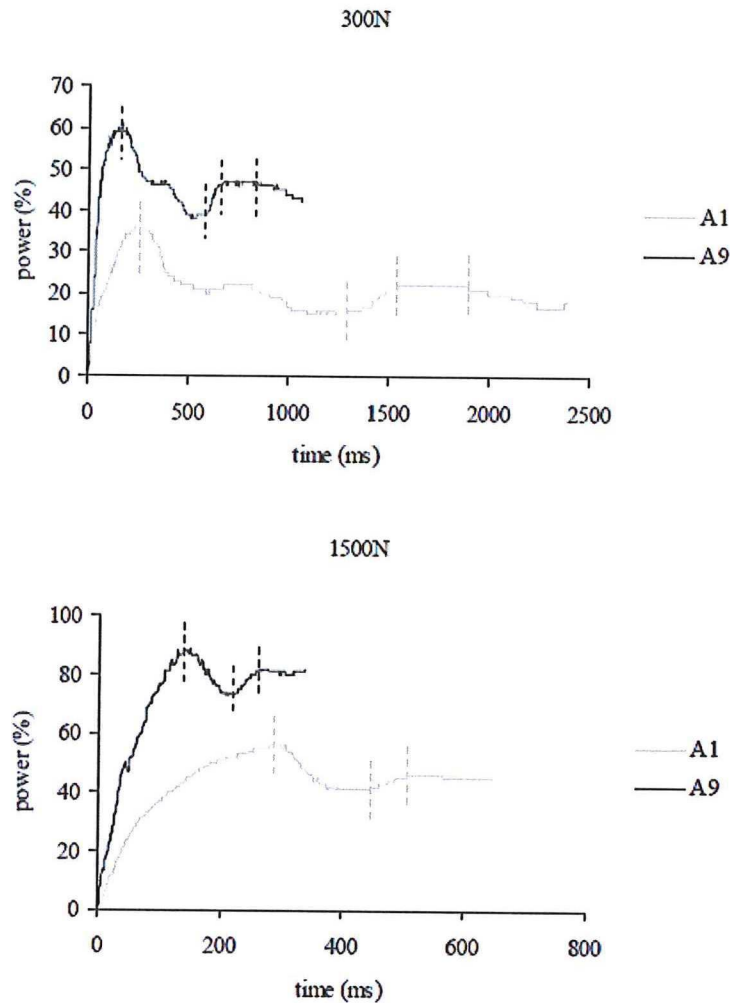


Figure 1-9 | Influence of the amplitude of vibration ( $A1 = 51.8 \text{ [}\mu\text{m]}$ ,  $A9 = 86.2 \text{ [}\mu\text{m]}$ ) on the power curves for a low welding force (300 [N], top) and a high welding force (1500 [N], bottom) [22]. Depicting less change considering duration of stage 3 in the 1500 [N] welds with varying amplitude compared to the 300 [N] welds.

Also for the fourth stage the welding force is the most important factor. Increasing the welding force significantly decreases the duration due to the faster flow of the molten ED.

For the final stage it has been noted that a low welding force provides a better defined stage (using the same total displacement as in a higher welding force process). It is normally considered to stop welding before this stage (namely at stage 4 as explained), therefore this is deemed less important.

All the process parameters described thus far are directly controllable by the settings of the USW machine. In the welding process however, other factors influence the result as well. Although virtually no research is found in literature on some the following parameters and their influence on the USW process, they might be important in further development and up-scaling of the process.



Firstly the effect welding two different material configurations to each other is not been researched yet. H. Potente mentions briefly that some different polymers are compatible and can be welded to each other [23]. The research of A. Benatar also showed that in some cases this was possible with dissimilar composites (J polymer graphite and PEEK graphite composites). [24] The effect of welding short fibre TPC to continuous fibre TPC however, has not been researched yet. The difference in stiffness and heat dissipation might form some issues in producing high quality welds; although literature suggest that if the ED has a lower stiffness than the composite parts it will be sufficient to promote preferential heating at the interface [5].

Secondly the welding setup itself has influence on the process as well. Two main parts of the setup that can be readily changed (or need to be changed to change the welding configuration), are the sonotrode and the jig (or welding fixture). The effect of different sonotrodes has been studied for plastic welding and it can be shown that changing the shape and / or size of the sonotrode affects the energy dissipated during the process [25]. Therefore the temperature developed at the interface can change for the same settings (since the energy dissipation changes, a different amount of energy can be utilized in the heating of the ED). Also the amplitude differs per sonotrode (different sonotrodes have different gains) [25]. However, using different settings in the USW machine can counteract some of these changes. No research on the effect of the welding jig is found in literature, except for the fact that it has some influence on the welding process [22], [24]. It is stated for example in the research by I. F. Villegas that the welded samples showed some preferential heating at one of the edges of the overlap due to the jig design [22].

### ***Mechanics and modelling of the joining process***

As explained by A. Benatar and T. G. Gutowski the USW process is very complex and is still not completely understood. The process however can be divided in 5 separate yet highly coupled sub-processes (not to confuse with the 5 stages of USW process). The mechanics (and proposed modelling) of these sub-processes are described here:

1. Mechanics and vibrations of the parts

To evaluate the strain distribution in the parts (from which the heating can be determined), a mechanics and vibrations model of the entire setup is needed. In the research of A. Benatar and T. G. Gutowski a lumped parameter model was used (however with triangular EDs moulded to the substrates). An overview of this can be seen in Figure 1-10. It is important to note that all masses and their mechanical properties of all the parts in the entire welding column (from the converter to the fixture on the base) play a role in this model for USW. This means that when one or several parts are changed, it influences the mechanics and vibrations of the entire welding setup.

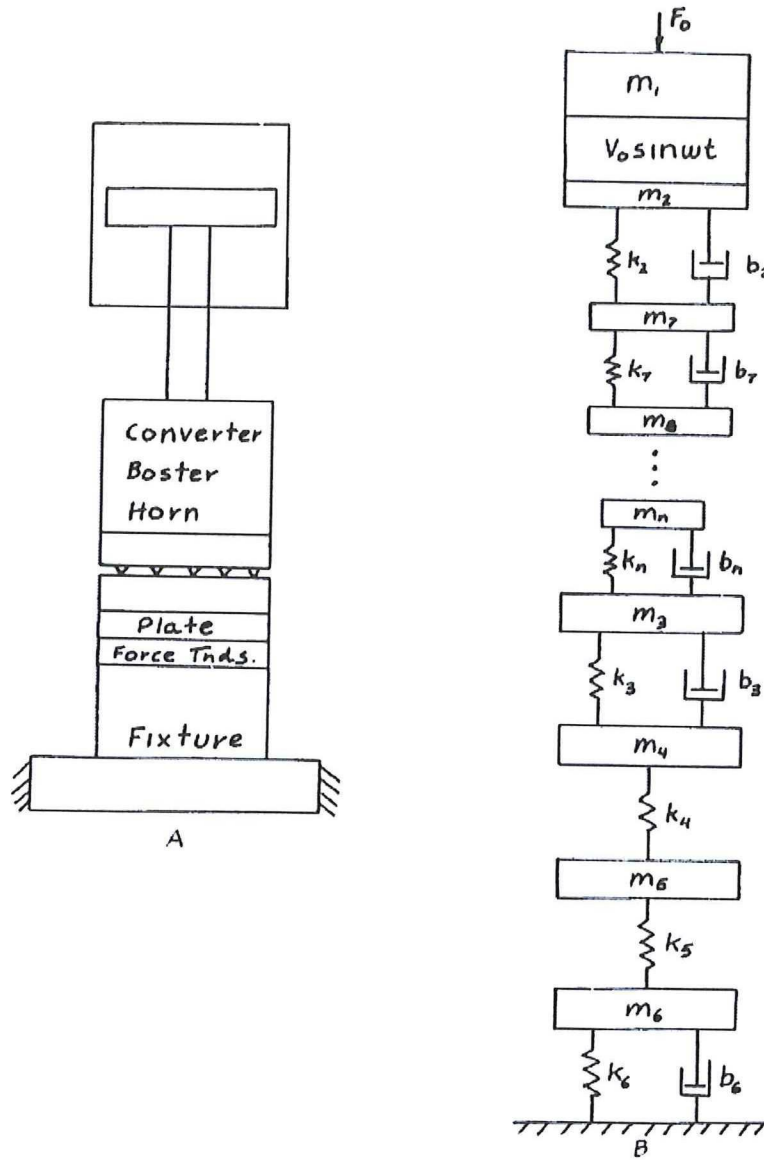


Figure 1-10 | Schematic overview of an USW system (A) and the corresponding lumped parameter model (B) as described by A. Benatar and T. G. Gutowski. [24] The masses  $m_7$ ,  $m_8$ ,  $m_n$  describe the triangular ED used in this parameter model, were the other masses represent all the other separate parts in the welding column for this setup.

## 2. Viscoelastic and interfacial friction, heating of the ED

If the USW process is well designed, the energy is focussed on the ED. Viscoelastic materials (like thermoplastic ED) subjected to this energy (the sinusoidal strain from the vibrations under the applied pressure) dissipate some of it into heat through intermolecular friction. This process is called viscoelastic heating. The average viscoelastic heating rate ( $\dot{Q}_{avg}$ ) is described by Equation 1-1, in which  $\omega$  is the frequency of vibration,  $\epsilon_0$  is the (cyclic) amplitude of strain of the ED and  $E''$  is the loss modulus of the thermoplastic (viscoelastic) resin material (this material property is dependent on temperature and frequency, so it needs to be determined for different welding frequencies along the entire temperature range) [24].

$$\dot{Q}_{avg} = \frac{\omega \epsilon_0^2 E''}{2}$$

Equation 1-1 [24]



Although viscoelastic heating is an important parameter in the heating of the ED, recent research performed by Zhang et al. [26] shows that the viscoelastic heating is only the dominant heating mechanism above the  $T_g$ . Not considered in the study of A. Benatar and T. G. Gutowski is the interfacial friction (combined with thermal conduction), which is dominant below the  $T_g$  and causes the initial temperature rise. The interfacial heating is higher at the edges (causing a faster temperature rise at the edges) due to stress concentrations and a high relative sliding velocity. The experimental results published in the research of Zhang et al. [26] confirm the theory that interfacial friction rather than viscoelastic heat starts the welding process. It is only above the  $T_g$  that viscoelastic heating becomes dominant.

Another important factor to consider is the so called hammering effect. For ideal welding conditions the sonotrode stays in contact with the upper sample, transferring all energy to the ED (which has the lowest stiffness and deforms most significantly). However, it has been observed that during welding of TPCs contact between the upper sample and the sonotrode has been lost (negative / upward travel seen in the travel curves), making the sonotrode ‘hammer’ on the parts to be welded. For the viscoelastic heating it was proposed by Levy in [27] to use an empirical hammering correction factor, changing Equation 1-1 to Equation 1-2.

$$\dot{Q}_{avg} = \frac{\alpha_h^2 \omega \epsilon_0^2 E''}{2} \quad \text{Equation 1-2 [27]}$$

In the analyses done by Levi in [27], it was found that a curve showing 13 [%] transmitted power of the USW machine, accurately fitted the predicted power dissipation. Making the efficiency of the overall process only 13 [%].

### 3. Heat transfer

When the EDs heat up, they dissipate heat through conduction to the relatively colder composite material and through convection to the surrounding air (where the setup has free edges to the air, for example in welding lap shear specimen). It was found that heat transfer through conduction is far greater than through convection, partly because carbon fibres have a high thermal conductivity. [24] In the research of A. Benatar and T. G. Gutowski the heat transfer was modelled using a modified version of the finite element program FEAP [28] and again using triangular ED. [24]

### 4. Flow and wetting

When a part of the ED is molten it starts to flow (mainly due to the applied pressure). Due to high viscosity of thermoplastic polymers the wetting of the composite surface depends on this squeezing flow. In the research of A. Benatar and T. G. Gutowski [24] the importance of inertia, compressibility and elasticity on the process are estimated. It is assumed that the whole amplitude of vibration is taken up by the molten ED. Their results show that at the beginning of the USW process the ED behaves like a soft spring in parallel with a soft damper (lumped parameter model) under the static loading and like a moderately hard spring under the dynamic loading. While the USW process progresses, dynamically the ED behaves like a stiffer spring. At

the point where the complete ED is molten (all the different melt fronts meet) the static behaviour is similar to that of a quasi-steady-state squeeze flow. Dynamically compressibility becomes an important aspect. This is the point where the impedance of the molten ED becomes very large, which can be measured indirectly by the power increase (because some of the vibration amplitude is now taken up by other parts like the composite, the fixture and the base which behave differently).

### 5. Intermolecular diffusion

The part where a fusion bond derives its strength from is the diffusion and entanglement of the long polymer chains throughout the bond interface [24]. This happens when two similar (or compatible) polymers are brought above the  $T_g$  (amorphous) /  $T_m$  (semi-crystalline). The interface gradually disappears through a healing process and the mechanical strength develops [6]. This healing process can be described by five sequential stages as described by C. Ageorges et al. [6], 1) surface rearrangement; 2) surface approach; 3) wetting 4) diffusion and 5) randomisation. This healing process is displayed schematically in Figure 1-11.

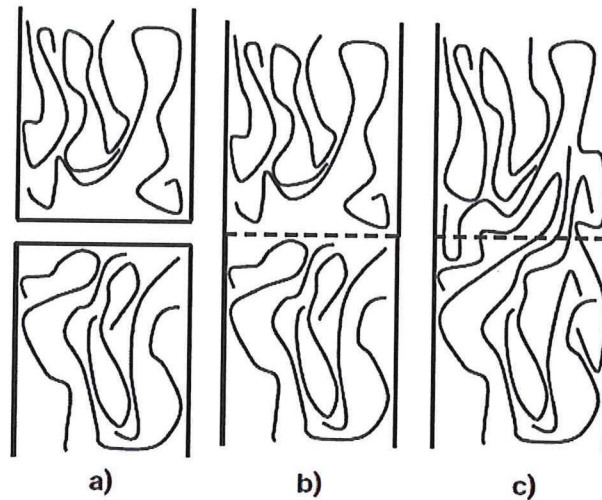


Figure 1-11 | Healing of a polymer interface (ED-joining parts) showing: a) two distinct interfaces; b) intimate contact; and c) inter-diffusion of the polymer chains [6]

Because the ends of the polymer chains are free to move the chains can move away from their initial position (which can be represented by a tube) and create the (partial) entanglement forming the bond. This healing process is called autohesion and relies on the phenomena described by the reptation theory [6]. The process of the reptation theory over time can be seen in Figure 1-12 in which  $t=0$  is at the start of the bonding process and  $t=t_r$  at the completion of it.

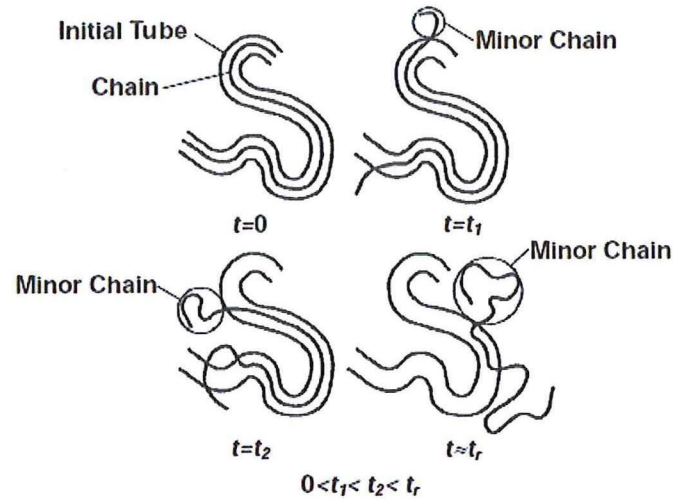


Figure 1-12 | Polymer chain movement from its initial to its final position as described in the reptation theory [6]

Intermolecular diffusion is not important for modelling of the process because of the extremely short healing times (estimated to be at least 6 orders of magnitude less than the weld time for USW) [24]. Therefore it can be assumed that intermolecular diffusion occurs almost immediately after melting of the ED and achieving intimate contact at the bonding interface [24].

From the 5 sub-processes in which the USW process can be divided according to A. Benatar and T. G. Gutowsky [24], it can be derived that information on the impedance or energy absorption of the fixture/base is dependent on the design/type of fixture used (assuming the same material is used, since different materials also have different impedances). If the impedance of the ED (or composite) increases, the fixture and base dissipate more energy [24]. It can be concluded that changing the welding setup or changing the materials of the samples, which is needed for example in (sequential) welding of the hinges, changes the energy dissipation.



### 1.3 Research goals

Quite some research in identifying the most influential welding parameters in different stages of the USW process and in optimizing several process parameters has already been done. Virtually all research, however, regards single lap shear specimen, for welding two similar substrates to each other.

The aim of this work is to perform a preliminary study on the up-scaling of the USW process for larger overlaps, for the practical purpose of welding structural elements as brackets, clips and hinges. The focus is on researching the possibilities of sequential welding and welding of dissimilar materials. This is done with a specific practical case of the Clean Sky project in mind: Welding of the CF/PEEK short fibre composites hinges (produced by FHNW), to a CF/PEEK continuous UD fibre C-frame (produced by the NLR).

Since sequential welding of practical applications is not yet attempted, many different aspects need to be investigated. Therefore the research is divided in several parts:

- Establishment of control / baseline parameters: use USW to join the specific materials used in this research and identify optimum welding conditions in lap shear samples
- Identify possible challenges for sequential USW and up-scaling
- Propose new concepts: research and analyse new welding approaches in standard lap shear sample tests
- Up-scale: design a setup and produce a joint with ultrasonic sequential spot welding, attaching the hinge from the Clean Sky project to continuous CF/PEEK material, creating a weld which can withstand a load case provided by FHNW of 3411 [N] in tension [29], as depicted in Figure 1-13

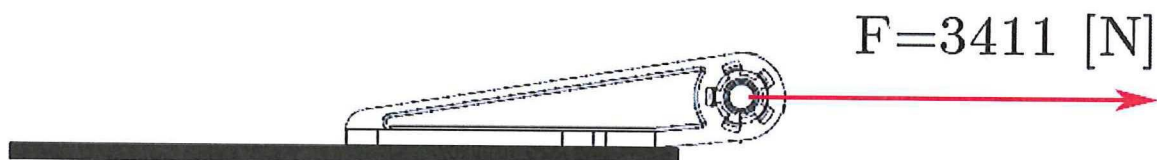


Figure 1-13 | Tension load case for the Clean Sky hinge

### 1.4 Outline

In this research the proposed experiments towards the up-scaling of the USW process are described and their results are discussed. Starting with chapter 2, which describes the experimental procedure, presents the materials, manufacturing processes, equipment and testing processes used. Chapter 3 presents and reflects upon the acquired results, the energy determination experiments are discussed in chapter 4, the newly proposed concepts and process practicalities will be discussed in chapter 5 and the results will be used for the up-scaling and hinge welding presented in chapter 6. Chapter 7 will provide an overview of all the main conclusions and finally chapter 8 will present future research recommendations.

## 2 Experimental Procedure

### 2.1 Materials and manufacturing

All the materials used in this research have a PEEK matrix with carbon fibre reinforcements. Continuous weave laminates from Toho Tenax and Ten Cate and chopped fibre material from Toho Tenax are used. Both Toho Tenax Vestakeep® PEEK film and the Ten Cate Victrex® PEEK film are used separately for the production of EDs.

#### 2.1.1 Toho Tenax continuous fibre weave and chopped fibre PEEK composite

##### *Continuous weave material for lap shear samples*

For the baseline experiments, Toho Tenax CF/PEEK continuous fibre  $[[0^\circ/90^\circ]_3]_s$  5HS (Harness Satin) weave plate material was already available with an average thickness of 1.85 [mm] (Note, the amount of layers was estimated since no information was available). The plate material was cut into lap shear sized samples, dimensions shown in Figure 2-1, using water jet cutting at Van Nobelen Delft BV. This process produces fast and relatively clean cuts (good edge quality, not many signs of delamination). The samples are cut in the main apparent orientation of the fibres in the  $0^\circ$  direction (main orientation of the longest visible fibre bundles relative to the longitudinal axis of the sample), since this results in preferable (higher) lap shear strengths in the welded samples [30].

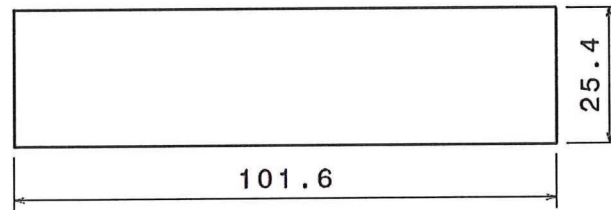


Figure 2-1 | Dimensions in [mm] for one sample used in the creation of lap shear samples following the ASTM D1002 standard

##### *Chopped tape lap shear samples and hinges*

For the production of the hinges and the chopped fibre test samples Toho Tenax PEEK (Vestakeep 2000) matrix / AS4 12k UD fibre - tape, with a 55% fibre volume, a  $T_m$  of  $345^\circ\text{C}$  and an average density of  $1.6\text{ [g/cm}^3\text{]}$  was used. The tape was cut in chopped parts using the Robust cutting machine available at FHNW.

Due to the maximum shear loads observed in previous welded samples (baseline and literature, approaching  $40\text{ [MPa]}$ ), a fibre length of  $20\text{ [mm]}$  was deemed appropriate for the lap shear samples as stated by [29] (the use of shorter fibres might result in breakage of the samples itself instead of failure at the weld). For the hinges, a fibre length of  $10\text{ [mm]}$  was found to be the optimum compared to various other compositions by [31], in terms of strength and processability.

For the production of the lap shear sample plate material and for the hinges, the Schwabenthan Polystat 200T,  $200\text{ [kN]}$  press at FHNW was used. The press has a top and bottom plate that



can be heated up to the desired temperature and the bottom plate is attached to a piston which can apply a maximum force of 200 [kN] on the part being produced.

For the lap shear sample plate material a simple mould available at FHNW was used with an inner die having a higher thermal expansion coefficient than the outer die, creating a perfect seal during heating. The mould allowed for the production of  $5.5 \cdot 25$  [cm] plates. The thickness was the only variable dimension and was kept identical to the thickness of the bottom plate of the hinge, namely 0.4 [cm]. With the dimensions of the plate and the average density of the chopped material known, the weight of the charge needed is calculated:

$$25 \text{ [cm]} \cdot 5.5 \text{ [cm]} \cdot 0.4 \text{ [cm]} \cdot 1.6 \text{ [g/cm}^3\text{]} = 88 \text{ [g]} \text{ of chopped material}$$

After applying release agent (Frekote 770-NC) to the mould, the charge of 88 gram was distributed evenly in the mould, closing it off with the inner die. The mould was placed in the press with a starting pressure of just under 1 [MPa] and heated up to an average temperature of 360 [°C] (measured manually with temperature sensors at 2 different mould positions) over a period of roughly 45 minutes (7.6 [°C/min]). At 360 [°C] the pressure was raised to 4 [MPa], and cooling (using air compressors) was initiated. After the temperature dropped to 340 [°C] (just below the  $T_m$  of the matrix material) the pressure was increased to 11 [MPa]. After cooling down the plate was demoulded. With the water jet cutting machine available at FHNW two samples were cut out of every plate, using the same dimensions as shown in Figure 2-1.

For the hinge production a more complex mould, designed and built at FHNW, was used [31]. The mould consists of a main outer mould, with three inner dies (left-side, right-side and bottom plate). One of these three, the bottom plate originally had 4 small cylindrical protrusions, designed for the creation of holes used for mechanical fastening. These protrusions were replaced by smaller parts, making one flat bottom plate, producing a hinge with a flat surface suitable for welding. The volume of the original design was 13.75 [cm<sup>3</sup>], the absence of the 4 protrusions (with a radius of 0.4 [cm] and a height of 0.4 [cm]) added a volume of:

$$4 \text{ [protrusions]} \cdot \pi [-] \cdot 0.4^2 \text{ [cm}^2\text{]} \cdot 0.4 \text{ [cm]} = 0.80 \text{ [cm}^3\text{]}$$

For the total of  $13.75 \text{ [cm}^3\text{]} + 0.80 \text{ [cm}^3\text{]} = 14.55 \text{ [cm}^3\text{]}$  a charge of  $14.55 \text{ [cm}^3\text{]} \cdot 1.6 \text{ [g/cm}^3\text{]} = 23.3 \text{ [g]}$  per hinge was used. After applying release agent (Frekote 770-NC) to the mould, the charge was distributed evenly throughout the mould. Subsequently the mould is placed in the press. The press applies pressure to the bottom plate, the left-side and right side dies can be moved inwards by tightening bolts on either side. Again starting with a low pressure the mould was heated up to an average temperature of 360 [°C] (measured manually with 1 temperature sensor) over a period of roughly 30 minutes (11 [°C/min]). At 360 [°C] the pressure was raised to 14 [MPa], and cooling (using air compressors) was initiated. After the temperature dropped to 340 [°C] (just below the  $T_m$  of the matrix material) the pressure was increased to 55 [MPa] and kept constant during cooling. Around 120 [°C] the process was stopped and the hinge was removed from the mould. The newly manufactured hinge, without the holes in the bottom plate, can be seen in Figure 2-2.



Figure 2-2 | Newly produced hinge, without holes in the bottom plate, using Toho Tenax CF/PEEK chopped fibre material

### 2.1.2 Ten Cate continuous carbon fibre weave PEEK composite

Next to the Toho Tenax weave material, two plates of 6 layer Ten Cate CF/PEEK continuous fibre  $[[0^\circ/90^\circ]_3]_s$  5HS (Harness Satin) weave material with an average thickness of 1.82 [mm] were already available, produced in the Delft Aerospace Structures and Materials Laboratory (DASML). The Ten Cate material was cut into lap shear sized samples (Figure 2-1) using the same company and method as for the Toho Tenax material (Van Nobelen Delft BV). Due to an error at the water jet cutting company however, one of the plates was cut in the wrong main apparent orientation of the fibres, namely in the  $90^\circ$  direction.

One extra laminate of Ten Cate CF/PEEK continuous fibre  $[[0^\circ/90^\circ]_4]_s$  weave was produced with an average total thickness of 2.44 [mm] (used as baseplate material to weld the hinges on) using the heated flat plate press in the DASML. 8 layers of Ten Cate CF/PEEK prepreg continuous fibre weave material ( $580 \cdot 580$  [mm]) were cut using the automatic sheet cutting machine, seen in Figure 2-3, A. These were stacked ( $[[0^\circ/90^\circ]_4]_s$ ) and attached to each other using plunge welds with the ultrasonic hand welder seen in Figure 2-3, B, for handling. After the plunge welds aluminium tape was applied around the edges to prevent the leakage of any molten matrix material onto the heated flat plate press. Subsequently the laminate was placed in the heated flat plate press (JoosPress, Figure 2-4) between two aluminium plates (cleaned using cloth and PF-QD quick drying cleaning solvent, and treated with 3 layers of 227CEE Marbocote release agent also applied using cloth), after which heat and pressure were applied to consolidate the laminate.



Figure 2-3 | DASML – A) Automatic sheet cutting machine, B) Ultrasonic hand plunge welder



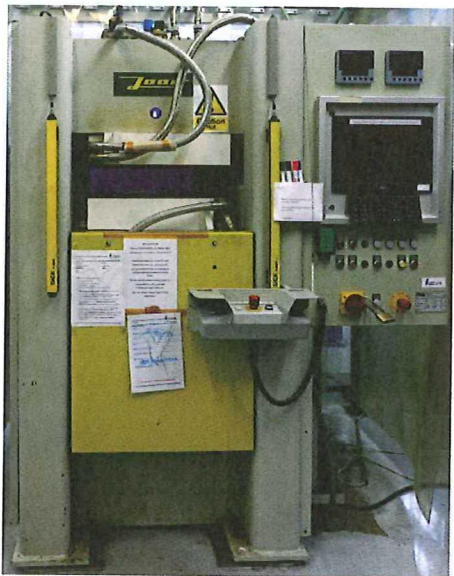


Figure 2-4 | DASML – Heated flat plate press (JoosPress) 1000 [kN], 450 [°C], 600 x 600 [mm]

The heat and pressure cycle used for the laminate production can be seen in Figure 2-5. This plate was cut using the shear cutting machine in the DASML. The edge delamination resulting from this process was deemed not to pose a problem since the welds on this plate were applied some distance from the edge.

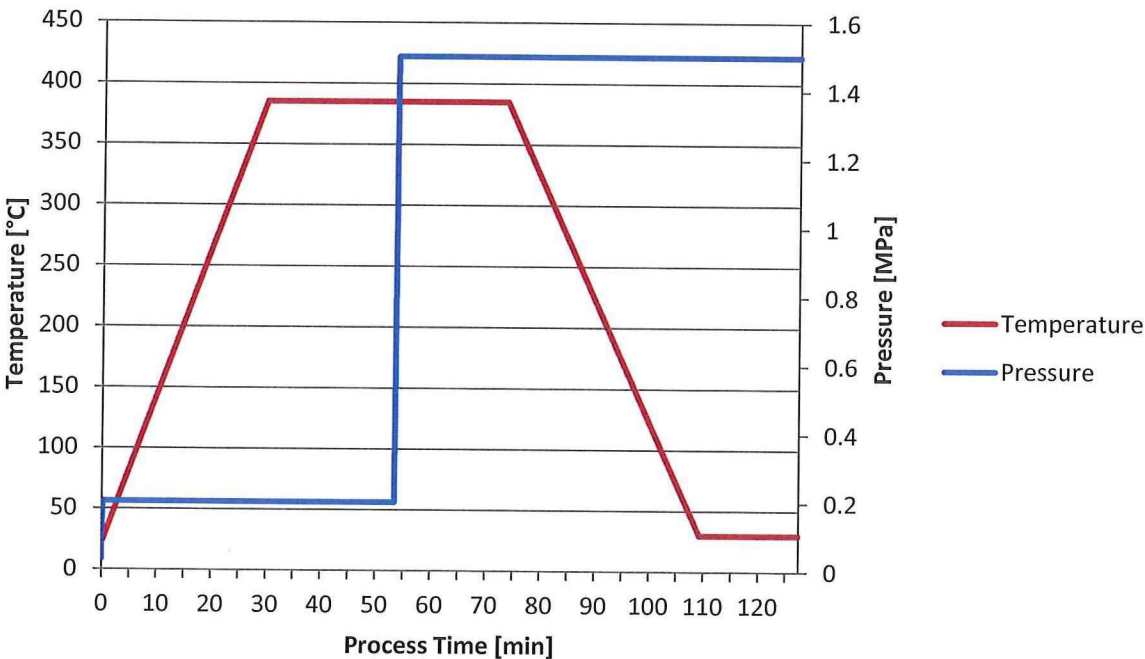


Figure 2-5 | Temperature and pressure curves from the JoosPress for the manufacturing of a 8 layer prepreg weave CF/PEEK Ten Cate laminate

### 2.1.3 Energy directors

In this research flat PEEK film EDs are used, produced using either Toho Tenax Vestakeep® PEEK film or Ten Cate Victrex® PEEK film. The films were cut in sheets of roughly  $140 \cdot 480$  [mm] (due to the sizing of the film on the roll) using the film cutter available in the DASML. These were stacked and attached to each other with plunge welds for handling using the ultrasonic hand welder. For the Toho Tenax material 2 layers were used (average thickness 0.12 [mm] per layer) and for the Ten Cate material 5 layers (average thickness 0.05 [mm] per layer). These stacked layers were placed in the hot plate press and heated up close to  $T_m$ , after which pressure was increased to make the layers stick together. The heat and pressure cycle used for this process can be seen in Figure 2-6. The stacked films were cut in the desired ED sizing needed for welding using the film cutter. This process was repeated several times to manufacture a sufficient amount of EDs.

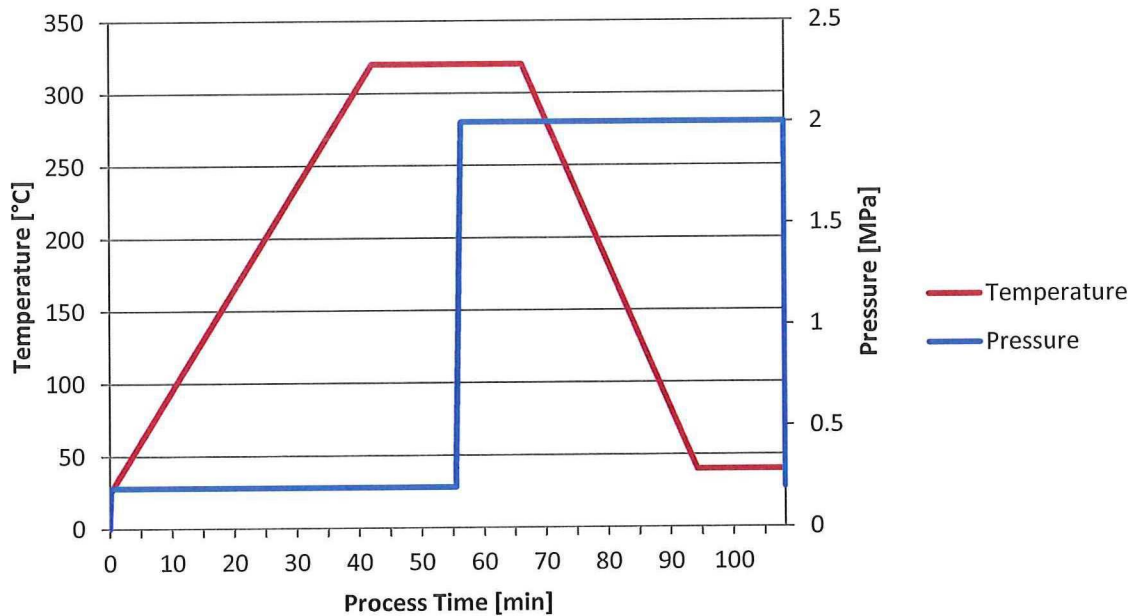


Figure 2-6 | Temperature and pressure curves from the JoosPress for the manufacturing of energy directors of Toho Tenax Vestakeep® PEEK film / Ten Cate Victrex® PEEK film

Alternatively, layers of neat resin were directly attached to some of the flat laminates manufactured with chopped material and to tow hinges as well, since this might prove valuable for later steps in the up-scaling of the USW process. Therefore several samples (chopped plates and hinges) were manufactured with one extra layer of PEEK polymer using the film stacking process, producing parts with ED already attached to the material. Using the press and moulds available at FHNW the film stacking cycle used for the hot plate press in the DASML was modified to stack the film to a plate of chopped fibre material. The film and the attachment to the plate are shown in Figure 2-7.



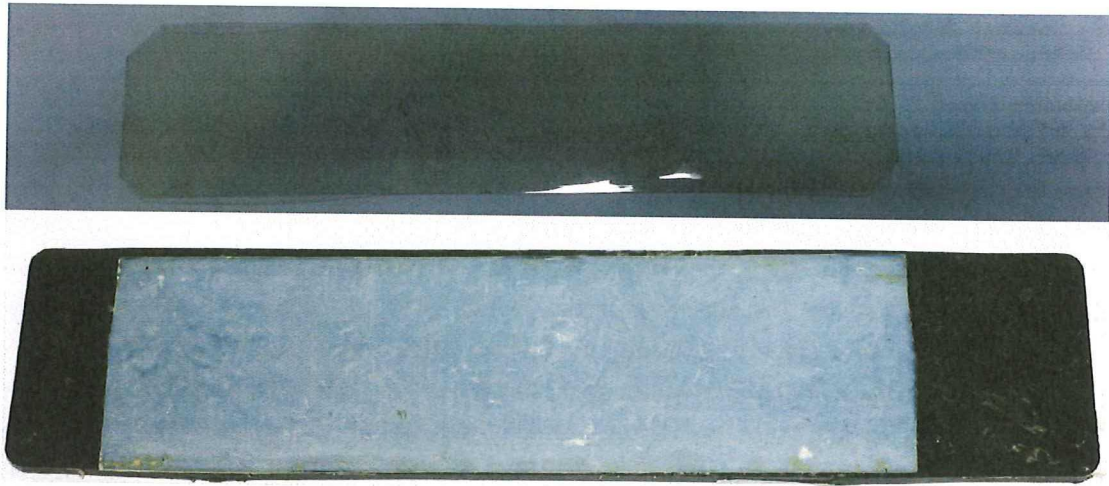


Figure 2-7 | PEEK film and the attachment to a chopped fibre composite plate using the film stacking process (temperature just below  $T_m$  and 0.9[MPa] pressure)



Figure 2-8 | Chopped fibre hinge with extra layer PEEK attached using the same film stacking process

The process cycle for the plates and hinge shown in Figure 2-7 and Figure 2-8, consists of heating up to 335 [°C], increasing the pressure to 0.9 [MPa], keeping these settings for 35 [min] and finally cooling down to 120 [°C] where the part could be removed. To apply pressure to the plates, the original mould at FHNW was used. For the hinges, however, two aluminium blocks were placed on either side of the flange on the bottom plate of the hinge, transferring the pressure and temperature of the press to the bottom plate. The slight variation with the regular film stacking cycle is due to the different press used at FHNW, the different materials used and the moulds used (higher pressure deforms the chopped fibre products). Although the layer seems to be properly attached, the adhesion is not strong enough for reprocessing using water jet cutting, which tears off the layer. Application of a layer on a finished product (the hinge) proved possible, but showed problems around the edges and at the flange due to uneven heating, shown in Figure 2-8.

## 2.2 Ultrasonic welding

### 2.2.1 Ultrasonic welding machine – Rinco Dynamic 3000 and ACU

For the USW process (described in section 1.2.2) the Rinco Dynamic 3000 from AESON equipped with the Advanced Control Unit (ACU), available in the DASML, was used (see Figure 2-9). The ACU is coupled to a computer with the software AcuCapture, which shows all the weld parameters, allows to store all the data for each weld and show graphs of the force, power and displacement curves, providing valuable feedback during the entire process.



Figure 2-9 | Rinco Dynamic 3000 ultrasonic welder equipped with an Advanced Control Unit

### 2.2.2 Machine settings

The ACU allows for several ‘Weld Modes’ (not to confuse with the welding parameters) allowing to change the controlling parameters of the process. The two modes used in this research are the TRAVEL MODE and the ENERGY MODE. In the TRAVEL MODE, the controlling parameter is the displacement (in [mm]) of the sonotrode. During welding, the ED melts and collapses under the applied force. This displacement is named travel, if the selected travel is reached the vibration part of the USW process ends and the process continues to the solidification stage. In the solidification stage, no vibrations but only pressure is applied by the sonotrode, for a certain amount of time (several seconds) to let the molten polymer in the overlap solidify. The travel option of the machine can be easily used to determine ideal welding conditions and produce consistent welding results as explained in section 1.2.2.

In the ENERGY MODE the controlling parameter is the total welding energy (in [Ws]). During welding the machine dissipates power. The amount of power (as a percentage of the total capacity of the machine) is dissipated is logged by the ACU. The welding energy is measured by integrating the area under the power curve as shown in Figure 2-10.



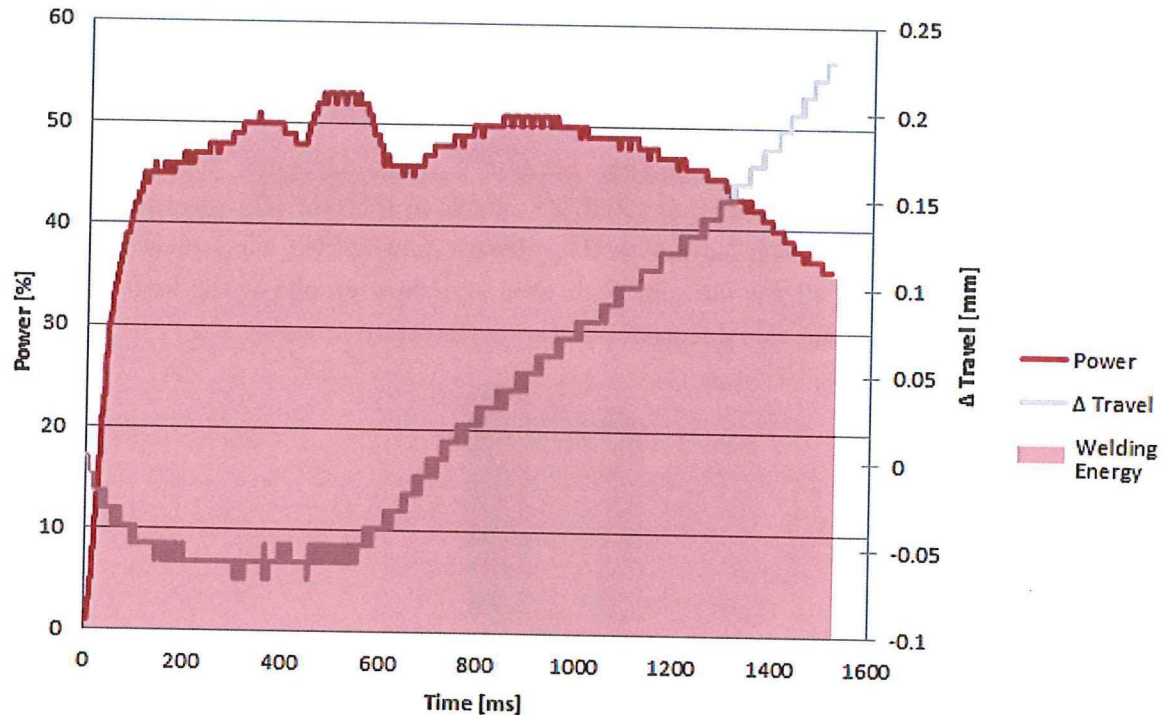


Figure 2-10 | A typical power and travel curve for the USW process, showing the welding energy as the highlighted area under the power curve

### 2.2.3 Samples and ED attachment

This research focusses on a variety of welding samples and welding strategies. For the alignment and clamping of the different samples to be welded different jigs were used, described in more detail in section 2.3. Prior to welding possible imperfections and protruding fibres (mainly at the edges, as a result from the cutting process) are removed from all samples sanding them using Scotch-Brite, after which the samples and the ED are wiped clean using cloth and PF-QD quick drying cleaning solvent.

### 2.2.4 Sonotrodes

In this research three different sonotrodes were used, a Ø 40 [mm] diameter cylindrical one, a Ø 10 [mm] cylindrical one and a 30 [mm] · 14.9 [mm] rectangular one (Figure 2-11). Due to the different size and shape of the sonotrodes their gain (or amplification factor) is different as shown in Figure 2-11. As explained in section 1.2.2, this means that with the same settings in the ACU, a sonotrode with a higher gain will generate a larger amplitude. The amplitude can be calculated with Equation 2-1, wherein a machine setting of 1 equals 60 [%] and a setting of 9 – 100 [%]

$$\text{Amplitude } [\mu\text{m}] = \frac{\text{Converter Amplitude } [\mu\text{m}] \cdot \text{Booster Gain } [-]}{\text{Sonotrode Gain } [-] \cdot \text{Machine Setting } [1-9 / 60\% - 100\%]} \quad \text{Equation 2-1}$$




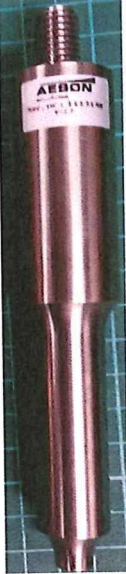

|   |   |   |
|---|---|---|
|  |  |  |
| Cylindrical (Ø40 [mm])  | Cylindrical (Ø10 [mm])  | Rectangular (14.9 · 30.0 [mm])  |
| Surface Area1,257 [mm²]   | Surface Area78.54 [mm²]   | Surface Area447.0 [mm²]   |
| Gain1.96 [-]  | Gain2.3 [-]   | Gain2.75 [-]  |
| Maximum Peak-to-peak Amplitude86.2 [µm]   | Maximum Peak-to-peak Amplitude101.2 [µm]  | Maximum Peak-to-peak Amplitude120.9 [µm]  |

Figure 2-11 | Three different sonotrodes used in this research and their specifications, note that the maximum peak-to-peak amplitude shown, is valid for the combination with the AESON Dynamic 3000 and the 1:2 booster

Changing the cylindrical sonotrodes is quite straight forward (unscrewing the first, screw in the second), since the orientation is not important. For the rectangular sonotrode used in this research, alignment is of importance. The long side is aligned with the baseplate using alignment blocks and a try square. For this the entire welding train (converter, booster, sonotrode) is loosened through the bolt displayed in Figure 2-12 (after the sonotrode has been properly fastened), so it can be aligned correctly.



Figure 2-12 | Front view USW machine, highlighted bolt is used to loosen the complete welding train

### 2.3 Welding jig configurations

On the baseplate of the AESON Dynamic 3000 two bolt holes and two T-slots are available for the attachment of a welding jig (see Figure 2-13). This welding jig is needed to ensure no movement of the samples during welding through clamping and consistent alignment for every repeating weld. In this research three different jigs were used, jig 9109, jig 9110 (two already existing jigs) and a newly developed jig (discussed in section 6.2) for up-scaling. Jig 9109 and 9110 are attached to the USW machine using the two bolt holes, whereas the newly designed jig uses the two T-slots for attachment.

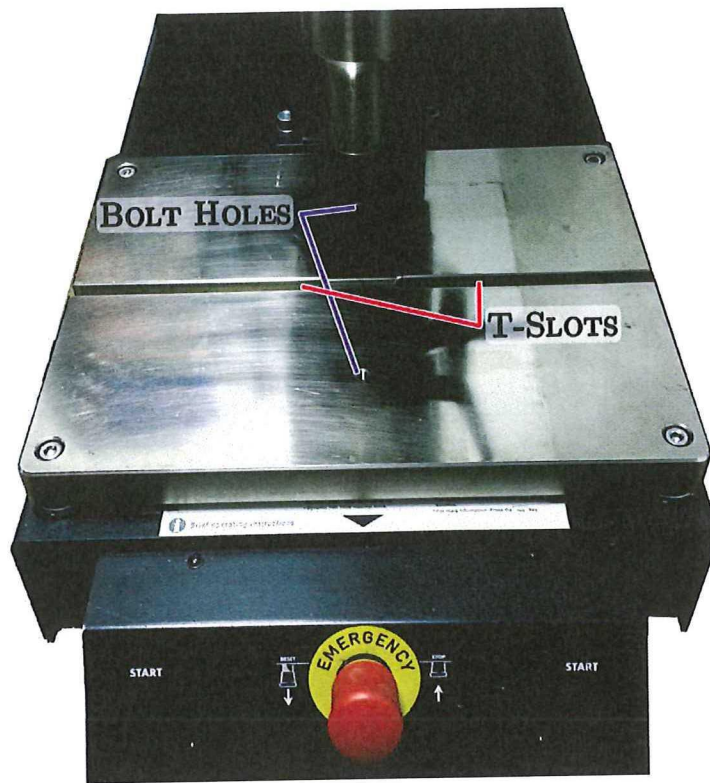


Figure 2-13 | Baseplate of the USW-machine showing the bolt holes and T-slots

### 2.3.1 9109 jig

The 9109 jig was the oldest jig used in this research and was designed and built at the faculty of Aerospace Engineering Delft University of Technology (DUT). This jig was designed to specifically weld a standard ASTM D1002 lap shear sample (Figure 2-1) in the configuration shown in Figure 2-13.

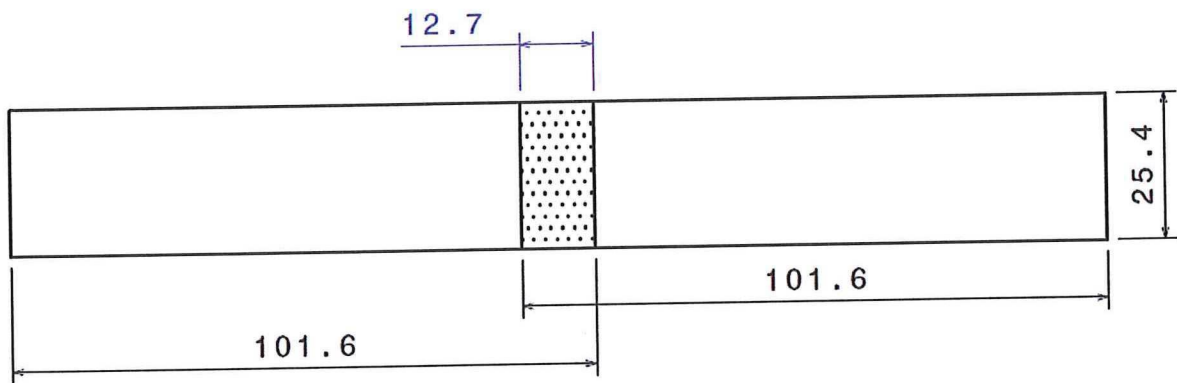
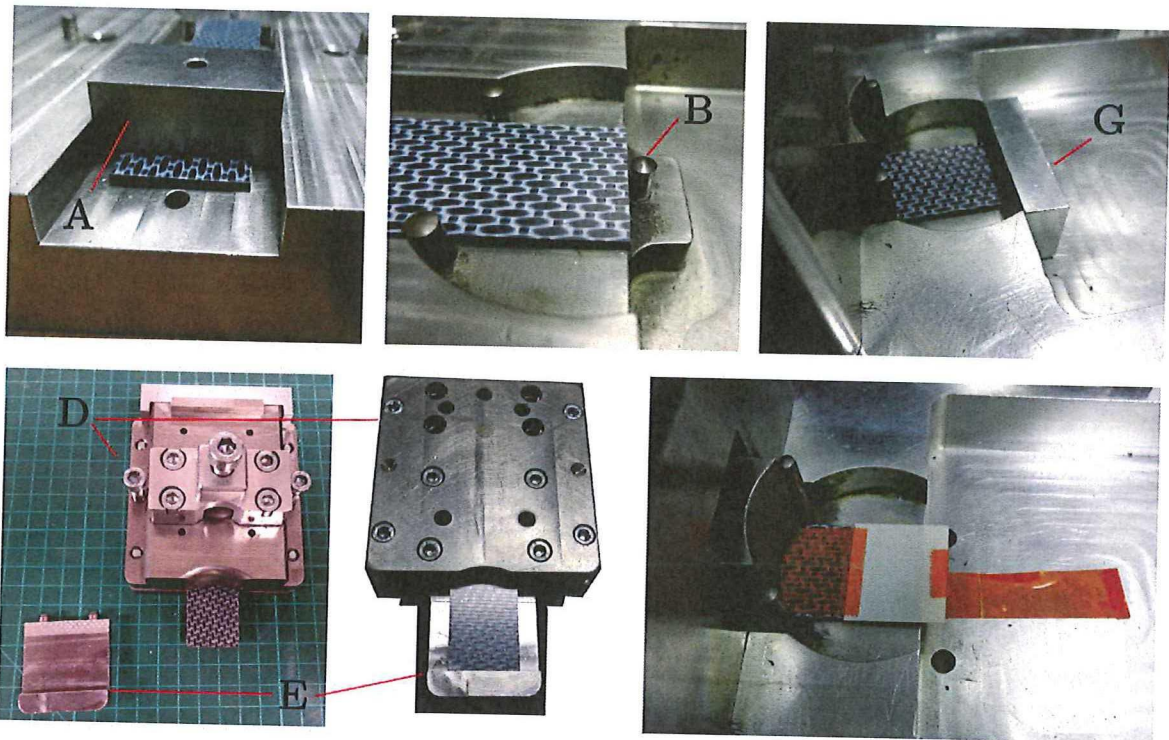


Figure 2-14 | Dimensions in [mm] following the ASTM D1002 standard for a lap shear sample showing the sample size and the  $\frac{1}{2}$  inch overlap

Figure 2-15 shows all parts of this clamping tool (and for the 9110 jig variation). First the bottom sample is aligned on the bottom plate of the jig using alignment block A and pin B, after which it is clamped by tightening bolt C. The ED is taped to the bottom sample and to the jig as can be seen in Figure 2-15. The top sample is clamped in block D by tightening the bolt and aligned with alignment block E ensuring the 12.7 [mm] overlap. This entire block is then attached



to the frame F. The frame is guided by four poles as can be seen in Figure 2-15 and is supported by four springs. This entire setup allows for perfect alignment, good clamping and only vertical movement of the parts (no sideways movement or bending) during every weld.



- A - ALIGNMENT BLOCK  
9109 JIG (BOTTOM SAMPLE)
- B - ALIGNMENT PIN  
(BOTTOM SAMPLE)
- C - CLAMPING BOLT  
(TOP SAMPLE)
- D - CLAMPING BLOCK  
(TOP SAMPLE)
- E - ALIGNMENT BLOCK  
(TOP SAMPLE)
- F - SLIDING FRAME  
(TOP SAMPLE)
- G - ALIGNMENT BLOCK  
9110 JIG (BOTTOM SAMPLE)

Figure 2-15 | Detailed overview of the 9109 and 9110 jig variations

### 2.3.2 9110 jig

The 9110 jig, also designed and built at the faculty of Aerospace Engineering DUT, is a modification of the 9109 jig allowing for a larger overlap of the samples to be joined. It uses the same parts to a large extent as the 9109 jig, except for the bottom plate and different alignment aids. The different bottom plates are shown in Figure 2-16. Even though the main difference between the jigs is the material used for the base plate, steel for the 9109 jig and aluminium for the 9110 jig, there are also some small geometrical differences. The 9110 bottom plate has the same main dimensions as the 9109 (both  $210 \cdot 210$  mm), but the milled away square area on the right is slightly smaller for the 9110 jig, as can be seen in Figure 2-16. The thickness of the bottom plate is the same for the part where the bottom sample for welding is placed (15 [mm]), the milled away square on the right, however, is deeper leaving less material (only 4 [mm] for the 9110 jig compared to the 8 [mm] for the 9109).

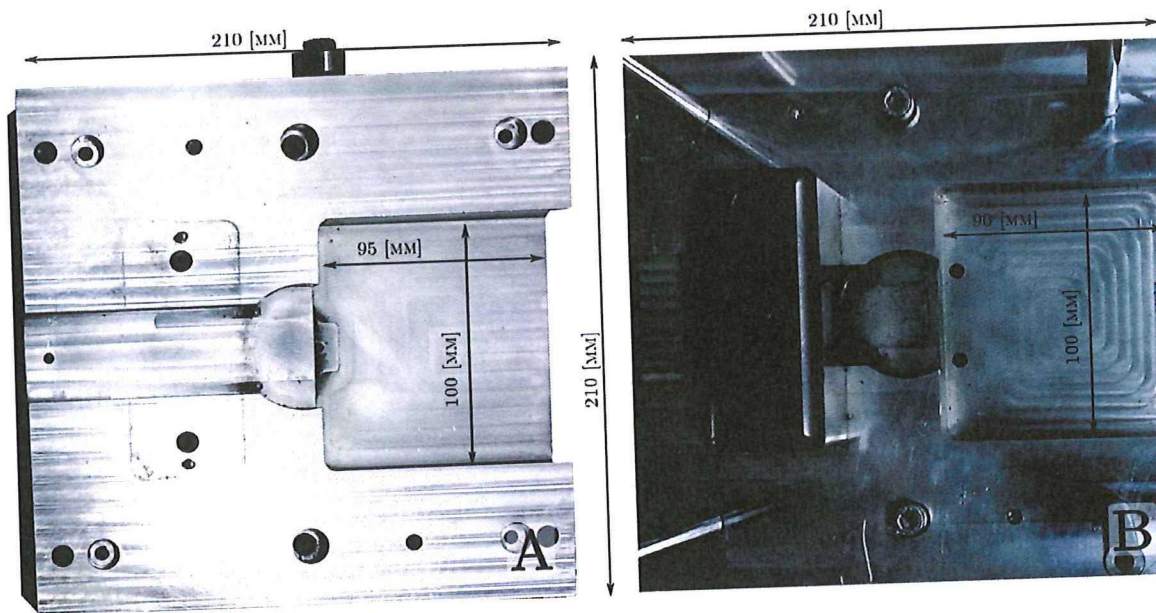


Figure 2-16 | Two different bottom plates for the: A) 9109 jig (steel bottom plate), B) 9110 (aluminium bottom plate), showing the clamping block of the bottom sample and the 4 poles on 9110 which are interchangeable with jig 9109

For the 9110 jig, the same guiding poles and frame for the top sample are used. The alignment of the bottom sample is different due to the new alignment block G depicted in Figure 2-17 (compared to pin B shown for the 9109 jig). For the top sample the same alignment block E can be used with an extension to reach an overlap with a maximum of 25.4 [mm] (1 inch). In the research several alignment aids on the bottom plate and for alignment block E are used to achieve variations in overlap between 12.7 [mm] and 25.4 [mm].



## 2.4 Universal testing machine – Zwick 250kN

The static single lap shear tests in this research were performed with the Zwick 250kN universal testing machine shown in Figure 2-17.



Figure 2-17 | Zwick 250 kN universal testing machine used for static lap shear strength determination

All static tests were carried out following the ASTM D1002 standard to provide lap shear strength (LSS) data for all welded samples. However, due to variations in overlap in the experiments, there is deviated from the ASTM D1002 standard overlap of 12.7 [mm] (up to 25.4 [mm]). For all variations in overlap, the cross head control rate was kept at the ASTM D1002 specified value of 1.3 [mm/min] and a clamping distance of 60 [mm]. The parts were clamped using hydraulic grips on the Zwick, which can be configured to have an offset compared to each other. With this offset proper alignment was achieved such that the centre line of the top and lower grips, and therefore the load direction (minimizing bending), passed through the weld line, shown in Figure 2-18.



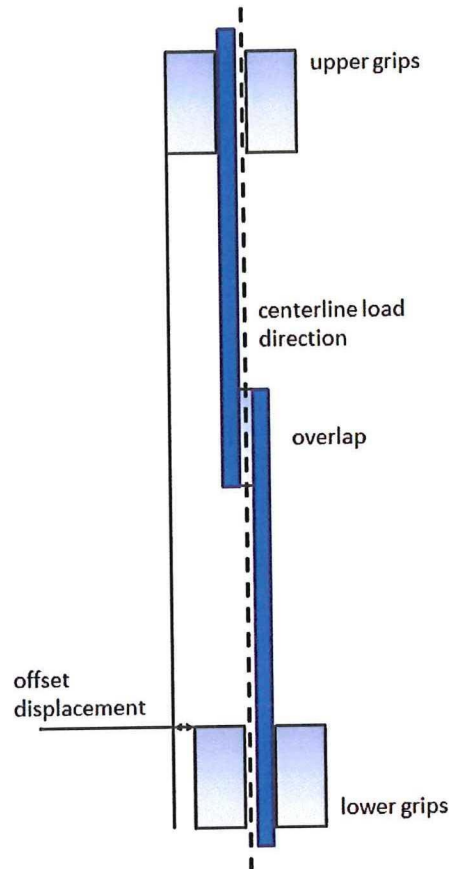


Figure 2-18 | Schematic view of the offset displacement between the top and lower grip of the Zwick 250 kN universal testing machine, allowing to align the load direction with the centre weld line to minimize bending during static the lap shear strength test

The variations of the standard 12.7 [mm] overlap up-to 25.4 [mm] in this experiment should be kept in mind. The effect of the larger overlap for the same testing conditions results in lower average shear strength for adhesive bonded joints. Also the variation in thickness between the samples (chopped fibre vs continuous weave) influences the eccentricity and the stress levels [32]. This is important to consider while comparing the results.

## 2.5 Optical microscopy and C-scan equipment and procedures

Next to evaluating the mechanical properties of the welded samples through single lap shear testing, the samples were also analysed through visual inspection of the fracture surfaces and optical microscopy of the cross sections and fracture surfaces. Furthermore, C-scans were made of the welded hinges and the laminates used, to obtain information about the weld and material quality. The optical microscopy and C-scan equipment and procedures are discussed here in more detail.

### **Optical microscopy**

The optical microscopes used were the (mostly used) Zeiss Discovery.V8 SteREO, equipped with a Zeiss AxioCam ERc5s digital camera and using an external (cold) light source available in the DASML, shown in Figure 2-19, and the Leica 2130 DMLM Optical Microscope with a Zeiss

AxioCam ICc3. The setups were connected to a computer with the AxioVision Rel. 4.6 software which allowed for easy capturing of the images viewed by the microscope.

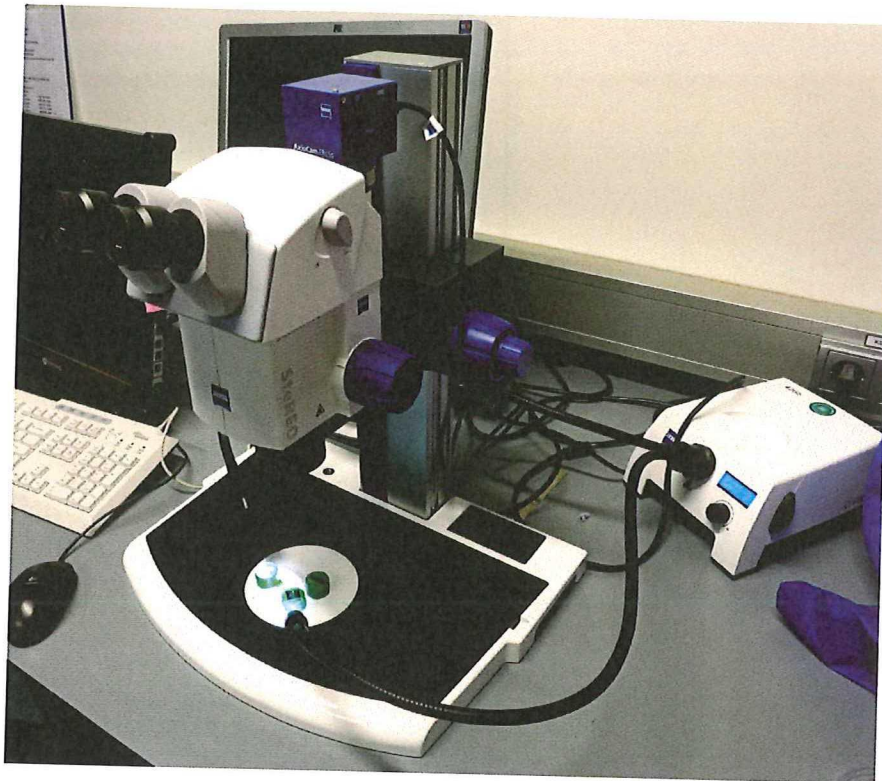


Figure 2-19 | Zeiss Discovery.V8 SteREO optical microscope, equipped with an Zeiss AxioCam ERc5s digital camera and external (cold) light source available at the DASML

To get a cross section of the joint, a water cooled diamond saw (M1D20 blade used in the Struers Secotom-10) was used to cut the sample at the desired location. The small retrieved part was embedded in Technovit 4071 fast curing two component resin. After curing, the embedded surface of the sample was sanded in several steps (roughness 75 [ $\mu\text{m}$ ] to 10 [ $\mu\text{m}$ ]) using the Struers Rotopolz & Pedemat and cleaned in an ultrasonic bath (Bandelin Sonorex) filled with acetone. After which the surface was polished with the same setup in several steps (roughness 6 [ $\mu\text{m}$ ] to 1 [ $\mu\text{m}$ ]) and cleaned again to get a smooth surface finish for microscopic analysis. A few samples were analysed without being embedded in the Technovit 4071 resin. This was either done for the fracture surfaces, or to get a different perspective of the cross section.

### **C-scan**

The C-scan equipment (Midas water jet, 10 [Mhz], 130 [dB]) available in the DASML was used for non-destructive testing of the materials used and for analysis of the weld quality of the welded hinges. The equipment is shown in Figure 2-20. The technique used sends ultrasound pulses through water and measures the attenuation through the material. Several factors, like voids and delaminations, influence this attenuation. The collected data can be plotted using the Automated Laminate Inspection Software (Alis), so these defects can be visualized.



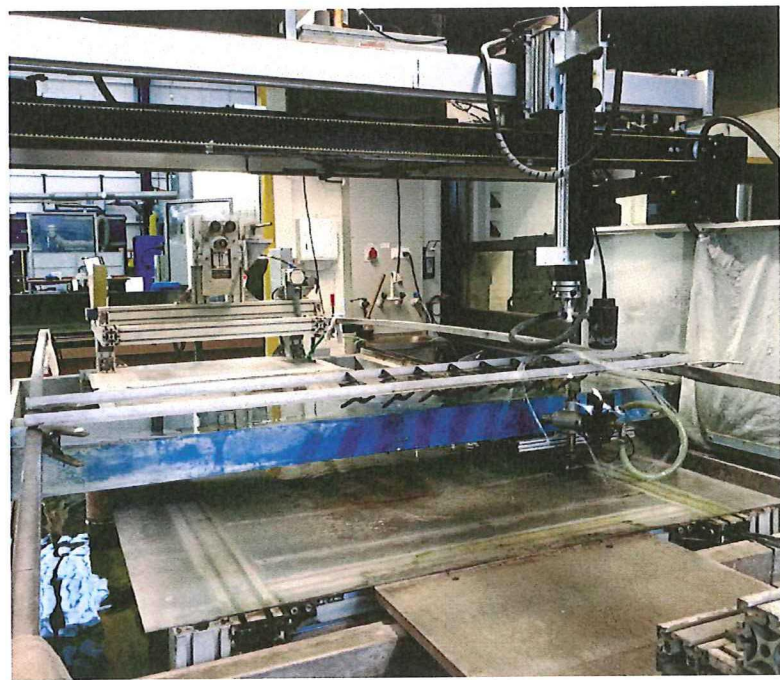


Figure 2-20 | C-scan equipment available in the DASML used for non-destructive testing of the used composite materials and analysis of the hinge weld quality

2.6 Experiment description

This section describes experiments conducted in this research. Considering the research goals mentioned in section 1.3 and the USW process, there are many different aspects which can be changed and investigated. It is important to note however that many of the aspects are linked, influencing each other as mentioned in section 1.2.2. To obtain an overview of the experimental approach, the roadmap in Figure 2-21 was created. The approach described here focusses on the Clean Sky case, where for other applications other factors might have more importance.

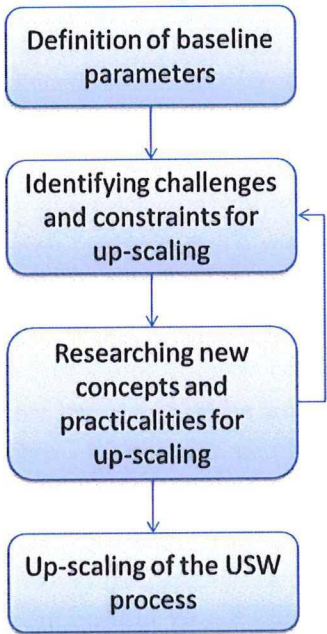


Figure 2-21 | Schematic roadmap of experimental approach towards up-scaling of the USW process



Most of the tests were repeated five times to get statistical valid data per set of conditions. However, for some preliminary experiments this was not done, due to the limited amount of samples available. For all sample sets a selection is made to test sets for LSS, visual analysis of the welding surfaces and optical microscopic analysis of the joints..

### **2.6.1 Standard welding process for baseline creation and parameter determination**

To establish control and baseline parameters, standard welds were produced for Toho Tenax continuous weave CF/PEEK and Toho Tenax CF/PEEK chopped material, in the combinations weave – weave, chopped – chopped and weave – chopped. This was done following the well-established method of welding samples using the travel as controlling parameter, as explained in section 1.2.2. From these tests controlling parameters and reference data for the other experiments in this research can be determined, keeping the limitations of the USW machine in mind. Also the challenges and practicalities of the machine and the USW can be studied during these baseline experiments.

The parameters that can be varied in the ACU for the travel controlled welding process are:

- Rise of force [N/s]
- Welding force (Trigger) [N]
- Rise of force during melting [N/s]
- Amplitude setting [-]
- Welding on [mm] (travel controlled parameter)
- Solidification force [N]
- Solidification holding time [ms]

Varying all these parameters to determine control parameters would require the welding of many samples. As explained in section 1.2.2, some parameters have more influence than others during different stages of the welding process. The importance of the rise of force is deemed insignificant and is simply set at half the welding force, if the welding force is larger than 300 [N], or equal to 300 [N/s] for a welding force of 300 [N]. For the welding force itself, it was decided for the baseline experiments to compare a low welding force of 300 [N] and high welding force of 1000 [N]. The effect of the rise of force during melting has been kept out of the scope of this research and is set at zero, keeping the welding force constant during welding. A high peak-to-peak amplitude setting of 86.2 [ $\mu\text{m}$ ] (setting 9 for the  $\varnothing$  40 [mm] cylindrical sonotrode) was selected as fixed value and researching an optimum value has been kept out of the scope of this research. The high value is selected due to the high  $T_m$  of PEEK, the amplitude has a high influence in the average viscoelastic heating ( $\epsilon_0$ , the amplitude of strain, has a quadratic influence on  $Q_{\text{avg}}$ , see section 1.2.2). The ideal travel (for both welding forces and the different material combinations) is determined from the welding graph for a 100 [%] travel weld (which means a melting on travel setting equal to the thickness of the ED), as explained in section 1.2.2. Finally, since they pose no limitations on the final goal of this research, the solidification force and solidification holding time are kept constant at 1000 [N] and 4000 [ms] respectively. It could be that a lower force and / or shorter holding time would suffice as well, but since the setting of 1000 [N] for 4000 [ms] is known to work from literature and does not impose any limitations on other parameters it is decided to leave them fixed.

The output of AcuCapture from the welds produced using travel as the controlling parameter (while varying other welding parameters) are compared, as well as their LSS results. This data is exported to Excel for further analysis. The coefficient of variation ( $c_v$ ) of these results, plus the visual and optical microscopy analysis of the joints are used as reference for the results of the newly proposed experiments. The  $c_v$  is calculated using Equation 2-2.

$$c_v = \frac{\sigma}{\mu} \cdot 100 [\%] \quad \text{Equation 2-2}$$

In which  $\sigma$  is the standard deviation and  $\mu$  is the mean of the values considered.

### ***2.6.2 Investigating new concepts for up-scaling using spot welding***

Since up-scaling USW of TPC for practical applications using sequential welding has not yet been researched, investigating new concepts gives rise to new challenges. The results of the baseline experiments are evaluated and are used to design experiments to research new concepts. This is done keeping the restrictions for sample dimensions and overlap of the current welding (and testing) setup in mind. For the new concepts probably the setup needs to be changed which will have influence on the results. The welding parameters determined by the baseline experiments are used for these new concepts as well if possible, to minimize their influence on the results. The results from these new concepts (welding curves, LSS, fracture surfaces,  $c_v$ ) are analysed and compared to the baseline to determine if it would be a feasible concept for up-scaling. The goal is to establish a spot welding strategy which has LSS and  $c_v$  values compared to the baseline.

To establish a possible spot welding strategy for up-scaling, some practical constraints may apply as well. In analysing the new concepts for the design of a welding setup for up-scaling, practicalities considering the sonotrode selection and the use and size of EDs are regarded. This is done for the Clean Sky specific case, meaning that the geometry and material properties of the hinge are used as constraining factors.

The results of the tested new welding concepts are used for the design of a new clamping design and welding strategy to weld the Clean Sky ITD hinges to a TPC plate. In the original ITD design the hinges are to be welded to CF/PEEK UD C-frames, but since neither C-frames nor CF/PEEK UD material was available it was decided to weld the hinges to continuous weave CF/PEEK plate material.





## II – Experiments, Results and Discussion



### 3 Baseline Results and Determined Welding Parameters

For the baseline experiments standard welds with travel as the controlling parameter are produced. For the test in this section Toho Tenax weave CF/PEEK and Toho Tenax chopped fibre CF/PEEK lap shear samples are used. For the ED, the 2 layer (average 0.23 [mm] thickness) Toho Tenax material was used.

A complete overview of the relevant USW parameters and LSS data of all the samples welded can be found in appendix B.

#### 3.1 Basic USW-machine control parameters

The materials used and the welding parameters (ACU settings) for the welds discussed in this section are summarized in Table 3-1.

Table 3-1 | Overview of the materials used (TT = Toho Tenax), sonotrodes used and input settings for the USW machine for the welding of the baseline samples for a standard 12.7 [mm] overlap using the 9109 jig and Toho Tenax 2 layer (0.23 [mm]) ED, comparing a 300 [N] and 1000 [N] welding force

|                  |           | I) Initial Phase    | II) Vibration Phase |                     |                                    |                       | III) Solidification Phase |                   |
|------------------|-----------|---------------------|---------------------|---------------------|------------------------------------|-----------------------|---------------------------|-------------------|
| Materials        | Sonotrode | Rise of Force [N/s] | Welding Force [N]   | Rise of Force [N/s] | Amplitude [ $\mu$ m] / setting [-] | Controlling Parameter | Force                     | Holding Time [ms] |
| TT weave – weave | Ø 40 [mm] | 300                 | 300                 | 0                   | 86.2 (9)                           | Travel                | 1000                      | 4000              |
| TT weave – weave | Ø 40 [mm] | 500                 | 1000                | 0                   | 86.2 (9)                           | Travel                | 1000                      | 4000              |

Two different settings are investigated for the determination of the welding force parameter. One with a low welding force of 300 [N], and one with a high welding force of 1000 [N]. First a 100 [%] travel (for the ED used, an average value of 0.23 [mm]) was carried out for both settings shown in Figure 3-1.



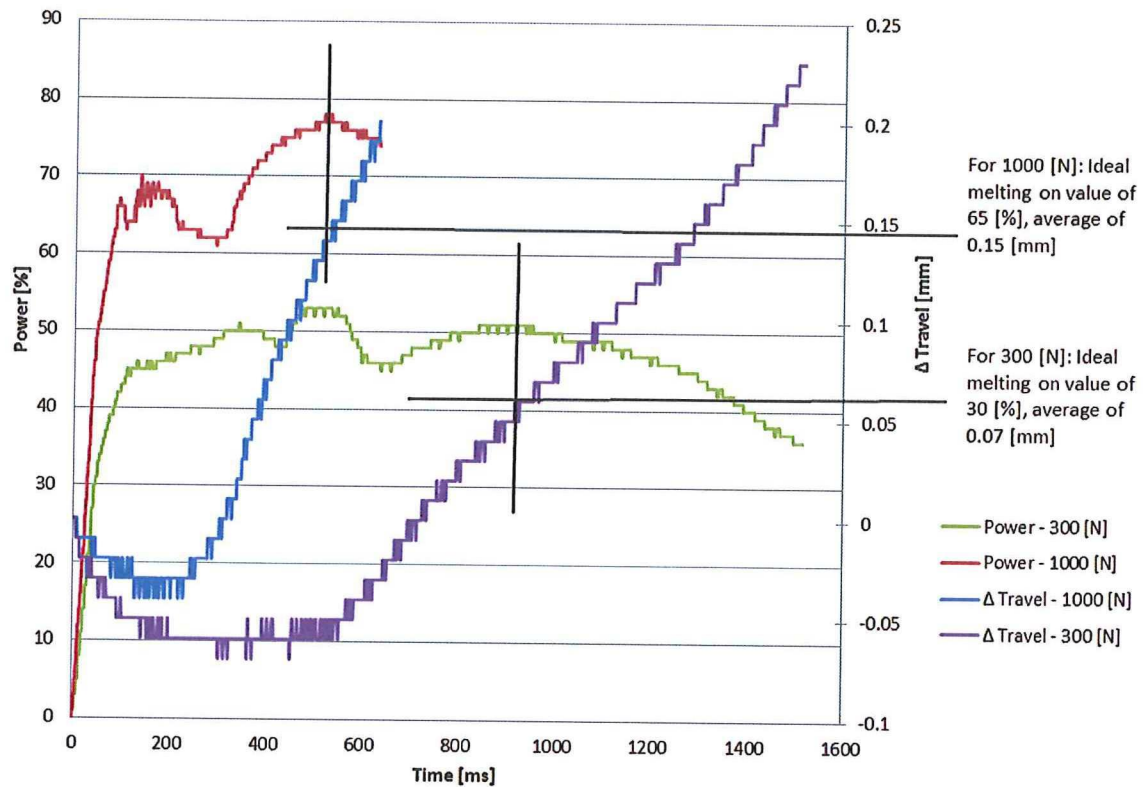


Figure 3-1 | Power and relative travel curves for a melting on setting of 100% travel, used for the determination of the ideal welding on setting for a 300 [N] and a 1000 [N] welding force, welding Toho Tenax CF/PEEK continuous weave standard size lap shear samples using 2 layer (0.23 [mm]) Toho Tenax ED (showing sample #01 and #10, appendix B)

The output of the ACU for these welds is shown in Figure 3-1. From Figure 3-1 the optimum travel setting for 300 [N] is determined to be 30 [%] (i.e. 0.07 [mm]) and for 1000 [N] 65 [%] (i.e. 0.15 [mm]). This difference in optimum travel is partly the result of the changed welding parameters, since for different parameters different heating rates exist. Next to that the determination of the optimum welding conditions does not use exact methods, so variation (even for similar samples welded with identical parameters) might exist. The difference in optimum travel distances, however, is not further investigated in this research. Using the optimum travel settings for both welding forces, five welds are produced; the welding graphs were consistent and can be found in appendix C. These samples are tested for static lap shear, which all follow the same stress strain curve (almost no deviations) as can be seen in appendix C. The resulting average values, and the range, of several parameters for the 300 [N] and 1000 [N] welded samples are plotted in Figure 3-2 and summarized in Table 3-2.

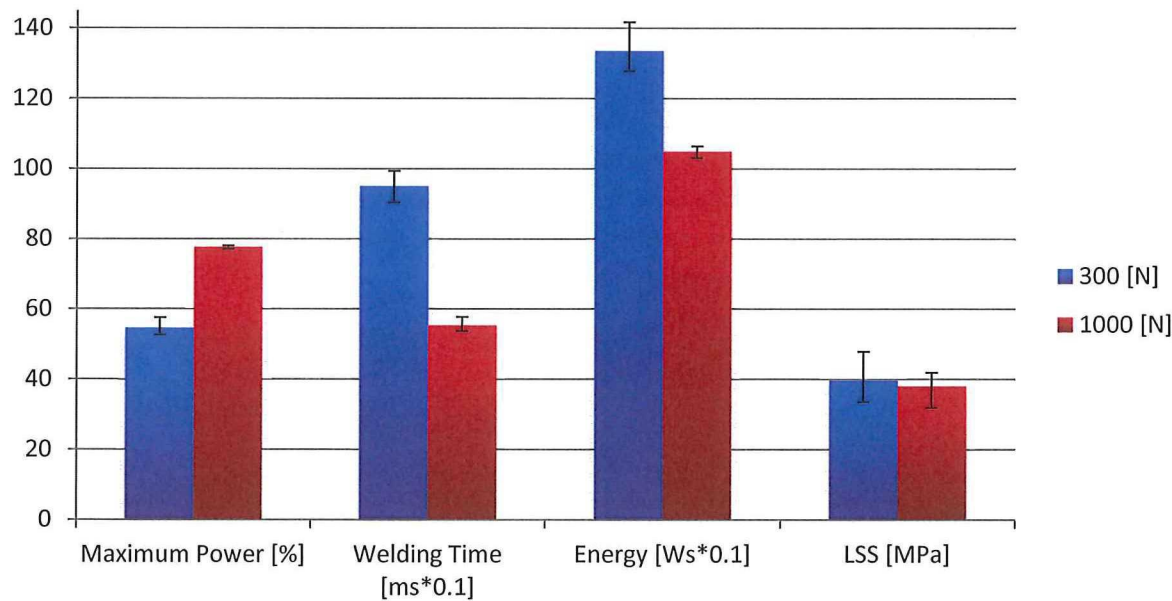


Figure 3-2 | Average values and range of values for the maximum power (maximum level reached during the weld as percentage of the total USW machine capacity), welding time, energy dissipated and LSS, for optimal welding conditions using 300 [N] and 1000 [N] welding force for a standard ASTM D1002 12.7 [mm] (Ø 40 [mm] sonotrode) overlap (samples #04-09, 300 [N], #11-15 1000 [N], appendix B)

Table 3-2 | Average values and their  $c_v$  for the maximum power (maximum level reached during the weld as percentage of the total USW machine capacity), welding time, energy dissipated and LSS, for optimal welding conditions using 300 [N] and 1000 [N] welding force for a standard ASTM D1002 12.7 [mm] (Ø 40 [mm] sonotrode) overlap (samples #04-09, 300 [N], #11-15 1000 [N], appendix B)

|                            | Maximum Power [%]<br>( $c_v$ [%]) | Welding Time [ms]<br>( $c_v$ [%]) | Energy [Ws]<br>( $c_v$ [%]) | LSS [MPa]<br>( $c_v$ [%]) |
|----------------------------|-----------------------------------|-----------------------------------|-----------------------------|---------------------------|
| 300 [N],<br>30 [%] travel  | 55 (6.42)                         | 950 (5.75)                        | 1335 (4.95)                 | 39.7 (4.71)               |
| 1000 [N],<br>65 [%] travel | 78 (2.16)                         | 553 (2.67)                        | 1049 (3.99)                 | 38.0 (4.80)               |

Looking at the values in Figure 3-2 and Table 3-2, it can be seen that the difference in LSS does not differ significantly for the two different welding forces. For 300 [N] the average LSS is slightly higher, and looking at  $c_v$ , also slightly more consistent. This means that changing the welding force does not significantly influence the LSS, so other parameters can be considered. It can be seen that the welding time and energy dissipated by the machine are significantly higher for the 300 [N] welding force (950 [ms] and 1335 [Ws] compared to 553 [ms] and 1049 [Ws] for 1000 [N]). These values are coupled of course, a longer welding time (although at a lower power level, looking at the power curves and the maximum power utilized) results in a higher value for the total dissipated energy. The maximum power utilized during the process, however, is significantly lower for the 300 [N] case, 55 [%] compared to 78 [%] for the 1000 [N] case. This is consistent with literature as described in section 1.2.2. Using the higher welding force could therefore reduce the energy and time consumed by the process. Since the amount of power available on the USW machine is limited, it was decided to use the lower welding force. The 300 [N] welding force



delivers the desired LSS, while leaving more power available to for welding experiments which require a higher maximum power usage.

Next to the welding and LSS data, the fracture surfaces and the cross section are analysed. Looking at the fracture surfaces in Figure 3-3 it can be seen that there are no big differences, and both EDs have been molten up to the first layer of the composite samples with limited fibre distortion. In Figure 3-4 it can be seen that the ED indeed is molten up to the first layer of the composite samples, showing a thin weld line.

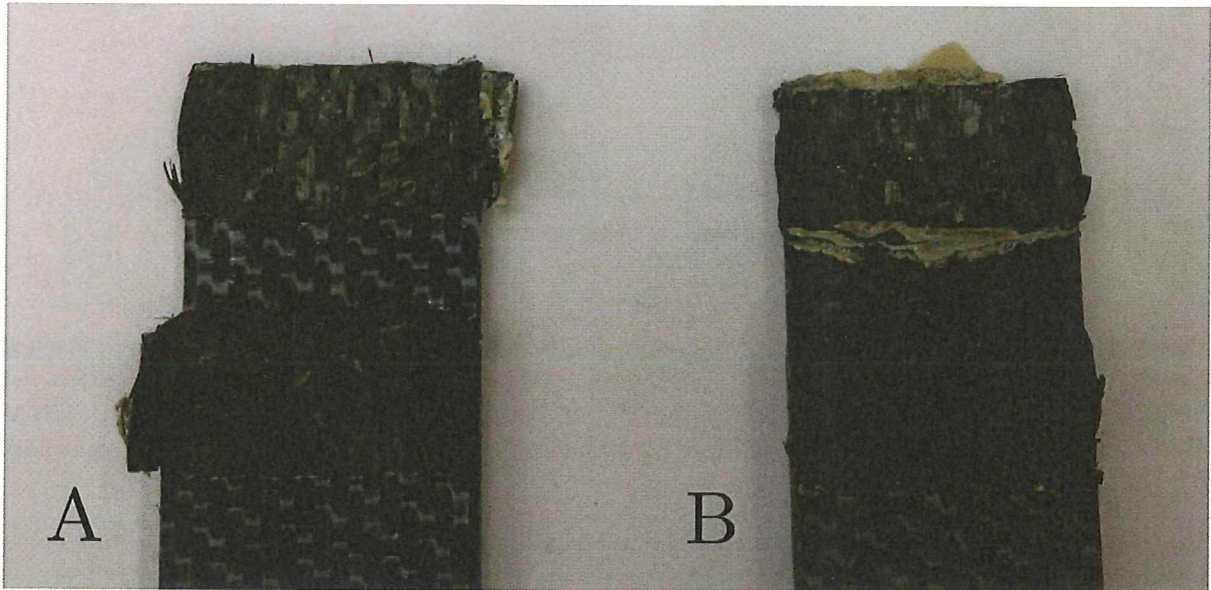


Figure 3-3 | Fracture surfaces of Toho Tenax material, 12.7 [mm] overlap, welded with the  $\varnothing$  40 [mm] cylindrical sonotrode and a welding force of A) 300 [N] (#4 appendix B), B) 1000 [N] (#12 appendix B) using optimum welding conditions



Figure 3-4 | Sample A (#09, appendix B) cross section of a Toho Tenax weave – weave weld using 300 [N] welding force, Sample B (#17, appendix B) cross section of a Toho Tenax weave – weave weld using 1000 [N] welding force, 1.25x magnified



3.2 Dissimilar materials

The welding parameters for welding chopped to chopped material discussed in this section are summarized in Table 3-3.

Table 3-3 | Overview of the materials used (TT = Toho Tenax), sonotrodes used and input settings for the USW machine for the welding of the baseline chopped fibre samples for a standard 12.7 [mm] overlap using the 9109 jig and 2 layer (0.23 [mm]) Toho Tenax EDs

|                     |           | I) Initial Phase    | II) Vibration Phase |                     |                              |                       | III) Solidification Phase |                   |
|---------------------|-----------|---------------------|---------------------|---------------------|------------------------------|-----------------------|---------------------------|-------------------|
| Materials           | Sonotrode | Rise of Force [N/s] | Welding Force [N]   | Rise of Force [N/s] | Amplitude [μm] / setting [-] | Controlling Parameter | Force                     | Holding Time [ms] |
| TT chop.<br>– chop. | Ø 40 [mm] | 300                 | 300                 | 0                   | 86.2 (9)                     | Travel                | 1000                      | 4000              |

As a first reference to materials welded in section 3.1, an experiment of welding chopped to chopped Toho Tenax CF/PEEK lap shear samples has been performed using the cylindrical sonotrode and the original setting of 300 [N] welding force. All the welding curves and LSS curves can be found in appendix D. Figure 3-5 shows the welding curves for two 100 [%] travel welds.

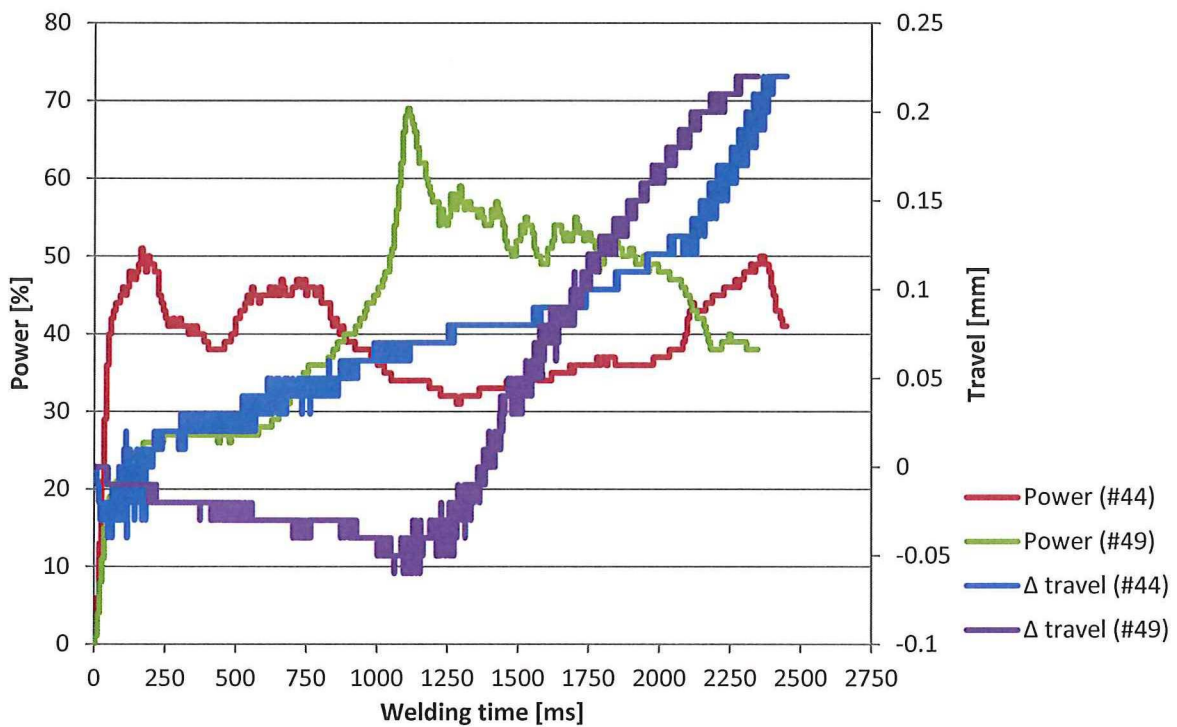


Figure 3-5 | Inconsistent welding curves for USW of chopped to chopped Toho Tenax CF/PEEK, for melting on 100 [%] travel using 300 [N] welding force , 12.7 [mm] overlap and the Ø 40 [mm] sonotrode (samples #45,#46, appendix B)

Using the power curves for welding chopped to chopped material to identify optimum welding conditions is not possible. The curves are inconsistent, showing much dissimilarity between the

two power curves and the two travel curves shown in Figure 3-5. The curves also do not resemble the regular curves, showing the different stages (as explained in section 1.2.2). Looking at the welding surfaces of the samples shown in Figure 3-6, it can be seen this is due to the fact that a random amount of energy goes to deconsolidation of the samples. Due to this random energy dissipation through deconsolidation it is not possible to weld the samples in this configuration using these welding parameters. It can be seen that the chopped fibre samples are unable to cope with the in plane loads at the edges, the lack of support at the edge combined with melting of the resin results in deconsolidation and damages the top sample.



Figure 3-6 | Melting on 100% travel chopped to chopped fibre welded sample, showing extensive deconsolidation mostly in the top sample, showing samples #45 and #46 (appendix B)

To prevent the deconsolidation at the edge of the chopped fibre samples, an experiment with the smaller Ø 10 [mm] cylindrical sonotrode was performed. The settings used are summarized in Table 3-4.

Table 3-4 | Overview of the material used (TT = Toho Tenax), sonotrode used and input settings for the USW machine for the experiment of the energy controlled welding using a small sonotrode in the 9110 jig with an 2 layer (0.23 [mm]) Toho Tenax ED of a chopped fibre sample

|                 |           | I) Initial Phase    | II) Vibration Phase |                     |                              |                       | III) Solidification Phase |                   |
|-----------------|-----------|---------------------|---------------------|---------------------|------------------------------|-----------------------|---------------------------|-------------------|
| Materials       | Sonotrode | Rise of Force [N/s] | Welding Force [N]   | Rise of Force [N/s] | Amplitude [µm] / setting [-] | Controlling Parameter | Force                     | Holding Time [ms] |
| TT chop – weave | Ø 10 [mm] | 300                 | 300                 | 0                   | 70.8 (3)                     | Energy 500 [Ws]       | 1000                      | 4000              |

Since the smaller sonotrode has a different gain, the amplitude is changed to a slightly lower value of 70.8 [µm] (setting 3 in the ACU). Since the sonotrode has a small surface area it was



decided to only deliver a limited amount of energy of 500 [Ws] (half of the average energy needed for the baseline welds, shown in Table 3-2) to the samples for this first experiment, to prevent overheating of the small area. Both these values could be adjusted but the preliminary experiment already showed much surface damage while no bond was formed yet. The surface damage can be seen in Figure 3-7. It could be that this surface damage is the result of the relative higher pressure, since the smaller sonotrode has a smaller surface area. Changing to a lower welding force, however, is not advised since this is close to the limits of the USW machine which might show unstable behaviour. Although the surface damage is expected to be lower for continuous fibre samples, the use of the smaller sonotrode was not further investigated.



Figure 3-7 | Surface damage as a result of an energy controlled welding experiment, delivering 500 [Ws] of energy with the Ø 10 [mm] cylindrical sonotrode, using a 300 [N] welding force, sample #94 (appendix B)

For the actual ITD hinge welding, chopped fibre material is welded to continuous fibre material. Since deconsolidation and surface damage is mostly found in the top sample for the previous experiments, the top sample is replaced with Toho Tenax continuous weave CF/PEEK material. Similar welds have been created using again the Ø 40 [mm] cylindrical sonotrode and the original setting of 300 [N] welding force, the other settings are summarized in Table 3-5.

Table 3-5 | Overview of the materials used (TT = Toho Tenax), sonotrode used and input settings for the USW machine for the welding of the weave - chopped baseline samples for a standard 12.7 [mm] overlap using the 9109 jig and 2 layer (0.23 [mm]) Toho Tenax ED

| Materials        | Sonotrode | I) Initial Phase    | II) Vibration Phase |                     |                              |                       | III) Solidification Phase |                   |
|------------------|-----------|---------------------|---------------------|---------------------|------------------------------|-----------------------|---------------------------|-------------------|
|                  |           | Rise of Force [N/s] | Welding Force [N]   | Rise of Force [N/s] | Amplitude [µm] / setting [-] | Controlling Parameter | Force                     | Holding Time [ms] |
| TT weave - chop. | Ø 40 [mm] | 300                 | 300                 | 0                   | 86.2 (9)                     | Travel                | 1000                      | 4000              |

All the welding curves and LSS curves can be found in appendix E. Figure 3-8 shows the welding curve for 80 [%] travel input setting. 100 [%] travel is normally used to show the complete cycle, but since the last part is of no interest and there was much deconsolidation in the previous samples, it was decided to start with a lower value for travel.



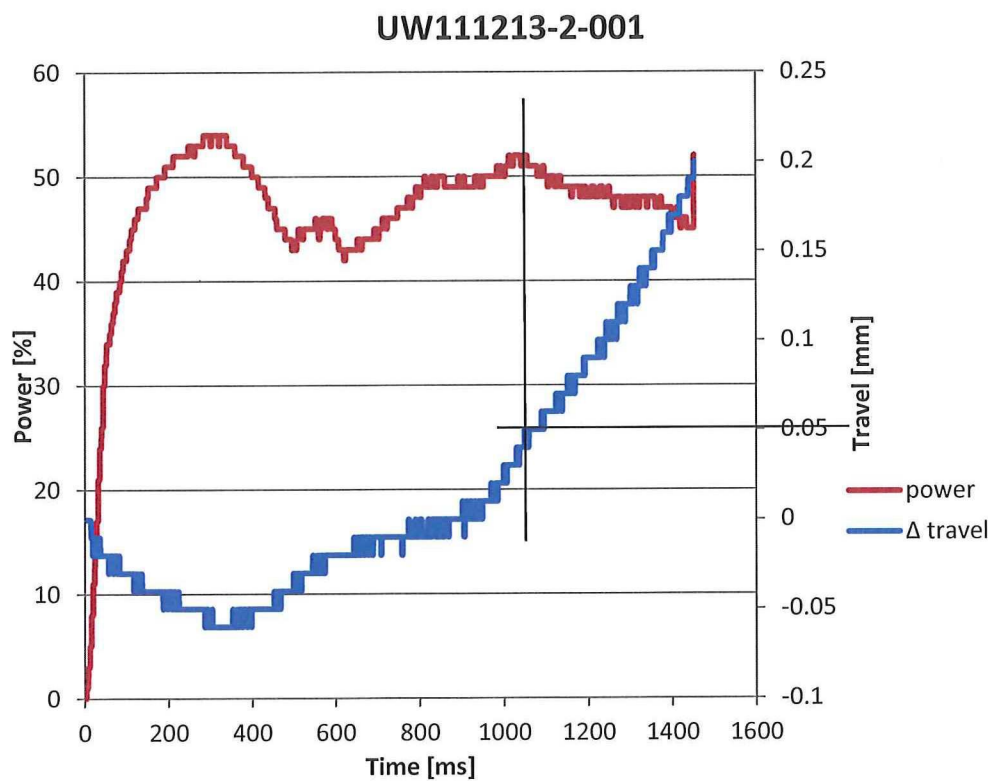


Figure 3-8 | Welding of sample #50 (appendix B) for continuous weave to chopped Toho Tenax CF/PEEK material, using melting on 80 [%] travel, 12.7 [mm] overlap, 300 [N] welding force and the Ø 40 [mm] sonotrode

Looking at Figure 3-8 it can be seen that the welding stages as described in section 1.2.2 are visible for this weld. Next to that, the welding curves are more consistent (showing similar patterns for each repeating weld), than for the chopped to chopped welding. The determined optimum travel has a value of 0.05 [mm] as can be seen in Figure 3-8, which amounts to 20 [%] of the ED thickness. This setting was used to weld five extra samples of which one was used for microscopy analysis, shown in Figure 3-9. The average values and  $c_v$  of the remaining samples were calculated and are shown in Table 3-6, compared to the values of the weave – weave welds.



Figure 3-9 | Sample #55 (appendix B) section of a continuous weave (top sample) to a chopped fibre (bottom sample) weld, 1.25x magnified

Looking at Figure 3-9, it can be seen that there are still some fibres that got pushed out of the weld with the squeeze flow, but the thickness and quality of the bond line is comparable to that of the continuous weave to continuous weave baseline samples shown in Figure 3-4.

Table 3-6 | Average values and their  $c_v$  for the maximum power, welding time, energy dissipated and LSS, for welding weave to chopped fibre samples using 300 [N], 12.7 [mm] ( $\varnothing$  40 [mm] sonotrode), all samples and excluding sample #52 (from #51-52, appendix B) compared to the values for the weave to weave welds

|  | Maximum Power [%]<br>( $c_v$ [%]) | Welding Time [ms]<br>( $c_v$ [%]) | Energy [Ws]<br>( $c_v$ [%]) | LSS [MPa]<br>( $c_v$ [%]) |
|--|-----------------------------------|-----------------------------------|-----------------------------|---------------------------|
| 300 [N],<br>30 [%] travel<br>weave - weave           | 55 (6.42)                         | 950 (5.75)                        | 1335 (4.95)                 | 39.7 (4.71)               |
| 1000 [N],<br>65 [%] travel<br>weave - weave          | 78 (2.16)                         | 553 (2.67)                        | 1049 (3.99)                 | 38.0 (4.80)               |
| (4 samples)<br>20 [%] travel<br>weave - chopped      | 59 (8.01)                         | 907 (17.0)                        | 1275 (10.2)                 | 33.6 (28.4)               |
| excl. sample #52<br>20 [%] travel<br>weave - chopped | 57 (4.96)                         | 937 (17.2)                        | 1285 (11.5)                 | 37.7 (15.1)               |

The  $c_v$  for all values considered in Table 3-6 are larger for the continuous weave to chopped material is than for the continuous weave to continuous weave baseline samples (added to Table 3-6), most significantly for the LSS. One of the samples was poorly welded because it moved during welding. Figure 3-10 shows the incomplete weld for sample #52 (appendix B) clearly. Without sample #52 the  $c_v$  for the LSS becomes questionable (since there are only 3 samples left, making the sample size too small for statistical analysis), but the LSS strength for this sample strongly influenced the  $c_v$  for the LSS. Due to the poorly welded surface the LSS was only 21 [MPa] compared to the average of 37 [MPa].



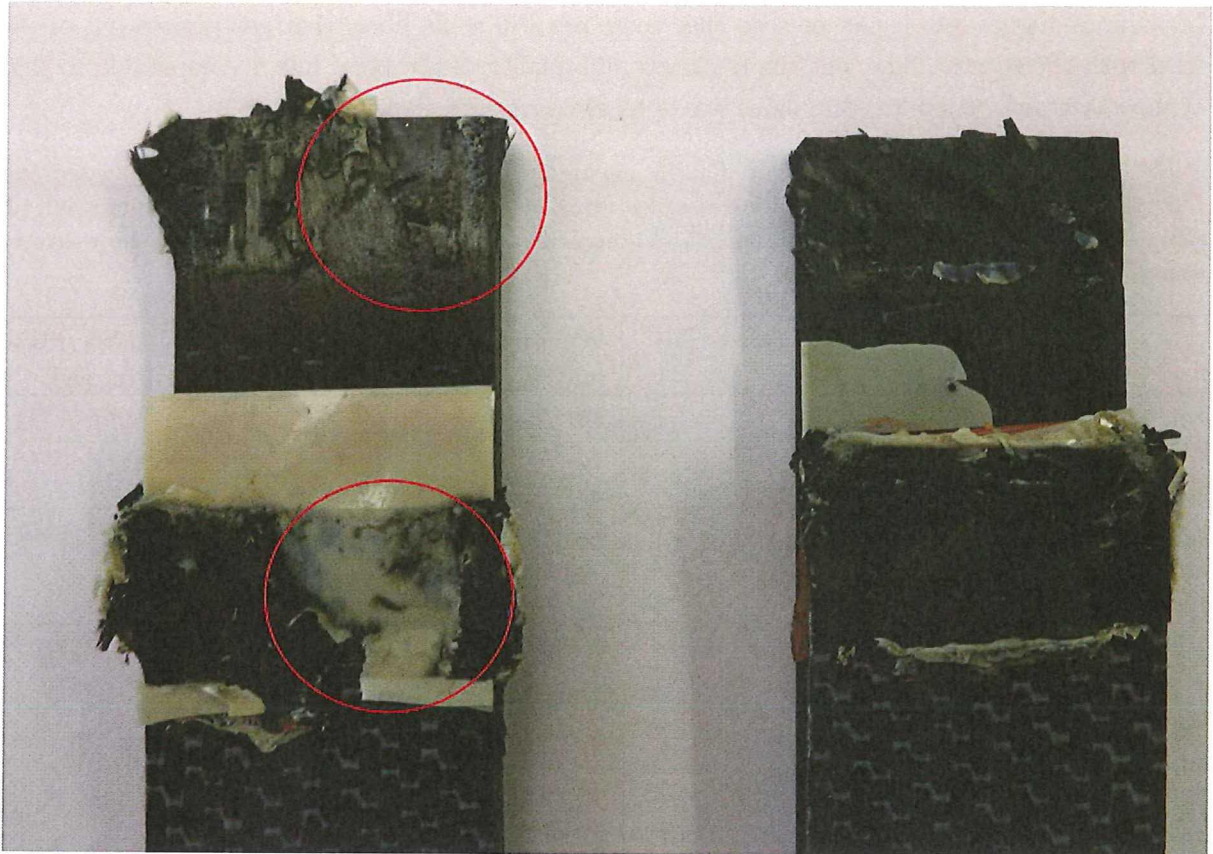


Figure 3-10 | Welding surfaces of weave to chopped material welded samples #52 (left) and #53 (right) (appendix B), highlighting the poorly welded area of the overlap for sample #52

Even without sample #52, the differences in  $c_v$  are still significant (4.7 [%] for the baseline compared to 15.1 [%] for the weave to chopped welds). Different factors can cause these irregularities (next to the random distribution of the short fibres). One can be the fact that the chopped samples show less polymer material at the sample surface (which can be seen in Figure 3-9 and Figure 3-10). The polymer poor surface can attribute to the difficulties in forming the weld, since there is less polymer material at the sample surface to bond with. Secondly the different surface composition might also influence the initiation of melting (and movement of the ED) due to different friction behaviour. Finally the higher stiffness in z-direction (higher out-of-plane stiffness, due to random orientation of the short fibres) can influence the response as well. From the welds created it was observed that this resulted in less energy dissipation (Table 3-6) compared to the weave to weave welds (Table 3-2), however, this difference is deemed insignificant. In optimization of welding chopped to continuous materials it is advised to research the influence of these mentioned factors.

### 3.3 Practical limitations for up-scaling and welding dissimilar materials

From the baseline of welding dissimilar materials it was found that using the chopped material as top sample (closest to the sonotrode) poses a restriction, since this results in deconsolidation of the sample. The use of a smaller sonotrode, further away from the edge of the sample, resulted in surface damage. It is therefore decided to use continuous material in the top sample. However,



the influence of using a different sonotrode, different weld settings or different material composition for the chopped samples is recommended for future research.

Another practical limitation is the travel (downward movement of the sonotrode) during the process. The travel during the vibration phase for the 1000 [N] and 300 [N] welding forces are 0.15 [mm] and 0.07 [mm]. The total travel of the entire process (including the solidification phase) is even higher. This poses some practical limitations on the up-scaling of USW using sequential spot welding. This is due to the fact that for spot welding it is expected that only a small spot of the (larger) overlap will be affected by the vibrations from the sonotrode. This means that only a small area will melt and travel would occur locally. If the ED is larger than the area covered by the sonotrode, the travel of this specific spot is prohibited by the surrounding ED material, which is outside of the influence of the sonotrode and therefore (far) colder and not yet molten. This problem is depicted schematically in Figure 3-11. If the ED would be of equal size as the area covered by the sonotrode, the same problem might arise due to the molten flow fronts around the ED. Using travel as the controlling parameter for the process would mean that the desired travel setting would never be reached and the welding process would continue until it reaches the machine limits (or the process is stopped manually).

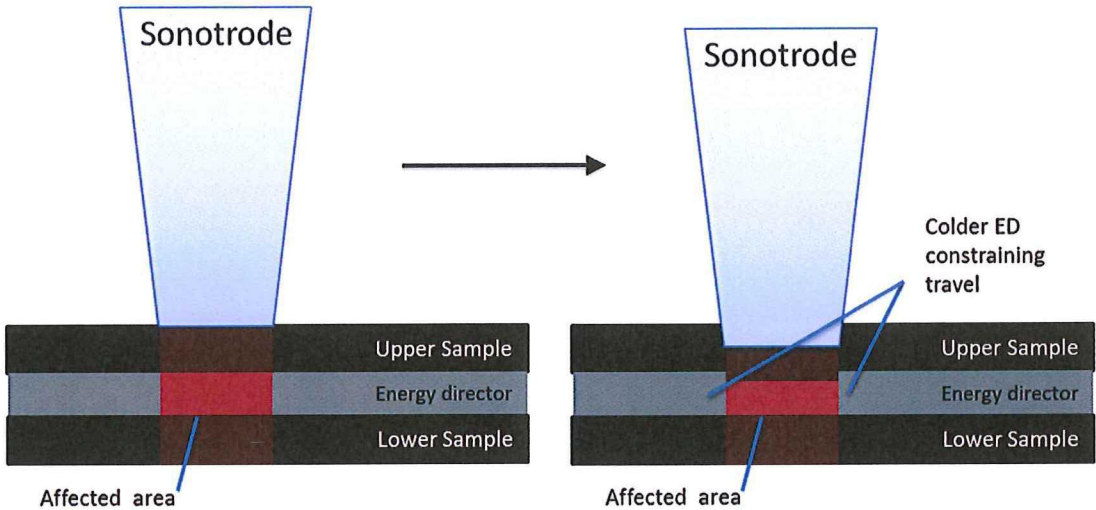


Figure 3-11 | Schematic view of the practical limitation of the travel controlled USW process: The colder ED surrounding the affected area by the sonotrode does not melt and therefore prohibits travel by the sonotrode

To circumvent this problem, not travel but energy or welding time could be selected as the controlling parameter. The duration of the vibration for the spot weld could then be controlled by this parameter, for which no restrictions apply. Considering Table 3-2 the dispersion of the welding time for 300 [N] is higher than for the welding energy. Therefore energy is selected as the controlling parameter for the experiments in which travel cannot be used as the controlling parameter.

As explained in section 2.2.1, this setting will measure the amount of energy already dissipated by the machine (by integrating the surface under the power curve) and will therefore stop once the predetermined energy level is reached. A challenge in welding with energy as the controlling parameter, however, is the influence of many different factors. The energy computed by the ACU

is the total energy dissipated, comprised of not only the energy needed to create the weld but including energy losses as well. Changing material or setup would change the energy levels. These energy levels and losses are investigated in more detail in chapter 4.

## 4 Energy Determination

As explained in section 3.3, welding with travel as the controlling parameter is not possible for spot welding, due to restrictions by the surrounding (ED) material. Welding using energy was deemed the most suitable alternative, although the determination of the needed energy can be complicated. Therefore the influence of several factors on the energy needed for the creation of a high quality weld is investigated. The factors that are of interest are the ones that are believed to change for up-scaling of the process for this specific case, compared to the baseline single lap shear samples. These are:

- The overlap or size of the welded area: No matter how the hinge will be welded, the welded area of one spot might differ from the area welded in a single lap shear joint. Changing the size of the area to be welded will result in a different amount of material to be melted and therefore influence the energy needed.
- The Jig design: For the welding of the hinges a new jig needs to be designed. Different jig geometry, material or clamping influences how the vibrations (heat and sound) dissipate throughout the jig and therefore influence the energy dissipation.
- The materials: In this research samples with different material (compositions) are used. The composition of the materials determines the material properties which also influence the dissipation of the vibrations, heat and sound and therefore the dissipated energy.

### 4.1 Energy determination experiments

The determination of the average welding energy needed is a complicated task. The energy dissipated by the machine during welding is influenced by many parameters, which can be basically divided in two parts. The first being the energy dissipated in actual welding, the second being the energy losses, seen in Equation 4-1. The energy losses are dependent on several parameters, the separate factors are shown in Equation 4-2.

$$E_{\text{tot}} \cdot \eta_{\text{hammering}} = E_{\text{weld}} + E_{\text{loss}} \quad \text{Equation 4-1}$$

$$E_{\text{loss}} = E_{\text{materials}} + E_{\text{machine}} + E_{\text{jig}} + E_{\text{hammering}} \quad \text{Equation 4-2}$$

In which  $E_{\text{tot}}$  is the total energy delivered, of this  $E_{\text{weld}}$  is the energy needed for the weld and  $E_{\text{loss}}$  are the energy losses. However, part of the energy of the machine is not delivered to the samples at all due to the hammering effect, therefore an efficiency factor  $\eta_{\text{hammering}}$  is introduced (in which 1 means no hammering effect, making energy transmission 100 [%] effective). The energy losses ( $E_{\text{loss}}$ ) can be divided in four different sources, in which  $E_{\text{materials}}$  are the losses in the ED and samples (due to composition, geometry or defects),  $E_{\text{machine}}$  the losses of the machine, baseplate and welding train,  $E_{\text{jig}}$  of the jig used to clamp the samples and  $E_{\text{hammering}}$  the energy that is lost through impact at the surface of the top sample.



As explained, the size of the overlap is an important factor on the energy needed for welding ( $E_{\text{weld}}$ ), since it is expected that a larger overlap needs more energy, since more material needs to be molten. The energy dissipated for the welding of samples with different overlaps is investigated. While keeping all other welding conditions identical (Sonotrode, Jig, Material, USW settings), overlaps of 12.7 [mm] (1/2 inch), 19.05 [mm] (3/4 inch) and 25.4 [mm] (1 inch) were welded using the 9110 jig and the proper alignment aids for each overlap. Using travel as the controlling parameter, welds can be created and the average energy dissipated for each overlap can be compared. With these results scaling of the area in different welding setups could possibly be used to give an indication of the energy needed. This can be used for energy controlled welding.

For up-scaling it is interesting to research all the energy loss variables considered in Equation 4-2. However, since only one USW machine is available and used in this research,  $E_{\text{machine}}$  is deemed to be constant with one exception. This is when the sonotrode of the machine is changed. Since the different sonotrodes have different gains (and geometry), the amplitudes are different for the sonotrodes, which influences the energy. However, the settings on the ACU allow for similar amplitude settings for all the sonotrodes. Since the amplitude will not be exactly similar, and the geometry of the sonotrode might influence the energy dissipation as well, there still might be a difference in energy loss. However, these effects were not researched. The hammering effect is also an important parameter, but this is also kept out of the scope of this research. Experiments determining the influence on the energy dissipation concerning the two other losses, the materials  $E_{\text{materials}}$  (ED and samples) and the jig  $E_{\text{jig}}$ , are performed. The influence on the energy levels of changing these factors (either material, or the jig) is compared while keeping all other weld settings (USW input settings, etc.) identical.

The influence of changing these parameters on the energy losses is analysed and can be used in providing an indication of the energy needed for the hinge welding, where two dissimilar materials will be welded in a new jig.

## 4.2 Area influence

As described in section 4.1, jig 9110 was used to weld samples with overlaps of A1: 12.7 [mm] (1/2 inch), A2: 19.05 [mm] (3/4 inch) and A3: 25.4 [mm] (1 inch). This was done using Ten Cate continuous weave CF/PEEK samples (cut in the right 0 [°] apparent fibre direction) and Ten Cate 5-layer EDs with an average thickness of 0.25 [mm]. The tests were conducted using the established technique of using travel as the controlling parameter. All the input welding parameters are summarized in Table 4-1.

Table 4-1 | Overview of the material used (TC = Ten Cate), sonotrodes used and the welding parameters for the welding of the samples for a 12.7 [mm], a 19.05 [mm] and a 25.4 [mm] overlap using the 9110 jig and 5 layer (0.25 [mm]) Ten Cate ED

|                  |           | I) Initial Phase    | II) Vibration Phase |                     |                              |                       | III) Solidification Phase |                   |
|------------------|-----------|---------------------|---------------------|---------------------|------------------------------|-----------------------|---------------------------|-------------------|
| Materials        | Sonotrode | Rise of Force [N/s] | Welding Force [N]   | Rise of Force [N/s] | Amplitude [μm] / setting [-] | Controlling Parameter | Force                     | Holding Time [ms] |
| TC weave – weave | Ø 40 [mm] | 300                 | 300                 | 0                   | 86.2 (9)                     | Travel                | 1000                      | 4000              |

The resulting welding curves, however, were dissimilar compared to the ones for the baseline experiment as shown in Figure 4-1. With the dissimilar curves, not showing the different stages discussed in section 1.2.2, it was not possible to determine the optimum welding conditions. To verify if the dissimilarities in the welding curves were caused by quality differences between the Ten Cate material and the Toho Tenax material used for the baseline, the test was repeated using Toho Tenax material (and Toho Tenax ED with an average thickness of 0.24 [mm]). The resulting welding curves are presented Figure 4-1 as well.

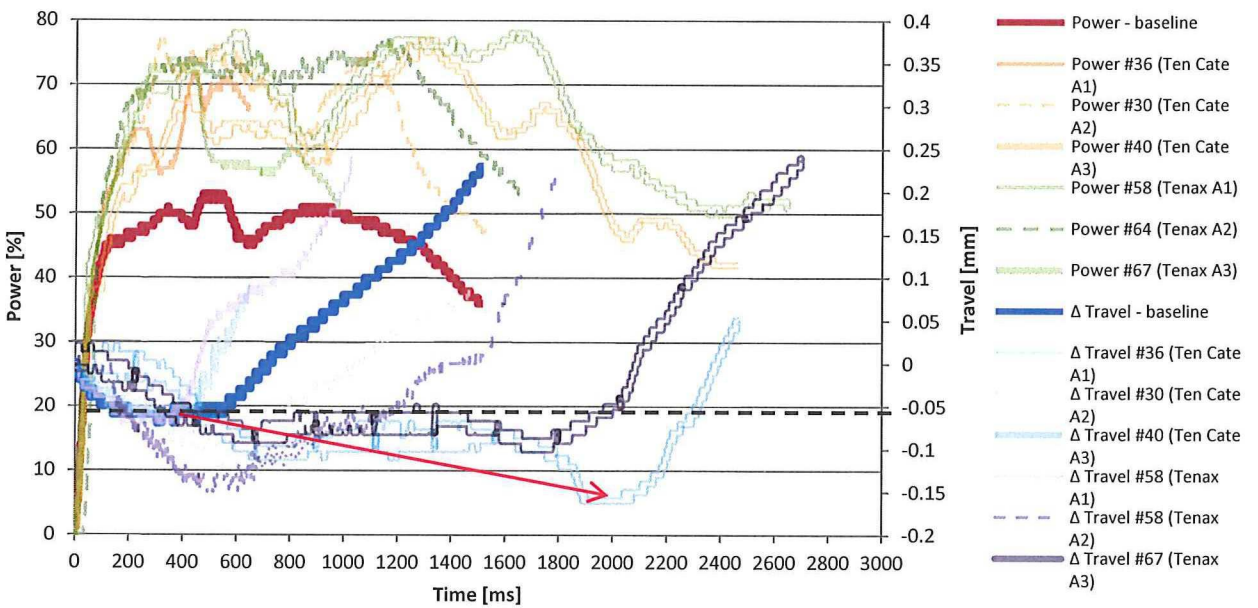


Figure 4-1 | Welding curves for different overlaps (A1 = 12.7 [mm], A2 = 19.05 [mm], A3 = 25.4 [mm]) comparing Ten Cate and Toho Tenax material to the baseline, with the red arrow highlighting the increasing negative travel for welding of larger overlaps

Several things can be observed by looking at Figure 4-1. The average power used is higher for these experiments. This is due to the different welding jig used in this experiment, elaborated upon in section 4.3. Next to that, the curves for both materials are different and do not comply with the regular curves seen in the baseline welds for overlaps A2 and A3. Only A1 showed a similar curve. Therefore it was not possible to determine the optimum welding conditions for overlaps A2 and A3, that is, the determination of the optimum travel. The travel was estimated with the irregular welding curves. However, these travel values seemed far too low compared to

the baseline results and the obtained welds have a low LSS as well. The travel used and the LSS results can be seen in Table 4-2, and the fracture surface quality is shown in Figure 4-2. Table 4-2 shows the LSS values for the A1 (12.7 [mm]) overlap to be of the same magnitude as the baseline, whereas the larger overlaps have strongly reduced strength. Looking at the fracture surfaces in Figure 4-2 it can be seen that the welding process did not form a good bond but instead overheated the overlap and melted the composite material through the thickness. The welding also created much fibre distortion, combined with the overheating strongly reducing the LSS. Since the results for the larger overlaps were not satisfying, welding was stopped and the set of 5 subsequent welds with the same conditions was not completed to save samples. The sample size is also depicted in Table 4-2. Even though the results were not satisfying it can be seen in Table 4-2, that the energy dissipated for a larger overlap increases compared to the 12.7 [mm] baseline overlap. The differences for the 12.7 [mm] (A1) overlap for the Ten Cate and Toho Tenax material compared to the baseline can be due to the different optimum travel found. Which could be caused by the different jig used compared to the baseline or due to the dissimilarities between the Ten Cate and Toho Tenax material (Composite and ED). The influence of these two parameters is elaborated upon in sections 0 and 4.4.

Table 4-2 | LSS and energy data for different overlap (A1 = 12.7 [mm], A2 = 19.05 [mm], A3 = 25.4 [mm]) welds comparing Ten Cate (with 5 layer, 0.25 [mm] ED) and Toho Tenax (with 2 layer, 0.23 [mm] ED) material (welded with the 9110 jig) with the baseline data (welded with the 9109 jig).

\*travel input used could not be determined with the established method and was estimated

|   | (Toho T.)<br>9109 jig | Ten Cate<br>9110 jig |                |                | Toho Tenax<br>9110 jig |                |             |
|---|-----------------------|----------------------|----------------|----------------|------------------------|----------------|-------------|
|   | Baseline              | A1                   | A2             | A3             | A1                     | A2             | A3          |
| Determined Travel [%]                       | 30                    | 16                   | 12*            | 8*             | 43                     | 12.5*          | 100*        |
| (sample size)                               | (5)                   | (4)                  | (3)            | (3)            | (4)                    | (3)            | (1)         |
| Average LSS [MPa]<br>(c <sub>v</sub> [%])   | 39.7<br>(4.71)        | 39.7<br>(15.2)       | 14.0<br>(29.3) | 17.4<br>(0.88) | 39.0<br>(4.85)         | 10.8<br>(32.6) | 11.0<br>(-) |
| Average Energy [Ws]<br>(c <sub>v</sub> [%]) | 1335<br>(4.95)        | 944<br>(18.7)        | 2780<br>(8.15) | 4413<br>(3.31) | 983<br>(20.1)          | 3330<br>(4.77) | 5235<br>(-) |



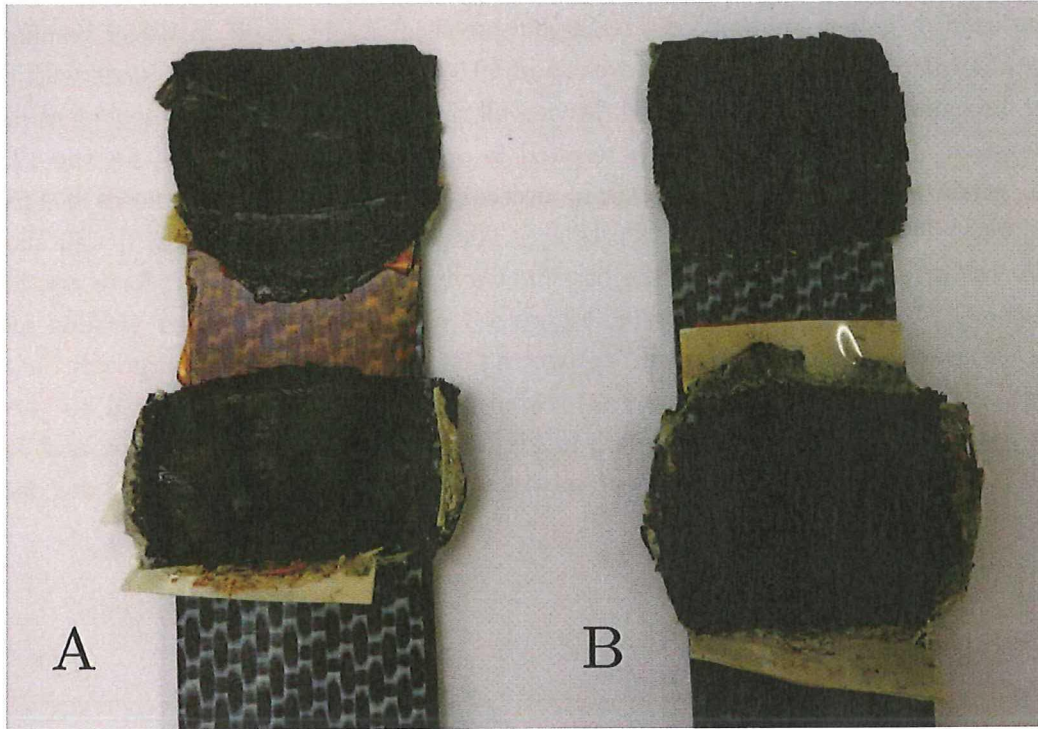


Figure 4-2 | Fracture surfaces of the samples poorly welded with 300 [N] for A) 19.05 [mm] overlap (#29 appendix B) and B) 25.4 [mm] overlap (#41 appendix B)

The difference of the welding curves shown in Figure 4-1 compared to the baseline welding curve, is attributed to the initially selected parameter for the welding force. The 300 [N] used proved sufficient for the 12.7 [mm] overlap, but was not high enough to create welds at the larger overlap. The increasing area automatically meant a decrease in pressure for the same welding force. This could decrease the rate at which initiation and growth of hot spots occurs as explained in section 1.2.2. Rather than keeping the force constant at 300 [N], a constant pressure (increasing force) might solve the mentioned issue of the poor welds (overheating, low LSS) for larger overlaps.

First, another interesting effect of this constant force, therefore decreasing pressure, is discussed. The decreasing pressure results in an increase of negative travel which represents an upward motion of the sonotrode, depicted by the red arrow shown in Figure 4-1. This is believed to come from an increasing hammering effect, which is the ‘hammering’ of the sonotrode on the material if it loses contact with the top sample. This means that the cyclic deformation of the ED under the vibrations and pressure of the sonotrode is not as high as it could have been without hammering. If hammering occurs, a great amount of energy is lost since it is not being transferred to the material (no cyclic deformation). A higher welding force or a smaller amplitude might both decrease the hammering effect. The higher pressure might influence how much the ED deforms under the cyclic load, allowing more deformation might decrease the hammering. With a smaller amplitude setting, less deformation of the ED is needed for the complete cyclic deformation of the ED, which also might decrease the hammering effect. However, further research on the hammering effect in USW of TPC is recommended.

As mentioned, a higher welding force (constant pressure) might result in better results for the welding of larger overlaps. For the A2 overlap of 19.05 [mm] two welds were made with a higher welding force and the Ten Cate material, leaving all the other welding parameters identical to the ones shown in Table 4-1. The 300 [N] resulted in a pressure of 0.93 [MPa] for the 12.7 [mm] overlap, which means that the 19.05 [mm] overlap, which is 1.5x larger, needs a 1.5x larger welding force of 450 [N] for the same pressure. The weld formed with 450 [N] still showed an irregular welding curve compared to the baseline curve, therefore the welding force was increased to 600 [N] (1.24 [MPa]), both shown in Figure 4-3. Even with the higher welding force, the welding curves do not show the separate stages as for the baseline welds, although the welding time and therefore energy needed was somewhat lower, but this is attributed to the higher welding force. Next to that, as can be seen in Figure 4-3, for this jig configuration and Ten Cate CF/PEEK material, it reaches the power limits of the USW machine. Therefore it was decided to stop these tests and save samples.

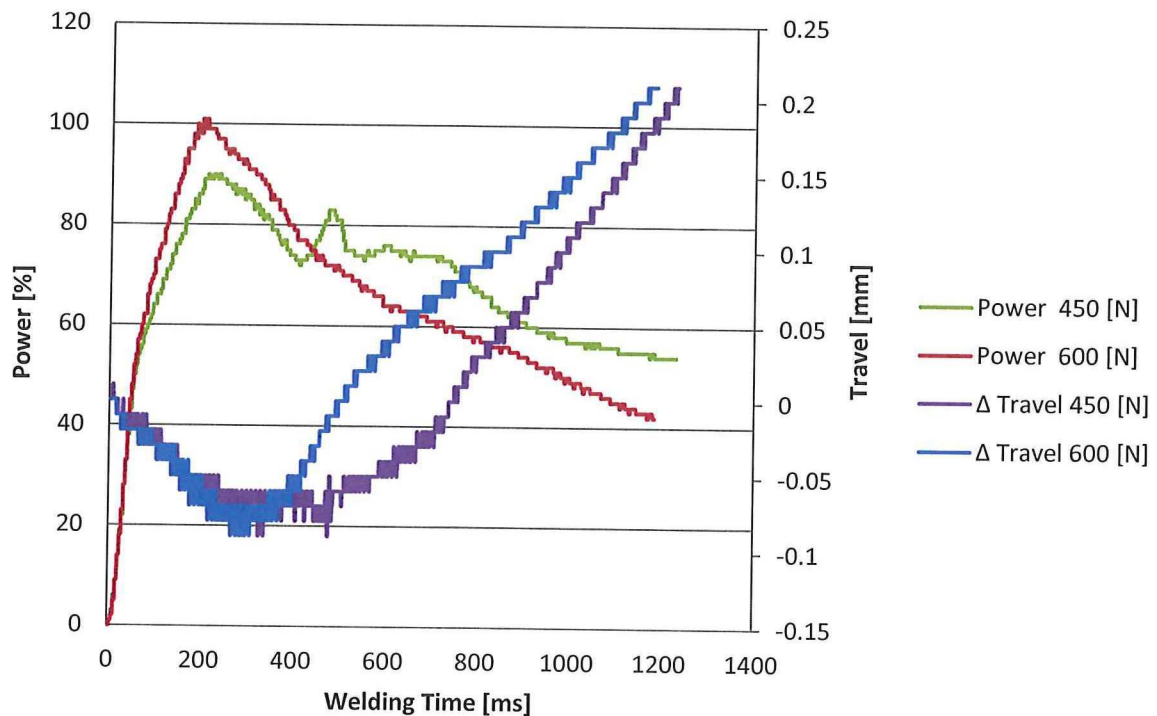


Figure 4-3 | (Irregular) Welding curves for sample #68 and #69 (appendix B), experiment with 450 [N] (0.93 [MPa]) and 600 [N] (1.24 [MPa]) welding force, 19.05 [mm] overlap, reaching the power limits of the USW machine for 100 [%] travel

Even though no optimum welds were obtained, the influence of increasing the area clearly shows an increase in energy dissipated (Table 4-2). It can be concluded that for the CF/PEEK material, using flat EDs, increasing the welding area reaches the limitations of the USW machine. For lower forces the overlap overheats and low LSS are obtained. Increasing to a higher force the machine reaches its maximum power levels.



### 4.3 Jig influence

To research the influence of the jig used, an identical set of samples was welded in both the 9109 jig and the 9110 jig (samples #4 - #8 for 9109, samples #59 - #63 for 9110, appendix B). The jigs do not differ very much in geometry, but the baseplate of the 9109 jig is manufactured from steel and the baseplate of the 9110 jig from aluminium, as explained in section 2.3. The settings used were a welding force of 300 [N], 12.7 [mm] overlap, using the 40 [mm] sonotrode for continuous weave Toho Tenax CF/PEEK material. All the welding parameters used are summarized in Table 4-3. The optimum travel found for the samples welded with the 9109 jig was slightly lower than for the samples welded with the 9110 jig (30 [%] i.e. 0.07 [mm] compared to 43 [%] i.e. 0.10 [mm]) The welding curves for both materials are shown in Figure 4-4.

Table 4-3 | Overview of the material used (TT = Toho Tenax), sonotrode used and the welding parameters for the welding of identical weave – weave samples for the 9109 jig and the 9110 jig using 2 layer (0.24 [mm]) Toho Tenax EDs

|                  |                       | I) Initial Phase    | II) Vibration Phase |                     |                                    |   | III) Solidification Phase |                   |
|------------------|-----------------------|---------------------|---------------------|---------------------|------------------------------------|---|---------------------------|-------------------|
| Materials        | Sonotrode             | Rise of Force [N/s] | Welding Force [N]   | Rise of Force [N/s] | Amplitude [ $\mu$ m] / setting [-] | Controlling Parameter                       | Force                     | Holding Time [ms] |
| TT weave – weave | $\varnothing$ 40 [mm] | 300                 | 300                 | 0                   | 86.2 (9)                           | Travel, opt.:<br>30 [%] 9109<br>43 [%] 9110 | 1000                      | 4000              |

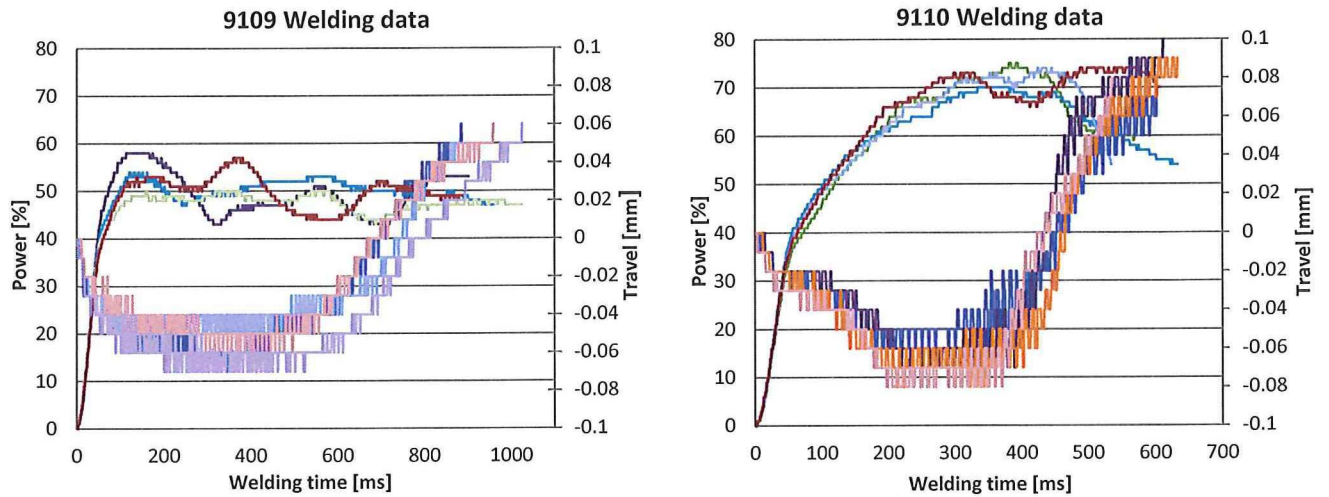


Figure 4-4 | Welding curves for identical welding conditions using the 9109 (left) and the 9110 jig (right)

Looking at Figure 4-4 several differences can be identified. Comparing the travel curves for both jigs, it can be seen that there is some vibration in all curves (due to the oscillating motion of the sonotrode). The vibrations for the 9110 jig, however, are somewhat larger (not to confuse with the total travel, which is also higher, but this is due to the higher optimum travel found for the samples welded with the 9110 jig, Table 4-3). An overview of the differences in maximum power, welding time and energy is presented in Figure 4-5, whereas a comparison in the  $c_v$  for these



parameters concerning both jigs is given in Table 4-4. Note that only 4 samples are shown for the 9110 jig, since in the welding of sample #62 the ED shifted, making the results invalid.

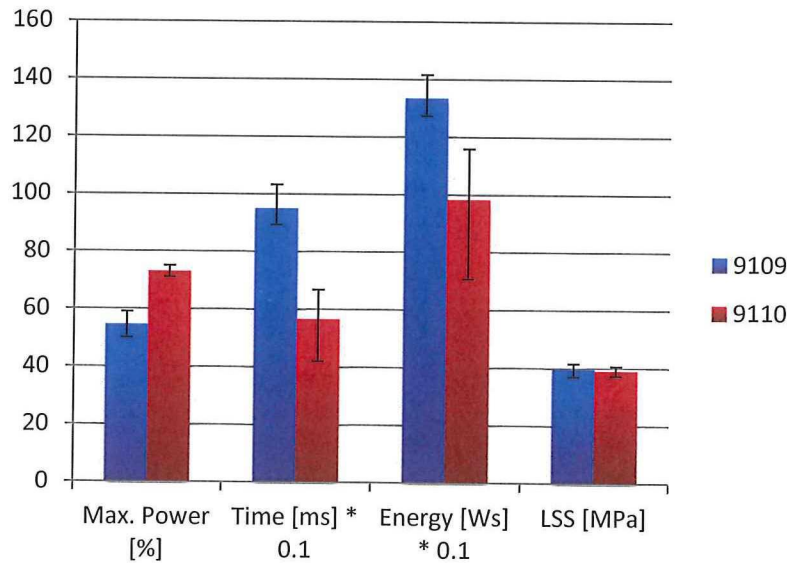


Figure 4-5 | Average and range values for several welding outcome parameters comparing identical welded samples for the 9109 and 9110 jig

Table 4-4 | Average and  $c_v$  values for several welding outcome parameters comparing identical welded samples the 9109 and 9110 jig

|   | Maximum Power<br>[%] ( $c_v$ [%]) | Welding Time [ms]<br>( $c_v$ [%]) | Energy [Ws]<br>( $c_v$ [%]) | LSS [MPa]<br>( $c_v$ [%]) |
|---|-----------------------------------|-----------------------------------|-----------------------------|---------------------------|
| <b>9109 jig</b><br>(5 samples)<br>(30 [%] travel) | 54.6 (6.42)                       | 950 (5.75)                        | 1335 (4.95)                 | 39.7 (4.71)               |
| <b>9110 jig</b><br>(4 samples)<br>(43 [%] travel) | 73 (2.50)                         | 566 (18.9)                        | 983 (20.1)                  | 39.0 (4.85)               |

It can be seen in Figure 4-5 and Table 4-4, that next to the aforementioned higher vibrations, the 9110 jig also requires a higher power (but has a lower energy level due to the shorter weld time) and has far less consistent results for the welding time and energy dissipation. This is believed to come from either the material used or some geometrical factors. The 9109 jig is made of steel whereas the 9110 jig is manufactured using aluminium, which Young modulus is a factor 3 lower [13]. This lower stiffness is believed to cause most of the differences since the geometry is almost identical. However, further research on the influence of the geometry and material properties of the jig on the energy dissipation is recommended.

From these experiments it is calculated that the 9110 jig, although having less consistent results for the energy dissipation, consumes 24 [%] less energy than 9109 jig for this particular weld. The maximum power used, however, is 34 [%] higher for the 9110 jig (which combined with the shorter weld time results in the mentioned lower energy consumption).

It can be concluded that the aluminium 9110 jig influences the dissipated energy such that it requires less energy on average for optimum weld conditions of identical samples compared to the steel 9109 jig. The variations in the energy levels for the welds made in the different jigs, however, are larger for the 9110 jig. The differences are mostly attributed to the different material of the baseplate. A final note is that changing the welding parameters and / or welding configuration (overlap, sonotrode, etc.) will influence these results. Also the influence of the geometry of the jig has yet to be determined since the difference for this comparison was limited.

#### 4.4 Material influence

For the influence of the material on the dissipated energy several combinations are investigated. First the difference in energy dissipated by welding a 12.7 [mm] overlap of a standard weave – weave weld (baseline) is compared to a weave (top sample) – chopped (bottom sample) weld. Since the chopped material is thicker (average 3.86 [mm] compared to the 1.85 [mm] for the weave material) and has a different composition (chopped fibres with random orientation compared to the (0/90) [°] oriented continuous fibres), it is expected to change the energy dissipation. Secondly the Toho Tenax weave and Ten Cate weave material are compared. Since they both have the same composition and roughly the same thickness (1.85 [mm] for Toho Tenax and 1.82 [mm] for Ten Cate), changes in energy are not expected for the same welding overlap of 12.7 [mm] using the same welding parameters.

The samples used for the sets are #4 – 8 (weave – weave Toho Tenax) and #51 – 55 (weave – chopped Toho Tenax) welded with the 9109 jig, #35 – 39 (weave – weave Ten Cate) and #59 – 64 (weave – weave Toho Tenax) welded on the 9110 jig (appendix B). All 4 sets were welded using travel as controlling parameter and the optimum welding conditions for a welding force of 300 [N] and an overlap of 12.7 [mm], using the 40 [mm] sonotrode. All the welding parameters are summarized in Table 4-5

Table 4-5 | Overview of the materials (TT = Toho Tenax weave thickness = 1.85 [mm] chopped thickness = 3.86 [mm], TC = Ten Cate weave thickness = 1.82 [mm]), jigs used and the welding parameters for the welding of different materials using the 9109 jig and the 9110 jig and using Toho Tenax 2 layer (0.24 [mm]) ED for the TT and Ten Cate 5 layer (0.25 [mm]) ED for the TC samples

| All welded with the<br>Ø 40 [mm] sonotrode |      | I) Initial<br>Phase       | II) Vibration Phase     |                           |                                    |                          | III) Solidification<br>Phase |                      |
|--|------|---------------------------|-------------------------|---------------------------|------------------------------------|--------------------------|------------------------------|----------------------|
| Materials<br>&<br>thickness                | Jig  | Rise of<br>Force<br>[N/s] | Welding<br>Force<br>[N] | Rise of<br>Force<br>[N/s] | Amplitude<br>[µm] /<br>setting [-] | Controlling<br>Parameter | Force                        | Holding<br>Time [ms] |
| TT weave<br>– weave                        | 9109 | 300                       | 300                     | 0                         | 86.2 (9)                           | Travel<br>opt.: 30 [%]   | 1000                         | 4000                 |
| TT weave<br>– chop                         | 9109 | 300                       | 300                     | 0                         | 86.2 (9)                           | Travel<br>opt.: 20 [%]   | 1000                         | 4000                 |
| TC weave<br>– weave                        | 9110 | 300                       | 300                     | 0                         | 86.2 (9)                           | Travel<br>opt.: 16 [%]   | 1000                         | 4000                 |
| TT weave<br>– weave                        | 9110 | 300                       | 300                     | 0                         | 86.2 (9)                           | Travel<br>opt.: 43 [%]   | 1000                         | 4000                 |



The resulting energy levels from these welds are shown in Figure 4-6 and their average values and  $c_v$  are presented in Table 4-6.

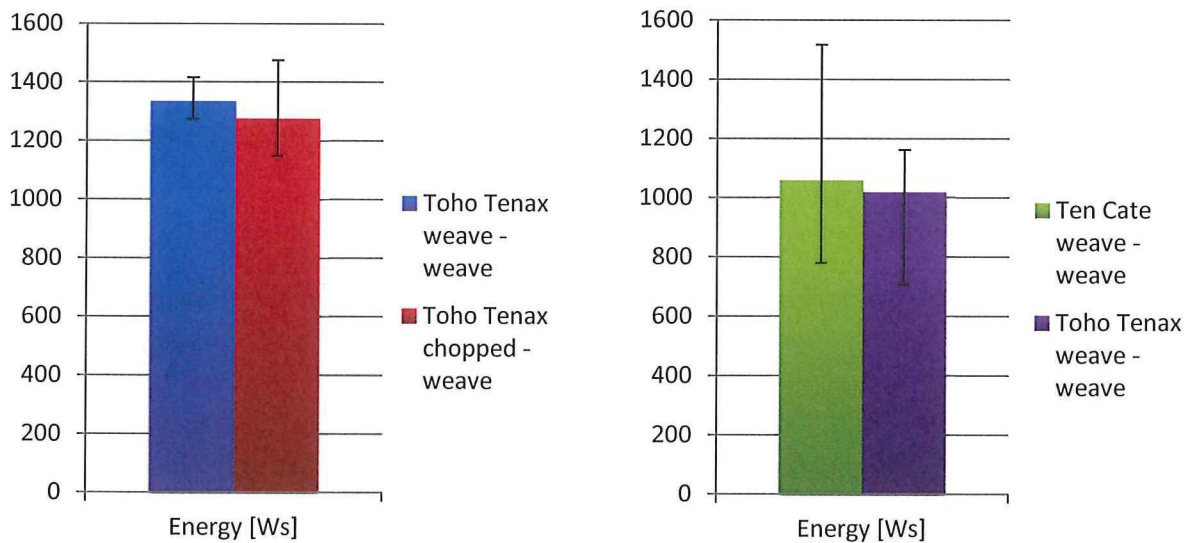


Figure 4-6 | Average energy levels for identical welds (optimal conditions for 300 [N], 12.7 [mm] overlap using the 40[mm] sonotrode) in different materials for the 9109 jig (left) and 9110 jig (right)

Table 4-6 |  $c_v$  for identical welds (optimal conditions for 300 [N], 12.7 [mm] overlap using the 40[mm] sonotrode) in different materials for the 9109 and 9110 jig (not all samples were lap shear tested or the test failed, \*1 = 3 samples, \*2 = 4 samples)

|                                   | Toho Tenax<br>weave - weave<br>(9109) | Toho Tenax<br>chopped - weave<br>(9109) | Ten Cate weave<br>- weave (9110) | Toho Tenax<br>weave - weave<br>(9110) |
|-----------------------------------|---------------------------------------|---|----------------------------------|---------------------------------------|
| Energy [Ws]<br>( $c_v$ [%])       | 1335<br>(4.95)                        | 1275<br>(10.22)                         | 1059<br>(28.16)                  | 1018<br>(18.53)                       |
| Average LSS [MPa]<br>( $c_v$ [%]) | 39.7<br>(4.71)                        | 37.7 (*1)<br>(15.1)                     | 39.7 (*2)<br>(15.2)              | 39.0 (*2)<br>(4.85)                   |

For the two sets compared for the 9109 jig, the Toho Tenax weave – chopped weld requires slightly less energy on average, however, due to the large scatter this does not mean a lot. For the 9110 jig the difference is even smaller, the Toho Tenax material shows a slightly lower energy dissipation on average, but again the scatter is significant. The average energy for the materials welded with the 9110 jig is lower than for the 9109 jig as expected by section 4.3. It is important to note that even though the composition might be slightly different (especially for the weave – chopped material, but also between the Ten Cate weave compared to the Toho Tenax material slight difference exist for example in thickness) the matrix for all samples is PEEK. This explains the fact that the differences in average energy required are relatively small, since the PEEK used will roughly have the same  $T_m$  and other material properties (although minor variations could exist between the polymers of different manufacturers, i.e. different grades).

The higher  $c_v$ , seen in Table 4-6, for the materials welded with the 9110 jig corresponds with the results in section 4.3. The difference in variation ( $c_v$ ) for the energy levels between the Ten Cate material and the Toho Tenax material however, is unexpected. One of the factors that might



influence the variations in energy levels ( $c_v$ ) is the difference in the EDs used, which only have 2 layers (average thickness of 0.12 [mm] per layer) for the Toho Tenax material and 5 layers (average thickness of 0.05 [mm] per layer) for the Ten Cate material. Although the layers are stacked to each other, under the vibrations the layers can separate again as shown in Figure 4-7. Figure 4-7 shows the separation of layers at the edge of the sample, however, during the vibration phase this might occur in the overlap as well which could contribute to the higher variation in energy for the Ten Cate samples. Further research with 1 layer EDs (with sufficient thickness for welding) or better stacked EDs could reduce the variation in energy levels.

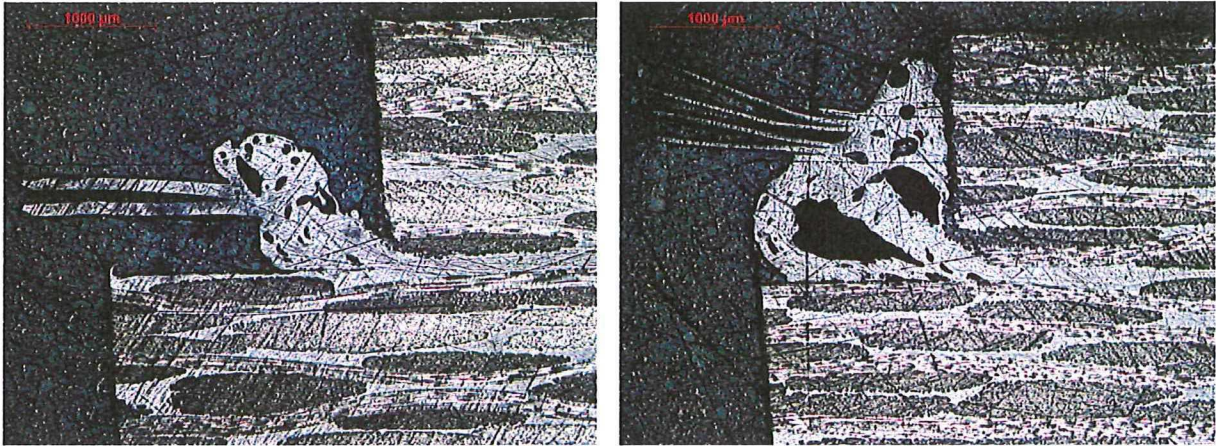


Figure 4-7 | 2.5x magnification of a Toho Tenax welded sample showing the two layer ED separation at the edge (left) and a Ten Cate welded sample showing the 5 layer ED separation at the edge (right)

Another factor that could clarify the inconsistency in energy levels for the Ten Cate welds is the material quality. Many of the samples manufactured with the hot plate press in the DASML using Ten Cate material showed delamination at the edges of the samples after water jet cutting, shown in Figure 4-8. It was therefore decided to do a C-scan of the material, of which the result is shown Figure 4-9. It is noted that the different colours in the C-scan image are used for relative comparison, not for absolute attenuation values.

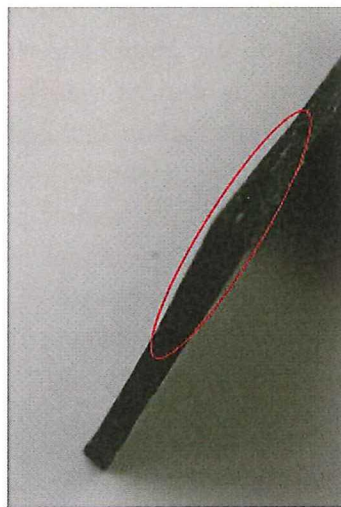


Figure 4-8 | Sample of a delaminated corner due to water jet cutting of the Ten Cate material

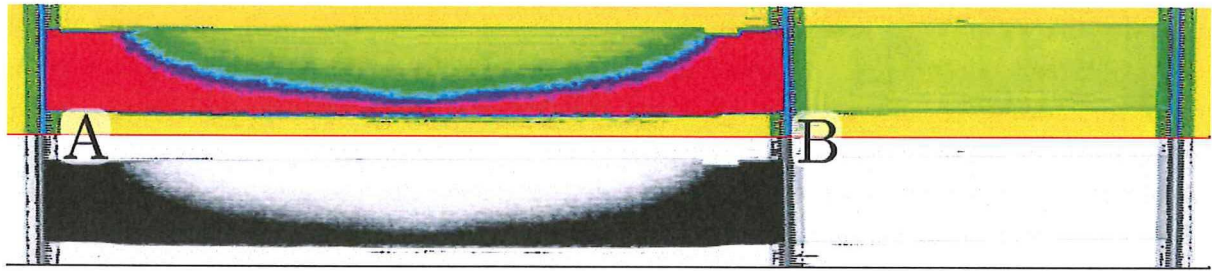


Figure 4-9 | Colour and black & white C-scan images of the edges of the laminate plates: A) Ten Cate material, B) Toho Tenax material, the dark/red colour indicates poorly consolidated material. The colours are used for relative comparison, not for absolute attenuation values.

Looking at the C-scan in Figure 4-9 for the Ten Cate material compared to the Toho Tenax material it can be seen that the edges are poorly consolidated (indicated by the dark/red colour). The reason for the poor consolidation can be found in the limitations of the hot plate press available in the DASML which does not provide completely uniform heating to the entire laminate. The samples were cut out of the plate, using the water jet cutting, with a margin of 25.4 [mm] from the edge. Although the middle of the plate shows a good consolidation, some samples might have been cut out too close to the edge. Together with the aforementioned deconsolidation of the edges, this might contribute to the wide range of welding energies (high  $c_v$ ) since part of the energy, depending on the sample, dissipates to the deconsolidated areas.

It can be concluded that the different material compositions and combinations studied in this experiment only have a slight influence on the dissipated energy. Considering the high variation (high  $c_v$ ) in the sets of welded samples this difference could be neglected. It is important to note, however, that changing the welding parameters might affect these results.

#### 4.5 Discussion on energy determination

Regarding the results of the experiments presented in this chapter, it is noted that the energy dissipation is influenced by many parameters. Some indications on the influence of several parameters on the energy dissipation can be given. For the increase of the welded area an increase in energy is shown, for the two jig designs, mostly different in material, changing to aluminium results in less average energy dissipation but higher  $c_v$  and for material selection / combination no significant effect on the energy levels was found, however, a higher  $c_v$  is observed for the Ten Cate material. However, changing of the welding parameters and / or the setup might influence these values. It is therefore in general recommended to perform experiments with the travel controlled process (if possible), to get an estimate of the average energy needed for an optimum weld (leaving the other welding parameters identical).



## 5 New Concepts: Zero Travel Spot Welding, Dedicated Area Sized ED Welding and Process Practicalities

### 5.1 Experiment design for spot welding of a larger overlap

One of the proposed welding strategies in this research is the welding of a small strip in the middle of a large overlap, or zero travel welding. The overlap will be completely covered with ED material, making the ED area larger than the area covered by the sonotrode. As stated in chapter 3, this process is travel restricted by the part of the ED which does not melt and calls for welding energy as the controlling parameter. For this experiment the rectangular sonotrode is used, having as advantage that a narrow strip of 14.9 [mm] can be welded in both a normal and a larger overlap, creating similar conditions for the energy determination. Before this concept is researched first a preliminary experiment was performed, to verify if a weld can be formed with energy as the controlling parameter in a setup where travel is restricted. In this test two samples are placed directly on top of each other with a large ED in between. Since the energy delivered by the sonotrode only melts part of the ED, the rest of the larger ED should restrict the travel. This test is shown schematically in Figure 5-1.

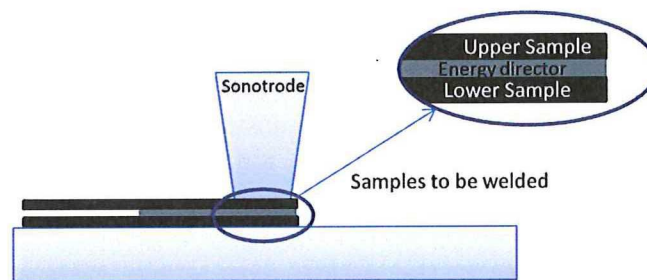


Figure 5-1 | Schematic view of the initial experiment to determine the possibility of energy controlled zero travel welding using the 9109 jig

For the spot welding experiment, first a set of normal, travel controlled welds for an overlap of 14.9 [mm] are conducted (Figure 5-2-A). Out of these welds the average energy dissipated for optimum welding conditions can be calculated, which is used as the controlling parameter to weld a spot (strip) in the middle of a large overlap, shown in Figure 5-2-B. The unequal overlap on the left (6 [mm]) and right (4.5 [mm]) of the spot weld (Figure 5-2-B) is due to the geometrical constraints and alignment of the used 9110 jig relative to the rectangular sonotrode.



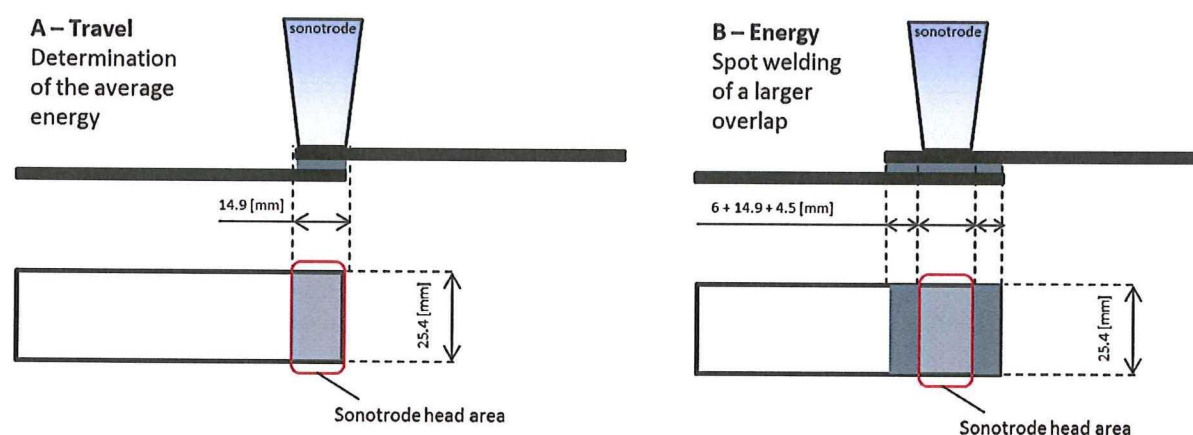


Figure 5-2 | Schematic view of the setup using the 9110 jig for: A) Energy determination 14.9 [mm] overlap using travel as the controlling parameter, B) Spot welding of a larger overlap using energy as the controlling parameter

Again the welding curves, output (energy, maximum power) and strength data of the specimen are analysed and compared to the baseline results.

### **Welding force**

The area welded in the described zero travel experiment is slightly larger than the area of the overlap in the baseline welds ( $14.9 \cdot 25.4 = 378.46 \text{ [mm}^2\text{]}$ , 17 [%] larger compared to the baseline area of  $12.7 \cdot 25.4 = 322.58 \text{ [mm}^2\text{]}$ ). As stated in chapter 4, using the welding force of 300 [N] (and therefore a relatively lower pressure) results in unstable results for the larger overlaps. Next to that, the rectangular sonotrode might have some influence on the energy dissipation as well. Therefore the welding force was reconsidered.

The welding pressure corresponding to the welding force of 300 [N] is 0.93 [MPa] for the 12.7 [mm] overlap. Experiment welds were produced with the rectangular sonotrode (welding area overlap of 14.9 [mm]) and a welding force of 500 [N], a pressure of 1.3 [MPa] for this overlap, with all other welding parameters summarized in Table 5-1. Note that the amplitude is slightly lower compared to the baseline amplitude (86.2 [ $\mu\text{m}$ ]), but since the settings of the ACU only allow for 5 [%] step changes this was the closest amplitude achievable. Since the difference is less than 2 [%] it is assumed this does not affect the welding process significantly. With these parameters a somewhat regular welding curve was obtained, seen in Figure 5-3. It can be seen that stage 4 (the power plateau) is shorter compared to the baseline results for a welding force of 300 [N] and is only a small peak instead of a plateau. This is expected due to higher welding force as described in section 1.2.2, and can also be seen for the baseline using a 1000 [N] welding force. Also, as expected, the rate at which the travel increases is higher than for the baseline using a 300 [N] welding force and lower than for the baseline using a 1000 [N] welding force.

Table 5-1 | Overview of the material used (TT = Toho Tenax), sonotrode used and the welding parameters for the welding experiments with a higher welding force using TT 2 layer, 0.24 [mm], EDs and the 9110 jig

| Materials        | Sonotrode                  | I) Initial Phase    | II) Vibration Phase |                     |                           |                       | III) Solidification Phase |                   |
|------------------|----------------------------|---------------------|---------------------|---------------------|---------------------------|-----------------------|---------------------------|-------------------|
|                  |                            | Rise of Force [N/s] | Weld. Force [N]     | Rise of Force [N/s] | Amplitude [μm] (set. [-]) | Controlling Parameter | Force                     | Holding Time [ms] |
| TT weave – weave | Rectangular 14.9 · 30 [mm] | 250                 | 500                 | 0                   | 84.6 (3)                  | Travel, opt.: 20 [%]  | 1000                      | 4000              |

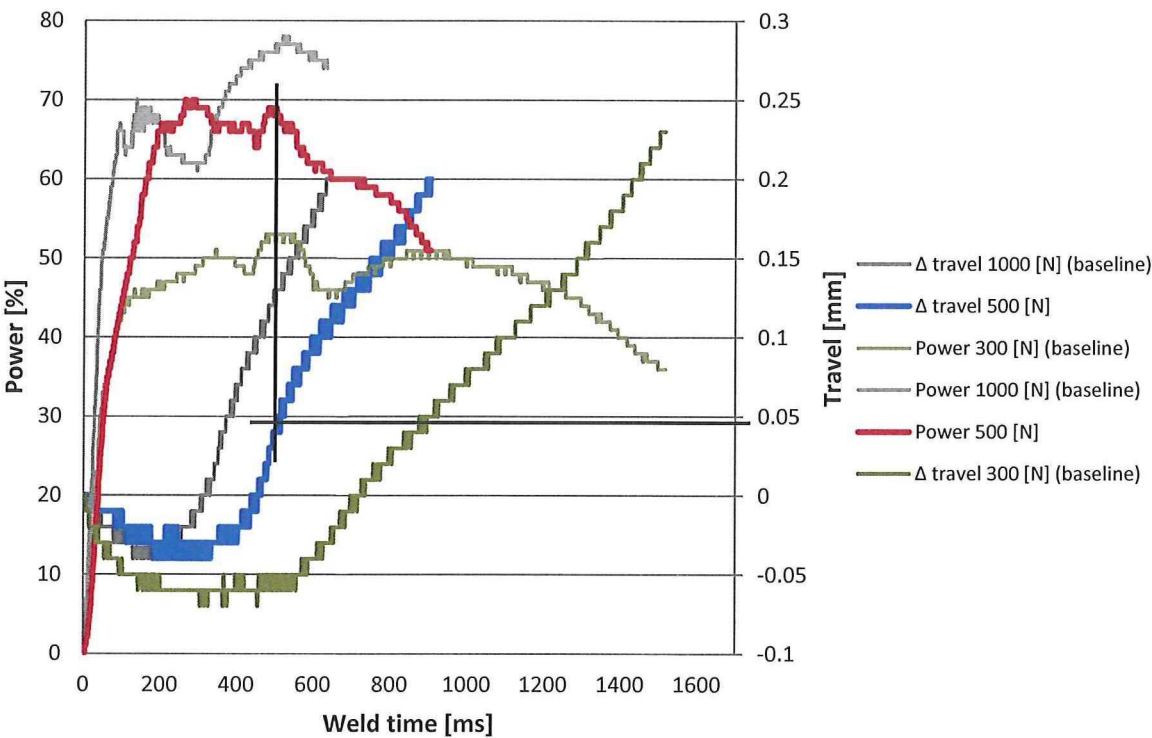


Figure 5-3 | Welding curve for the welding of a 14.9 [mm] overlap 100 [%] travel weld using the rectangular sonotrode, a welding force of 500 [N] and the 9110 jig, showing an optimum around 0.048 [mm] – 20 [%] travel (showing sample #79, appendix B) and a comparison to the baseline welding curves for 300 [N] and 1000 [N]

From the welding curve in Figure 5-3 an optimum travel of 20 [%] (i.e. 0.05 [mm]) was determined. With the 20 [%] travel (and the parameters of Table 5-1), 5 samples were welded. The results are compared to the values obtained for the baseline (welding forces of 300 [N] and 1000 [N]) welds for an overlap of 12.7 [mm] welded using the cylindrical 40 [mm] sonotrode, in Figure 5-4 and Table 5-2.

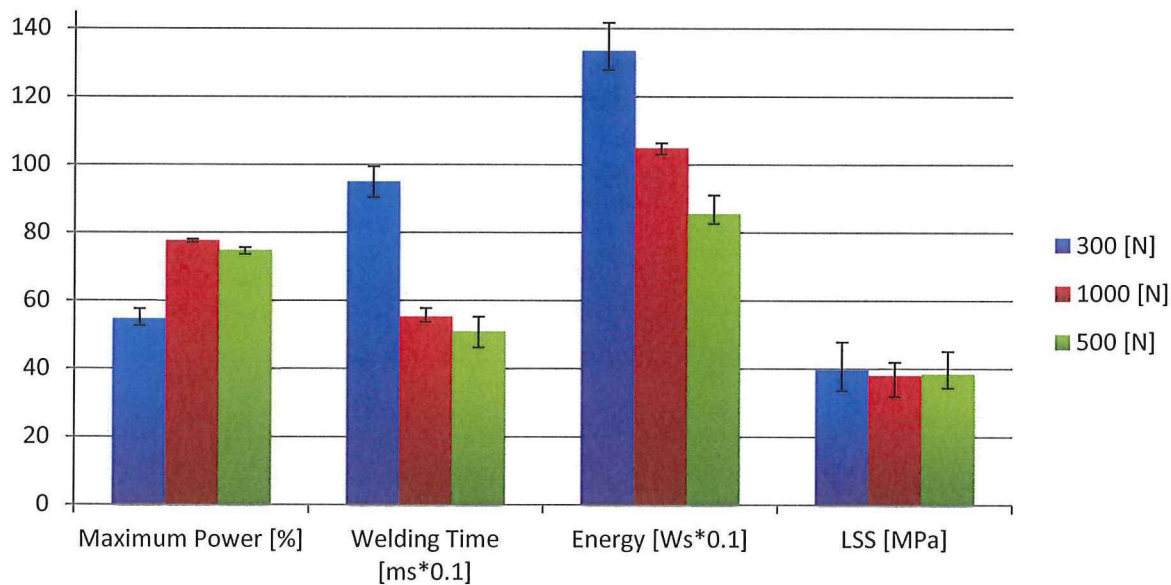


Figure 5-4 | Average values and range of values for the maximum power, welding time, energy dissipated and LSS, for optimal welding conditions using 300 [N] and 1000 [N] welding force for a standard 12.7 [mm] (cylindrical Ø 40 [mm] sonotrode, 9109 jig) overlap and 500 [N] for a 14.9 [mm] (rectangular sonotrode, 9110 jig) overlap

Table 5-2 | Average values and  $c_v$  for the maximum power, welding time, energy dissipated and LSS, for optimal welding conditions using 300 [N] and 1000 [N] welding force for a standard 12.7 [mm] (cylindrical Ø 40 [mm] sonotrode, 9109 jig) overlap and 500 [N] for a 14.9 [mm] (rectangular sonotrode, 9110 jig) overlap

|                            | Maximum Power [%]<br>( $c_v$ [%]) | Welding Time [ms]<br>( $c_v$ [%]) | Energy [Ws]<br>( $c_v$ [%]) | LSS [MPa]<br>( $c_v$ [%]) |
|----------------------------|-----------------------------------|-----------------------------------|-----------------------------|---------------------------|
| 300 [N],<br>30 [%] travel  | 55<br>(6.42)                      | 950<br>(5.75)                     | 1335<br>(4.95)              | 39.7<br>(4.71)            |
| 1000 [N],<br>65 [%] travel | 78<br>(2.16)                      | 553<br>(2.67)                     | 1049<br>(3.99)              | 38.0<br>(4.80)            |
| 500 [N],<br>20 [%] travel  | 75<br>(4.95)                      | 510<br>(6.59)                     | 855<br>(4.54)               | 38.5<br>(4.47)            |

Considering the values for the 500 [N] welding force, it can be seen that, although less significant, the maximum power utilized is still less than that of the 1000 [N] welding force and it does not reach the limits of the machine. Also the  $c_v$  for the LSS is slightly lower compared to the welded samples and with a lower  $c_v$  than for 300 [N] welding force. Overall it can be seen that the effect of changing the welding force does have a minimal effect on the obtained LSS. It is therefore decided to change to a 500 [N] (and 250 [N/s] rise of force) welding force while keeping the other values identical.



5.2 Thin energy directing surfaces

For the experiments considered in section 5.1 where zero or low travel is used, it might prove useful for the parts to be joined to already be closer to each other. This could mean the chance of unwanted loads (i.e. bending or peel forces) in the joint could decrease, making the design process easier. Experiments were carried out with the same conditions as in the baseline experiments, for an overlap of 12.7 [mm], with the only difference of only using one layer PEEK (Toho Tenax) film as ED, with a thickness of 0.12 [mm]. One 100 [%] travel weld was created using a welding force of 300 [N] and one using a welding force of 1000 [N]. All the welding parameters are summarized in Table 5-3. The welding curves are shown in Figure 5-5, compared to a baseline curve for 1000 [N] welded with a 2 layer, 0.23 [mm], ED in the 9109 jig.

Table 5-3 | Overview of the materials used (TT = Toho Tenax), sonotrode used and the welding parameters for the welding of samples using 1 layer ED (0.12 [mm]) in the 9109 jig

|                  |           | I) Initial Phase    | II) Vibration Phase |                     |                           |                       | III) Solidification Phase |                   |
|------------------|-----------|---------------------|---------------------|---------------------|---------------------------|-----------------------|---------------------------|-------------------|
| Materials        | Sonotrode | Rise of Force [N/s] | Weld. Force [N]     | Rise of Force [N/s] | Amplitude [μm] (set. [-]) | Controlling Parameter | Force                     | Holding Time [ms] |
| TT weave – weave | Ø 40 [mm] | 300                 | 300                 | 0                   | 86.2 (9)                  | Travel                | 1000                      | 4000              |
| TT weave – weave | Ø 40 [mm] | 500                 | 1000                | 0                   | 86.2 (9)                  | Travel                | 1000                      | 4000              |

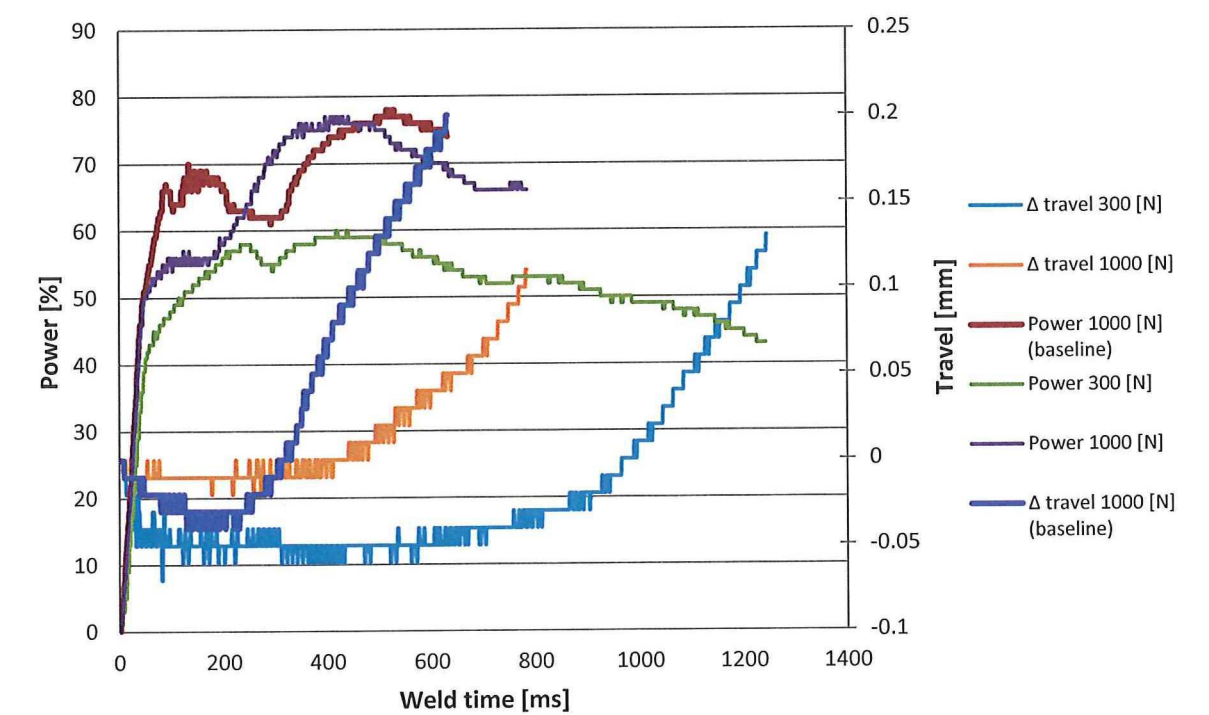


Figure 5-5 | Welding curves for 1 layer (thin, 0.12 [mm]) ED welds using melting on 100 [%] travel for 300 [N] and 1000 [N] using the 9109 jig, showing samples #20, #21 (appendix B) compared to the 100 [%] travel baseline (1000 [N]) welded sample with a 2 layer, 0.23 [mm] ED (sample #10)

The welding curves in Figure 5-5 of the samples welded with a thin ED do not resemble the regular curves found for the baseline welds. No clear power peak is visible in the beginning of the process and the expected power ramp up of stage 3, where the travel normally increases (onset of flow), cannot be distinguished as well. One of the reasons might be the volumetric heating process (one layer has relative more volume per area, although the total volume is less) and the fact that the absolute strain is lower for one layer of ED. Since the thin ED has relative more volume per area this might influence the through thickness heating and growth of hotspots. The lower absolute strain might however decrease this effect, both affecting the power curves. It is hard to say which factors are responsible for the different power curves, so further research is needed. Since the up-scaling could as well be achieved with thicker (regular) ED it was decided to not further research the effect of thin ED on the welding process.

5.3 Spot welding in a larger overlap area with zero (low) travel using energy as the controlling parameter

One of the concepts proposed for the up-scaling of USW, is to create a spot weld in the middle of a large overlap as described in section 5.1. As explained, initially two preliminary experiments are carried out to investigate if it is possible to create a fusion bond with zero travel. The average energy dissipated found in the baseline for a travel controlled weld using 1000 [N] welding force was around 1000 [Ws] (Table 3-2). This value was used as welding parameter for the energy controlled weld. All welding parameters are summarized in Table 5-4.

Table 5-4 | Overview of the material used (TT = Toho Tenax), sonotrode used and input settings for the USW machine for the zero travel welding using the 9109 jig using 0.24 [mm] Toho Tenax EDs

|                     |           | I) Initial Phase    | II) Vibration Phase |                     |                              |                       | III) Solidification Phase |                   |
|---------------------|-----------|---------------------|---------------------|---------------------|------------------------------|-----------------------|---------------------------|-------------------|
| Materials           | Sonotrode | Rise of Force [N/s] | Welding Force [N]   | Rise of Force [N/s] | Amplitude [µm] / setting [-] | Controlling Parameter | Force                     | Holding Time [ms] |
| TT weave<br>– weave | Ø 40 [mm] | 500                 | 1000                | 0                   | 86.2 (9)                     | Energy:<br>1000 [Ws]  | 1000                      | 4000              |

The samples are shown in Figure 5-6 A and B, following the method described in section 5.1. Since this sample could not be used for lap shear testing, the weld surface was inspected by manually breaking the weld open using a (small) pry tool and is shown in Figure 5-6 C.

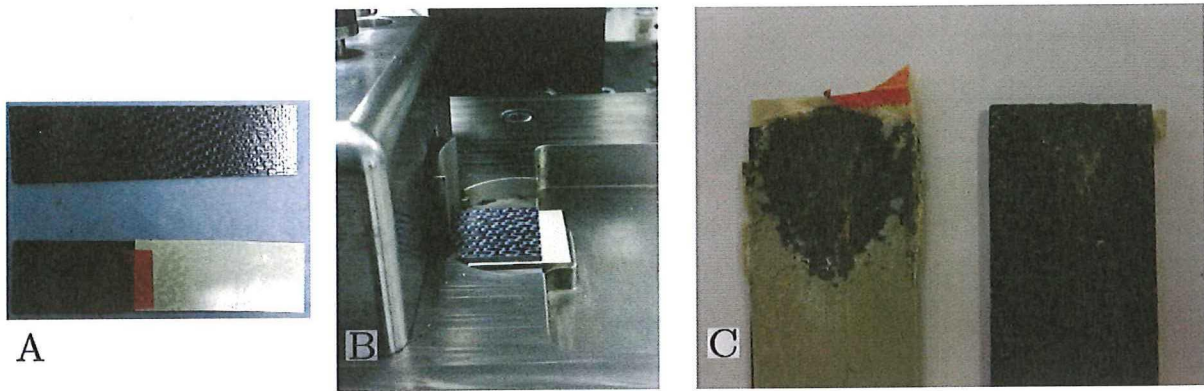


Figure 5-6 | Experiment for zero travel energy controlled welding of a larger overlap with, A) the large ED placement, B) the welding setup and C) the fracture surfaces, showing sample #19 (appendix B)

Opening the weld took quite some effort, indicating that certainly some fusion bonding has occurred in the overlap. As shown in Figure 5-6, the welding surface clearly shows molten ED at the part of the overlap affected by the sonotrode, indicating fusion bonding. The weld appears to be a bit hot at the centre of the overlap, indicated by some darker molten ED, which might indicate some oxidation. Also some molten ED can be noticed at the edges, even at the part where the ED adjacent to the edge is not molten yet (as can be seen in the left and right lower corner of the sample in Figure 5-6 C). The welding curves for these welds, shown in Figure 5-7, show similar results and indeed only show negative travel (upward movement of the sonotrode), which might indicate some hammering during the entire vibration phase. This negative travel, however, is seen for most of the other welding curves as well. The negative travel also has the same magnitude compared to the baseline welding curves. For the welding parameters used, it shows that it is possible to form a fusion bond with zero travel using USW.



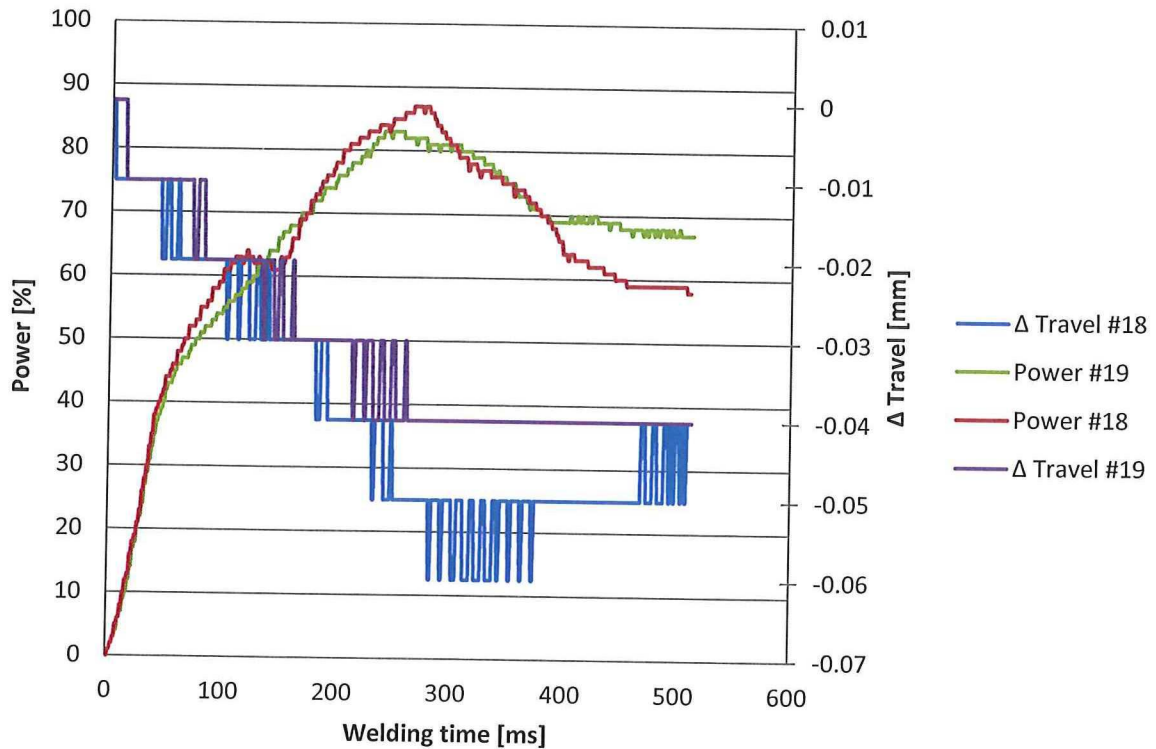


Figure 5-7 | Power and travel curves of samples #18 and #19 (appendix B) for the energy controlled zero travel welding of a larger overlap

Since the energy controlled zero travel welding proved possible, the second experiment can be conducted. For this experiment, using the rectangular sonotrode to create spot welds of 14.9 [mm] · 25.4 [mm] in the middle of a 25.4 [mm] · 25.4 [mm] overlap, first the average energy for optimum welding conditions is determined as described in section 5.1. Using the Toho Tenax material, the rectangular sonotrode and the regular travel controlled process (all other welding parameters are summarized in Table 5-5), a melting on 20% travel was found to be the optimum condition for an overlap of 14.9 [mm].

Table 5-5 | Overview of the materials used (TT = Toho Tenax), sonotrode used and the welding parameters for the welding experiments for the energy determination needed for the energy controlled spot welding using TT 2 layer, 0.24 [mm], EDs and the 9110 jig

|                  |                            | I) Initial Phase    | II) Vibration Phase |                     |                           |                       | III) Solidification Phase |                   |
|------------------|----------------------------|---------------------|---------------------|---------------------|---------------------------|-----------------------|---------------------------|-------------------|
| Materials        | Sonotrode                  | Rise of Force [N/s] | Weld. Force [N]     | Rise of Force [N/s] | Amplitude [μm] (set. [-]) | Controlling Parameter | Force                     | Holding Time [ms] |
| TT weave – weave | Rectangular 14.9 · 30 [mm] | 250                 | 500                 | 0                   | 84.6 (3)                  | Travel, opt.: 20 [%]  | 1000                      | 4000              |

With the 20 [%] travel 5 samples were welded, giving an average welding energy of 855 [Ws]. All the output data and their  $c_v$  are presented in Table 5-6 and all the welding and LSS curves can be found in appendix F. The scatter for the energy is low ( $c_v = 4.54$  [%]) almost identical to the

scatter for the LSS as can be seen in Table 5-6, making the values useful for the spot welding in the middle of a larger overlap.

Table 5-6 | Average values and  $c_v$  for the maximum power, welding time, energy dissipated and LSS, for optimal welding conditions using a 500 [N] welding force for a 14.9 [mm] (rectangular sonotrode) overlap

|                           | Maximum Power [%]<br>( $c_v$ [%]) | Welding Time [ms]<br>( $c_v$ [%]) | Energy [Ws]<br>( $c_v$ [%]) | LSS [MPa]<br>( $c_v$ [%]) |
|---------------------------|-----------------------------------|-----------------------------------|-----------------------------|---------------------------|
| 500 [N],<br>20 [%] travel | 75<br>(4.95)                      | 510<br>(6.59)                     | 855<br>(4.54)               | 38.5<br>(4.47)            |

Using the 855 [Ws] energy setting, the energy controlled spot (strip) welds in the centre of a larger overlap are created using the rectangular sonotrode as described in section 5.1. All welding parameters are summarized in Table 5-7. The welding curves for an energy controlled weld in this experiment, compared to the curves for a regular travel controlled process, are shown in Figure 5-8.

Table 5-7 | Overview of the materials used (TT = Toho Tenax), sonotrode used and the welding parameters for the welding experiments for the energy welded spot in the middle of a larger overlap, using TT 2 layer, 0.24 [mm], EDs and the 9110 jig

|                     |                               | I) Initial Phase    | II) Vibration Phase |                     |                              |                           | III) Solidification Phase |                   |
|---------------------|-------------------------------|---------------------|---------------------|---------------------|------------------------------|---------------------------|---------------------------|-------------------|
| Materials           | Sonotrode                     | Rise of Force [N/s] | Weld. Force [N]     | Rise of Force [N/s] | Amplitude [μm]<br>(set. [-]) | Controlling Parameter     | Force                     | Holding Time [ms] |
| TT weave<br>– weave | Rectangular<br>14.9 · 30 [mm] | 250                 | 500                 | 0                   | 84.6 (3)                     | Energy, opt.:<br>855 [Ws] | 1000                      | 4000              |

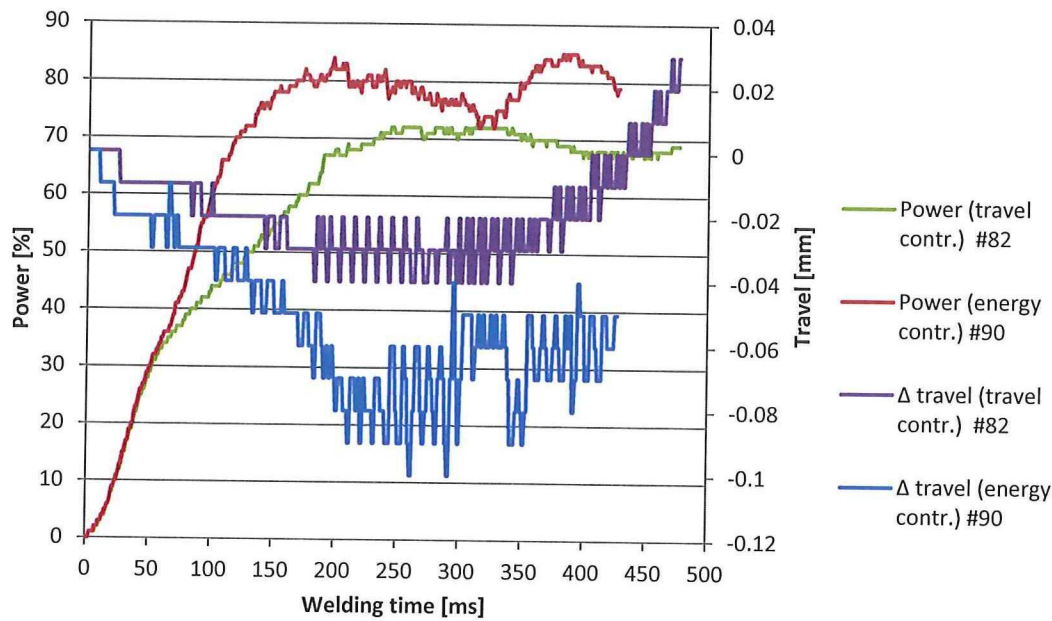


Figure 5-8 | Welding curves for the travel controlled process for energy determination and the energy controlled process for the zero travel welding of a spot in a larger overlap, showing sample #82, travel welded, and #90, energy spot welded, (appendix B)

Looking at Figure 5-8, it can be seen that the travel curve for the spot weld shows more vibration and more negative values than the travel controlled weld. This could indicate more hammering in the spot welding case. This could be caused by the fact that the surrounding material is not melting and restricting downward movement (positive travel) of the sonotrode, however, further research is needed. This also seems to cause slightly higher maximum power levels (the shorter weld time even it out with the amount of energy required for the welded area).

Both sets are also tested for LSS, the curves are shown in Figure 5-9. It can be seen that the stress strain curves of the spot welded samples are less consistent in terms of failure strength than the curves of the travel controlled welded samples. An overview of the average value for LSS, welding distance (complete travel during the vibration and solidification phase), maximum power used, weld time and their  $c_v$  is provided in Figure 5-10 and Table 5-8.

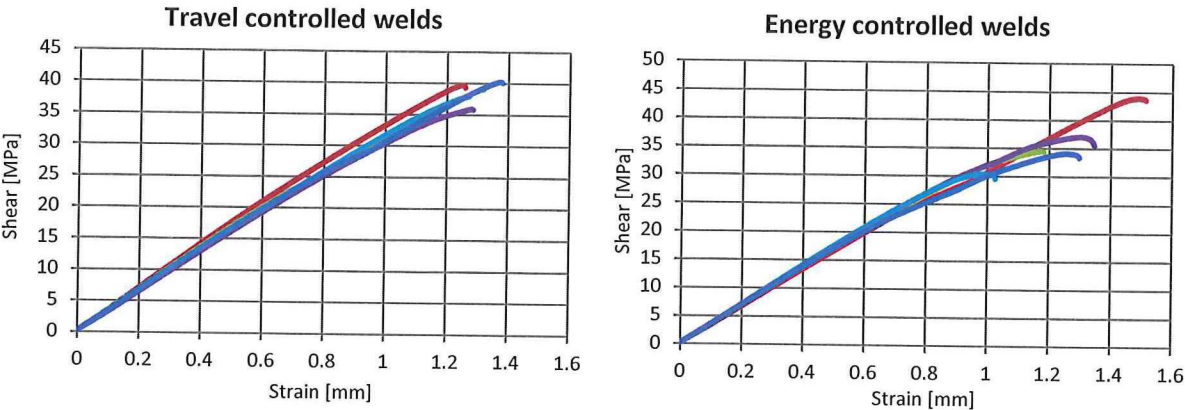


Figure 5-9 | Stress – strain curves depicting the LSS for regular travel controlled welded samples (used for energy determination) and the energy controlled zero travel spot welds of a larger overlap



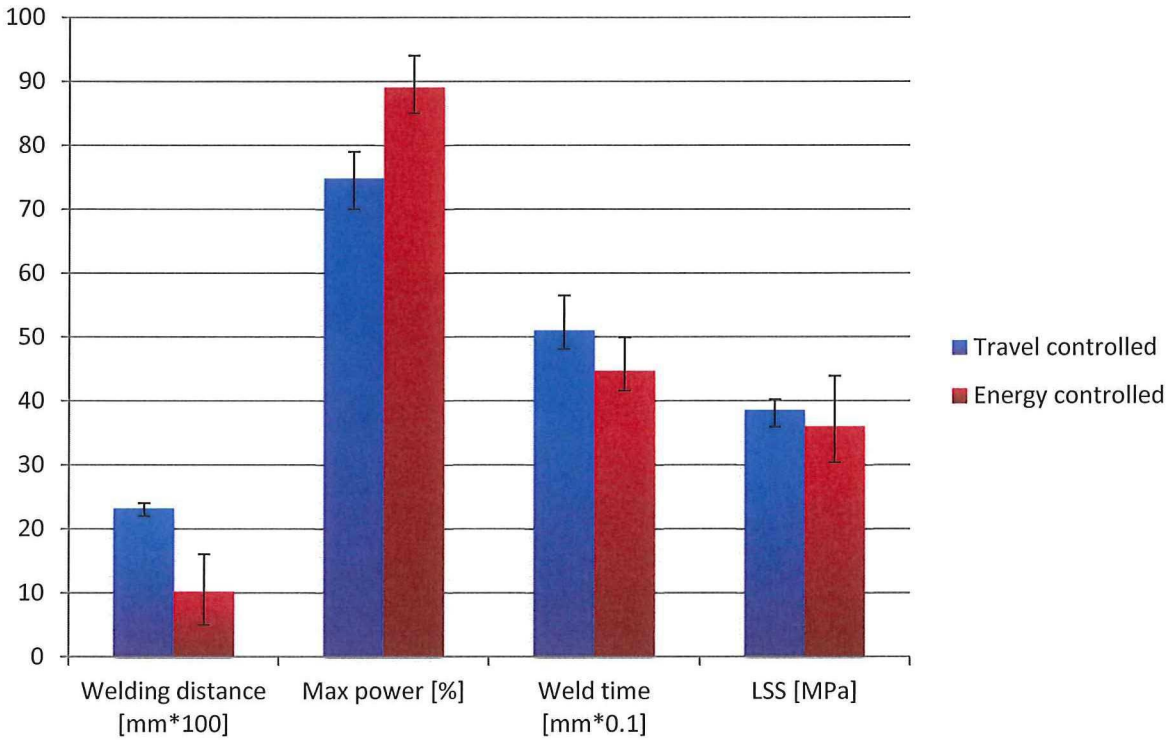


Figure 5-10 | Difference in average values for welding parameters comparing the regular travel controlled welds with energy controlled spot welds

Table 5-8 | Average values and their  $c_v$  for welding parameters comparing the regular travel controlled welds with energy controlled spot welds

|                   | Welding distance [mm]<br>( $c_v$ [%]) | Max power [%]<br>( $c_v$ [%]) | Weld time [ms]<br>( $c_v$ [%]) | LSS [MPa]<br>( $c_v$ [%]) |
|-------------------|---------------------------------------|-------------------------------|--------------------------------|---------------------------|
| travel controlled | 0.23 (3.61)                           | 75 (4.95)                     | 510 (6.59)                     | 38.5 (4.47)               |
| energy controlled | 0.10 (52.5)                           | 89 (3.97)                     | 447 (7.07)                     | 36.0 (14.0)               |

Evaluating Figure 5-10 and Table 5-8, several things are noted. Firstly, it can be seen that the maximum power used and weld time show a clear difference for the regular travel controlled process compared to the energy controlled spot weld. The increase in power is cancelled by the reduced weld time for the energy welded samples. Secondly the welding distance (total travel measured during the vibration phase and the solidification phase), decreased by more than 50 [%] to an average of 0.1 [mm]. Although the displacement during welding (the vibration phase) only shows hammering or negative travel, during solidification (when the force increases to 1000 [N]) some minor travel is still present. This average travel, however, is identical to the compression in [mm] of the samples and ED found for applying an external force of 1000 [N] with the sonotrode. This was tested by applying increasing force with the rectangular sonotrode, on two (not welded) Toho Tenax samples with ED in between, using the ADJUST mode on the ACU and manually collecting the corresponding displacement. The results are shown in Figure 5-11. It can be seen in Figure 5-11 that for 1000 [N] the compression is slightly higher than 0.1 [mm], which could mean the total travel (welding distance) found for the energy welded samples, is only the result of the compression of the samples under the applied force which is 1000 [N] during the solidification

phase. This is not confirmed however. Finally, it can be seen that the variation and the  $c_v$  for the LSS is far higher for the spot welded samples (213 [%] more compared to the travel controlled samples). This inconsistency is not ideal for up-scaling, and is investigated further by analysing of the fracture surfaces, shown in Figure 5-12.

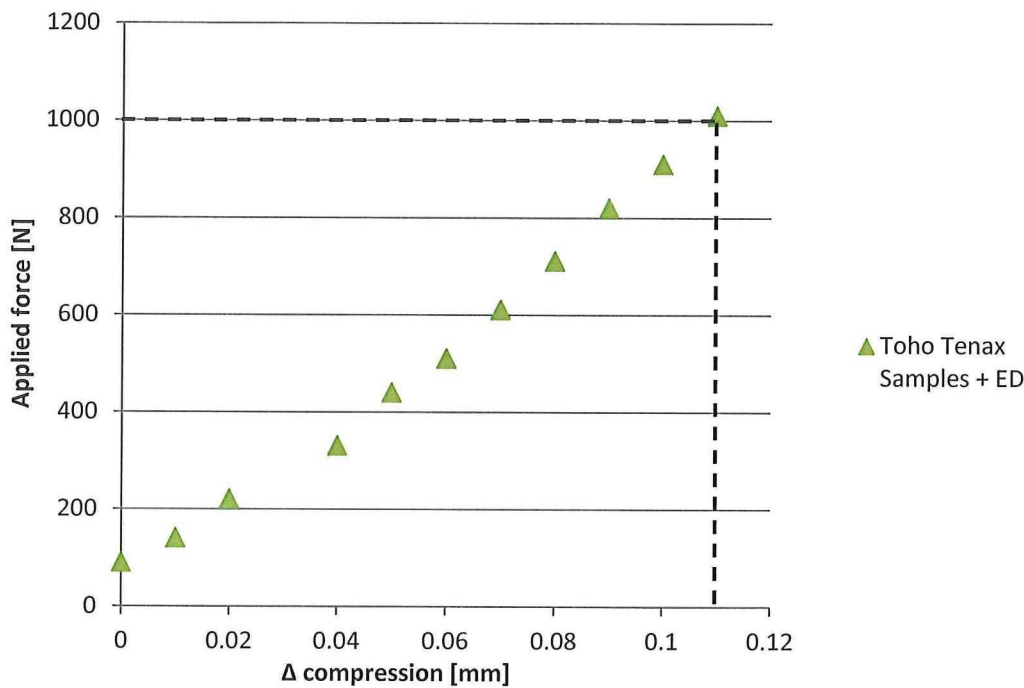


Figure 5-11 | Relative compression due to the applied force of the rectangular sonotrode for Toho Tenax samples with a 2 layer (0.24 [mm]) ED, highlighting the compression related to a force of 1000 [N]



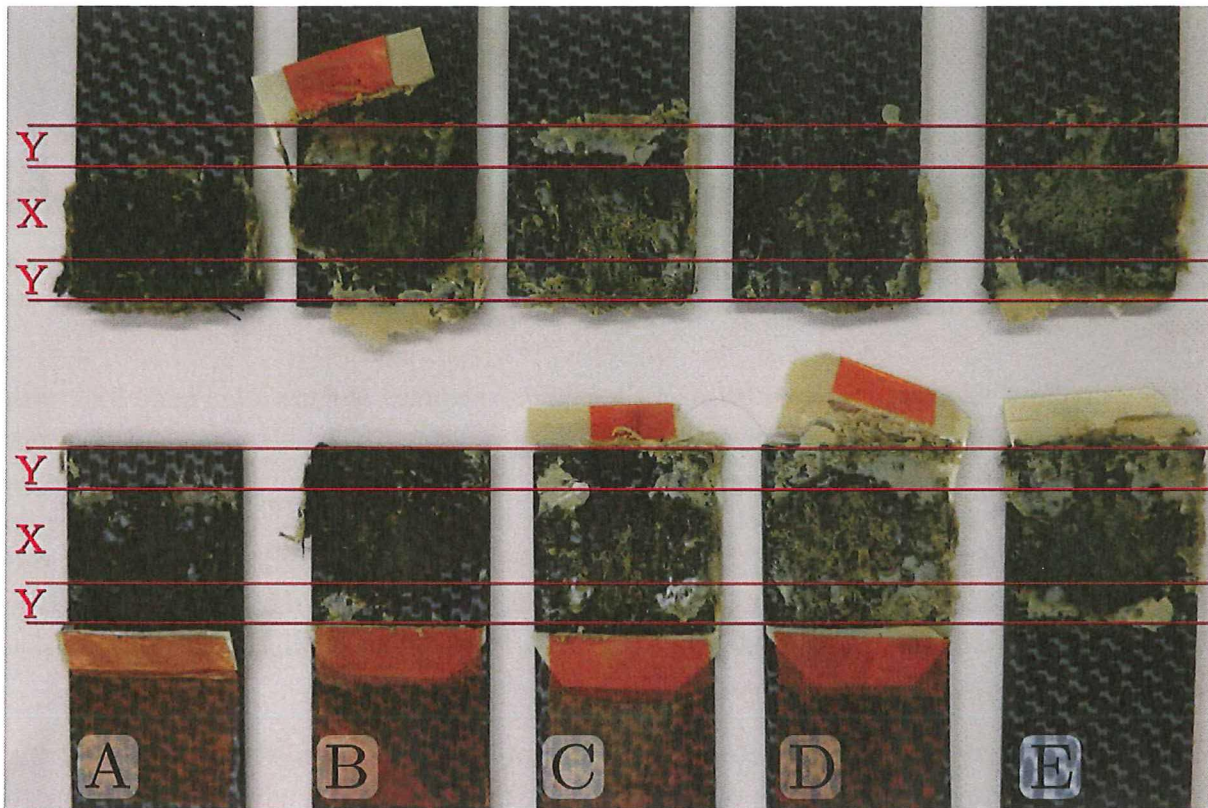


Figure 5-12 | Fracture surfaces for energy controlled zero travel spot welds in a larger overlap showing sample A-E (#88 - #92, appendix B), where X shows the area of the overlap directly affected by the sonotrode (14.9 [mm]) and Y the remainder of the total overlap (10.5 [mm])

Looking at Figure 5-12, it can be seen that the welded areas differ in size for each weld, explaining the inconsistencies in LSS. Since it is calculated dividing the force over the expected welded area (the area covered by the sonotrode), which is different from the actual welded area. The fact that the welded areas are not consistent and do not match the area covered by the sonotrode is deemed to come from the high stiffness of the TPC material. Although the stiffness is less than that of the complete welding system, the TPC material is stiff enough to transfer a part of the oscillating motion of the sonotrode (welding energy) to other areas, initiating melting. This means that the welding force is also redistributed over a larger area to some extent, resulting in a relatively lower pressure. The edge effects and the weld in the centre of the overlap are more closely analysed using optical microscopy, shown in Figure 5-13. It can be clearly seen that welding is initiated at the edges of the overlap as well, where the interfacial friction is the highest. Also the centre of the weld shows many bubbles, which affects the LSS as well. These bubbles could be due to a relative shortage of pressure during welding and solidification (which is restricted due to the not molten material around the welding area), or due to overheating of the centre of the weld. Overheating seems a bit unlikely, since the amount of energy delivered is limited (energy controlled process) and the cross section does not depict any signs of through the thickness heating of the samples which should be expected. However, further research would be needed.



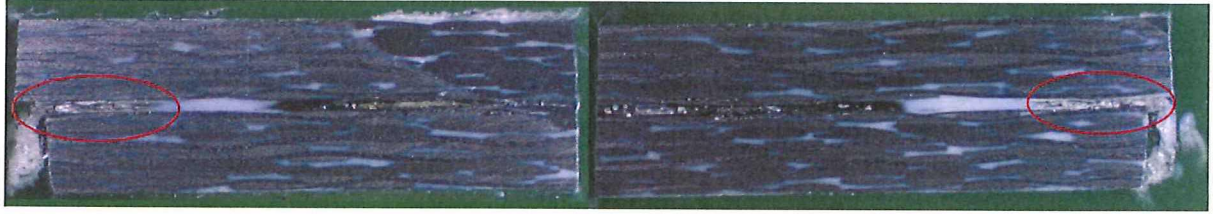


Figure 5-13 | 1.25x enlarged image of the cross-section of sample #87 (appendix B) zero travel welded using energy as controlling parameter, showing the edge effect and bubble forming in the centre of the weld

There are some differences observed between the initial experiment (Figure 5-1, Figure 5-6), with the two samples directly overlapping each other with a large ED in between, and the spot welding of the larger overlap. The initial experiment had more benefit of this mentioned edge effect, due to the fact that it was not a spot weld but had 3 edges free at the overlap. Next to that, due to the different configuration for the initial experiment in the 9109 jig which clamped the a large part of the two samples, might have damped the vibration in the sample further away from the area covered by the sonotrode to some extent. This could also reduce the effect of fusion bonding in areas away from area covered by the sonotrode.

Considering the results for this proposed welding concept it can be concluded that is spot welding of two parts whose joining areas are completely covered with ED is not advised. This is due to the fact that the stiffness of the TPC samples aids in the welding of the complete overlap, resulting in inconsistent LSS results. Up-scaling might increase the inconsistency since the area that might be unintentionally affected increases as well. The melting of the ED at different locations than the area covered by the sonotrode (especially at the edges of the overlap), however, could be decreased by using sufficient damping as stated in literature [7]. As explained in section 2.2.3, it was found to be possible to pre-attach one layer of film to either plate material or to the hinge. The process is, however, time and energy consuming. Although the process could be optimized and automated, it still would consume much time and energy compared to manual attachment. Combined with the unsatisfying results for the zero travel spot welding of a larger overlap, it was decided not to use this process.

#### 5.4 Experiment design for area sized energy director welding

A second concept considered, a variation on the spot welding of a larger overlap, is the use of a dedicated area sized ED for welding. In this setup the ED does not cover the entire overlap, but only occupies the area covered by the sonotrode, schematically shown in Figure 5-14. The geometry of the overlap is identical to the experiment designed for the spot welding of the larger overlap. The EDs in this setup are attached in a small strip covering only the designated area by taping them to the welding jig as shown in Figure 5-14. The results of this welding approach are compared to the ones from the spot welding of a larger overlap and to the baseline.

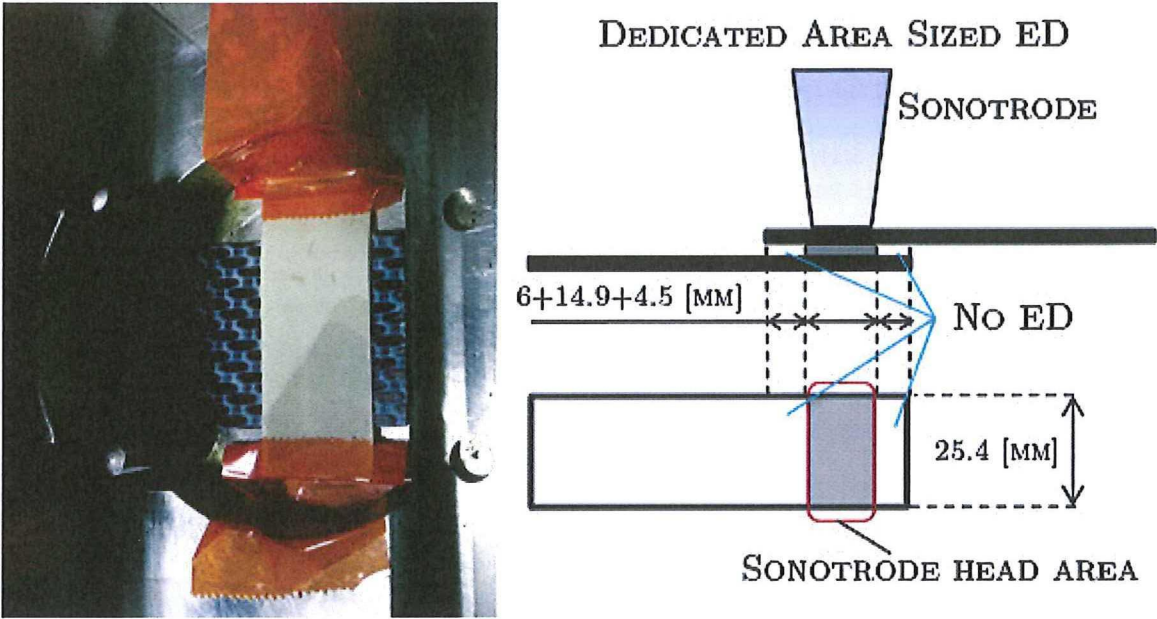


Figure 5-14 | Dedicated ED size welding showing ED attachment to the jig on the left and a schematic view on the right

5.5 Dedicated area sized energy director spot welding

Different from the approach for the spot weld of a larger overlap, where the entire overlap is covered with ED, for this experiment only a small area is covered with ED, equal to the area that is directly affected by the sonotrode. The alignment of the ED, as described in section 5.4, requires a bit more effort compared to the energy spot weld of the larger overlap (where the ED simply covers the entire overlap). This process could however be automated.

Although the results for the welds made with Ten Cate material showed more variation in energy dissipation compared to the Toho Tenax material (section 4.4), the Ten Cate material is used in this experiment due to the limited sample availability of the Toho Tenax material. Since section 4.4 also showed that the average energy dissipation for Toho Tenax and Ten Cate material does not differ significantly, the optimum energy was not redefined. However, the determined weld energy of 855 [Ws] of section 5.3 (Toho Tenax material) was used to weld a Ten Cate sample in the standard configuration with 14.7 [mm] overlap (comparable to the baseline welds, having only an overlap of the area that is going to be welded). This resulted in a LSS of 43 [MPa] which was deemed expectable. The dedicated area sized ED welds were therefore created with 855 [Ws] as well. All the welding parameters are summarized in Table 5-9. The welding curves for these welds are shown in Figure 5-15 (all separate data can be found in appendix G).



Table 5-9 | Overview of the materials used (TC = Ten Cate), sonotrode used and the welding parameters for the welding experiments for the energy welded dedicated area sized ED, using TC 5 layer, 0.25 [mm], EDs and the 9110 jig

|                     |                               | I) Initial Phase    | II) Vibration Phase |                     |                           |                           | III) Solidification Phase |                   |
|---------------------|-------------------------------|---------------------|---------------------|---------------------|---------------------------|---------------------------|---------------------------|-------------------|
| Materials           | Sonotrode                     | Rise of Force [N/s] | Weld. Force [N]     | Rise of Force [N/s] | Amplitude [μm] (set. [-]) | Controlling Parameter     | Force                     | Holding Time [ms] |
| TC weave<br>- weave | Rectangular<br>14.9 · 30 [mm] | 250                 | 500                 | 0                   | 84.6 (3)                  | Energy, opt.:<br>855 [Ws] | 1000                      | 4000              |

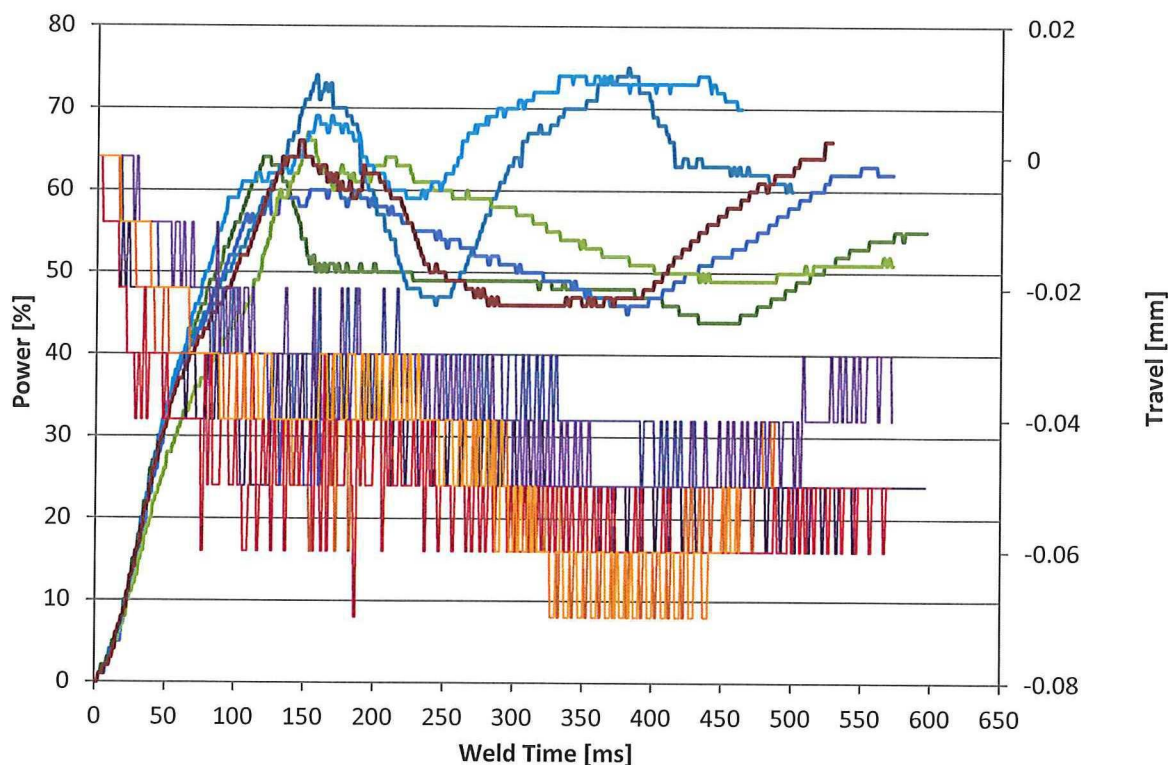


Figure 5-15 | Welding curves for the welding of dedicated area sized ED welds of samples #100 - #106 (appendix B)

Looking at Figure 5-15 it is observed that the power curves are somewhat inconsistent relative to each other. Two samples seem to have a (second) power peak at 350 [ms], where the other welds seem to reach this peak a bit later at 550 [ms] towards the end of the vibration phase. Furthermore there appears to be a peak around 150 [ms] into the weld for the power curve, where the travel curve stays constant around -0.04 [mm] for some time, after which the travel decreases further and the power usage rises again. Figure 5-16 shows two of the dedicated area sized ED welding curves compared to the curves of the travel controlled weld and the spot weld of the larger overlap (welding parameters seen in Table 5-5 and Table 5-6). The first peak is believed to be similar to travel controlled curves for the onset of welding, and the remainder of the power curve looks similar to the ones found for travel controlled welds as well. The second peak in the power curves for travel controlled welds is attributed to the part where the ED starts to flow. However, as can be seen in Figure 5-15 and Figure 5-16, the travel stays negative for the



dedicated area sized ED welds. This might be caused by the flow fronts around the ED which could restrict the downwards displacement of the sonotrode. However, further research into these effects is necessary.

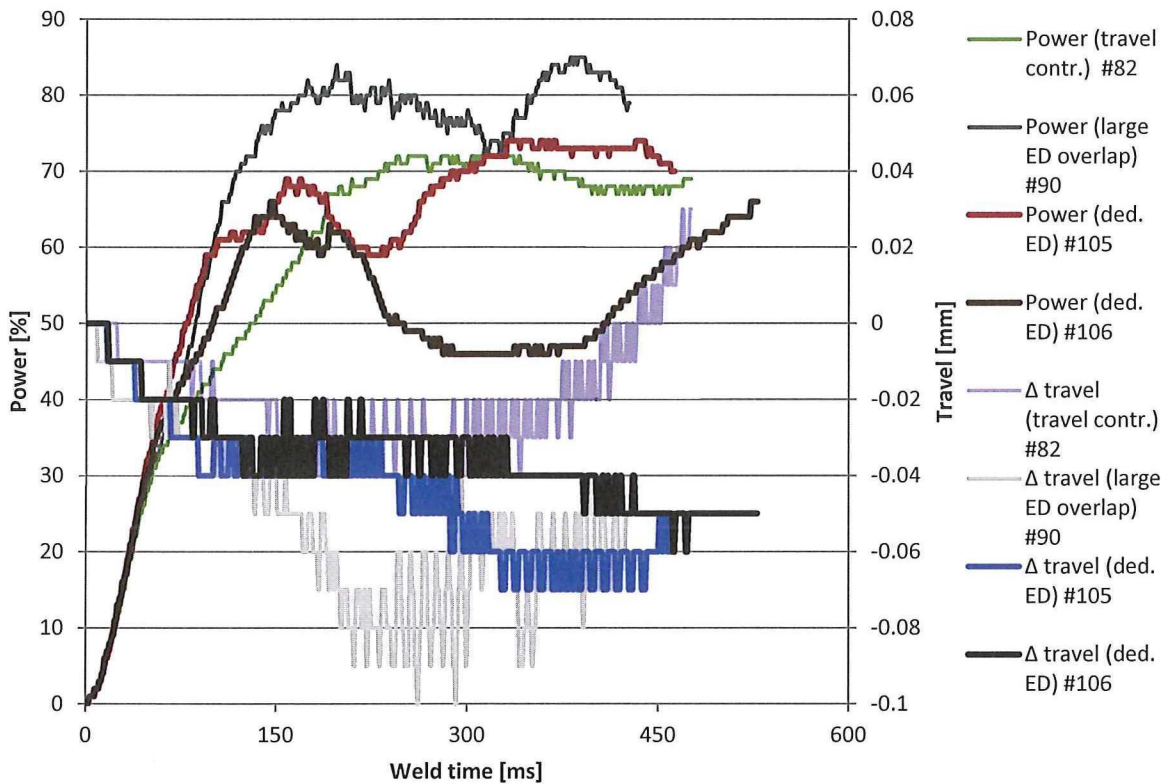


Figure 5-16 | Comparison of two different dedicated area sized ED welding curves (power & travel) with the travel controlled welding curves and the welding curves for the spot welding of the large overlap. All for Ten Cate samples and 5 layer (0.25 [mm]) ED, welded with the rectangular sonotrode, in the 9110 jig using a welding force of 500 [N]

Next to the welding curves, the average LSS and other output values of the dedicated area sized ED welds and their  $c_v$  are presented in Figure 5-17 and Table 5-10, compared to the travel controlled welds and the spot welds in the larger overlap. It can be seen that the average LSS is 23 [%] higher and the  $c_v$  is down to 11.9 [%], which is a decrease of 15.1 [%] compared to the spot weld of the larger overlap. Also the fracture surface analysis shows more consistency in the welded areas as can be seen in Figure 5-18. Figure 5-18 also shows however that for most welds the flow fronts of the molten ED are squeezed out of the area covered by the sonotrode.

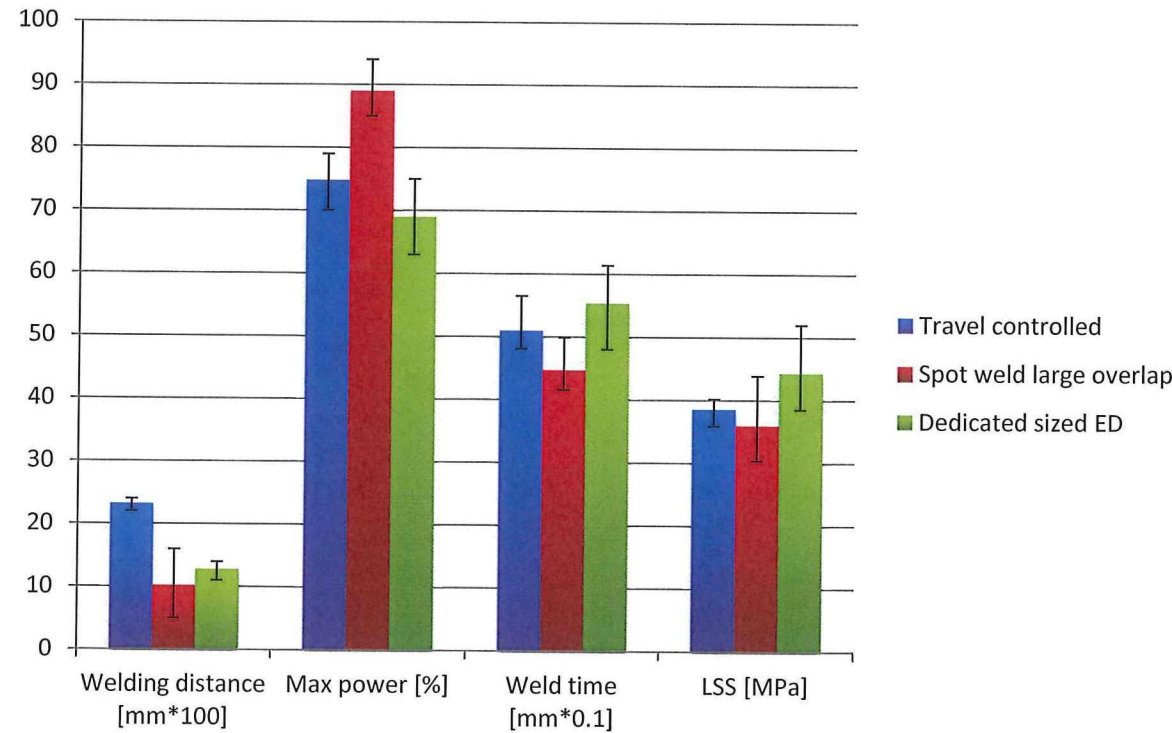


Figure 5-17 | Average and range values, comparing the regular travel controlled welds and the energy controlled spot welds of the larger overlap with the dedicated area sized ED welds

Table 5-10 | Average values and their  $c_v$  for welding parameters comparing the regular travel controlled welds and the energy controlled spot welds of the larger overlap with the dedicated area sized ED welds

|   | Welding distance [mm]<br>( $c_v$ [%]) | Max power [%]<br>( $c_v$ [%]) | Weld time [ms]<br>( $c_v$ [%]) | LSS [MPa]<br>( $c_v$ [%]) |
|---|---------------------------------------|-------------------------------|--------------------------------|---------------------------|
| Travel controlled<br>(normal 14.7 [mm]<br>overlap)  | 0.23 (3.61)                           | 75 (4.95)                     | 510 (6.59)                     | 38.5 (4.47)               |
| Energy controlled<br>(spot weld, in the<br>middle of a large<br>ED covered<br>overlap)        | 0.10 (52.5)                           | 89 (3.97)                     | 447 (7.07)                     | 36.0 (14.0)               |
| Energy controlled<br>(spot weld, with a<br>dedicated area<br>sized ED for a<br>large overlap) | 0.13 (10.2)                           | 69 (7.60)                     | 554 (9.85)                     | 44.4 (11.9)               |



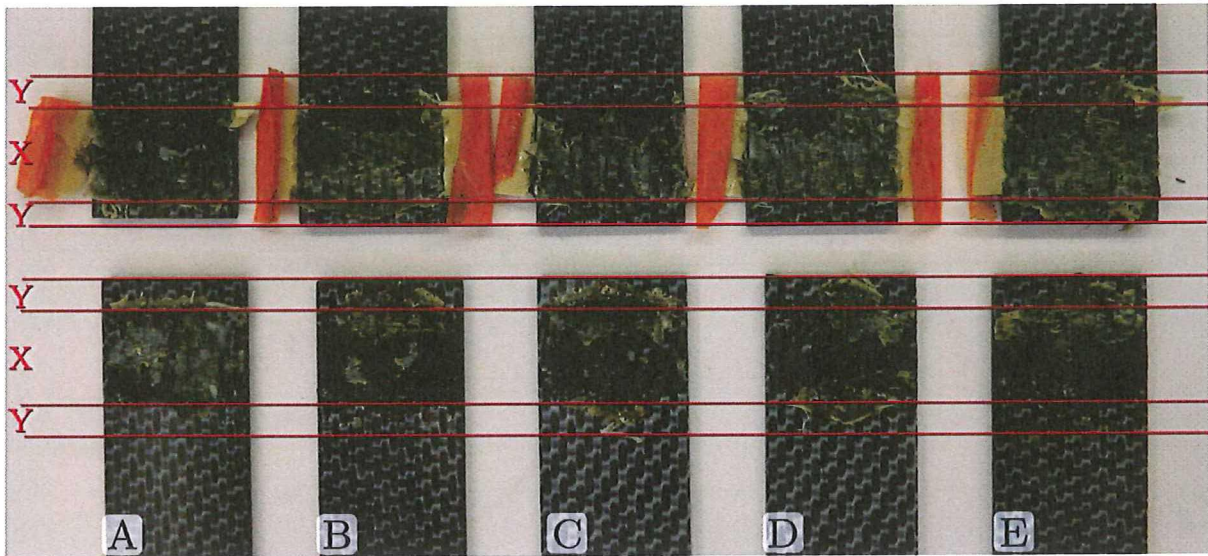


Figure 5-18 | Fracture surfaces of the dedicated area sized ED welded samples A – E: #101 – #105 (appendix B)

The results presented in the previous paragraph are promising, however they are still not as consistent as the results obtained with travel controlled welding. Since the ED has a starting thickness of around 0.24 [mm], there is space around the ED to melt and flow, it might be possible to use travel as the controlling parameter. Using travel might decrease the  $c_v$  even further. Therefore a preliminary investigation has been done into the possibilities for welding with travel. It is noted that, due to an error at the water jet cutting facility for these experiments only Ten Cate material with a 90 [°] apparent fibre direction was available. The first experiment was not successful in forming a weld, which was expected since it used the same welding force as the dedicated area sized ED welds of 500 [N], which showed only negative travel. The welding force seemed to be too low to get to the desired 100 [%] travel, and therefore overheated the overlap through the thickness (the sonotrode continued to input energy since the set value for travel was not reached). The welding force was raised from 500 [N] to 1000 [N] and the travel was decreased to 50 [%]. This allowed for the formation of a weld, but the welding curves are irregular as can be seen in Figure 5-19. The welding parameters for these experiments are summarized in Table 5-11.

Table 5-11 | Overview of the materials used (TC = Ten Cate 90 [°]), sonotrode used and the welding parameters for the welding experiments for the travel welded dedicated area sized ED, using TC 5 layer, 0.25 [mm], EDs and the 9110 jig

|                  |                            | I) Initial Phase    | II) Vibration Phase |                     |                           |                       | III) Solidification Phase |                   |
|------------------|----------------------------|---------------------|---------------------|---------------------|---------------------------|-----------------------|---------------------------|-------------------|
| Materials        | Sonotrode                  | Rise of Force [N/s] | Weld. Force [N]     | Rise of Force [N/s] | Amplitude [μm] (set. [-]) | Controlling Parameter | Force                     | Holding Time [ms] |
| TC weave – weave | Rectangular 14.9 · 30 [mm] | 250                 | 500                 | 0                   | 84.6 (3)                  | Travel 100 [%]        | 1000                      | 4000              |
| TC weave – weave | Rectangular 14.9 · 30 [mm] | 500                 | 1000                | 0                   | 84.6 (3)                  | Travel 50 [%]         | 1000                      | 4000              |



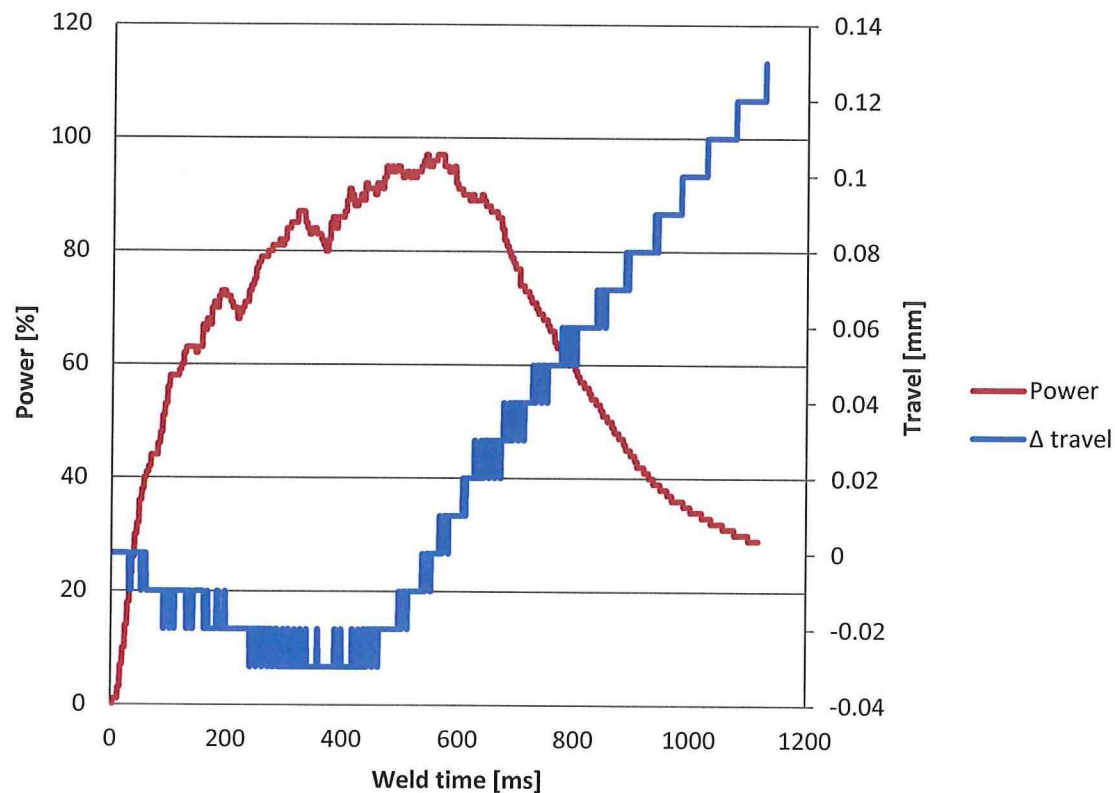


Figure 5-19 | Welding curves for sample #108 (appendix B), experiments for the dedicated area sized ED welding using travel with 1000 [N] welding force, 50% travel, the rectangular sonotrode and jig 9110 for Ten Cate samples with a 90 [°] apparent fibre direction

Looking at the welding curve in Figure 5-19 and at the welding overlap shown in Figure 5-20, it can be seen that for the higher force the flow fronts are completely squeezed out. The small peaks seen in the welding curve are therefore believed to come from the flow fronts around the molten ED (still between the samples), which flow for a short distance but then solidify due to the colder surrounding sample material. This requires an extra input of energy (the small peaks) to re-melt and flow them again until they are completely squeezed out. The solidification of the flow fronts is also deemed to be the cause of the problems that occurred with welding using travel for a 500 [N] welding force were the welding was unsuccessful. These weld fronts therefore prevent the use of travel as controlling parameter in this configuration. The travel observed in Figure 5-19 is attributed to the through thickness deformation seen in Figure 5-20, elaborated upon in the next paragraph. It could be researched if different shaped EDs might provide room for the fronts to flow, by not posing any restrictions to the displacement when they solidify.

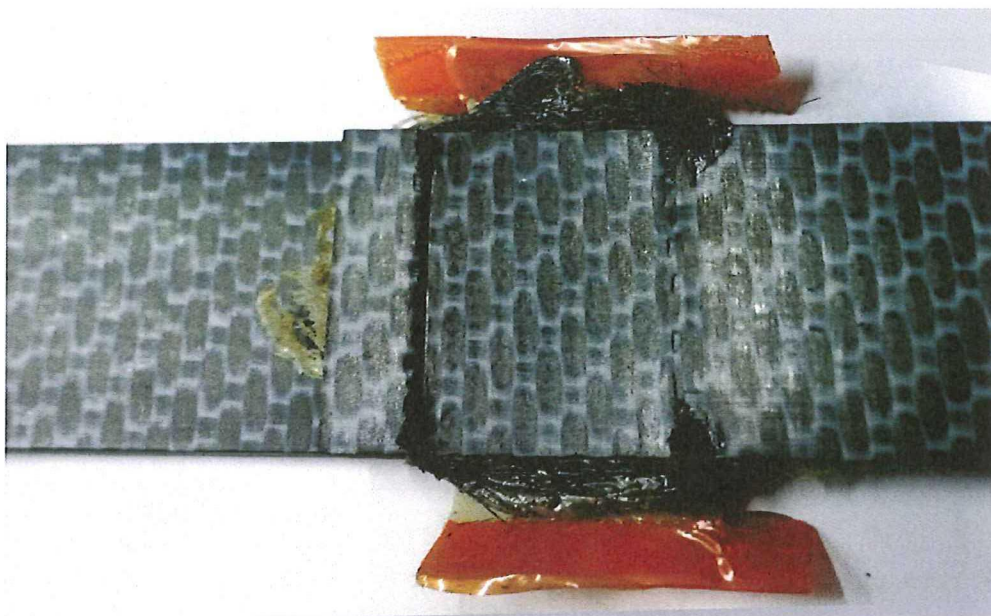


Figure 5-20 | Overlap for the #109 (appendix B) welded sample, showing surface damage and ED squeeze out on all sides

As stated, the overlap shown in Figure 5-20 also shows extensive surface deformation. This is believed to be caused by the overheating through the thickness, which allows for deformation of the samples under the high welding force and hammering loads. The fact that the rectangular sonotrode (with the straight edges on the overlap and a relative higher force / area) was used, might have amplified the surface deformations. The experiment was repeated with the  $\varnothing 40$  [mm] sonotrode. Since this sonotrode is larger than the used dedicated ED and large enough to cover the entire (large) overlap, it might affect the rest of the welding process as well. The difference found compared to the use of the rectangular sonotrode, was that less surface damage was formed, even more ED material got squeezed out of the overlap (since now the complete overlap is covered) and a higher maximum power was reached. The welding curves for 500 [N] (100% travel) and 1000 [N] (30 [%] travel) are shown in Figure 5-21. The 500 [N] the samples overheated more extensively than the samples welded with the rectangular sonotrode. For the 1000 [N] the flow front were complete squeezed out of the overlap. More importantly, using these welding parameters and this setup, the power levels of the USW machine are well exceeded as shown in Figure 5-21. Regardless of the sonotrode, it was concluded that due to the flow fronts of the molten ED, welding with travel as the controlling parameter is not possible for this setup.

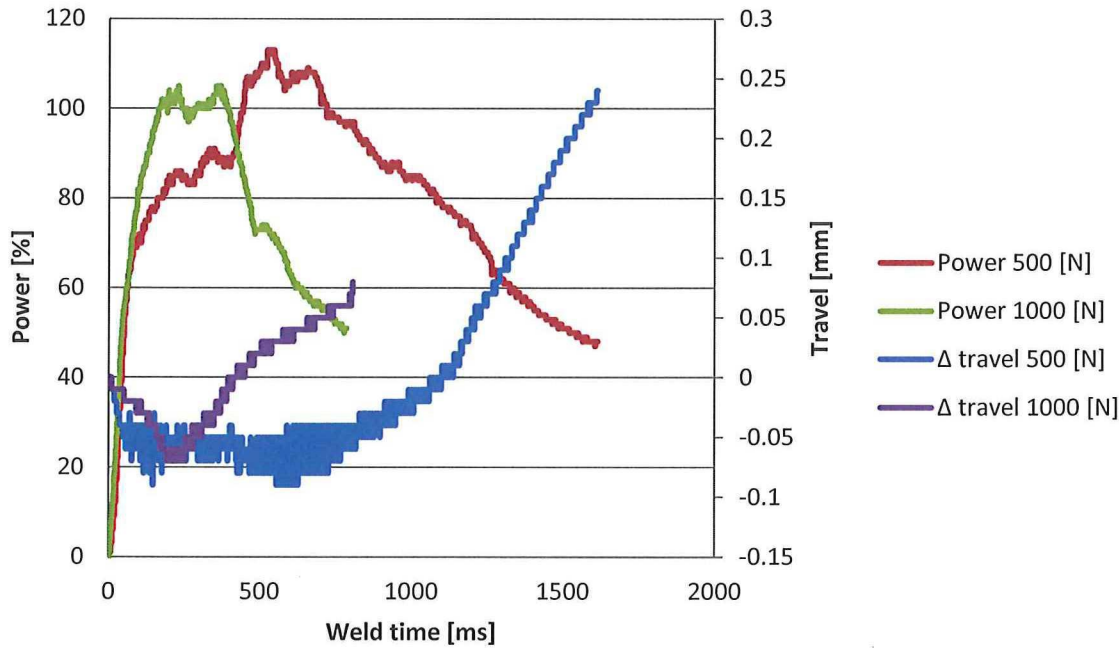


Figure 5-21 | Welding curves for the welding of a small ED with a larger sonotrode using the 9110 jig, 90 [°] Ten Cate weave and 5-layer (0.25 [mm] ED), with a welding force of 500 [N] and 100 [%] travel and 1000 [N] and 30 [%] travel (samples #119 and #121, appendix B)

The energy controlled process was used for an experiment welding dissimilar materials using a dedicated area sized ED as well. Again, however, only 90 [°] weave CF/PEEK Ten Cate material was available to weld to the chopped fibre samples. Therefore the results were only used as indication, to verify if the process works with dissimilar materials as well. The determined welding energy of 855 [Ws] was used again, since the energy needed was expected to be similar as explained in section 4.4. All the welding parameters are summarized in Table 5-12.

Table 5-12 | Overview of the materials used (TC = Ten Cate 90 [°], TT = Toho Tenax), sonotrode used and the welding parameters for the welding experiments for the travel welded dedicated area sized ED, using TC 5 layer, 0.25 [mm], EDs and the 9110 jig

|                       |                            | I) Initial Phase    | II) Vibration Phase |                     |                           |                       | III) Solidification Phase |                   |
|-----------------------|----------------------------|---------------------|---------------------|---------------------|---------------------------|-----------------------|---------------------------|-------------------|
| Materials             | Sonotrode                  | Rise of Force [N/s] | Weld. Force [N]     | Rise of Force [N/s] | Amplitude [μm] (set. [-]) | Controlling Parameter | Force                     | Holding Time [ms] |
| TC weave – TT chopped | Rectangular 14.9 · 30 [mm] | 250                 | 500                 | 0                   | 84.6 (3)                  | Energy 855 [Ws]       | 1000                      | 4000              |

Also for the dissimilar materials it was possible to form welds, however the average welding energy of 855 [Ws] was not enough to form completely welded areas, of which an example is shown in Figure 5-22. For the welding parameters and materials used in this setup, more energy was lost for the weave to chopped welded samples compared to the weave to weave samples for the dedicated area sized ED. Two welding curves for a weave to chopped weld are compared to the curves for a weave to weave weld in Figure 5-23, whereas all the curves for the weave to chopped welds are shown in Figure 5-24. Looking at Figure 5-23 it can be seen that the travel



curve for the weave to chopped weld show a twice as large vibration compared to the weave to weave weld. This trend can be seen for all the weave to chopped welds in Figure 5-24. This could be caused by hammering as a result of the different material properties for the chopped and Ten Cate 90 [°] material. However further research on the subject is required. As already mentioned, researching the effects (and possible reduction), of hammering could make the process more efficient. For this research it is noted that a higher welding energy is needed to get the desired welded area. All welding curves for these experiments can be found in appendix H.



Figure 5-22 | Typical fracture surface for the welding of weave (Ten Cate 90 [°]) to chopped fibres using the dedicated area sized ED welding (sample #117, appendix B)

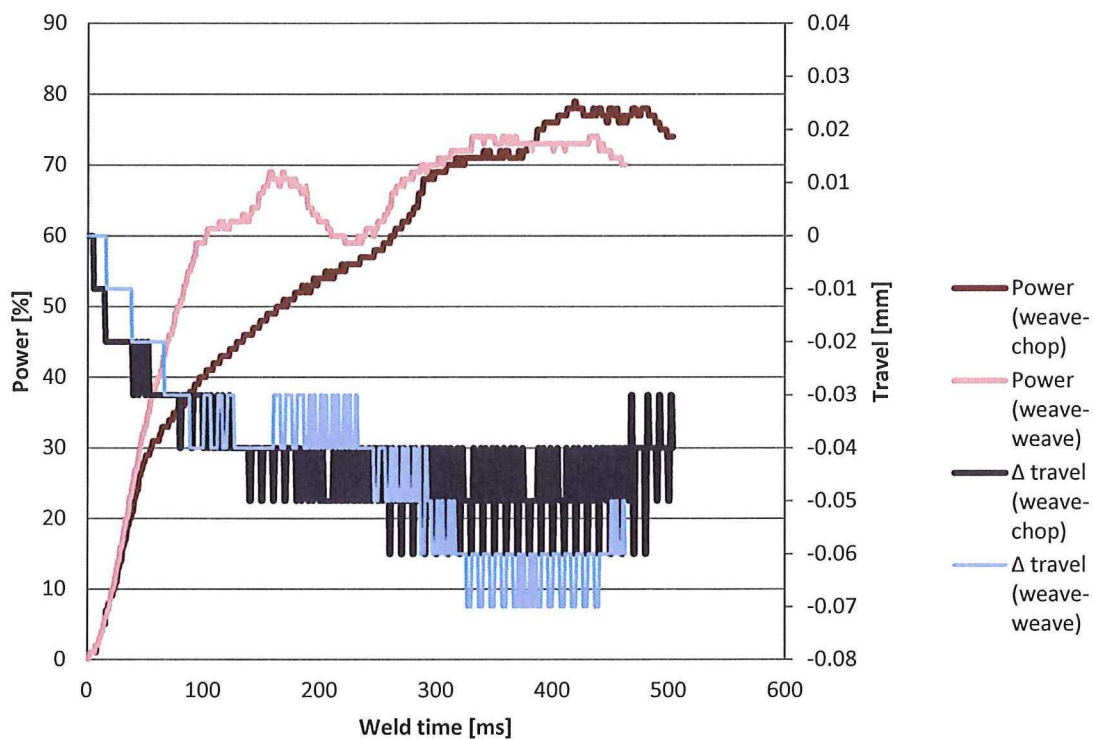


Figure 5-23 | Welding curves comparing a weave – chopped weld to a weave – weave weld for the welding of a dedicated area sized ED

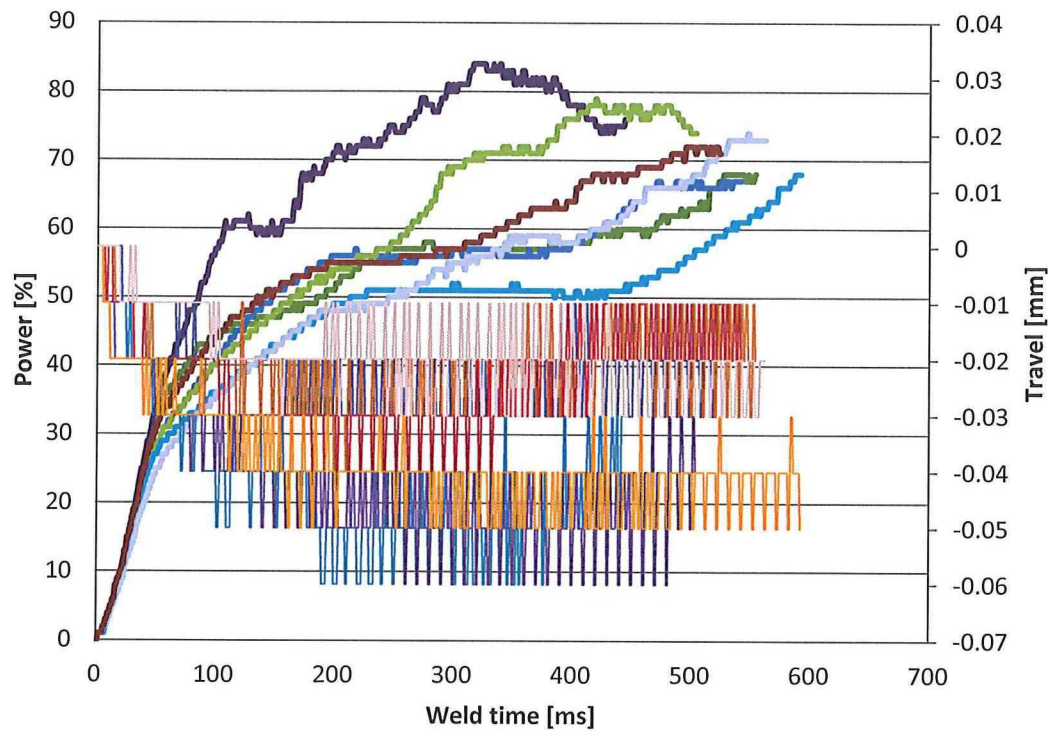


Figure 5-24 | Welding curves for the welding of weave (Ten Cate 90 [°]) to chopped fibre using the dedicated area sized EDs for samples #112 – #118, appendix B

The results for the LSS and other average values are presented in Table 5-13. As expected, the use of Ten Cate 90 [°] material and the low welding energy resulted in poor values. With similar quality material as for the weave to weave welds and a new energy determination, it is expected that the average LSS will increase and the  $c_v$  will decrease. However, as explained in the baseline for welding dissimilar materials (section 4.4), the LSS is still expected to be lower and the  $c_v$  to be higher for the welding of weave to chopped material.

Table 5-13 | Average values and  $c_v$  for the welding distance, maximum power, welding time and LSS, for the dedicated area sized ED welding using a 500 [N] welding force, the rectangular sonotrode and the 9110 jig and welding energy of 855 [Ws]. Presenting the results for the weave to chopped welded samples compared to the weave to weave welded samples.

|                 | Welding distance<br>[mm] ( $c_v$ [%]) | Max power [%] ( $c_v$ [%]) | Weld time<br>[ms] ( $c_v$ [%]) | LSS [MPa]<br>( $c_v$ [%]) |
|-----------------|---------------------------------------|----------------------------|--------------------------------|---------------------------|
| weave - weave   | 0.13 (10.2)                           | 69 (7.60)                  | 554 (9.85)                     | 44.4 (11.9)               |
| weave - chopped | 0.13 (9.05)                           | 76 (7.86)                  | 541 (11.3)                     | 18.9 (20.6)               |

The results of welding with dedicated area sized EDs proved successful for the welding of a spot in the middle of a large overlap. Although the process could be further optimized by investigating the influence of other settings which might decrease hammering for example which could lower the  $c_v$  (or by using better quality PEEK/CF material), for this research the LSS results are deemed consistent enough for a first experiment into further up-scaling. It is noted that ED



attachment is an important aspect to consider for this approach, since for a larger overlap the ED cannot be taped to the welding jig or to the sample. This poses a challenge which is investigated more in the next section (5.6).

## 5.6 Pre-attached energy directors

For the welding of standard lap shear specimen, and for the new concepts proposed in this research, the EDs were taped to either the sample or the jig, to constrain them from moving under the high vibrations loads imposed by the sonotrode. This was possible, since the ED always protrudes from the overlap. For the welding of a larger overlap, e.g. the hinge, this might not be possible. Therefore experiments were performed with welding of pre-attached ED on a sample, which was used to weld a 14.9 [mm] overlap. For this experiment only Ten Cate 90 [°] weave samples were available. Using the ultrasonic hand plunge welder (shown in Figure 2-3-B, also used for the attachment of several layers of film or prepreg to each other for handling), a 5 layer (0.25 [mm]) Ten Cate ED is plunge welded to a sample covering the 14.9 [mm] overlap (one plunge in every corner of the overlap). The result is shown in Figure 5-25, depicting the bottom sample clamped in the jig with the ED pre-attached.

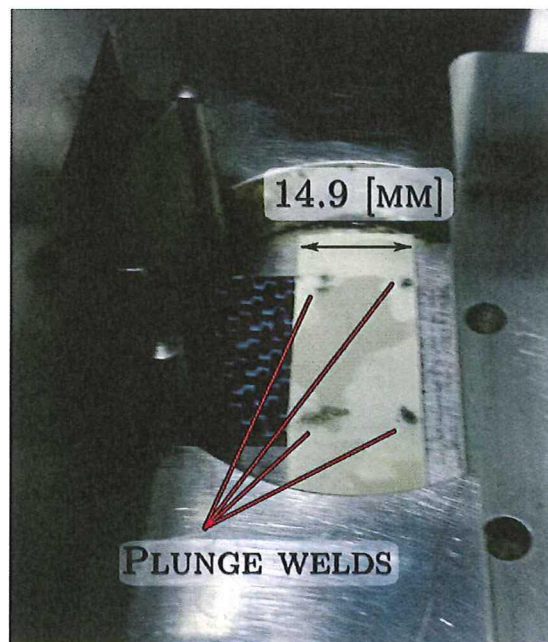


Figure 5-25 | Ten Cate 90 [°] sample with Ten Cate 5 layer (0.25 [mm]) ED pre-attached to it with four plunge welds, clamped in the 9110 jig

Using this setup and the welding conditions summarized in Table 5-14, the optimum travel was determined to be 20 [%] and one weld was made (limited samples) with this optimum setting.



Table 5-14 | Overview of the materials used (TC = Ten Cate 90 [°]), sonotrode used and the welding parameters for the welding experiments welding a 14.9 [mm] overlap with pre-attach ED, using TC 5 layer, 0.25 [mm], EDs and the 9110 jig

|                  |                            | I) Initial Phase    | II) Vibration Phase |                     |                           |                       | III) Solidification Phase |                   |
|------------------|----------------------------|---------------------|---------------------|---------------------|---------------------------|-----------------------|---------------------------|-------------------|
| Materials        | Sonotrode                  | Rise of Force [N/s] | Weld. Force [N]     | Rise of Force [N/s] | Amplitude [μm] (set. [-]) | Controlling Parameter | Force                     | Holding Time [ms] |
| TC weave – weave | Rectangular 14.9 · 30 [mm] | 250                 | 500                 | 0                   | 84.6 (3)                  | Travel, opt.: 20 [%]  | 1000                      | 4000              |

The welding curve is compared to the welding curve of a ‘normal’ taped ED (the samples used for the energy determination, using the same welding parameters, Toho Tenax material and 2 layer, 0.24 [mm] ED), shown in Figure 5-26. All welding and LSS curves are shown in appendix I) The average power, time, energy and LSS data is presented in Table 5-15, compared to the data for the taped ED as well.

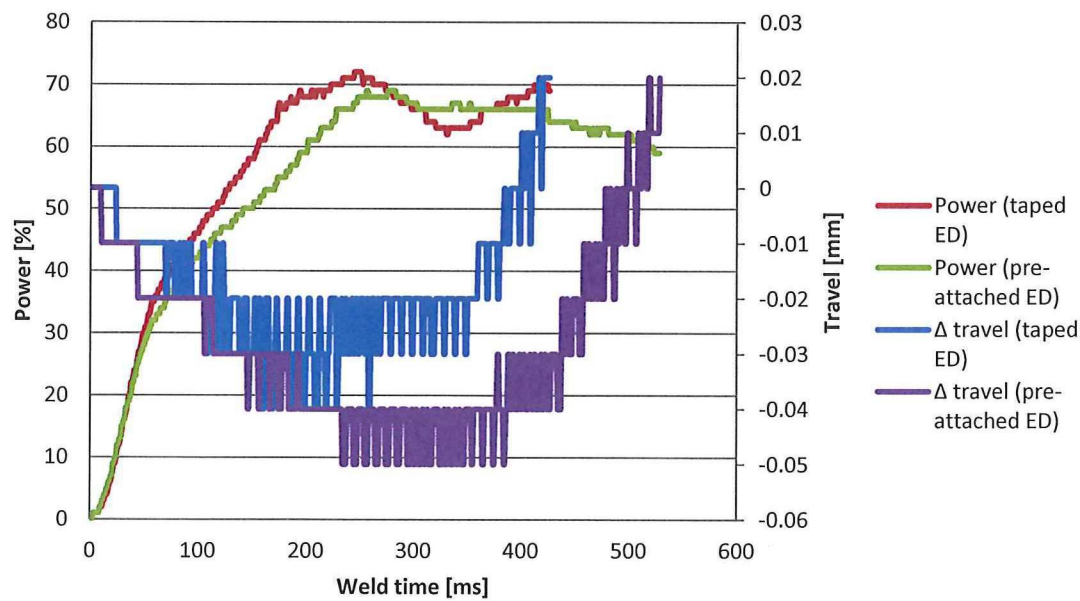


Figure 5-26 | Welding curves for the samples with the (regular) taped ED (Toho Tenax 0 [°] weave samples, and Toho Tenax 0.24 [mm] ED) and the plunge welded pre-attached ED (Ten Cate 90 [°] weave samples and Ten Cate 0.25 [mm] ED welded with a 500 [N] welding force, the rectangular sonotrode for a 14.9 [mm] overlap and the 9110 jig.

Table 5-15 | Average values and  $c_v$  (if applicable) for the maximum power, welding time, energy dissipated and LSS, for optimal welding conditions using a 500 [N] welding force, the rectangular sonotrode for a 14.9 [mm] overlap and the 9110 jig, comparing the samples with the (regular) taped ED (Toho Tenax 0 [°] weave samples, and Toho Tenax 0.24 [mm] ED) and the plunge welded pre-attached ED (Ten Cate 90 [°] weave samples and Ten Cate 0.25 [mm] ED)

|  | Maximum Power [%]<br>( $c_v$ [%]) | Welding Time [ms]<br>( $c_v$ [%]) | Energy [Ws]<br>( $c_v$ [%]) | LSS [MPa]<br>( $c_v$ [%]) |
|--|-----------------------------------|-----------------------------------|-----------------------------|---------------------------|
| 500 [N], (5 samples)<br>20 [%] travel<br>(taped ED)          | 75<br>(4.95)                      | 510<br>(6.59)                     | 855<br>(4.54)               | 38.5<br>(4.47)            |
| 500 [N], (sample #125)<br>20 [%] travel<br>(pre-attached ED) | 69<br>(-)                         | 582<br>(-)                        | 954<br>(-)                  | 37.7<br>(-)               |

Looking at Figure 5-26, it can be seen that the power curve for the pre-attached ED does not show a power increase at the point where the travel starts to increase. Also the power peak in the beginning of the process is less distinct compared to the taped ED curves. This could be due to a different initiation of the heating, since the plunge welds might influence the friction between the samples and the ED. Overall, the differences are not significant. Looking at Table 5-15, it can be seen that the values closely match those of the taped ED welds. The slightly lower LSS could be attributed to the different material (and apparent fibre direction) used for the pre-attached ED welds. The fracture surfaces, shown in Figure 5-27, also closely resemble that of the baseline (taped ED) welded samples, showing the ED molten up to the first fibre layer of the sample and minimal fibre distortion (due to the 90 [°] fibre orientation, however, some fibres got a bit squeezed out at the edge of the overlap, top of the left part in Figure 5-27).



Figure 5-27 | Fracture surfaces of sample #125 (appendix B), welded with pre-attached ED

The results of the experiment in this section show similar results (welding curves, output values) for the plunge weld pre-attached ED compared to the ‘regular’ taped ED. Therefore, it was decided to use plunge welds for the pre-attachment of ED on larger areas for up-scaling.





## 6 Sequential Spot Welding of the Clean Sky Hinge

---

Based on the results described in this research the USW process was up-scaled for which a sequential welding approach was conceived. First the sonotrode selection and spot welding strategy is discussed, after which the new jig design is presented. The complete detailed design (excluding the off-the-shelf DE-STA-CO clamps, T-nuts and bolts) can be found in appendix A. The design choices and usage of the new jig are discussed. After which the results of welding the hinges are presented.

### 6.1 Sonotrode selection and sequential spot welding strategy

As described in section 2.2.4, three different types of sonotrodes are used in this research, of which the  $\varnothing 40$  [mm] sonotrode and the rectangular sonotrode for the most experiments. To make a decision on which sonotrode and procedure would be best suited for up-scaling and welding the hinges, three different aspects are regarded.

Firstly the difference of the obtained weld quality produced with the different sonotrodes is considered (the small  $\varnothing 10$  [mm] sonotrode was only used in a few experiments and is therefore excluded from this comparison). Throughout the experiments similar results have been achieved with both the  $\varnothing 40$  [mm] sonotrode and the rectangular sonotrode. As described in section 5.5, changing from the rectangular sonotrode to the  $\varnothing 40$  [mm] sonotrode did not cause significant effects in the weld LSS. Although the settings for an optimum weld will change for every sonotrode, good welds (high LSS) can be achieved with both. It has to be noted that the used amplitude setting used for the rectangular sonotrode is slightly lower (due to limitations in the step-size of 5 [%] available in the ACU) than the 86.2 [ $\mu$ m] of the baseline, namely 84.6 [ $\mu$ m]. This might affect the hammering and / or the welding time, but since the change is only 2 [%] this is neglected.

Secondly the unwanted surface damage, which occurs occasionally, is regarded. The rectangular sonotrode has, as the name implies, a rectangular surface area with 90 [°] corners and straight edges. This makes the chance of surface damage a little higher compared to the circular sonotrode. Also, which is believed to have more influence, is the fact that the surface area is smaller making the pressure (force per area) relatively larger.

Finally some practicalities are regarded. Considering the hinge bottom plate dimensions (42 [mm] · 63 [mm] = 2646 [mm<sup>2</sup>]), using the  $\varnothing 40$  [mm] sonotrode would mean close proximity to the edges during welding. Furthermore it would be difficult to weld separate spots, since if the area of the  $\varnothing 40$  [mm] sonotrode is centred on one spot it would partly overlap another spot as well. For the rectangular sonotrode, however, it would be possible to do two separate spots on the bottom plate on either side of the flange, creating a symmetrical joint. This also provides a practicality for the ED. Cutting EDs in the shape of the rectangular sonotrode is easily achieved with the film cutter. The straight edges of the shape make it convenient for positioning and alignment as well.

Considering these three points it was decided to opt for a two spot welding approach using the rectangular sonotrode, with one spot weld on both sides of the flange, using the rectangular sonotrode. It is noted that the selection is made from the sonotrodes available. Another sonotrode for this specific application could be designed and manufactured to create more favourable conditions.

The proposed strategy of using two rectangular spots, will add up to a welded area of:  $2 \cdot 14.9 \cdot 30 = 894 \text{ [mm}^2\text{]}$ , which is 33.7 [%] of the hinge base plate area (2646 [mm<sup>2</sup>]), The load case provide for the Clean Sky project in tension is 3411 [N] [33] (Figure 6-1), which would mean a LSS of  $3411 \text{ [N]} / 894 \text{ [mm}^2\text{]} = 3.82 \text{ [MPa]}$ , which is significantly lower than the LSS obtained in this research. It is noted that this value only provides an indication. The geometry of the joint is expected to introduce some peel forces in the test and is significantly different from a single lap shear specimen. It can therefore not be compared directly. The difference between the 3.82 [MPa] and the LSS obtained in the preceding experiments (ranging from an average of 18.9 [MPa] to 44.4 [MPa], Table 5-13), was deemed large enough to ensure enough strength to cope with the provided load case.

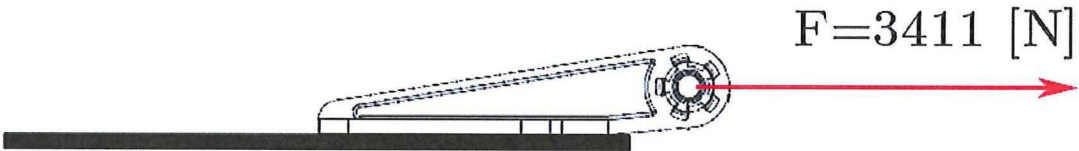


Figure 6-1 | Tension load case for the Clean Sky hinge

Considering the ED needed for each spot weld, it was decided to pre-attach both EDs using plunge welds as explained in section 5.6. The plates where the hinges would be welded too were easily clamped to the workbench. Therefore it was decided to pre-attach the ED to the plates. However, attachment to the hinges would be possible as well (although a bit more difficult to clamp). The effect of the attachment to the surface of the hinge on the bonding quality could be researched as well. To pre-attach the EDs on either side of the flange, not adjacent to the edge, some extra tooling was required. An alignment tool was manufactured to perfectly align the ED for plunge weld attachment, shown in Figure 6-2.

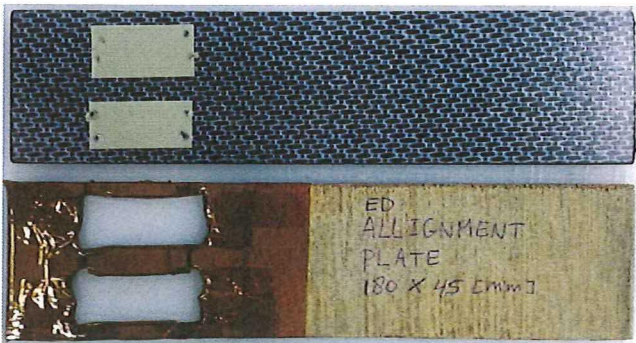


Figure 6-2 | ED alignment aid for plunge welding EDs to larger plates for hinge welding with square holes identical to the ED dimensions an rounded corners for accessibility of the USW hand plunge welder. The edges are covered with Kapton tape against possible overheating.

The conceived sequential spot welding approach for the welding of the Clean Sky hinge, uses dedicated area sized ED in combination with the rectangular sonotrode. With the geometrical



constraints (size of the hinge, size of the sonotrode, minimum distance of the clamping and length needed for the Zwick testing machine) considered it was decided to use two spot next to each other on either side of the flange of the hinge, welding it to a continuous CF/PEEK plate of  $180 \cdot 45$  [mm]. The manufacturing process of the plates can be found in section 2.1.2. A schematic view of the setup is presented in Figure 6-3.

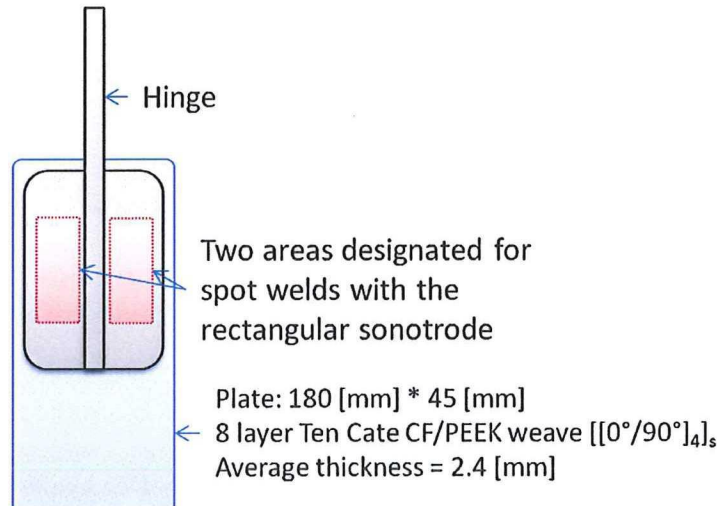


Figure 6-3 | Schematic view of the sequential spot weld configuration used showing plate dimensions (manufacturing process is described in section 2.1.2)

## 6.2 New jig design for sequential spot welding of the Clean Sky hinges

### 6.2.1 Jig design and manufacturing

As part of this research a new jig was designed and manufactured, using the presented results as design input. The new jig is especially designed and manufactured for this research with the goal of welding the Clean Sky chopped fibre CF/PEEK hinges to TPC plate material. The jig was manufactured by DEMO at the faculty of Aerospace Engineering DUT. Figure 6-4 shows the end result and the complete baseplate design can be found in appendix A.



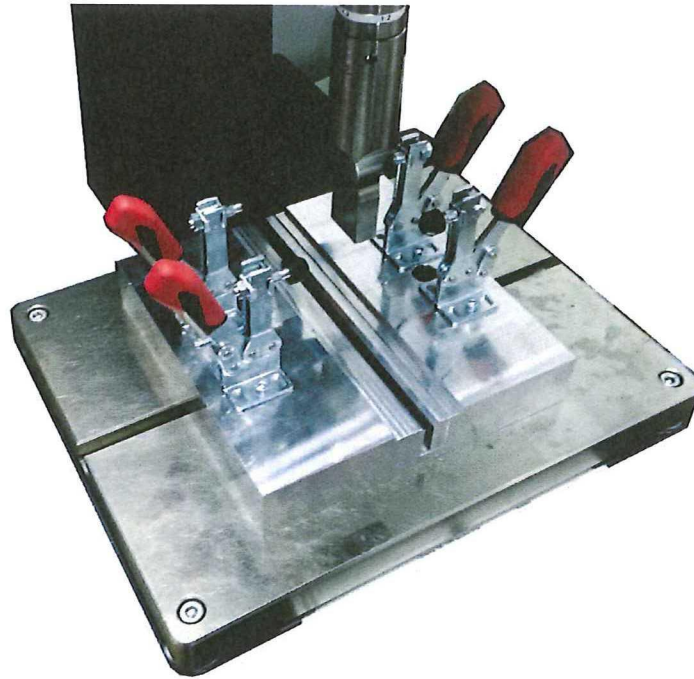


Figure 6-4 | New jig designed for welding of (chopped fibre) Clean Sky ITD hinges

The new jig allows for movement in the x- and y- direction (depicted in Figure 6-5). Movement along the x-direction of the entire jig is possible by moving it across the baseplate of the USW machine. Movement of the y-direction is possible by moving the part through the cavity in the jig. Thereby allowing multiple spot welds. In this research the hinges were welded with two spots using the rectangular sonotrode. In this setup only movement along the x-axis was required. Markings applied to the jig and baseplate of the USW machine ensured identical alignment for all subsequent welds. With these marks the clamping, alignment and welding of a hinge to a TPC plate can be achieved in a few simple steps. The different features of the jig are depicted in Figure 6-5.

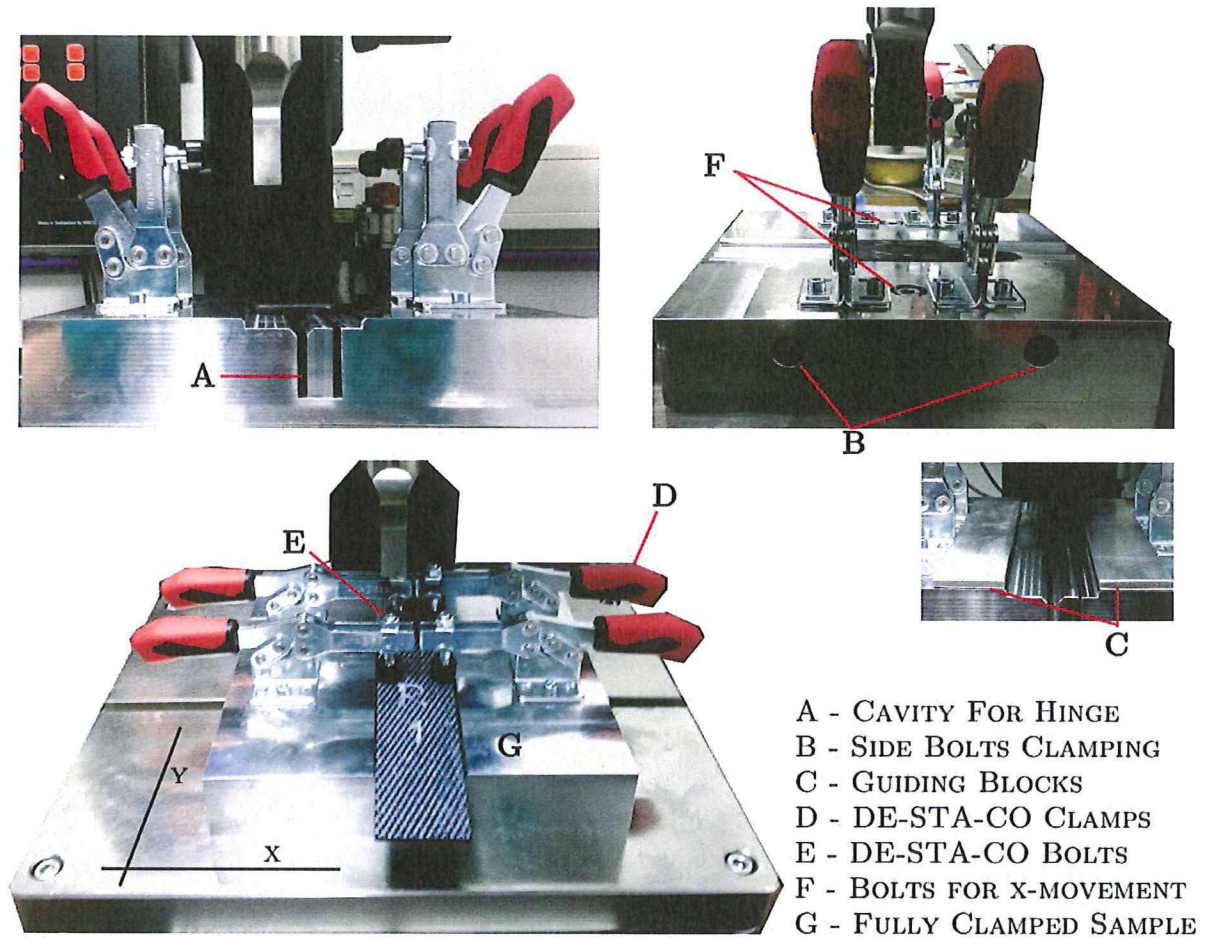


Figure 6-5 | Detailed overview of the new jig for hinge welding

First the hinge is placed upside down in the cavity A, aligning it with the markings. Bolts B are tightened simultaneously to ensure clamping of the hinge. Secondly the plate is placed on top of the hinge, with the pre-attached ED facing the hinge. The plates used in this research are aligned with the markings at the top and the two aluminium guiding blocks C on either side. Closing all four of the DE-STA-CO clamps D ensures clamping of the plate, after which the first weld can be made. The pressure each DE-STA-CO clamp can apply varies between the 1000 [N] and 1200 [N], depending on how far on the arm the pressure point is mounted (1000 [N] in the displayed configuration). Also the extension of each pressure point (controlled by the bolts E) changes the amount of pressure per point. Loosening bolts F allows for movement in the x-direction (x/y-direction are depicted in Figure 6-5) through the T-slots of the USW baseplate. Using the markings it can be aligned and bolts E can be tightened again after which the second weld is created.

The jig is designed to leave room to weld the hinge to larger plates (with the same clamping) or even to the C-frame. For welding the hinge to the C-frame, however, different clamping is necessary, for which room is left on the baseplate of the new jig.



### **6.2.2 *Elaboration on the design choices***

From the research presented it was found preferable to weld the continuous material to the chopped fibre material, having the continuous material closest to the sonotrode, since it was observed that having the chopped fibre sample close to the sonotrode results in delamination of the sample. Also it is advised for the same reason to have the welded area at some distance from the edge of the parts. The baseplate was therefore shaped to fit the hinge upside down so the bottom plate would be level for attachment to continuous plate material. The depth of the surface area supporting the hinge was designed slightly smaller (3.8 [mm]) than the average thickness of the hinge plate (4 [mm]) for two reasons:

- To cope with variations in base plate thickness
- To ensure good surface to surface pressure (top – bottom sample) during welding

The cavity, the supporting surface that supports the hinge and the block that is used for clamping of the hinge all are designed to leave enough space in the y-direction to allow for movement of the hinge in that direction. The DE-STA-CO clamps which were selected and their positioning on the block are ideal for this situation where this particular plate is clamped. However, other clamps and / or configurations can be mounted on the base for the welding of different parts to the hinge (e.g. the corners). Even though the steel jig (9109) had preferable results in terms of  $c_v$  and maximum power used compared to the aluminium jig (9110), the material selected for the new jig is aluminium as well. This is done because the influence of the geometry is not yet fully understood, meaning that this completely different geometry might have more influence than the variation of material, and aluminium is far lighter and therefore has better handling.

### **6.2.3 *Discussion on the operations of the new jig***

During welding several observations and slight adjustments were made. Operating the jig is less time consuming than the older jigs due to the easy clamping with the DE-STA-CO clamps. Only two bolts were needed for clamping of the hinge, however, it is recommended for future design to use clamps similar to the DE-STA-CO clamps for that as well. For the movement in the x-direction two bolts with off-the-shelf T-nuts were used to guide the base through the T-profiles in the USW machine baseplate. Since there was a slight mismatch, custom-made T-nuts are recommended for more accuracy. The dampening of the rubber pods at the end of the DE-STA-CO clamps proved to work well, but had the unintended side effect of melting to the samples. This did not do any harm, but left some molten material on the surface of the plate. This problem was fixed by the application of Kapton tape (which can handle temperatures up-to 400 [°C] [13]) on the rubber pads, seen in Figure 6-6. The wear of these pods inside the tape however still continues and it is recommend using material which can withstand higher temperatures for future welds. Another addition was the use of extra supporting (dampening) silicone rubber material to support the protruding portion of the plate material, also shown in Figure 6-6. This was done because the plates were observed to bend slightly into the jig cavity under the force of the DE-STA-CO clamps. A final observation was movement of the plate at an experiment welding with 1000 [N] welding force. At a welding force of 500 [N] no problems occurred, but somewhere between 500 [N] and 1000 [N] the welding force induces to much sideways vibrations



in the part for the clamping to handle. If the hinge needs to be welded with a higher welding force (not needed for this research), extra or stronger clamping will be needed for welding.

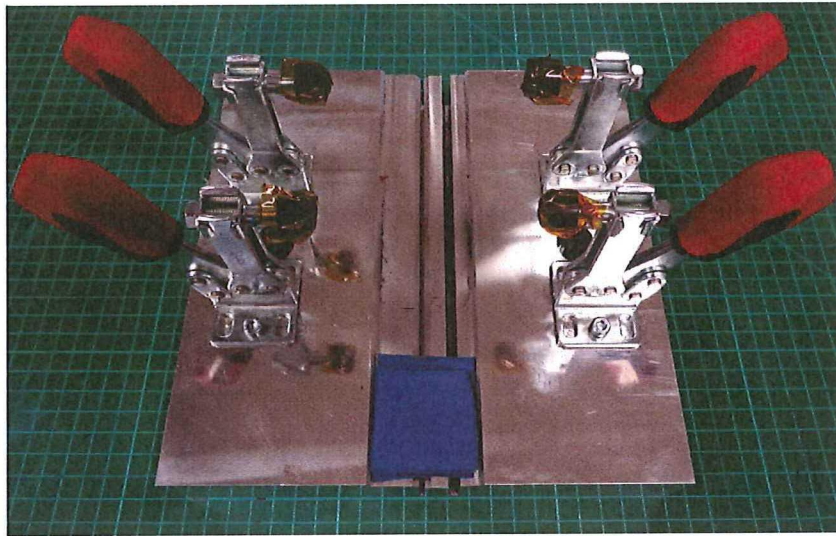


Figure 6-6 | New jig design with Kapton tape on the DE-STA-CO dampening pods and extra silicone rubber supporting material (the blue stack down in the middle of the jig) for the protruding plates

### 6.3 Tension strength test setup for the welded hinges

The setup and procedure described in section 2.4 for the LSS testing of single lap specimen is adjusted to test the tension strength of the hinges welded to the plates.

For the hinges, the cross head control rate was kept at the ASTM D1002 specified value of 1.3 [mm/min], but a special set-up was used shown in Figure 6-7. The plate (where the hinge was welded on) was clamped in a similar manner as the lap shear samples, between the hydraulic grips of the Zwick. An aluminium cylinder (A) was custom made to fit in the hinge hole and allowed for connection to a metal pin. This metal pin was connected to a 90 [°] rotated frame (B) which could be easily connected to the upper clamp of the Zwick, allowing for the machine to exert tension on the welded parts.

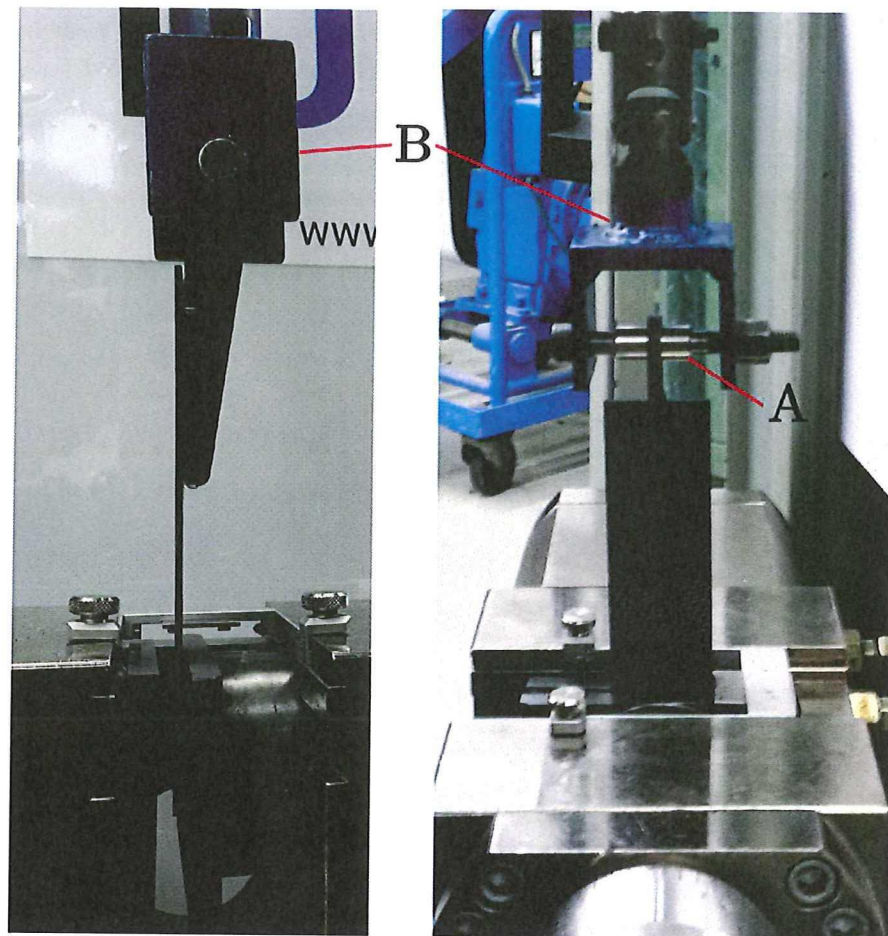


Figure 6-7 | Setup of the Zwick 250 kN universal testing machine for hinge tension testing showing: A) custom made aluminium cylinder for fitting the hinge to the frame, B) 90 [°] rotated frame

#### 6.4 Ultrasonic sequential spot welding of chopped fibre hinges to continuous fibre plates

Using the welding strategy and the new jig design presented in section 6.1 and 6.2, the chopped fibre hinges (Toho Tenax CF/PEEK) can be welded to the continuous fibre weave plates (Ten Cate CF/PEEK). The welding parameters used are kept identical to the parameters used for the energy controlled dedicated area sized ED welding (section 5.5). However, for this new setup first the energy needed needs to be determined. The welding parameters for the hinge welding are summarized in Table 6-1.



Table 6-1 | Overview of the materials used (TC = Ten Cate, hinge is produced from chopped fibre Toho Tenax material), sonotrode used and the welding parameters for the welding experiments sequentially welding a plate with two pre-attached ED to the hinge, using TT 2 layer, 0.24 [mm], EDs and the 9110 jig

|                  |                            | I) Initial Phase    | II) Vibration Phase |                     |                           |                       | III) Solidification Phase |                   |
|------------------|----------------------------|---------------------|---------------------|---------------------|---------------------------|-----------------------|---------------------------|-------------------|
| Materials        | Sonotrode                  | Rise of Force [N/s] | Weld. Force [N]     | Rise of Force [N/s] | Amplitude [µm] (set. [-]) | Controlling Parameter | Force                     | Holding Time [ms] |
| TC weave – hinge | Rectangular 14.9 · 30 [mm] | 250                 | 500                 | 0                   | 84.6 (3)                  | Energy tbd            | 1000                      | 4000              |

From chapter 4 it was still found difficult to predict the energy needed for the welding of the continuous weave CF/PEEK Ten Cate plate to the chopped fibre hinge. However the 855 [Ws] is used as starting point and is scaled using some indications provided by this research.

First of all the jig influence from the steel 9109 jig to aluminium 9110 jig showed a 24 [%] decrease in energy (section 4.3). Although the 9110 jig and the newly designed jig are manufactured using the same material, it cannot be assumed that the energy levels should stay the same due to the highly different geometry and clamping. Therefore its influence could not be taken into account. The change from continuous weave material as bottom sample to chopped fibre material indicated that more energy was needed (section 4.4). However, a higher energy value was not yet determined. Next to that, the influence of an increasing welding area on the energy dissipation was investigated as well (section 4.2). Even though these experiments did not provide successful welds (overheated, poor LSS), the output values did indicate an increase in energy dissipation. Although the welds were of poor quality, it is still believed that for the increase in welded area from 14.9 [mm] · 25.4 [mm] to 14.9 [mm] · 30 [mm] (since now not the width of the lap shear sample, but the size of the sonotrode is dictating the size), more energy is needed as well. Additionally, the fact that the flow fronts of the molten ED will now be constricted at all edges, not only on two sides of the ED as explained in section 5.5, the energy dissipation is expected to rise.

Since these conclusions only provide rough indications it was decided to start with 1.5 times the energy needed for the normal lap shear samples (855 [Ws]) and to perform experiments to find the optimum energy needed with the tension load case as goal for the strength. This was done through welding one hinge with two spots using a starting energy value of 1200 [Ws], increasing the energy in five steps of 200 [Ws] for subsequent hinges up to 2000 [Ws], and comparing the obtained strength in the tension test (using the setup as described in section 6.3). The 1600 [Ws] energy weld was welded using a welding force of 1000 [N], to research if this influenced the weld strength in this setup. However, the clamping could not cope with the vibrations and the plate moved making it unusable for a tension strength test. The input welding parameters are summarized in Table 6-2 and the tension strength results ( $F_{max}$ ) for the welds are shown in Figure 6-8.



Table 6-2 | Overview of the materials used (TC = Ten Cate, hinge is produced from chopped fibre Toho Tenax material), sonotrode used and the welding parameters for the energy determination for hinge welding, using TT 2 layer, 0.24 [mm], EDs and the 9110 jig

|                  |                            | I) Initial Phase    | II) Vibration Phase |                     |                            |   | III) Solidification Phase |                   |
|------------------|----------------------------|---------------------|---------------------|---------------------|----------------------------|---|---------------------------|-------------------|
| Materials        | Sonotrode                  | Rise of Force [N/s] | Weld. Force [N]     | Rise of Force [N/s] | Amplitu de [µm] (set. [-]) | Controlling Parameter                             | Force                     | Holding Time [ms] |
| TC weave – hinge | Rectangular 14.9 · 30 [mm] | 250                 | 500                 | 0                   | 84.6 (3)                   | Energy 1200 [Ws], 1400 [Ws], 1800 [Ws], 2000 [Ws] | 1000                      | 4000              |
| TC weave – hinge | Rectangular 14.9 · 30 [mm] | 500                 | 1000                | 0                   | 84.6 (3)                   | Energy 1600 [Ws]                                  | 1000                      | 4000              |

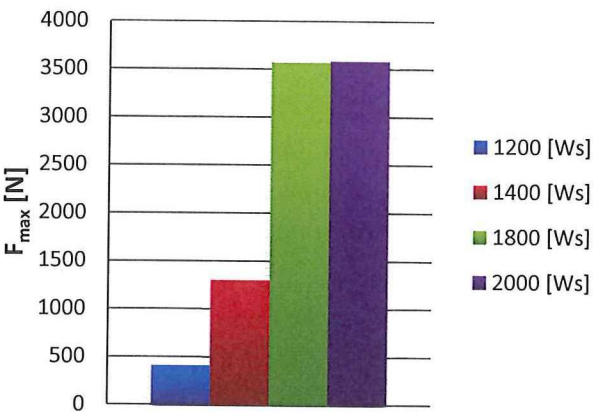


Figure 6-8 | Experiments for the energy determination for hinge welding, welding one hinge per setting with two sequential spot welds, showing hinge 1 (1200 [Ws]), 2 (1400 [Ws]), 4 (1800 [Ws]) and 3-2 (2000 [Ws])

It is noted that even though a sufficient offset was used, this test induced much peel in the joint next to the shear load, which should be taken into account when regarding the tension strength data. This effect is shown in Figure 6-9.

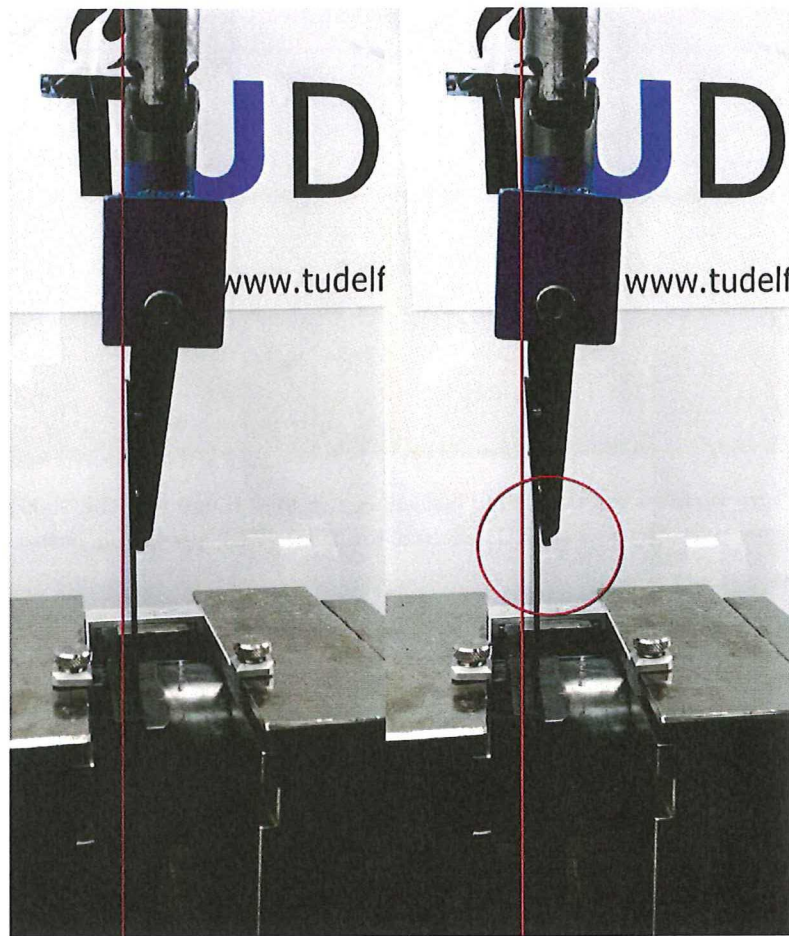


Figure 6-9 | Tension test using the Zwick universal testing machine to test the hinge weld strength, showing clear signs of induced peel forces

Although the welded areas obtained for the 2000 [Ws] were not completely melted, as can be seen in Figure 6-10, the strength of the bond met the Eurocopter loading case of 3411 [N] and was therefore deemed sufficient for subsequent welds. The strength for 1800 [Ws] was only slightly less as seen in Figure 6-8, but in the case of 2000 [Ws] the weld did not fail, instead the hinge broke. This hinge was, however, manually detached from the plate using a small pry tool for analysis of the welded area. The surfaces shown in Figure 6-10, show that a larger part of the two EDs melted for the hinge welded with 2000 [Ws] energy, providing better attachment of the hinge.

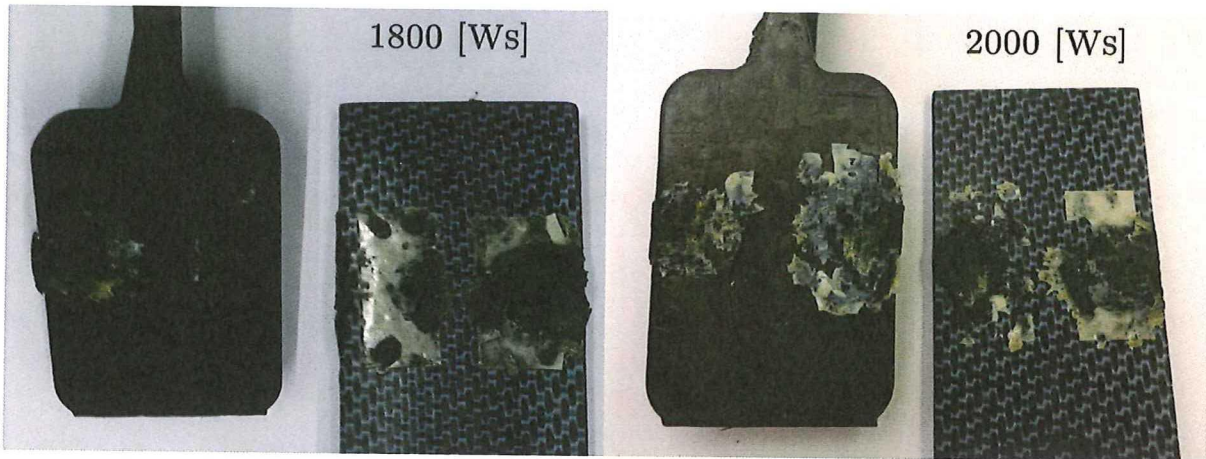


Figure 6-10 | Fracture surfaces for the 1800 [Ws] energy welded hinge and the 2000 [Ws] welded hinge, showing that a larger part of the two EDs melted for 2000 [Ws], providing better attachment of the hinge

The strength obtained using a welding energy of 2000 [Ws] to sequentially weld a hinge with to spots to the TPC plate, met the tension strength requirements for the Clean Sky project. The high energy level needed (2.5 times more than for the dedicated area sized ED single lap shear welding), could be due to several extra reasons next to the aforementioned influences for the energy determination. First of all the continuous weave plate was thicker than the plates used for the lap shear samples (8 layers vs 6 layers). Secondly the plates where shear cut instead of water jet cut, creating a more delaminated edge. It is noted that the welds were created away from the edge, but the delaminated edge could still have some influence in the dissipation of the energy explaining why more energy was needed to obtain sufficient tension strength. Next to that the hinge has a different geometry and shorter fibres (10 [mm] instead of 20 [mm]) than the chopped plates used in the other experiments. Also the effect of the dampening pods changes the energy dissipation. Further research into these effects is needed for better energy prediction.

Using the selected 2000 [Ws] as energy setting, 7 extra welds are created. The typical welding curves for a first and second, sequential, welds are shown in Figure 6-11. All the weld data can be found in appendix J.

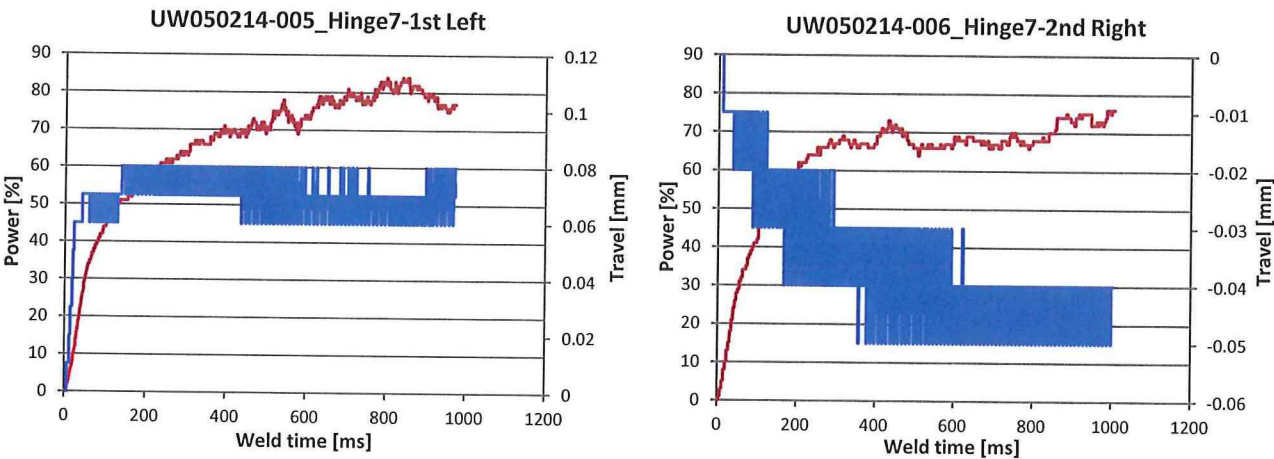


Figure 6-11 | Typical welding curves for the first and second spot weld for hinge welding, showing a large positive (downward motion of the sonotrode) travel at the beginning of the first weld and more hammering (negative travel) for the second weld



In Figure 6-11 it can be seen that generally the first weld shows large positive travel at the beginning of the USW process. This is believed to come from the asperities from the ED plunge weld attachment. These asperities are the result of the use of the alignment tool (presented in section 6.1), since they were not formed in the preliminary experiment for the welding of the pre-attached ED for a normal overlap (discussed in section 5.6). The alignment tool ensured straight plunge welds perpendicular to the surface of the plate material (creating asperities), whereas the plunge welded ED for the normal overlap were welded at an angle almost to the edge of the sample (creating no asperities). The initial vibrations, combined with the welding force, very quickly flatten these small areas resulting in positive travel. Afterwards power and travel stay roughly constant. For the second weld however, it can be seen that the constrictions created by the first weld imposes some changes in the second weld. Whereas the first weld shows almost a constant position for the sonotrode (except for the increase in the beginning) of around 0.08 / 0.06 [mm], the second weld shows a gradual negative travel from 0 [mm] to -0.04/-0.05 [mm]. This might be caused by an increased hammering effect for the second weld, which could be due to the fact that the first weld already presses the parts together (partly compressing the second ED), leaving less possible deformation of the ED for the second weld. The onset of welding starts by a smaller absolute travel of the sonotrode (58,23 [mm]) for the first weld compared to the second weld (58.3 [mm]). Meaning that for the second weld the part is already compressed to some extent by the first weld, leaving a longer path for the sonotrode to reach the part for the second weld, hence more travel.

Using the tension strength test, presented in section 6.3, four extra joints were tested. The stress strain curves for hinges 4 (1800 [Ws]), 3-2, 7, 10 and 11 (2000 [Ws]) are shown in Figure 6-12. The curve for hinge 9 is strongly different from the other curves, which could be due to a misalignment or defect in the hinge used, since for this test the hinge failed as well. As mentioned, the weld of hinge 4 (1800 [Ws]) failed above the Eurocopter load case of 3411 [N], all the other (2000 [Ws]) welds did not fail. Instead the hinge broke at the support bushing used in the Zwick as shown in Figure 6-13.

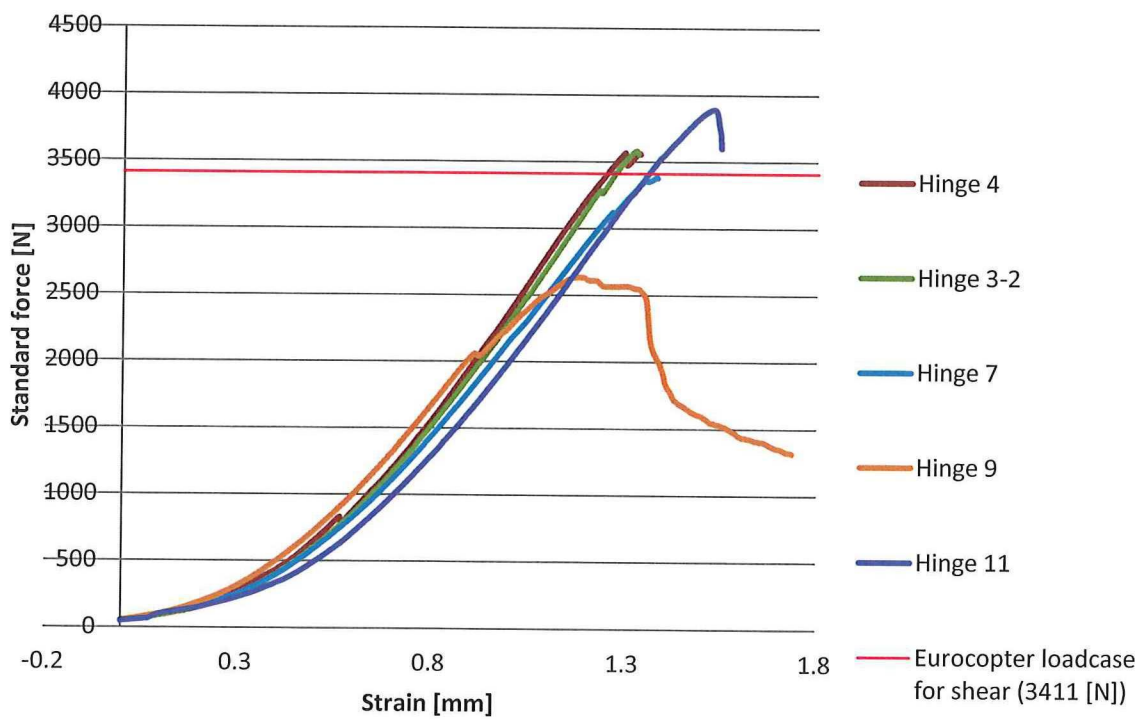


Figure 6-12 | Zwick strain curves for the welded hinges 4 (1800 [Ws]), 3-2, 7, 9 and 11 (2000 [Ws]) compared to the Eurocopter load case, hinge 4 failed in the weld, for the other welds the hinge failed

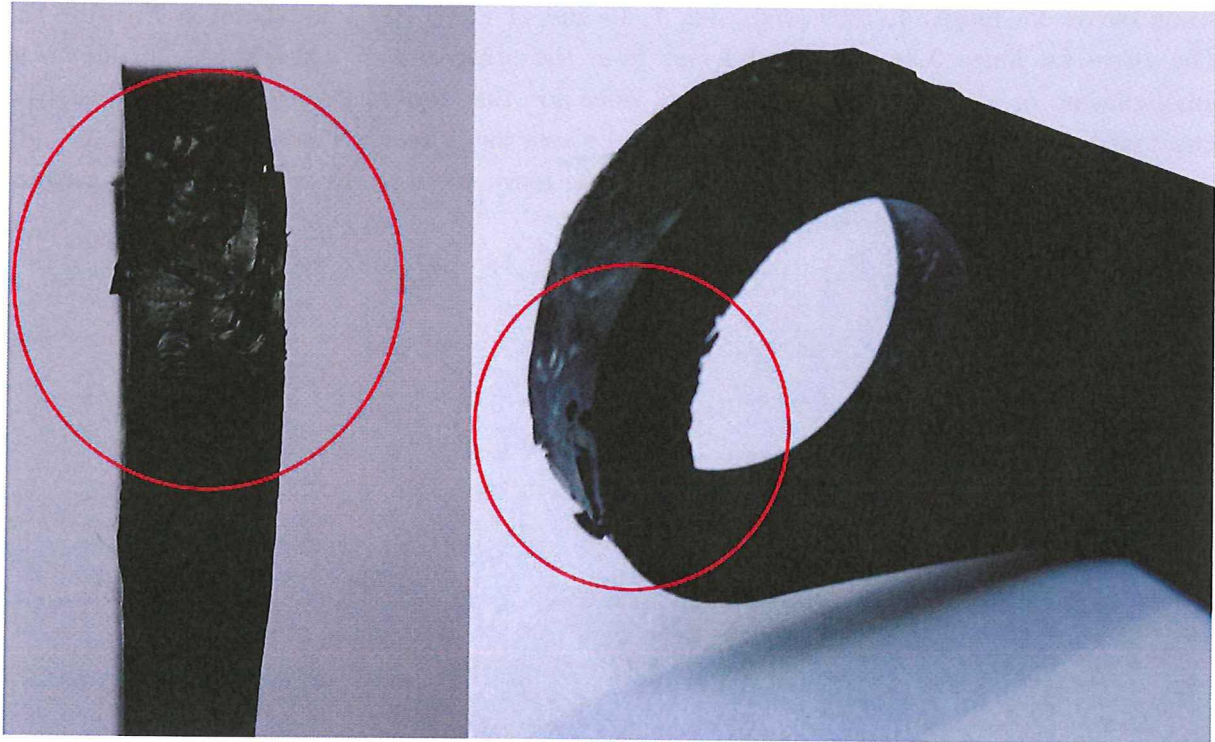


Figure 6-13 | Broken hinge as result of the Zwick strength test of the weld

Even though the bond was stronger than the hinges, the welded areas were inspected in several ways. Before testing hinges 5 to 11 were inspected using the C-scan to obtain an indication of the weld quality. These images are shown in Figure 6-13, showing that the areas of the weld generally

show low attenuation (light green coloured area) in the centre, which means the ED has melted and bonded for a large part of the overlap forming a good bond. It is noted that the colours in the C-scan image are used for relative comparison, not for absolute attenuation values. At the edges more blue areas are seen depicting more damping, possibly indicating parts of the ED that did not melt. The red areas depict parts with maximum damping, meaning that the bond quality is not good (considering the part where the bond is located, the clamps and flange of the hinge also show maximum damping). Figure 6-14 also shows that the first weld generally is of worse quality indicated by the red area, compared to the second weld, discussed more with the analyses of the fracture surfaces (Figure 6-15 and Figure 6-16) in this section.

It is noted that around the welded area no connection exist between the hinge and the plate, the reason that this does not show red (the air between the parts should show damping) is because during the process of C-scanning water accumulates between the two parts, transmitting the sound waves. It can be seen that still some air might have been trapped at the back end of hinge 8 depicted by the red area. Hinge 6 shows a partly good bond on the left side, but a bond with much damping on the right side. This hinge was investigated more thoroughly using microscopy of the cross-section depicted in Figure 6-14. The cross-section is shown in Figure 6-15, and it can be seen that the right bond indeed shows more air inclusions, responsible for the damping shown in the C-scan image.

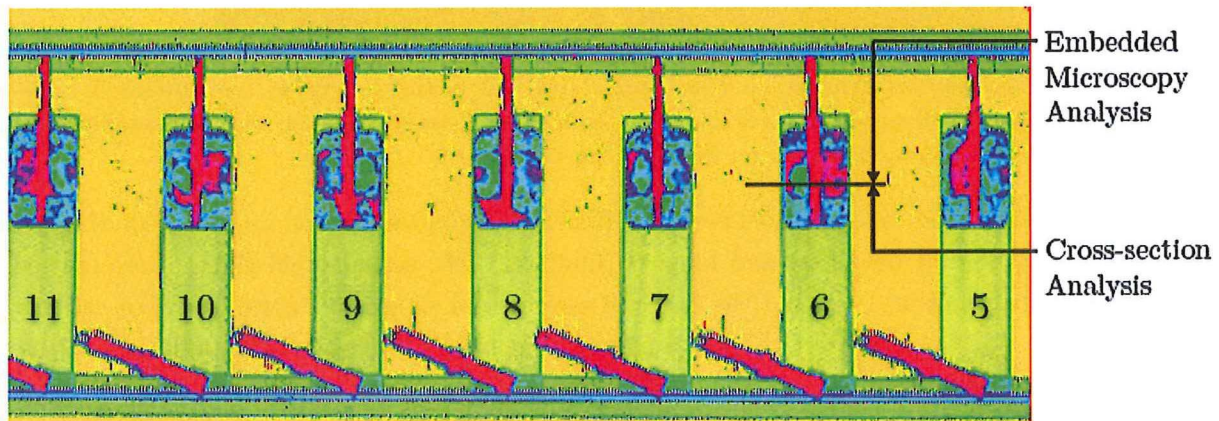


Figure 6-14 | C-scan for 2000 [Ws] energy welded hinges 5-11, showing the cross-section that was investigated with microscopy, first and second spot welds for all hinges are, L=Left, R=Right: 5 (1: L, 2: R), 6 (1: R, 2: L), 7 (1: L, 2: R), 8 (1: R, 2: L), 9 (1: L, 2: R), 10 (1: R, 2: L), 11 (1: L, 2: R), showing that the first weld generally is of worse quality indicated by the red area. The colours are used for relative comparison, not for absolute attenuation values.



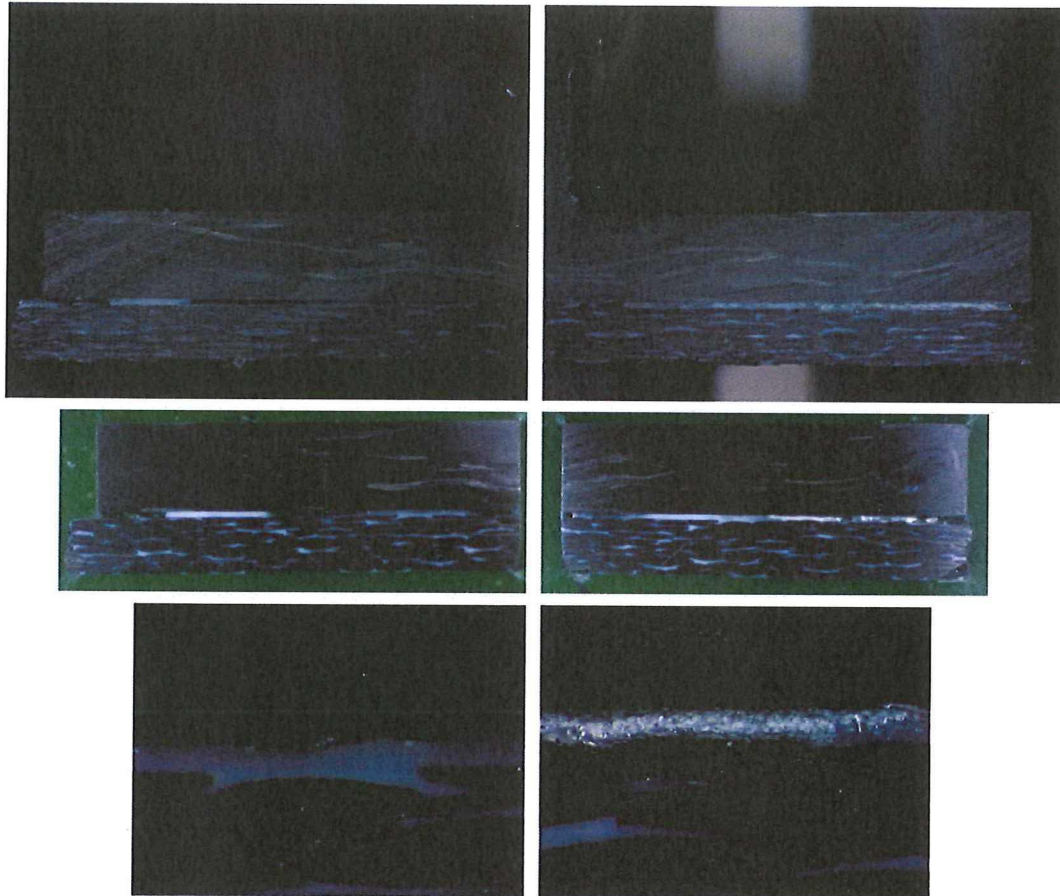


Figure 6-15 | Cross-section depicted in the C-scan, top two pictures showing the untreated cross-section, bottom four (mirrored) pictures show the embedded cross-section (1x and 8x magnification) showing more air in the first spot weld on the right side for hinge 6

Next to the C-Scan the difference between the first and second weld was investigated. Hinge 8 (first weld right, second weld left) and hinge 9 (first weld left, second weld right), were opened manually using a small pry tool and the fracture surfaces are shown in Figure 6-16. For another hinge, only one side was welded and opened manually as well, to investigate the influence of the first weld on the second (not welded) ED. This fracture surface is also shown in Figure 6-16.



Figure 6-16 | Fracture surfaces of welded hinges 8 (left), 9 (middle) and a one side welded hinge (right), first and second spot welds for the hinges are, L=Left, R=Right: 8 (1: R, 2: L), 9 (1: L, 2: R) and only the left one for the last hinge

It can be seen that generally the first spot weld results in less molten ED and therefore a lower quality bond than the second weld. The mentioned extra constrictions of the first weld seem to benefit the welding of the second spot. The first weld, however, does not seem to affect the ED

for the second weld as can be seen in the right of Figure 6-16. Extra clamping for the first weld might prove to induce similar restrictions on the first spot weld as well, increasing its quality. Also it might be considered to use different welding parameters for the first spot compared to the second spot. For the first spot it might be tried to use more energy and / or force, compared to the second weld, to get equally molten surfaces (and therefore a better bond). Also the amplitude settings should be investigated for both spots, since they might contribute to lower hammering and therefore increase the efficiency.

A final interesting observation is the initiation of the melting process looking at the ED. The parts where the ED was plunge welded to the plate did not melt as can be seen in Figure 6-10 and Figure 6-16. Since the ED is fixed to the plate, interfacial friction is minimized at that point. Therefore it is recommended to perform experiments with EDs attached only at one spot in the middle for example and leave the edges as free as possible so they can benefit from the relative higher interfacial frictions at these points.

The results in this section present a successful initial approach for the welding of the chopped fibre CF/PEEK hinges to a continuous weave CF/PEEK plate. In optimizing the process and taking further steps into up-scaling, some final remarks should be considered. Firstly just one particular approach is considered here. With different sonotrodes, adjusted clamping or other process parameters the process could be further optimized. It can be even considered to design a specific sonotrode which can weld several spots on the hinge at once, joining it to the plate material in one shot. The total area cannot be too large, however, unless a more powerful USW machine is used. Finally for a true practical application, it should be considered that in the current joint a small gap is left between the hinge, the plate and the ED welded areas. The ED only covers slightly more than 30 [%] of the overlap, whereas water could find its way in the remaining 70 [%] and could damage the joint. A sealant (or different ED configuration) would be recommended.





### **III – Conclusions and Recommendations**



## 7 Conclusions

---

This thesis presents the initial study of the possibilities and limitations for up-scaling of the USW process. USW can help to further improve the cost-effectiveness of the manufacturing process of TPCs. The process cycle of USW is extremely short and therefore consumes less energy than other fusion bonding processes. Next to that no foreign materials are introduced in the joint regardless of the composition of the thermoplastic composites used. Other advantages of the process are that it does not require extensive surface treatment of the parts, it is well suited to be automated and it can be on-line monitored which provides insight in the joint quality. The Clean Sky JTI, which promotes a more sustainable future for the aerospace industry, provides an ideal specific case in the welding of chopped fibre hinges to continuous fibre CF/PEEK material. USW can contribute to the goals of the Clean Sky project, since USW potentially can be used to create an energy efficient and clean joint. Therefore the main goal presented is the design of a sequential welding procedure suited for the welding of these hinges.

To reach this goal, first baseline experiments were conducted, establishing a reference frame for newly proposed welding concepts and determining a baseline for the main welding parameters. This is done for all materials considered in this experiment, i.e. the continuous weave and the chopped fibre CF/PEEK material. These preliminary experiments led to the following main conclusion and challenge:

- For the welding of dissimilar materials, the continuous weave material should be the top sample, close to the sonotrode. The chopped material cannot cope with the high cyclic load at the edges where there is no surrounding support and therefore results in deconsolidated edges.
- The process for up-scaling using spot welds is going to be energy controlled rather than travel controlled, due to travel constrictions imposed by the surrounding colder ED. The surrounding ED will not melt and flow, therefore prohibiting the travel of the top sample towards the bottom sample. Energy controlled welding does not rely on the travel, rather on the energy delivered and can therefore still be used.

To create good energy controlled welds, the energy determination for each type of weld was researched more elaborately. Therefore the energy dependence on factors changed in this research was investigated. These factors were the dimensions of the area welded, the difference in clamping jig and the influence of different materials.

- Increased area size welding proved more difficult compared to the baseline, due to overheating through the thickness of the samples. A increasing negative travel was observed for the increasing area sizes, caused by increased hammering, making the process increasingly less efficient. This was partly solved with a higher welding force setting but the power limits of the USW machine were reached. It can only be said that generally a larger area requires more power.
- The material of the jig has an influence on the energy dissipation as well. The aluminium jig showed to require less energy on average, but reached a higher maximum power



consumed, compared to the steel jig. This is believed to come from the material stiffness, which is a factor 3 lower for aluminium compared to steel. The influence of the geometry and clamping of the jig was not considered, but could have an influence as well.

- Studying the influence of different materials with identical welds between Toho Tenax and Ten Cate material, showed no significant difference in energy levels. The difference between welding of weave to weave material compared to weave to chopped material showed a slight reduction in energy needed. However, taking the variation of the energy values into account, this difference was deemed insignificant.

Based on the inconclusive results it was found that the energy required remains extremely difficult to determine. Therefore it would be best to determine the energy required with experiments in the exact welding configuration, using the same settings as for the final weld creation.

In the up-scaling several new concepts and practicalities were researched of which the main conclusions are presented here. For the concept of the energy controlled spot welding in the middle of a large overlap it was found that:

- There was a large variation in the welding curves, size and shape of the consolidated welding areas and therefore the lap shear strength (LSS). The average LSS was also significantly lower than for the baseline welds.
- The reason for the large variation and low average LSS, was found in the fact that the whole overlap started to weld. Not only the area directly affected by the sonotrode but also surround areas and areas at the edge of the samples. It was found that due to the high stiffness the vibrations from the sonotrode were transmitted to other regions initiating welding, especially at the edges where the interfacial friction is highest.

A second concept that was investigated was the use of a dedicated area sized energy directors (EDs), having only ED material in area directly affected by the sonotrode.

- This concept showed a higher average LSS compared to the baseline welds, but still showed more variation in the LSS values as well. The variation found, however, was lower than for the spot welding of the larger overlap.
- Since there is some space around the ED in this concept, it was investigated if the process could be controlled using the easier travel as controlling parameter. It was found not to be suited for travel controlled welding. The flow fronts which squeeze out around the ED area cool down due to the colder surrounding material, and solidify. This makes it impossible to reach travel for the regular used welding force. Higher welding forces damage the samples and squeeze the flow fronts of the ED completely out of the overlap.

Next to the newly proposed concepts, several practicalities were considered regarding the up-scaling of the USW process.

- First the thickness and the attachment of the ED were considered
  - Using a thinner ED would result in less variation in the distance between the two parts, potentially decreasing secondary loads. However it was found that the energy consumption was higher and the welding curves were irregular compared

to the baseline. Due to this, and the minor impact on the main goal, it was decided to disregard this topic.

- Using the same technique as used for stacking several layers of polymeric film it was found possible to attach a layer to composite material. However the adherence proved not to be strong enough for processing with water jet cutting, and more importantly, the process was time and energy consuming.
- The attachment of ED to the sample using ultrasonic plunge spot welds proved to be a fast and easy solution. Although welding with these pre-attached EDs showed good results, it was found that heating does not commence at the fixated points. It is believed that this is caused by restrictions in interfacial friction which are responsible for the onset of the heating process. It is therefore concluded to minimize the fixation of the ED and preferably position the plunge welds away from the edge.
- Secondly, the sonotrode selection and sequential welding procedure were considered
  - Three types of sonotrodes were regarded, and it was concluded that the rectangular sonotrode proved to be most practical for the sequential welding of the hinges. Next to that the ED can be easily sized and positioned for the rectangular contact area of this sonotrode.
  - It is noted however that the chance of getting surface damage, especially if much hammering occurs, is higher for the rectangular sonotrode due to the relative sharp edges.

Based on these conclusions a sequential welding procedure was conceived. A new jig was designed and manufactured and a welding process was developed. The main findings are presented here:

- The jig design and clamping made it possible to easily create consistent welds for the settings used. The jig design is also flexible enough to be used for different welding configurations.
- The strength of the welded hinges met the Eurocopter load case in most of the tests. However, for all tests the hinge failed before the weld. It was also observed that much peel was introduced in the simple tension strength tests used.
- Furthermore it was found that in using this setup, the energy delivered by the sonotrode for the first weld does not affect the other ED for the second weld. This proves that the designed damping works sufficiently.

This research proves that it is possible to weld a chopped fibre hinge to a continuous weave plate, and proposes the method to do so. The method is believed to be applicable for similar applications as well. However, there are many areas which could be researched to improve the process. The most important ones are discussed in the next chapter (Future Research Recommendations).





## 8 Future Research Recommendations

---

The research presented shows the successful welding of the hinge to a continuous weave composite plate. The setup should be verified for the welding of the hinges to the continuous UD composite C-frames as well.

Next to that, to improve the sequential welding process proposed in this research several additional areas for future research are identified. First of all the settings of the USW machine were kept constant during this process, however the following two research topics are proposed:

- Researching the amplitude setting. Although a high amplitude is needed for the viscoelastic heating, it might be possible that a lower amplitude in the onset of the process will reduce the hammering effect. This would make the process eventually more efficient (not only for sequential welding but in general for TPCs). The USW available at the DASML allows for a variable amplitude in different welding stages which aids in investigating this topic.
- Since the difference of the weld quality between the left and right weld was apparent, it is recommended to identify different settings for the first and second (or subsequent) welds. The first weld might need more energy or a higher welding force relative to the second weld to make the overall process more efficient.

Secondly, since prediction of the energy needed for a weld proved to be complicated due to so many interactions, it is recommended to work on a prediction model which includes the mentioned variables (jig, machine, area overlap and the materials used). No (good) models exist and the energy prediction is best done using experiments.

Thirdly changes to the hardware are proposed to optimize the process:

- The clamping of the jig could be fitted with a frame to more precisely control the damping and clamping force. Also the current material used for damping, wears quickly due to the fact that it melts as well. Increasing the damping force might prove beneficial for higher welding forces.
- Relative simple sonotrodes were used in this research. However more complicated sonotrode configurations (welding four spots in one go for example) are possible and might prove useful in increasing the efficiency of the process.

Finally concerning the EDs:

- Even though the results for thinner ED was inconclusive for this research, it is recommended to further research the influence of the thickness of the ED. The use of thinner ED could result in a more efficient joint.
- Using plunge weld to attach the EDs proved successful but showed lack of melting at the joined spots. It is therefore recommended to use an approach in which the ED is welded in only one spot (the middle) and leave all edges free for interfacial friction. This approach could result in a better welded area.

- For practical purposes it might prove more convenient to weld the ED to the hinge (or other part considered). It is not likely that this would pose any problems, however this should be.

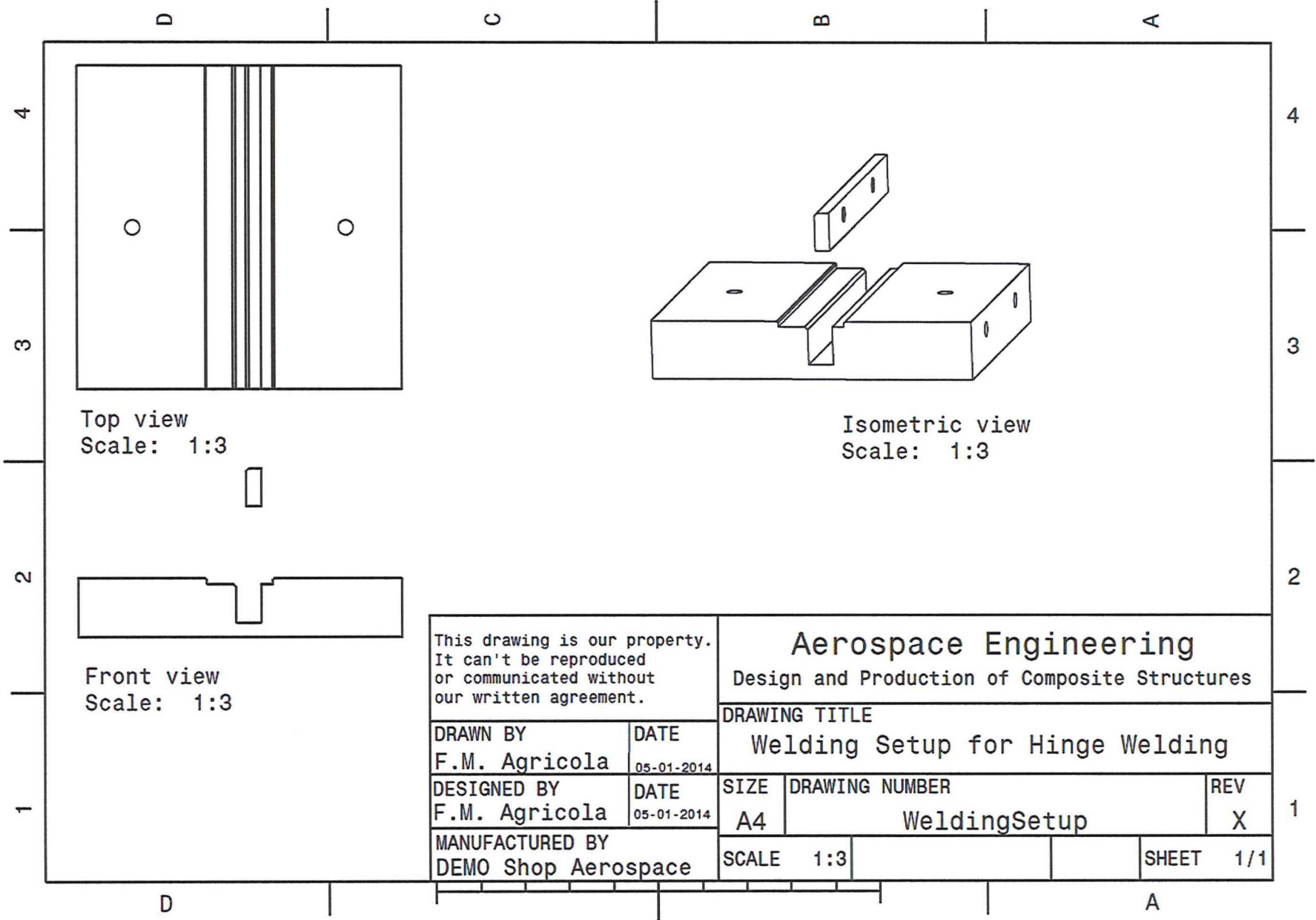
## Appendices

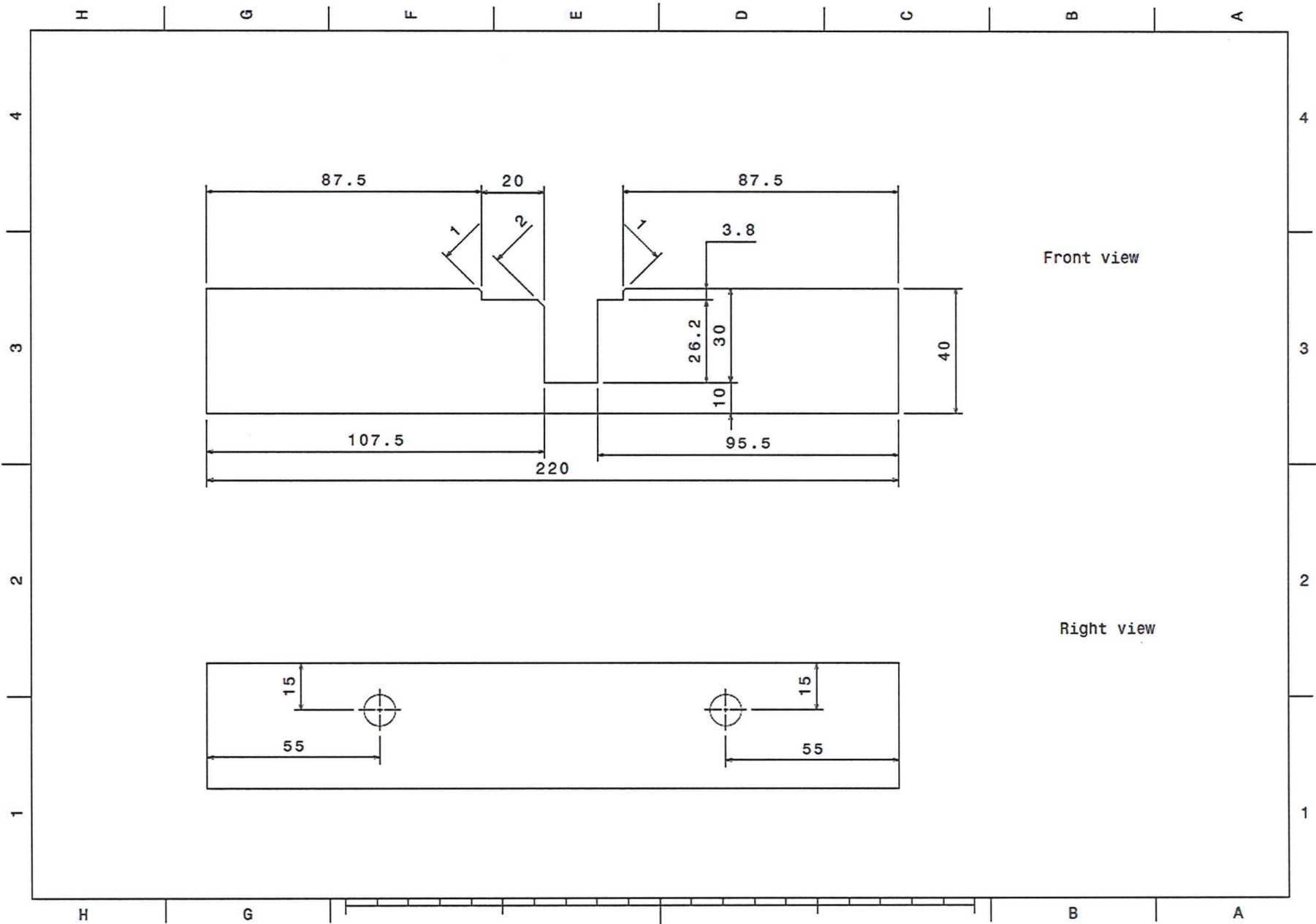
- A. Drawings of the New Jig Design
- B. Relevant Welding and LSS Parameters of All Welded Samples
- C. Welding and LSS Curves for 300 [N] and 1000 [N] Travel Controlled Welding of Continuous Weave CF/PEEK Toho Tenax Material Using a 2 Layer PEEK Toho Tenax ED
- D. Welding and LSS Curves for 300 [N] Travel Controlled Welding of chopped to chopped CF/PEEK Toho Tenax Material Using a 2 Layer PEEK Toho Tenax ED
- E. Welding and LSS Curves for 300 [N] Travel Controlled Welding of continuous weave to chopped CF/PEEK Toho Tenax Material Using a 2 Layer PEEK Toho Tenax ED
- F. Welding and LSS Curves for 500 [N] Travel Controlled Energy Determination Welds and Energy Controlled Spot Welding of s Larger Overlap
- G. Welding and LSS Curves for 500 [N] Energy Controlled Spot Welds Using Dedicated Area Sized ED
- H. Welding and LSS Curves for 500 [N] Energy Controlled Spot Welds Using Dedicated Area Sized ED Welding Weave (90 [°] Ten Cate) – Chopped Material
- I. Welding and LSS Curves for Pre-attached ED Welding
- J. Welding and LSS Curves for Hinge Welding



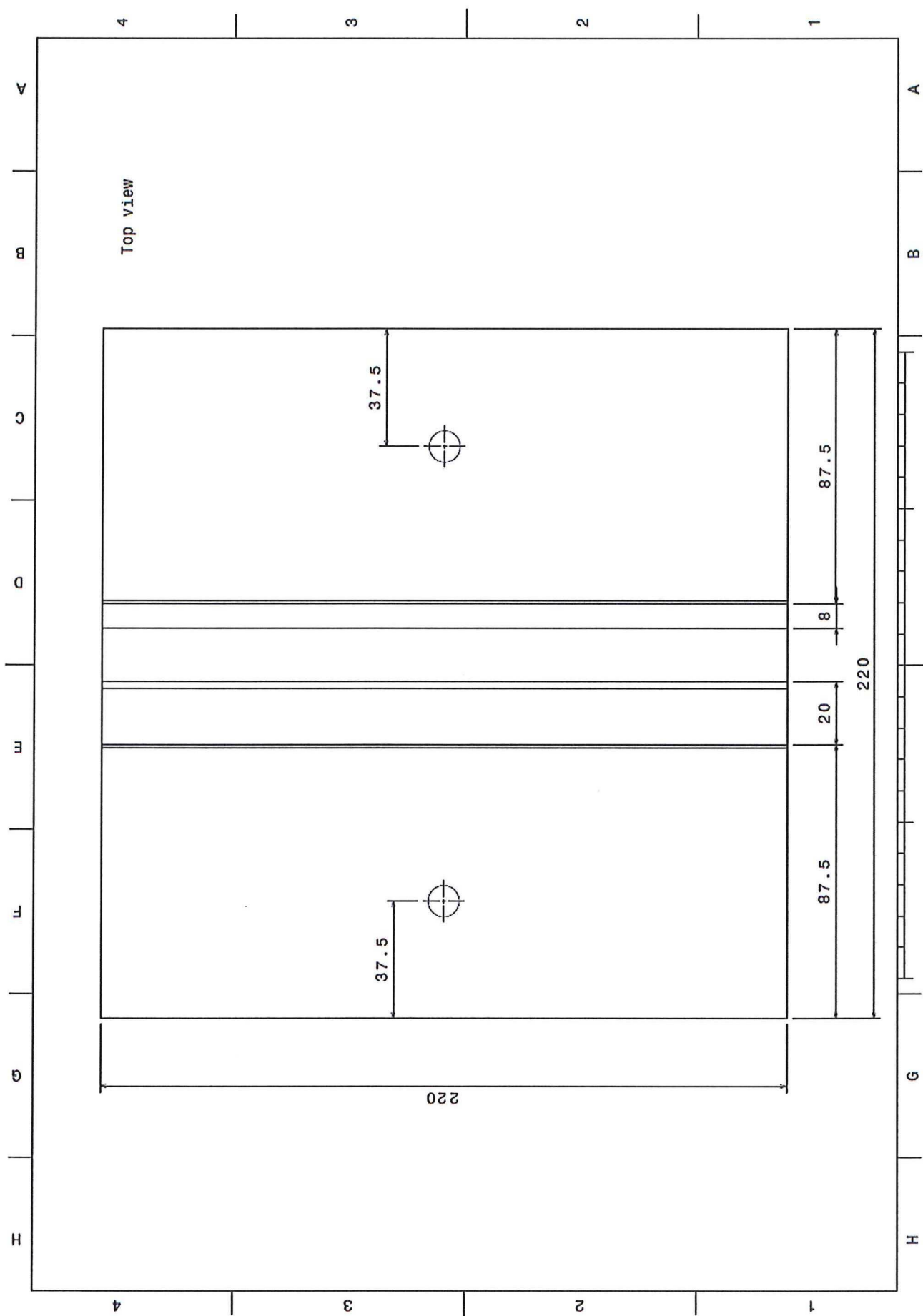


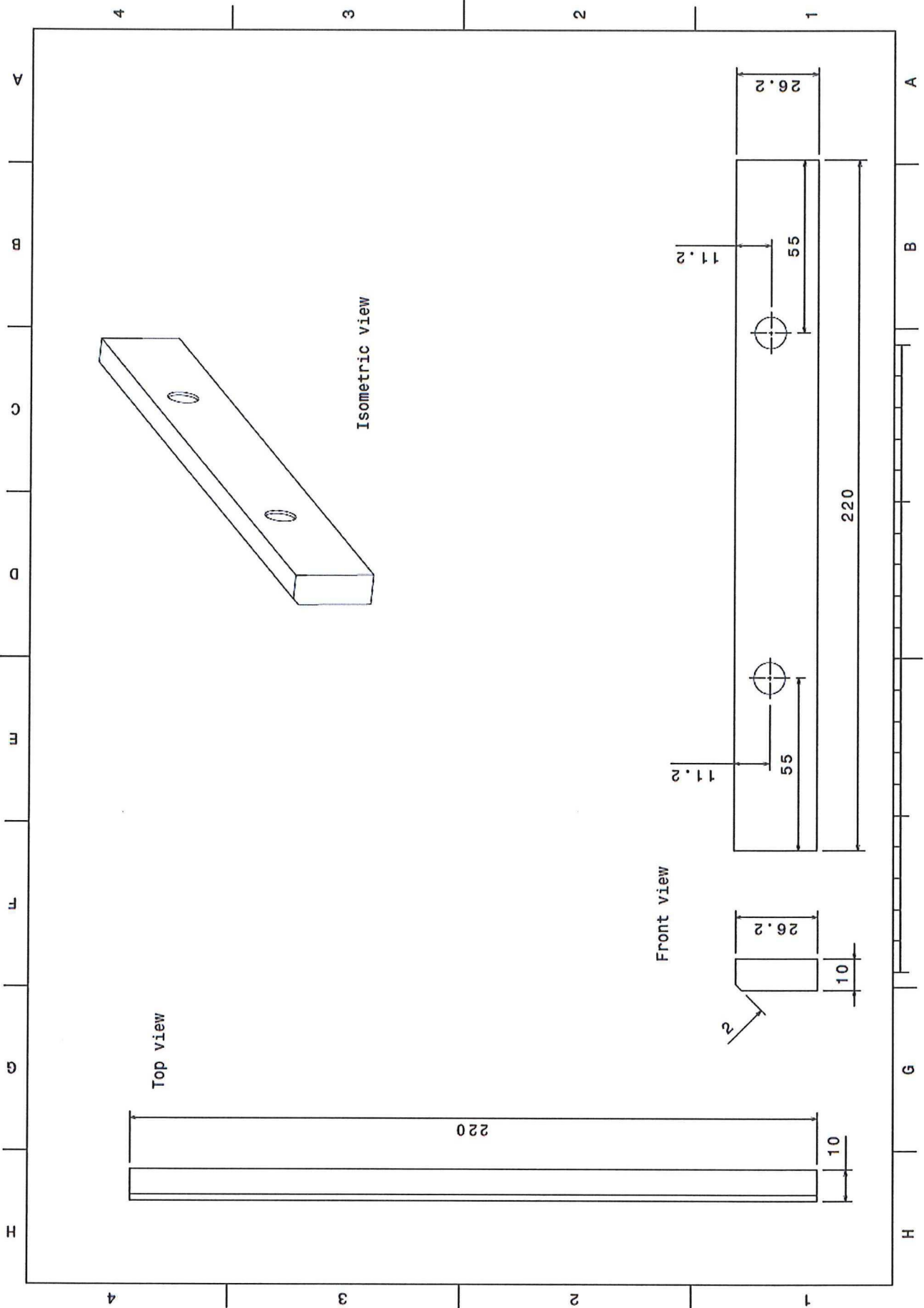
A. Drawings of the New Jig Design











## **B. Relevant Welding and LSS Parameters of All Welded Samples**



TT = Toho Tenax, TC = Ten Cate

| #  | Sample-ID           | Material B | Material T | ED           | Welding Conditions |          |           |                          |               |                 |                             |               |            |      |         | LSS Testing      |                |           |
|----|---------------------|------------|------------|--------------|--------------------|----------|-----------|--------------------------|---------------|-----------------|-----------------------------|---------------|------------|------|---------|------------------|----------------|-----------|
|    |                     |            |            |              | Overlap            | Jig-Type | Sonotrode | Rise of force (build-up) | Welding Force | Amplitude / ACU | Welding on: Travel - Energy | Weld distance | Max. Power | Time | Energy  | F <sub>max</sub> | S <sub>0</sub> | LSS       |
|    |                     |            |            |              | [-], [mm]          | [-]      | [-], [mm] | [N/s]                    | [N]           | [um]            | [%] - [Ws]                  | [mm]          | [%]        | [ms] | [Ws]    | [N]              | [mm²]          | [MPa]     |
| 1  | UW050713-001        | 0-deg (TT) | 0-deg (TT) | 2-layer (TT) | normal, 12.7       | 9109     | circ., 40 | 300                      | 300           | 9               | 100.00%                     | 0.9           | 53%        | 1327 | 2093.22 | 8351.125         | 322.199        | 25.919152 |
| 2  | UW050713-002        | 0-deg (TT) | 0-deg (TT) | 2-layer (TT) | normal, 12.7       | 9109     | circ., 40 | 300                      | 300           | 9               | 70.00%                      | 0.71          | 54%        | 1306 | 1865.54 | 12805.879        | 322.072        | 39.76092  |
| 3  | UW180913_2309-1-001 | 0-deg (TT) | 0-deg (TT) | 2-layer (TT) | normal, 12.7       | 9109     | circ., 40 | 300                      | 300           | 9               | 20.00%                      | 0.31          | 58%        | 697  | 997.14  | 12615.03         | 322.072        | 39.168355 |
| 4  | UW180913_2309-1-002 | 0-deg (TT) | 0-deg (TT) | 2-layer (TT) | normal, 12.7       | 9109     | circ., 40 | 300                      | 300           | 9               | 30.00%                      | 0.32          | 59%        | 908  | 1293.52 | 13388.231        | 321.945        | 41.585462 |
| 5  | UW180913_2309-1-003 | 0-deg (TT) | 0-deg (TT) | 2-layer (TT) | normal, 12.7       | 9109     | circ., 40 | 300                      | 300           | 9               | 30.00%                      | 0.35          | 54%        | 964  | 1395.71 | 12897.212        | 322.326        | 40.012943 |
| 6  | UW180913_2309-1-004 | 0-deg (TT) | 0-deg (TT) | 2-layer (TT) | normal, 12.7       | 9109     | circ., 40 | 300                      | 300           | 9               | 30.00%                      | 0.37          | 50%        | 1032 | 1416.17 | 13265.631        | 322.326        | 41.155944 |
| 7  | UW180913_2309-1-005 | 0-deg (TT) | 0-deg (TT) | 2-layer (TT) | normal, 12.7       | 9109     | circ., 40 | 300                      | 300           | 9               | 30.00%                      | 0.32          | 57%        | 893  | 1273.32 | 12471.07         | 322.326        | 38.690861 |
| 8  | UW180913_2309-1-006 | 0-deg (TT) | 0-deg (TT) | 2-layer (TT) | normal, 12.7       | 9109     | circ., 40 | 300                      | 300           | 9               | 30.00%                      | 0.34          | 53%        | 952  | 1294.21 | 11933.239        | 322.326        | 37.022267 |
| 9  | UW180913_2309-1-007 | 0-deg (TT) | 0-deg (TT) | 2-layer (TT) | normal, 12.7       | 9109     | circ., 40 | 300                      | 300           | 9               | 30.00%                      | 0.31          | 58%        | 762  | 1154.4  |                  |                |           |
| 10 | UW230913-001        | 0-deg (TT) | 0-deg (TT) | 2-layer (TT) | normal, 12.7       | 9109     | circ., 40 | 500                      | 1000          | 9               | 100.00%                     | 0.36          | 78%        | 698  | 1351.83 | 11267.56         | 323.088        | 34.874584 |
| 11 | UW230913-002        | 0-deg (TT) | 0-deg (TT) | 2-layer (TT) | normal, 12.7       | 9109     | circ., 40 | 500                      | 1000          | 9               | 65.00%                      | 0.25          | 76%        | 566  | 1072.89 | 12207.301        | 322.707        | 37.827815 |
| 12 | UW230913-003        | 0-deg (TT) | 0-deg (TT) | 2-layer (TT) | normal, 12.7       | 9109     | circ., 40 | 500                      | 1000          | 9               | 65.00%                      | 0.25          | 78%        | 556  | 1071.12 | 12959.913        | 322.072        | 40.23918  |
| 13 | UW230913-005        | 0-deg (TT) | 0-deg (TT) | 2-layer (TT) | normal, 12.7       | 9109     | circ., 40 | 500                      | 1000          | 9               | 65.00%                      | 0.26          | 76%        | 541  | 986.89  | 11604.829        | 322.707        | 35.960884 |
| 14 | UW230913-006        | 0-deg (TT) | 0-deg (TT) | 2-layer (TT) | normal, 12.7       | 9109     | circ., 40 | 500                      | 1000          | 9               | 65.00%                      | 0.26          | 80%        | 535  | 1024.91 | 11781.08         | 321.818        | 36.607897 |
| 15 | UW230913-007        | 0-deg (TT) | 0-deg (TT) | 2-layer (TT) | normal, 12.7       | 9109     | circ., 40 | 500                      | 1000          | 9               | 65.00%                      | 0.26          | 78%        | 568  | 1087.72 | 12758.192        | 323.088        | 39.488289 |
| 16 | UW300913-001        | 0-deg (TT) | 0-deg (TT) | 2-layer (TT) | large, 12.7        | 9109     | circ., 40 | 500                      | 1000          | 9               | 1000Ws                      | 0.25          | 81%        | 545  | 1000.19 | 13189.6          | 322.707        | 40.871749 |
| 17 | UW300913-002        | 0-deg (TT) | 0-deg (TT) | 2-layer (TT) | large, 12.7        | 9109     | circ., 40 | 500                      | 1000          | 9               | 1000Ws                      | 0.22          | 84%        | 509  | 1001.98 |                  |                |           |
| 18 | UW300913-003        | 0-deg (TT) | 0-deg (TT) | 2-layer (TT) | large, var (eWeld) | 9109     | circ., 40 | 500                      | 1000          | 9               | 1000Ws                      | 0             | 87%        | 535  | 1001.12 |                  |                |           |
| 19 | UW300913-004        | 0-deg (TT) | 0-deg (TT) | 2-layer (TT) | large, var (eWeld) | 9109     | circ., 40 | 500                      | 1000          | 9               | 1000Ws                      | 0.01          | 83%        | 528  | 1001.84 |                  |                |           |
| 20 | UW300913-2-001      | 0-deg (TT) | 0-deg (TT) | 1-layer (TT) | normal, 12.7       | 9109     | circ., 40 | 300                      | 300           | 9               | 100.00%                     | 0.68          | 60%        | 1252 | 1915.37 | 10104.989        | 321.945        | 31.387315 |
| 21 | UW300913-2-002      | 0-deg (TT) | 0-deg (TT) | 1-layer (TT) | normal, 12.7       | 9109     | circ., 40 | 500                      | 1000          | 9               | 100.00%                     | 0.26          | 77%        | 834  | 1592.84 | 11407.135        | 321.437        | 35.487933 |
| 22 | UW300913-2-003      | 0-deg (TT) | 0-deg (TT) | 1-layer (TT) | normal, 12.7       | 9109     | circ., 40 | 300                      | 300           | 9               | 33.00%                      | 0.49          | 62%        | 1004 | 1590.35 | 11284.84         | 322.326        | 35.010641 |
| 23 | UW300913-2-004      | 0-deg (TT) | 0-deg (TT) | 1-layer (TT) | normal, 12.7       | 9109     | circ., 40 | 300                      | 300           | 9               | 33.00%                      | 0.47          | 62%        | 1111 | 1788.66 | 11360.979        | 321.564        | 35.330384 |
| 24 | UW300913-2-005      | 0-deg (TT) | 0-deg (TT) | 1-layer (TT) | normal, 12.7       | 9109     | circ., 40 | 300                      | 300           | 9               | 33.00%                      | 0.47          | 58%        | 1189 | 1762.61 | 12025.319        | 322.58         | 37.278564 |
| 25 | UW300913-2-006      | 0-deg (TT) | 0-deg (TT) | 1-layer (TT) | normal, 12.7       | 9109     | circ., 40 | 300                      | 300           | 9               | 33.00%                      | 0.49          | 60%        | 1119 | 1646.35 | 10221.394        | 322.326        | 31.711353 |
| 26 | UW300913-2-007      | 0-deg (TT) | 0-deg (TT) | 1-layer (TT) | normal, 12.7       | 9109     | circ., 40 | 300                      | 300           | 9               | 33.00%                      | 0.49          | 65%        | 1141 | 1833.56 | 10554.999        | 321.945        | 32.7851   |
| 27 | UW300913-3-001      | 0-deg (TT) | 0-deg (TT) | 1-layer (TT) | large, var (eWeld) | 9109     | circ., 40 | 300                      | 300           | 9               | 1600Ws                      | 0.12          | 80%        | 809  | 1600.81 |                  |                |           |
| 28 | UW300913-3-002      | 0-deg (TT) | 0-deg (TT) | 1-layer (TT) | large, var (eWeld) | 9109     | circ., 40 | 300                      | 300           | 9               | 1400Ws                      | 0.09          | 64%        | 960  | 1400    |                  |                |           |
| 29 | UW151113-001        | 0-deg (TC) | 0-deg (TC) | 5-layer (TC) | normal, 19.05      | 9110     | circ., 40 | 300                      | 300           | 9               | 100.00%                     | 1.2           | 74%        | 1874 | 3263.37 |                  |                |           |
| 30 | UW151113-002        | 0-deg (TC) | 0-deg (TC) | 5-layer (TC) | normal, 19.05      | 9110     | circ., 40 | 300                      | 300           | 9               | 60.00%                      | 0.87          | 78%        | 1566 | 2963.07 |                  |                |           |
| 31 | UW151113-003        | 0-deg (TC) | 0-deg (TC) | 5-layer (TC) | normal, 19.05      | 9110     | circ., 40 | 300                      | 300           | 9               | 12.00%                      | 0.85          | 76%        | 1461 | 2828.73 | 6234.5254        | 483.2985       | 12.899948 |
| 32 | UW151113-004        | 0-deg (TC) | 0-deg (TC) | 5-layer (TC) | normal, 19.05      | 9110     | circ., 40 | 300                      | 300           | 9               | 12.00%                      | 0.88          | 76%        | 1553 | 2977.56 | 5127.415         | 483.2985       | 10.60921  |
| 33 | UW151113-005        | 0-deg (TC) | 0-deg (TC) | 5-layer (TC) | normal, 19.05      | 9110     | circ., 40 | 300                      | 300           | 9               | 12.00%                      | 0.42          | 78%        | 775  | 1503.72 |                  |                |           |
| 34 | UW151113-006        | 0-deg (TC) | 0-deg (TC) | 5-layer (TC) | normal, 19.05      | 9110     | circ., 40 | 300                      | 300           | 9               | 12.00%                      | 0.67          | 74%        | 1306 | 2532.4  | 8986.9297        | 483.108        | 18.60232  |
| 35 | UW181113-001        | 0-deg (TC) | 0-deg (TC) | 5-layer (TC) | normal, 12.7       | 9110     | circ., 40 | 300                      | 300           | 9               | 50.00%                      | 0.43          | 70%        | 918  | 1516.88 |                  |                |           |
| 36 | UW181113-002        | 0-deg (TC) | 0-deg (TC) | 5-layer (TC) | normal, 12.7       | 9110     | circ., 40 | 300                      | 300           | 9               | 41.67%                      | 0.44          | 72%        | 654  | 1136.02 | 12186.873        | 321.818        | 37.868836 |
| 37 | UW181113-003        | 0-deg (TC) | 0-deg (TC) | 5-layer (TC) | normal, 12.7       | 9110     | circ., 40 | 300                      | 300           | 9               | 16.00%                      | 0.28          | 61%        | 552  | 810.1   | 14620.438        | 321.437        | 45.484613 |
| 38 | UW181113-004        | 0-deg (TC) | 0-deg (TC) | 5-layer (TC) | normal, 12.7       | 9110     | circ., 40 | 300                      | 300           | 9               | 16.00%                      | 0.28          | 66%        | 492  | 779.66  | 13995.873        | 321.818        | 43.490026 |
| 39 | UW181113-005        | 0-deg (TC) | 0-deg (TC) | 5-layer (TC) | normal, 12.7       | 9110     | circ., 40 | 300                      | 300           | 9               | 16.00%                      | 0.31          | 70%        | 617  | 1051.25 | 10319            | 321.564        | 32.090035 |
| 40 | UW181113-2-001      | 0-deg (TC) | 0-deg (TC) | 5-layer (TC) | normal, 25.4       | 9110     | circ., 40 | 300                      | 300           | 9               | 48.00%                      | 0.61          | 77%        | 2617 | 4641.48 |                  |                |           |
| 41 | UW181113-2-002      | 0-deg (TC) | 0-deg (TC) | 5-layer (TC) | normal, 25.4       | 9110     | circ., 40 | 300                      | 300           | 9               | 8.33%                       | 0.59          | 81%        | 2265 | 4277.83 | 11321.91         | 642.874        | 17.611398 |
| 42 | UW181113-2-003      | 0-deg (TC) | 0-deg (TC) | 5-layer (TC) | normal, 25.4       | 9110     | circ., 40 | 300                      | 300           | 9               | 8.00%                       | 0.65          | 72%        | 2578 | 4567.63 | 11141.84         | 643.636        | 17.310778 |
| 43 | UW181113-2-004      | 0-deg (TC) | 0-deg (TC) | 5-layer (TC) | normal, 25.4       | 9110     | circ., 40 | 300                      | 300           | 9               | 16.67%                      | 0.7           | 72%        | 2369 | 4392.34 | 11190.494        | 642.874        | 17.406979 |
| 44 | UW10122013-001      | 0-deg (TT) | 0-deg (TT) | 2-layer (TT) | normal, 12.7       | 9109     | circ., 40 | 300                      | 300           | 9               | 30%                         | 0.33          | 64%        | 924  | 1519.18 |                  |                |           |
| 45 | UW10122013-002      | chop. (TT) | chop (TT)  | 2-layer (TT) | normal, 12.7       | 9109     | circ., 40 | 300                      | 300           | 9               | 100.00%                     | 0.38          | 51%        | 2460 | 2882.12 |                  |                |           |
| 46 | UW10122013-003      | chop. (TT) | chop (TT)  | 2-layer (TT) | normal, 12.7       | 9109     | circ., 40 | 300                      | 300           | 9               | 100.00%                     | 0.36          | 51%        | 2298 | 2705.21 |                  |                |           |
| 47 | UW11122013-001      | chop. (TT) | chop (TT)  | 2-layer (TT) | normal, 12.7       | 9109     | circ., 40 | 300                      | 300           | 9               | 44.00%                      | 0.31          | 47%        | 3560 | 4076.07 | 8424.2646        | 323.596        | 26.033278 |



TT = Toho Tenax, TC = Ten Cate

|           | Sample-ID        | Material B  | Material T  | ED           | Welding Conditions |           |                          |               |                 |                             |               |            |      |        |                  | LSS Testing    |          |           |
|-----------|------------------|-------------|-------------|--------------|--------------------|-----------|--------------------------|---------------|-----------------|-----------------------------|---------------|------------|------|--------|------------------|----------------|----------|-----------|
| Overlap   |                  |             |             |              | Jig-Type           | Sonotrode | Rise of force (build-up) | Welding Force | Amplitude / ACU | Welding on: Travel - Energy | Weld distance | Max. Power | Time | Energy | F <sub>max</sub> | S <sub>0</sub> | LSS      |           |
| [-], [mm] |                  |             |             |              | [-]                | [-], [mm] | [N/s]                    | [N]           | [um]            | [%] - [Ws]                  | [mm]          | [%]        | [ms] | [Ws]   | [N]              | [mm²]          | [MPa]    |           |
| #         |                  |             |             |              |                    |           |                          |               |                 |                             |               |            |      |        |                  |                |          |           |
| 48        | UW11122013-002   | chop. (TT)  | chop (TT)   | 2-layer (TT) | normal, 12.7       | 9109      | circ., 40                | 300           | 300             | 9                           | 44.00%        | 0.28       | 61%  | 452    | 620.84           |                |          |           |
| 49        | UW11122013-003   | chop. (TT)  | chop (TT)   | 2-layer (TT) | normal, 12.7       | 9109      | circ., 40                | 300           | 300             | 9                           | 100.00%       | 0.4        | 69%  | 2354   | 2928.44          |                |          |           |
| 50        | UW11122013-2-001 | chop. (TT)  | 0-deg (TT)  | 2-layer (TT) | normal, 12.7       | 9109      | circ., 40                | 300           | 300             | 9                           | 80.00%        | 0.59       | 54%  | 1458   | 2041.68          | 7543.499       | 308.864  | 24.423368 |
| 51        | UW11122013-2-002 | chop. (TT)  | 0-deg (TT)  | 2-layer (TT) | normal, 12.7       | 9109      | circ., 40                | 300           | 300             | 9                           | 20.00%        | 0.35       | 59%  | 948    | 1328.37          | 13517.65       | 313.182  | 43.162284 |
| 52        | UW11122013-2-003 | chop. (TT)  | 0-deg (TT)  | 2-layer (TT) | normal, 12.7       | 9109      | circ., 40                | 300           | 300             | 9                           | 20.00%        | 0.18       | 66%  | 788    | 1235.11          | 6581.5024      | 312.42   | 21.066201 |
| 53        | UW11122013-2-004 | chop. (TT)  | 0-deg (TT)  | 2-layer (TT) | normal, 12.7       | 9109      | circ., 40                | 300           | 300             | 9                           | 20.00%        | 0.31       | 57%  | 834    | 1148.05          | 11950.999      | 312.801  | 38.206396 |
| 54        | UW11122013-2-005 | chop. (TT)  | 0-deg (TT)  | 2-layer (TT) | normal, 12.7       | 9109      | circ., 40                | 300           | 300             | 9                           | 20.00%        | 0.27       | 53%  | 1160   | 1474.94          | 9960.708       | 313.309  | 31.791963 |
| 55        | UW11122013-2-006 | chop. (TT)  | 0-deg (TT)  | 2-layer (TT) | normal, 12.7       | 9109      | circ., 40                | 300           | 300             | 9                           | 20.00%        | 0.24       | 59%  | 805    | 1189.29          |                |          |           |
| 56        | UW12122013-001   | 0-deg (TT)  | 0-deg (TT)  | 2-layer (TT) | normal, 12.7       | 9110      | circ., 40                | 300           | 300             | 9                           | 50.00%        | 0.44       | 75%  | 934    | 1546.18          |                |          |           |
| 57        | UW12122013-002   | 0-deg (TT)  | 0-deg (TT)  | 2-layer (TT) | normal, 12.7       | 9110      | circ., 40                | 300           | 300             | 9                           | 75.00%        | 0.61       | 69%  | 894    | 1559.61          |                |          |           |
| 58        | UW12122013-003   | 0-deg (TT)  | 0-deg (TT)  | 2-layer (TT) | normal, 12.7       | 9110      | circ., 40                | 300           | 300             | 9                           | 100.00%       | 0.65       | 74%  | 1020   | 1777.47          |                |          |           |
| 59        | UW12122013-004   | 0-deg (TT)  | 0-deg (TT)  | 2-layer (TT) | normal, 12.7       | 9110      | circ., 40                | 300           | 300             | 9                           | 43.00%        | 0.35       | 75%  | 616    | 1080.65          | 13105.29       | 321.945  | 40.706611 |
| 60        | UW12122013-005   | 0-deg (TT)  | 0-deg (TT)  | 2-layer (TT) | normal, 12.7       | 9110      | circ., 40                | 300           | 300             | 9                           | 43.00%        | 0.35       | 71%  | 668    | 1158.89          | 12113.189      | 323.215  | 37.477188 |
| 61        | UW12122013-006   | 0-deg (TT)  | 0-deg (TT)  | 2-layer (TT) | normal, 12.7       | 9110      | circ., 40                | 300           | 300             | 9                           | 43.00%        | 0.34       | 74%  | 558    | 984.96           | 13093.278      | 322.072  | 40.653265 |
| 62        | UW12122013-007   | 0-deg (TT)  | 0-deg (TT)  | 2-layer (TT) | normal, 12.7       | 9110      | circ., 40                | 300           | 300             | 9                           | 43.00%        | 0.33       | 74%  | 630    | 1162.15          | 7402.5532      | 322.326  | 22.966044 |
| 63        | UW12122013-008   | 0-deg (TT)  | 0-deg (TT)  | 2-layer (TT) | normal, 12.7       | 9110      | circ., 40                | 300           | 300             | 9                           | 43.00%        | 0.34       | 72%  | 420    | 706.65           | 12021.425      | 322.072  | 37.325271 |
| 64        | UW12122013-009   | 0-deg (TT)  | 0-deg (TT)  | 2-layer (TT) | normal, 19.05      | 9110      | circ., 40                | 300           | 300             | 9                           | 100.00%       | 0.94       | 77%  | 1670   | 3373.61          | 6204.2617      | 483.2985 | 12.837329 |
| 65        | UW12122013-010   | 0-deg (TT)  | 0-deg (TT)  | 2-layer (TT) | normal, 19.05      | 9110      | circ., 40                | 300           | 300             | 9                           | 75.00%        | 0.94       | 78%  | 1672   | 3462.99          | 3265.0137      | 483.2985 | 6.7556876 |
| 66        | UW12122013-011   | 0-deg (TT)  | 0-deg (TT)  | 2-layer (TT) | normal, 19.05      | 9110      | circ., 40                | 300           | 300             | 9                           | 12.50%        | 0.74       | 78%  | 1515   | 3154.47          | 6216.7466      | 482.727  | 12.87839  |
| 67        | UW12122013-012   | 0-deg (TT)  | 0-deg (TT)  | 2-layer (TT) | normal, 25.4       | 9110      | circ., 40                | 300           | 300             | 9                           | 100.00%       | 0.72       | 79%  | 2704   | 5235.31          | 7108.2354      | 644.144  | 11.035165 |
| 68        | UW171213-001     | 0-deg (TC)  | 0-deg (TC)  | 5-layer (TC) | normal, 19.05      | 9110      | circ., 40                | 300           | 450             | 9                           | 100.00%       | 0.61       | 90%  | 1265   | 2548.79          |                |          |           |
| 69        | UW171213-002     | 0-deg (TC)  | 0-deg (TC)  | 5-layer (TC) | normal, 19.05      | 9110      | circ., 40                | 300           | 600             | 9                           | 93.00%        | 0.55       | 101% | 1242   | 2380.38          |                |          |           |
| 70        | UW181213-001     | 0-deg (TC)  | 0-deg (TC)  | 5-layer (TC) | normal, 12.7       | 9110      | circ., 40                | 250           | 500             | 9                           | 100.00%       | 0.55       | 77%  | 871    | 1507.9           |                |          |           |
| 71        | UW181213-002     | 0-deg (TT)  | 0-deg (TT)  | 5-layer (TC) | normal, 12.7       | 9110      | circ., 40                | 250           | 500             | 9                           | 100.00%       | 0.5        | 73%  | 932    | 1659.46          |                |          |           |
| 72        | UW181213-003     | 90-deg (TC) | 90-deg (TC) | 5-layer (TC) | normal, 12.7       | 9110      | rect, 30.1*14            | 250           | 500             | 3                           | 100.00%       | 0.54       | 68%  | 769    | 1252.55          |                |          |           |
| 73        | UW191213-001     | 0-deg (PPS) | 0-deg (PPS) | PPS          | normal, 14.9       | 9110      | rect, 30.1*14            | 250           | 500             | 3                           | 100.00%       | 0.58       | 68%  | 574    | 945.84           | 13779.427      | 380.099  | 36.252205 |
| 74        | UW191213-002     | 0-deg (PPS) | 0-deg (PPS) | PPS          | normal, 14.9       | 9110      | rect, 30.1*14            | 250           | 500             | 3                           | 43.00%        | 0.36       | 74%  | 308    | 459.05           | 11535.517      | 378.907  | 30.44419  |
| 75        | UW191213-003     | 0-deg (TT)  | 0-deg (TT)  | 2-layer (TT) | normal, 14.9       | 9110      | rect, 30.1*14            | 250           | 360             | 3                           | 100.00%       | 0.67       | 61%  | 1297   | 1901.23          | 14981.536      | 377.566  | 39.679251 |
| 76        | UW191213-004     | 0-deg (TT)  | 0-deg (TT)  | 2-layer (TT) | normal, 14.9       | 9110      | rect, 30.1*14            | 250           | 360             | 3                           | 100.00%       | 0.68       | 72%  | 1045   | 1793.33          | 13661.621      | 377.864  | 36.154863 |
| 77        | UW191213-005     | 0-deg (TT)  | 0-deg (TT)  | 2-layer (TT) | normal, 14.9       | 9110      | rect, 30.1*14            | 250           | 360             | 3                           | 100.00%       | 0.69       | 73%  | 1042   | 1782.23          |                |          |           |
| 78        | UW191213-006     | 0-deg (TT)  | 0-deg (TT)  | 2-layer (TT) | normal, 14.9       | 9110      | rect, 30.1*14            | 250           | 500             | 3                           | 100.00%       | 0.57       | 72%  | 902    | 1645.49          | 13658.862      | 377.715  | 36.161821 |
| 79        | UW191213-007     | 0-deg (TT)  | 0-deg (TT)  | 2-layer (TT) | normal, 14.9       | 9110      | rect, 30.1*14            | 250           | 500             | 3                           | 100.00%       | 0.54       | 70%  | 944    | 1643.9           |                |          |           |
| 80        | UW191213-008     | 0-deg (TT)  | 0-deg (TT)  | 2-layer (TT) | normal, 14.9       | 9110      | rect, 30.1*14            | 250           | 500             | 3                           | 20.00%        | 0.24       | 79%  | 481    | 873.4            | 14989.32       | 377.715  | 39.684207 |
| 81        | UW191213-009     | 0-deg (TT)  | 0-deg (TT)  | 2-layer (TT) | normal, 14.9       | 9110      | rect, 30.1*14            | 250           | 500             | 3                           | 20.00%        | 0.23       | 78%  | 517    | 942.05           | 14773.467      | 378.46   | 39.035742 |
| 82        | UW191213-010     | 0-deg (TT)  | 0-deg (TT)  | 2-layer (TT) | normal, 14.9       | 9110      | rect, 30.1*14            | 250           | 500             | 3                           | 20.00%        | 0.22       | 73%  | 490    | 834.56           | 13570.24       | 378.162  | 35.884727 |
| 83        | UW191213-011     | 0-deg (TT)  | 0-deg (TT)  | 2-layer (TT) | normal, 14.9       | 9110      | rect, 30.1*14            | 250           | 500             | 3                           | 20.00%        | 0.23       | 74%  | 496    | 864.75           | 14337.52       | 378.46   | 37.883844 |
| 84        | UW191213-012     | 0-deg (TT)  | 0-deg (TT)  | 2-layer (TT) | normal, 14.9       | 9110      | rect, 30.1*14            | 250           | 500             | 3                           | 20.00%        | 0.21       | 70%  | 725    | 1258.59          |                |          |           |
| 85        | UW191213-013     | 0-deg (TT)  | 0-deg (TT)  | 2-layer (TT) | normal, 14.9       | 9110      | rect, 30.1*14            | 250           | 500             | 3                           | 20.00%        | 0.24       | 70%  | 565    | 865.24           | 15222.061      | 378.46   | 40.221055 |
| 86        | UW191213-014     | 0-deg (TT)  | 0-deg (TT)  | 2-layer (TT) | normal, 14.9       | 9110      | rect, 30.1*14            | 250           | 500             | 3                           | 20.00%        | 0.23       | 72%  | 448    | 747.44           |                |          |           |
| 87        | UW201213-001     | 0-deg (TT)  | 0-deg (TT)  | 2-layer (TT) | large, var (eWeld) | 9110      | rect, 30.1*14            | 250           | 500             | 3                           | 855           | 0.08       | 91%  | 419    | 856.86           |                |          |           |
| 88        | UW201213-002     | 0-deg (TT)  | 0-deg (TT)  | 2-layer (TT) | large, var (eWeld) | 9110      | rect, 30.1*14            | 250           | 500             | 3                           | 855           | 0.16       | 87%  | 451    | 856.17           | 16607.441      | 378.311  | 43.898912 |
| 89        | UW201213-003     | 0-deg (TT)  | 0-deg (TT)  | 2-layer (TT) | large, var (eWeld) | 9110      | rect, 30.1*14            | 250           | 500             | 3                           | 855           | 0.16       | 91%  | 499    | 856.26           | 13045.776      | 378.609  | 34.457122 |
| 90        | UW201213-004     | 0-deg (TT)  | 0-deg (TT)  | 2-layer (TT) | large, var (eWeld) | 9110      | rect, 30.1*14            | 250           | 500             | 3                           | 855           | 0.07       | 85%  | 434    | 855.86           | 14004.321      | 378.162  | 37.032598 |
| 91        | UW201213-005     | 0-deg (TT)  | 0-deg (TT)  | 2-layer (TT) | large, var (eWeld) | 9110      | rect, 30.1*14            | 250           | 500             | 3                           | 855           | 0.07       | 88%  | 435    | 855.74           | 11497.563      | 378.46   | 30.379862 |
| 92        | UW201213-006     | 0-deg (TT)  | 0-deg (TT)  | 2-layer (TT) | large, var (eWeld) | 9110      | rect, 30.1*14            | 250           | 500             | 3                           | 855           | 0.05       | 94%  | 416    | 857.29           | 12890.356      | 378.46   | 34.060023 |
| 93        | UW100114-001     | 90-deg (TC) | chop (TT)   | 2-layer (TT) | large, var (eWeld) | 9110      | circ., 10                | 300           | 300             | 70.8                        | 500           | 0.08       | 21%  | 1494   | 500.06           |                |          |           |
| 94        | UW100114-002     | 90-deg (TC) | chop (TT)   | 2-layer (TT) | large, var (eWeld) | 9110      | circ., 10                | 250           | 500             | 70.8                        | 800           | 0.07       | 58%  | 1622   | 800              |                |          |           |



TT = Toho Tenax, TC = Ten Cate

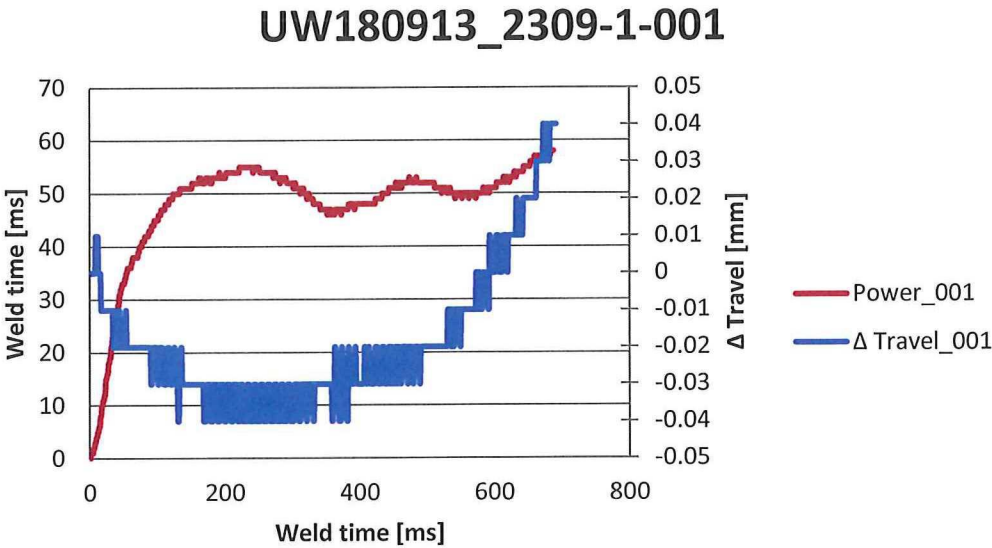
|     | Sample-ID    | Material B  | Material T  | ED           |                     | Welding Conditions |               |                          |               |                 |                             |               |            |      |         |                  | LSS Testing    |           |  |
|-----|--------------|-------------|-------------|--------------|---------------------|--------------------|---------------|--------------------------|---------------|-----------------|-----------------------------|---------------|------------|------|---------|------------------|----------------|-----------|--|
|     |              |             |             |              | Overlap             | Jig-Type           | Sonotrode     | Rise of force (build-up) | Welding Force | Amplitude / ACU | Welding on: Travel - Energy | Weld distance | Max. Power | Time | Energy  | F <sub>max</sub> | S <sub>0</sub> | LSS       |  |
| #   |              |             |             |              | [-], [mm]           | [-]                | [-], [mm]     | [N/s]                    | [N]           | [um]            | [%] - [Ws]                  | [mm]          | [%]        | [ms] | [Ws]    | [N]              | [mm²]          | [MPa]     |  |
| 95  | UW160114-001 | 0-deg (TC)  | 0-deg (TC)  | 5-layer (TC) | normal, 14.9        | 9110               | rect, 30.1*14 | 250                      | 500           | 2               | 100                         | 0.61          | 69%        | 1168 | 1765.8  |                  |                |           |  |
| 96  | UW160114-002 | 0-deg (TC)  | 0-deg (TC)  | 5-layer (TC) | normal, 14.9        | 9110               | rect, 30.1*14 | 250                      | 500           | 3               | 855                         | 0.25          | 69%        | 532  | 856.08  |                  |                |           |  |
| 97  | UW160114-003 | 0-deg (TC)  | 0-deg (TC)  | 5-layer (TC) | normal, 14.9        | 9110               | rect, 30.1*14 | 250                      | 500           | 3               | 880                         | 0.25          | 72%        | 512  | 881.38  | 15837.837        | 378.162        | 41.88109  |  |
| 98  | UW160114-004 | 0-deg (TC)  | 0-deg (TC)  | 5-layer (TC) | normal, 14.9        | 9110               | rect, 30.1*14 | 250                      | 500           | 3               | 865                         | 0.21          | 68%        | 531  | 866.28  | 14231.597        | 378.013        | 37.648432 |  |
| 99  | UW160114-005 | 0-deg (TC)  | 0-deg (TC)  | 5-layer (TC) | normal, 14.9        | 9110               | rect, 30.1*14 | 250                      | 500           | 3               | 855                         | 0.24          | 77%        | 468  | 856.03  |                  |                |           |  |
| 100 | UW160114-006 | 0-deg (TC)  | 0-deg (TC)  | 5-layer (TC) | normal, 14.9        | 9110               | rect, 30.1*14 | 250                      | 500           | 3               | 855                         | 0.22          | 77%        | 493  | 855.97  | 16598.607        | 377.864        | 43.927464 |  |
| 101 | UW160114-007 | 0-deg (TC)  | 0-deg (TC)  | 5-layer (TC) | small ED, 14.9      | 9110               | rect, 30.1*14 | 250                      | 500           | 3               | 855                         | 0.11          | 66%        | 614  | 855.46  | 17024.271        | 378.013        | 45.036206 |  |
| 102 | UW160114-008 | 0-deg (TC)  | 0-deg (TC)  | 5-layer (TC) | small ED, 14.9      | 9110               | rect, 30.1*14 | 250                      | 500           | 3               | 855                         | 0.14          | 75%        | 515  | 856.55  | 15240.543        | 377.715        | 40.349319 |  |
| 103 | UW160114-009 | 0-deg (TC)  | 0-deg (TC)  | 5-layer (TC) | small ED, 14.9      | 9110               | rect, 30.1*14 | 250                      | 500           | 3               | 855                         | 0.13          | 63%        | 578  | 855.56  | 19668.027        | 378.162        | 52.009529 |  |
| 104 | UW160114-010 | 0-deg (TC)  | 0-deg (TC)  | 5-layer (TC) | small ED, 14.9      | 9110               | rect, 30.1*14 | 250                      | 500           | 3               | 855                         | 0.14          | 67%        | 581  | 855.51  | 17308.416        | 377.864        | 45.805941 |  |
| 105 | UW160114-011 | 0-deg (TC)  | 0-deg (TC)  | 5-layer (TC) | small ED, 14.9      | 9110               | rect, 30.1*14 | 250                      | 500           | 3               | 855                         | 0.12          | 74%        | 480  | 855.66  | 14574.756        | 378.013        | 38.556229 |  |
| 106 | UW160114-012 | 0-deg (TC)  | 0-deg (TC)  | 5-layer (TC) | small ED, 14.9      | 9110               | rect, 30.1*14 | 250                      | 500           | 3               | 855                         | 0.13          | 67%        | 571  | 855.67  |                  |                |           |  |
| 107 | uw280114-001 | 90-deg (TC) | 90-deg (TC) | 5-layer (TC) | small ED, 14.9      | 9110               | rect, 30.1*14 | 250                      | 500           | 3               | 100                         | 0             | 55%        | 3161 | 3025.5  |                  |                |           |  |
| 108 | uw280114-002 | 90-deg (TC) | 90-deg (TC) | 5-layer (TC) | small ED, 14.9      | 9110               | rect, 30.1*14 | 500                      | 1000          | 3               | 50                          | 0.3           | 98%        | 1138 | 2184.52 |                  |                |           |  |
| 109 | uw280114-010 | 90-deg (TC) | 90-deg (TC) | 5-layer (TC) | small ED, 14.9      | 9110               | rect, 30.1*14 | 500                      | 1000          | 3               | 100                         | 0.46          | 86%        | 2797 | 3118.02 |                  |                |           |  |
| 110 | uw280114-011 | 90-deg (TC) | 90-deg (TC) | 5-layer (TC) | small ED, 14.9      | 9110               | rect, 30.1*14 | 500                      | 1000          | 3               | 0.08(32)                    | 0.27          | 86%        | 1327 | 2490.68 | 14564.403        | 378.758        | 38.453058 |  |
| 111 | uw280114-012 | 90-deg (TC) | 90-deg (TC) | 5-layer (TC) | small ED, 14.9      | 9110               | rect, 30.1*14 | 500                      | 1000          | 3               | 0.08(32)                    | 0.25          | 84%        | 1287 | 2153.01 |                  |                |           |  |
| 112 | uw280114-003 | chop. (TT)  | 90-deg (TC) | 5-layer (TC) | small ED, 14.9      | 9110               | rect, 30.1*14 | 250                      | 500           | 3               | 865                         | 0.11          | 74%        | 578  | 856.49  | 7557.5796        | 378.162        | 19.985032 |  |
| 113 | uw280114-004 | chop. (TT)  | 90-deg (TC) | 5-layer (TC) | small ED, 14.9      | 9110               | rect, 30.1*14 | 250                      | 500           | 3               | 855                         | 0.14          | 79%        | 517  | 857.15  | 7260.8799        | 378.311        | 19.192886 |  |
| 114 | uw280114-005 | chop. (TT)  | 90-deg (TC) | 5-layer (TC) | small ED, 14.9      | 9110               | rect, 30.1*14 | 250                      | 500           | 3               | 855                         | 0.12          | 84%        | 454  | 855.95  | 4673.667         | 377.864        | 12.368648 |  |
| 115 | uw280114-006 | chop. (TT)  | 90-deg (TC) | 5-layer (TC) | small ED, 14.9      | 9110               | rect, 30.1*14 | 250                      | 500           | 3               | 855                         | 0.12          | 69%        | 564  | 856.81  |                  |                |           |  |
| 116 | uw280114-007 | chop. (TT)  | 90-deg (TC) | 5-layer (TC) | small ED, 14.9      | 9110               | rect, 30.1*14 | 250                      | 500           | 3               | 855                         | 0.13          | 72%        | 542  | 856.93  | 7578.9072        | 378.609        | 20.017768 |  |
| 117 | uw280114-008 | chop. (TT)  | 90-deg (TC) | 5-layer (TC) | small ED, 14.9      | 9110               | rect, 30.1*14 | 250                      | 500           | 3               | 855                         | 0.13          | 69%        | 615  | 856.43  | 8531.5059        | 373.692        | 22.830314 |  |
| 118 | uw280114-009 | chop. (TT)  | 90-deg (TC) | 5-layer (TC) | small ED, 14.9      | 9110               | rect, 30.1*14 | 250                      | 500           | 3               | 855                         | 0.12          | 67%        | 561  | 856.42  |                  |                |           |  |
| 119 | UW020214-001 | 90-deg (TC) | 90-deg (TC) | 5-layer (TC) | small ED, 14.9      | 9110               | circ., 40     | 250                      | 500           | 9               | 100                         | 0.44          | 114%       | 1636 | 3875.32 |                  |                |           |  |
| 120 | UW020214-002 | 90-deg (TC) | 90-deg (TC) | 5-layer (TC) | small ED, 14.9      | 9110               | circ., 40     | 250                      | 500           | 9               | 855                         | 0.11          | 95%        | 373  | 856.26  | 12915.965        | 378.46         | 34.127688 |  |
| 121 | UW020214-003 | 90-deg (TC) | 90-deg (TC) | 5-layer (TC) | small ED, 14.9      | 9110               | circ., 40     | 500                      | 1000          | 9               | 0.08                        | 0.15          | 105%       | 810  | 1833.96 |                  |                |           |  |
| 122 | UW020214-004 | 90-deg (TC) | 90-deg (TC) | 5-layer (TC) | pre-attach ED, 14.9 | 9110               | rect, 30.1*14 | 250                      | 500           | 3               | 100 (0.25)                  | 0.51          | 72%        | 794  | 1338.8  | 13837.895        | 378.758        | 36.534923 |  |
| 123 | UW020214-005 | 90-deg (TC) | 90-deg (TC) | 5-layer (TC) | pre-attach ED, 14.9 | 9110               | rect, 30.1*14 | 250                      | 500           | 3               | 100 (0.25)                  | 0.57          | 71%        | 994  | 587.65  |                  |                |           |  |
| 124 | UW020214-006 | 90-deg (TC) | 90-deg (TC) | 5-layer (TC) | pre-attach ED, 14.9 | 9110               | rect, 30.1*14 | 250                      | 500           | 3               | 50 (0.12)                   | 0.36          | 70%        | 667  | 1146.98 |                  |                |           |  |
| 125 | UW020214-007 | 90-deg (TC) | 90-deg (TC) | 5-layer (TC) | pre-attach ED, 14.9 | 9110               | rect, 30.1*14 | 250                      | 500           | 3               | 20 (0.05)                   | 0.27          | 69%        | 582  | 954.39  | 14251.08         | 378.162        | 37.685119 |  |



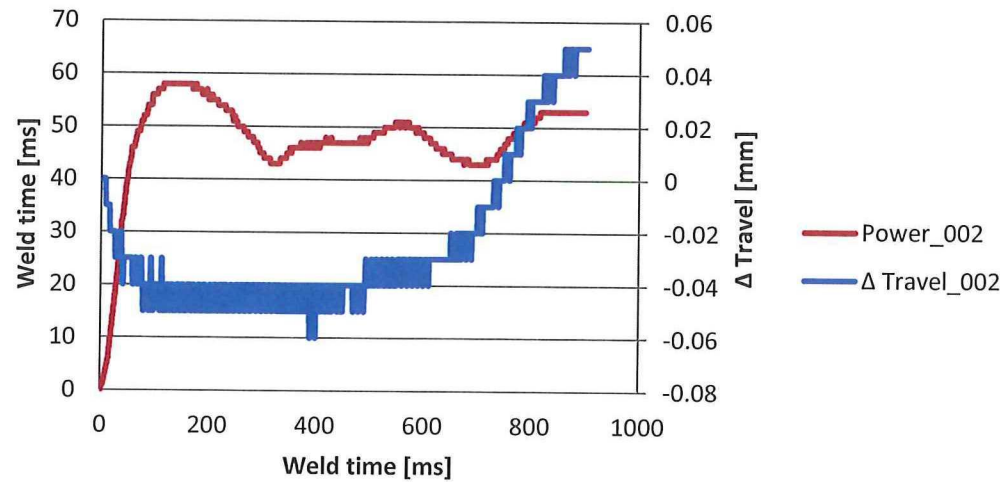
C. Welding and LSS Curves for 300 [N] and 1000 [N] Travel Controlled Welding of Continuous Weave CF/PEEK Toho Tenax Material Using a 2 Layer PEEK Toho Tenax ED

|                  |           | I) Initial Phase    | II) Vibration Phase |                     |                              |                       | III) Solidification Phase |                   |
|------------------|-----------|---------------------|---------------------|---------------------|------------------------------|-----------------------|---------------------------|-------------------|
| Materials        | Sonotrode | Rise of Force [N/s] | Welding Force [N]   | Rise of Force [N/s] | Amplitude [μm] / setting [-] | Controlling Parameter | Force                     | Holding Time [ms] |
| TT weave – weave | Ø 40 [mm] | 300                 | 300                 | 0                   | 86.2 (9)                     | Travel                | 1000                      | 4000              |
| TT weave – weave | Ø 40 [mm] | 500                 | 1000                | 0                   | 86.2 (9)                     | Travel                | 1000                      | 4000              |

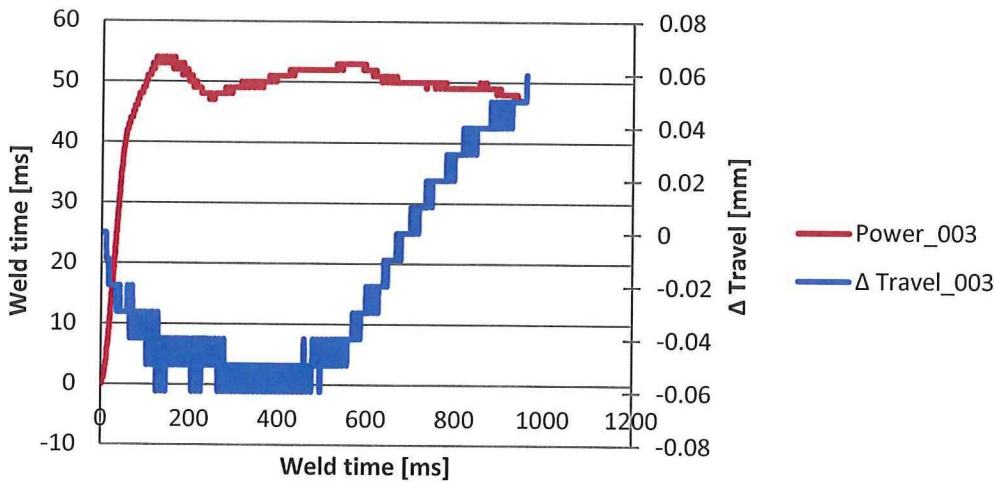
300 [N]



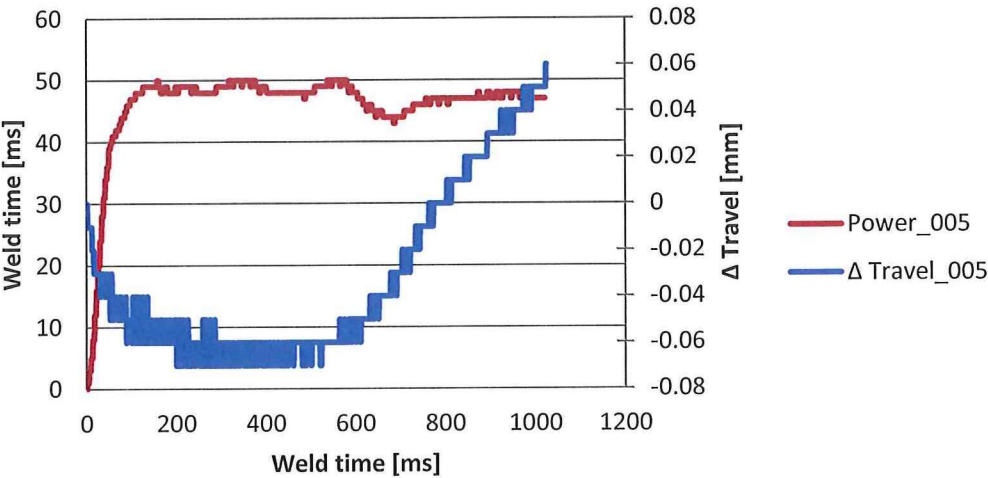
UW180913\_2309-1-002



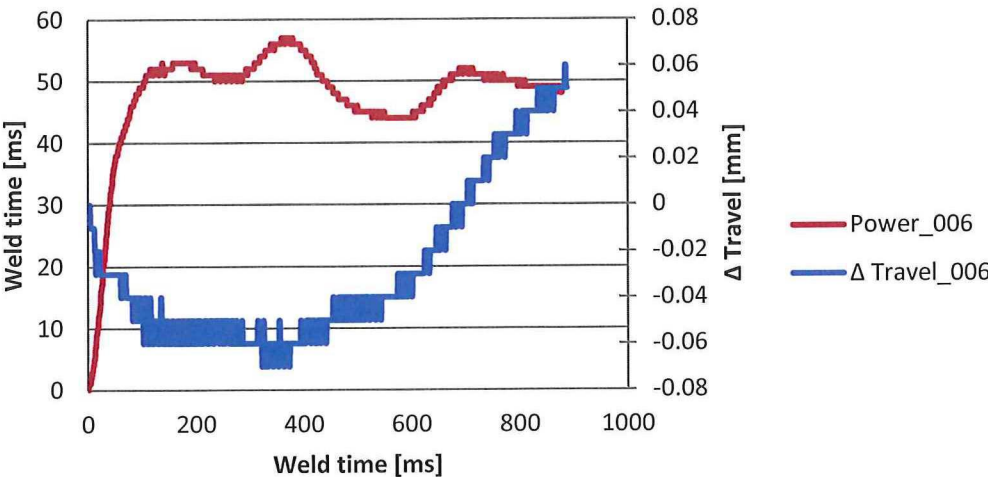
UW180913\_2309-1-003



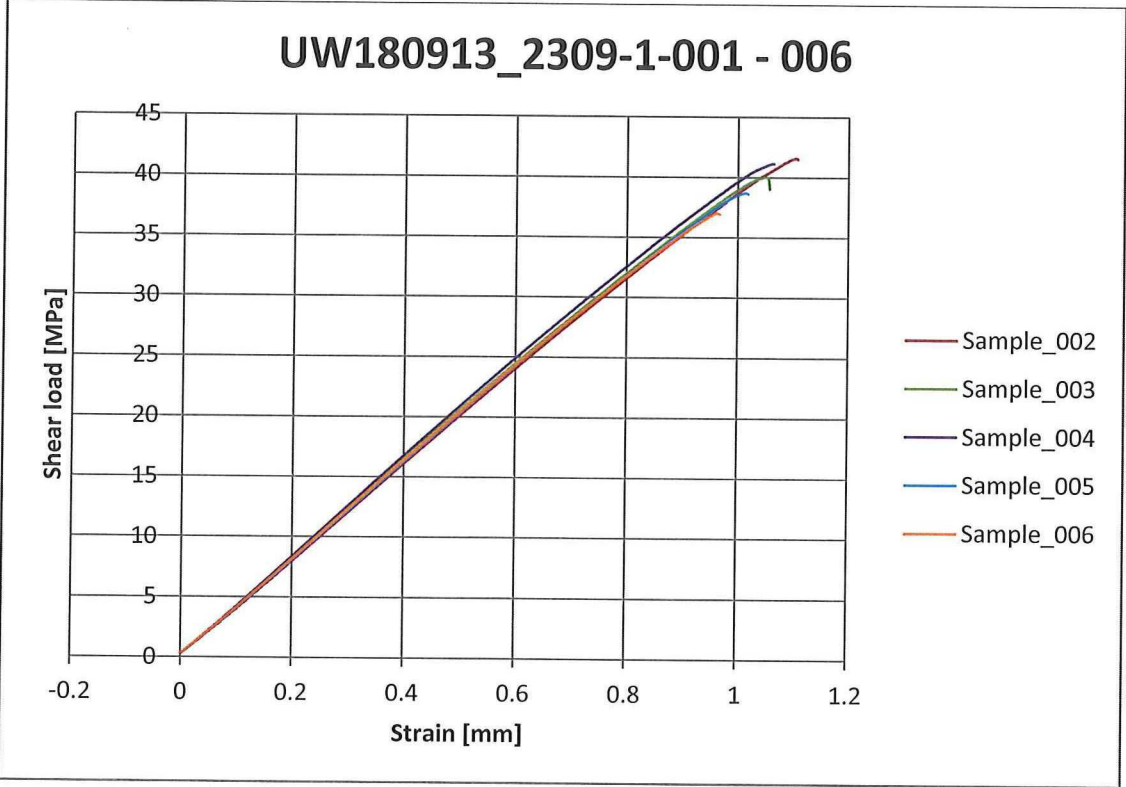
UW180913\_2309-1-005



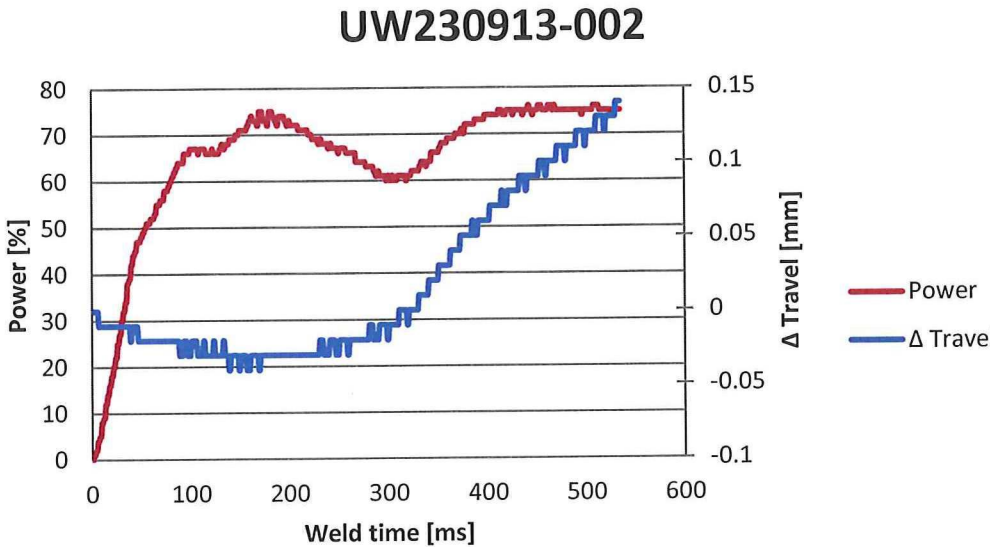
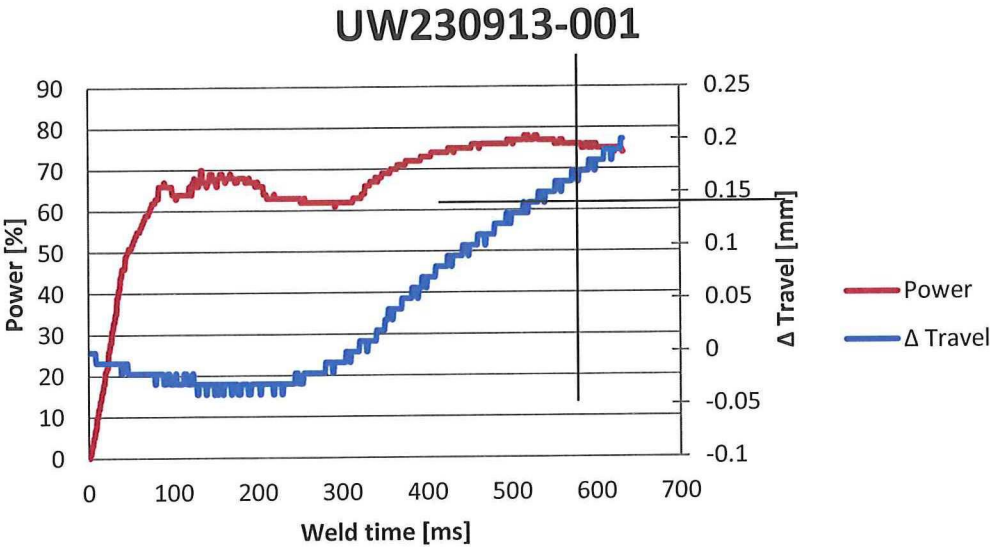
UW180913\_2309-1-006



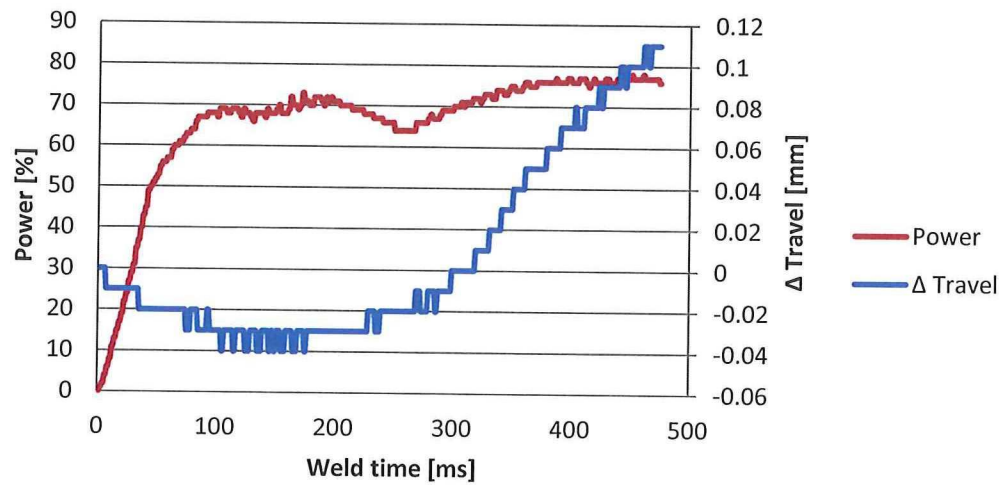




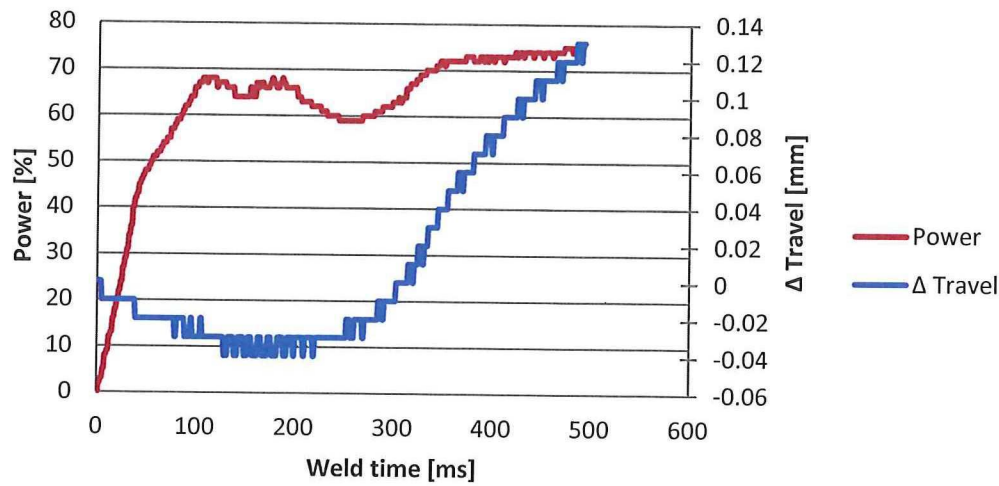
1000 [N]



UW230913-003

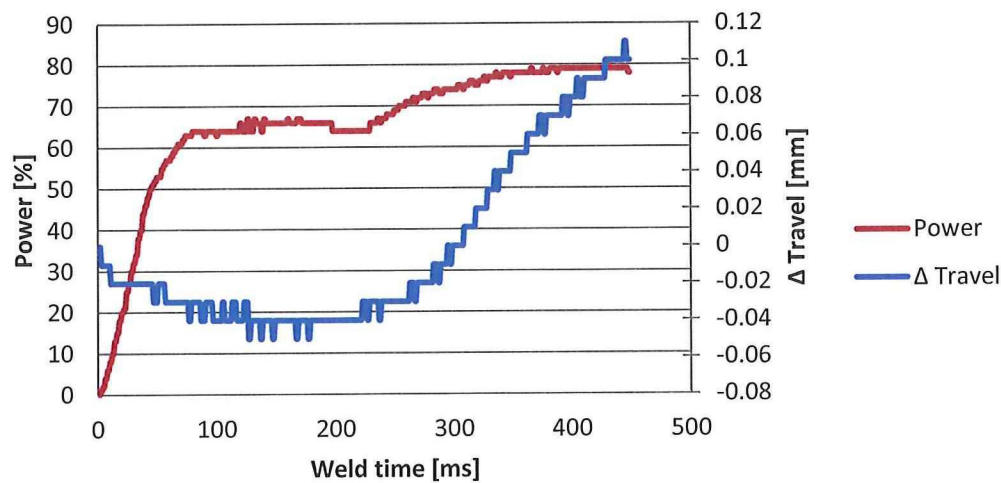


UW230913-005

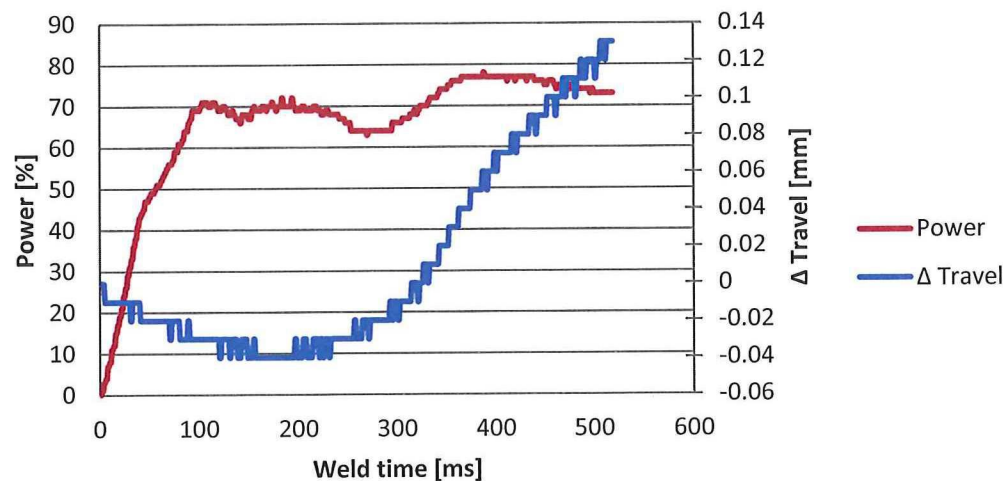


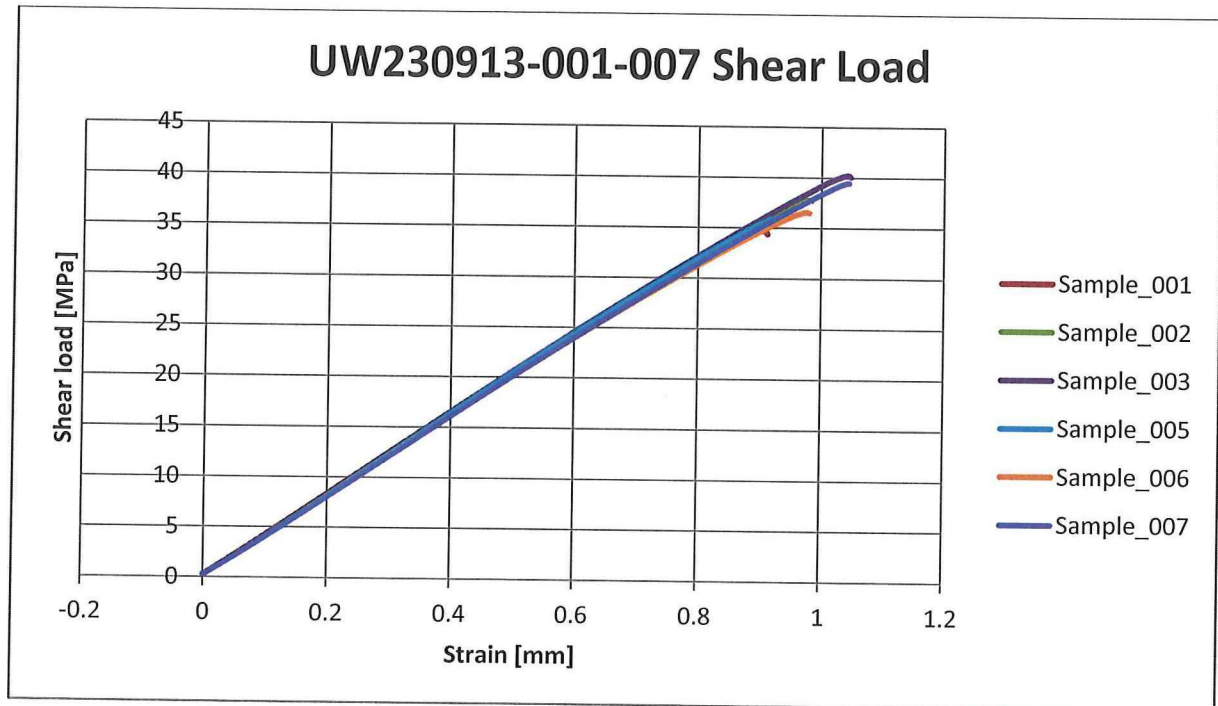


UW230913-006



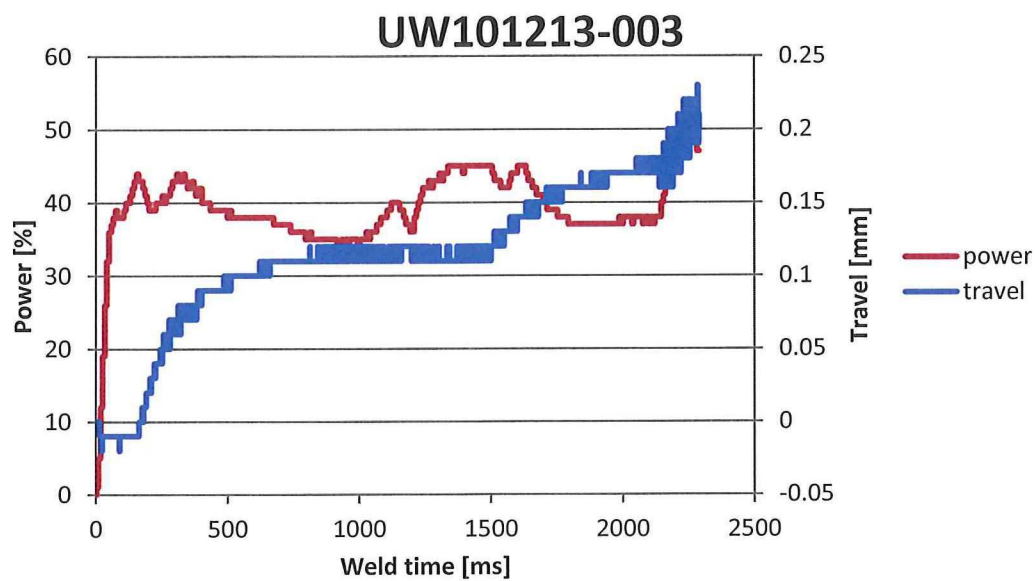
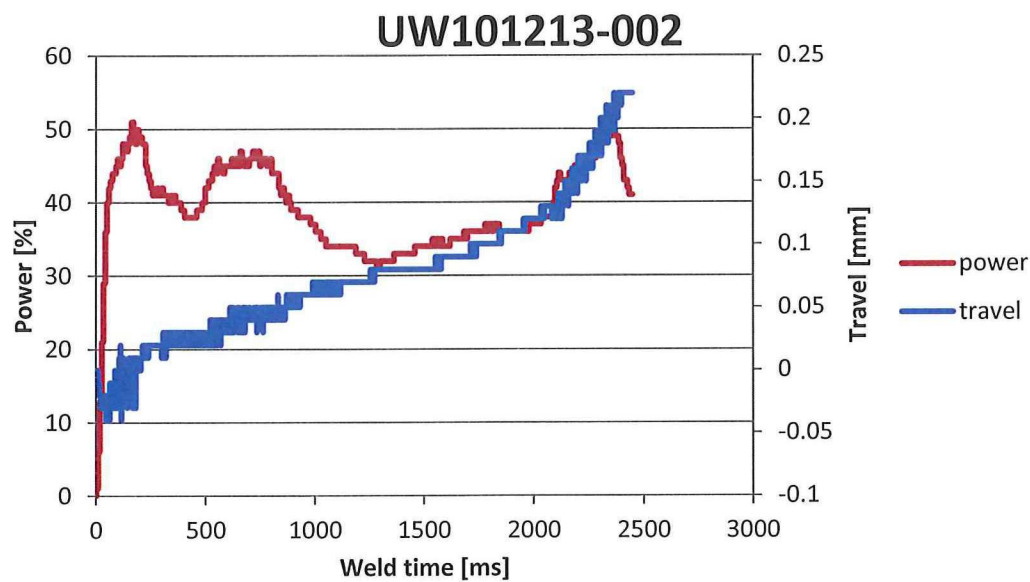
UW230913-007



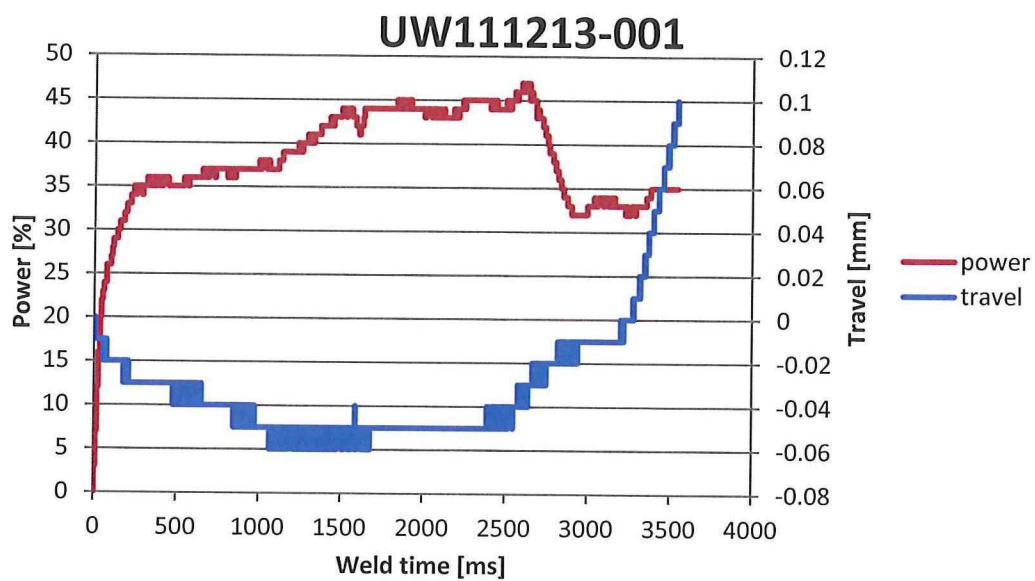
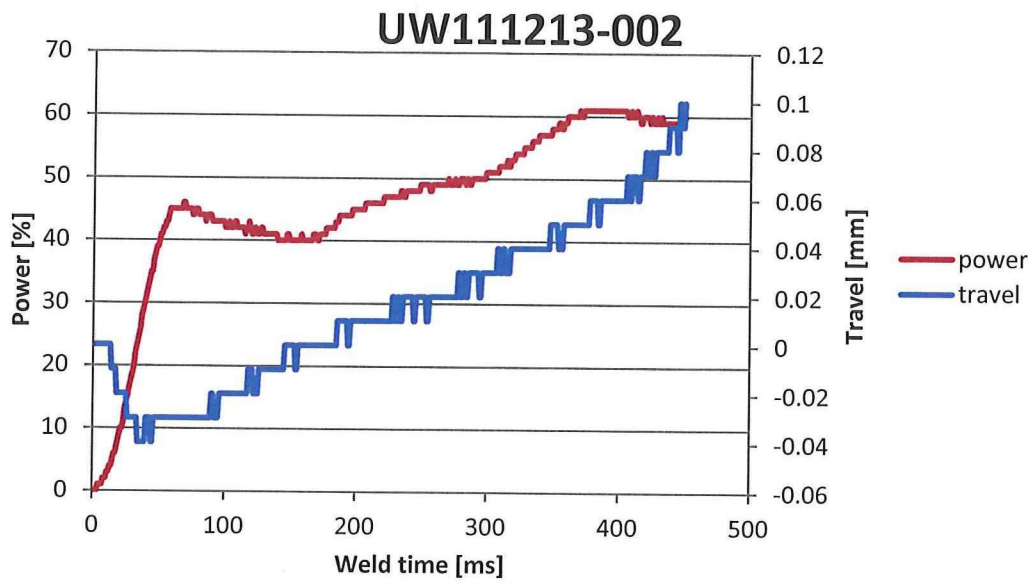
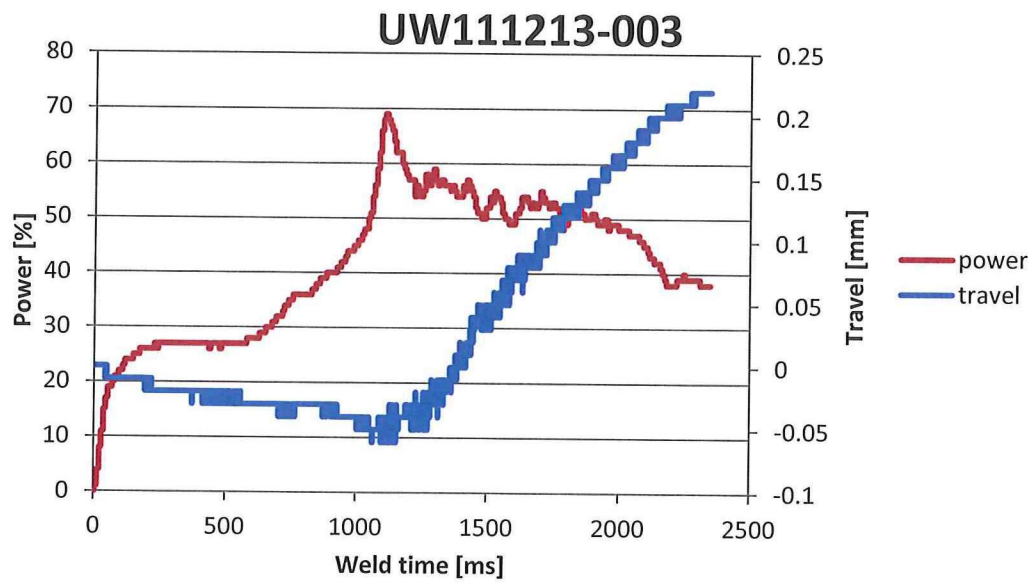


D. Welding and LSS Curves for 300 [N] Travel Controlled Welding of chopped to chopped CF/PEEK Toho Tenax Material Using a 2 Layer PEEK Toho Tenax ED

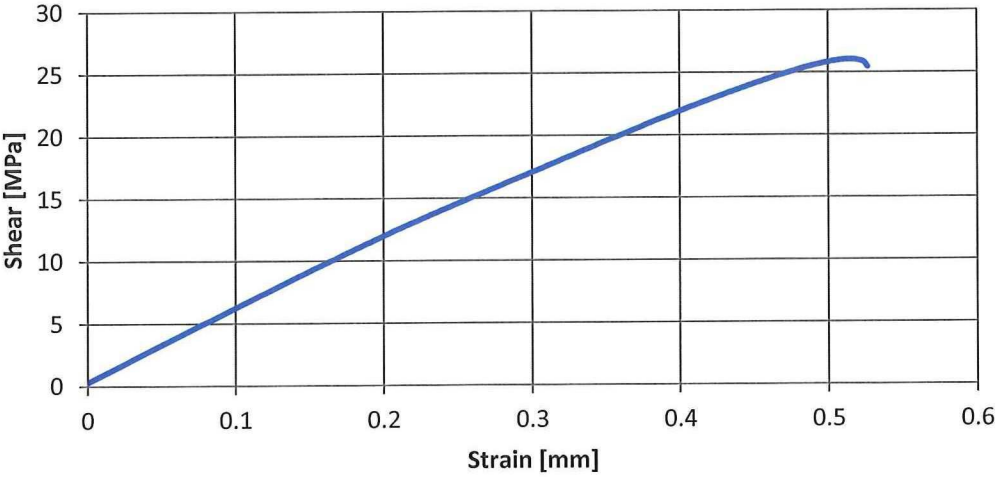
|                     |           | I) Initial Phase    | II) Vibration Phase |                     |                              |                       | III) Solidification Phase |                   |
|---------------------|-----------|---------------------|---------------------|---------------------|------------------------------|-----------------------|---------------------------|-------------------|
| Materials           | Sonotrode | Rise of Force [N/s] | Welding Force [N]   | Rise of Force [N/s] | Amplitude [µm] / setting [-] | Controlling Parameter | Force                     | Holding Time [ms] |
| TT chop.<br>- chop. | Ø 40 [mm] | 300                 | 300                 | 0                   | 86.2 (9)                     | Travel                | 1000                      | 4000              |







UW11122013-001

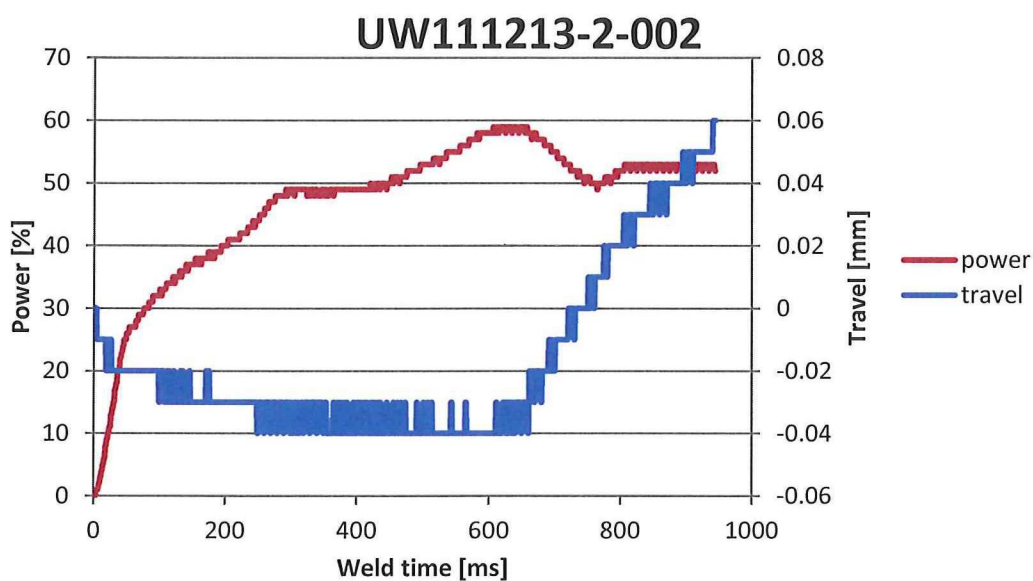
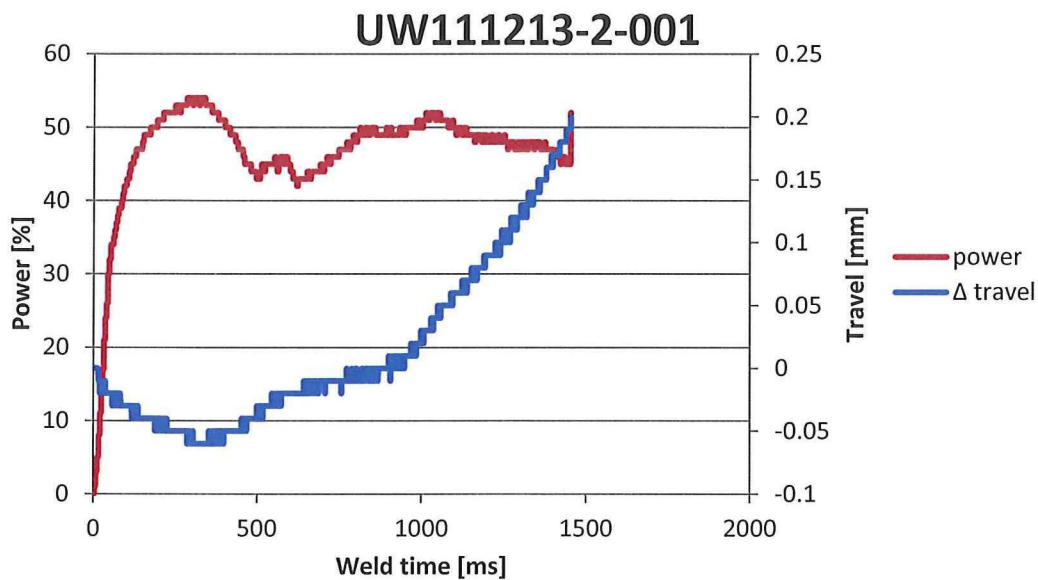


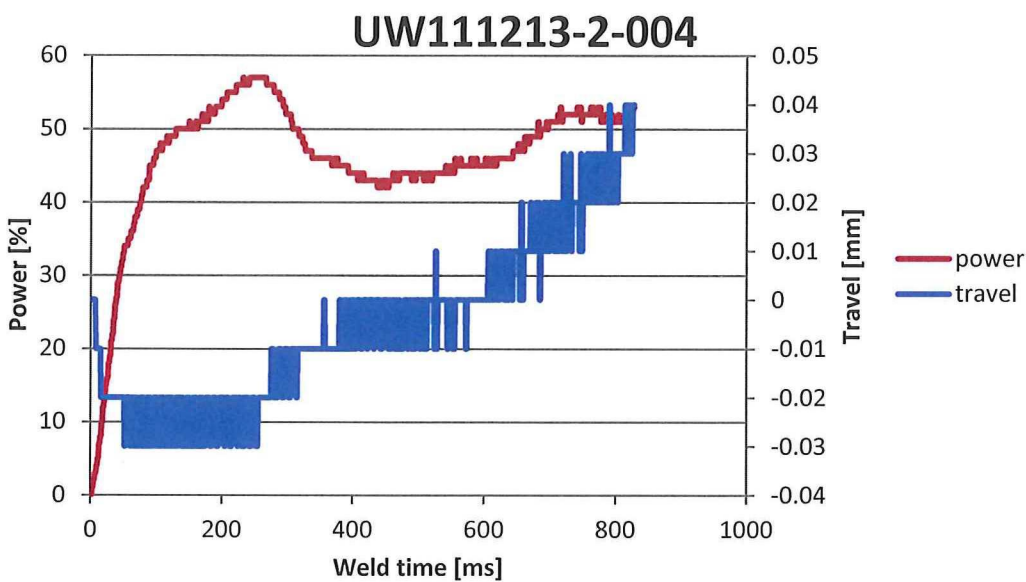
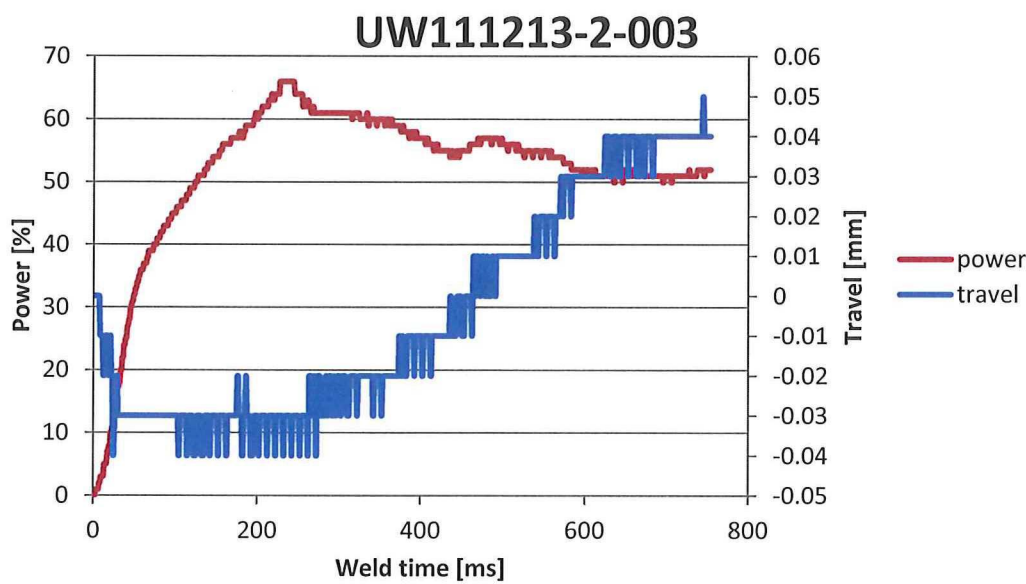


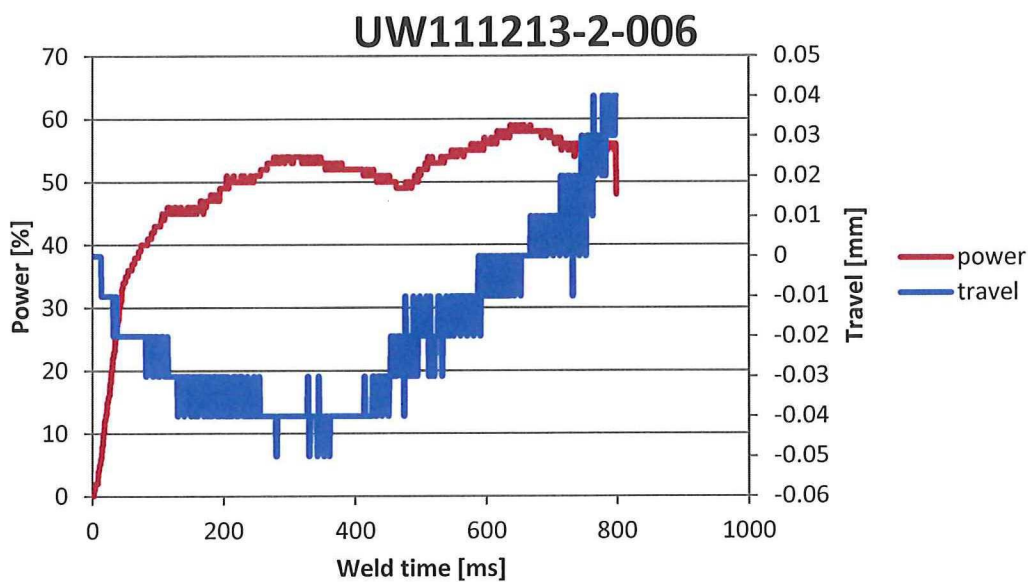
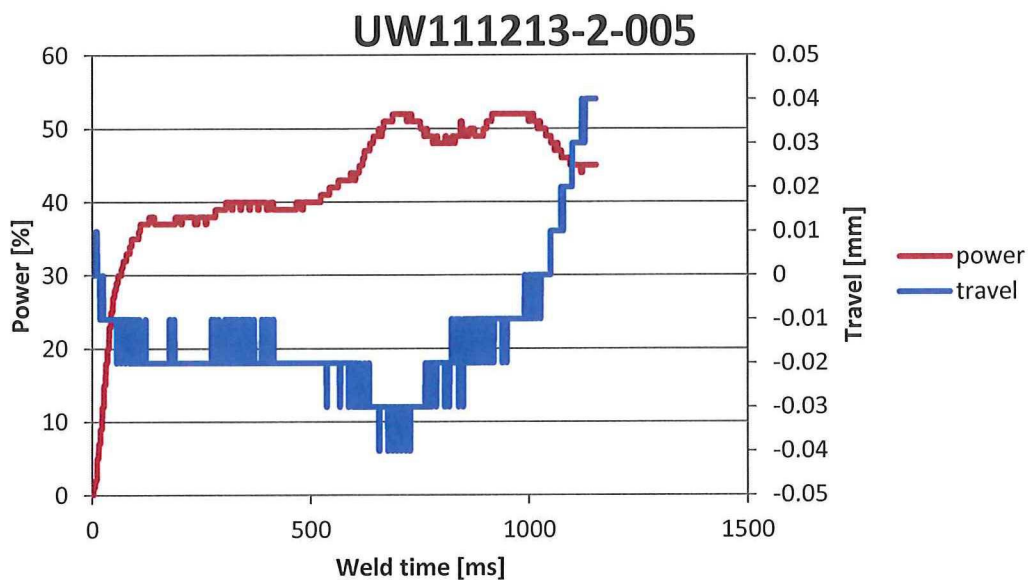


### E. Welding and LSS Curves for 300 [N] Travel Controlled Welding of continuous weave to chopped CF/PEEK Toho Tenax Material Using a 2 Layer PEEK Toho Tenax ED

|                  |                       | I) Initial Phase    | II) Vibration Phase |                     |   |                       | III) Solidification Phase |                   |
|------------------|-----------------------|---------------------|---------------------|---------------------|---|-----------------------|---------------------------|-------------------|
| Materials        | Sonotrode             | Rise of Force [N/s] | Welding Force [N]   | Rise of Force [N/s] | Amplitude [ $\mu\text{m}$ ] / setting [-] | Controlling Parameter | Force                     | Holding Time [ms] |
| TT weave - chop. | $\varnothing 40$ [mm] | 300                 | 300                 | 0                   | 86.2 (9)                                  | Travel                | 1000                      | 4000              |

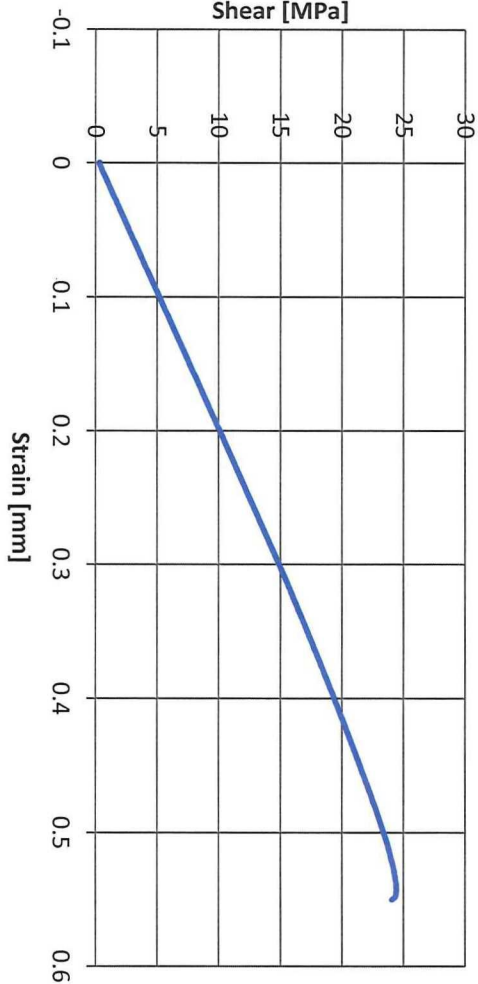




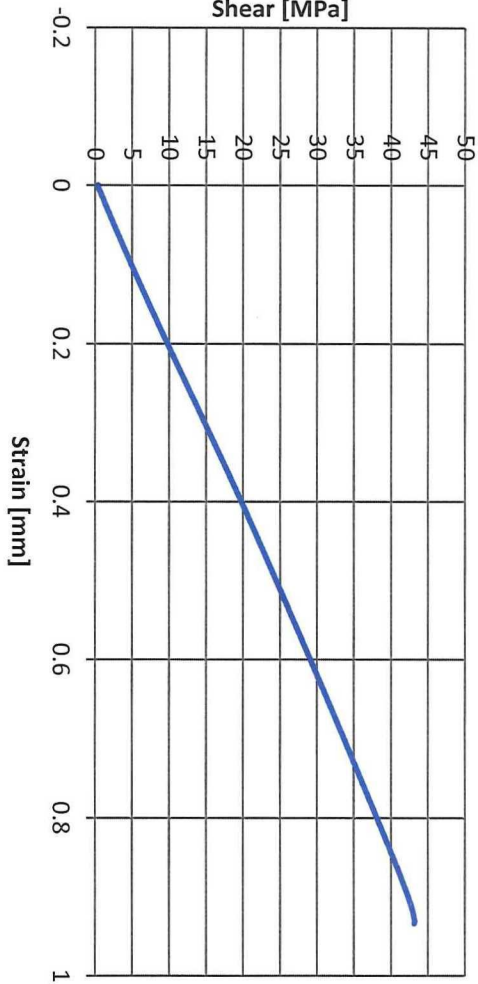




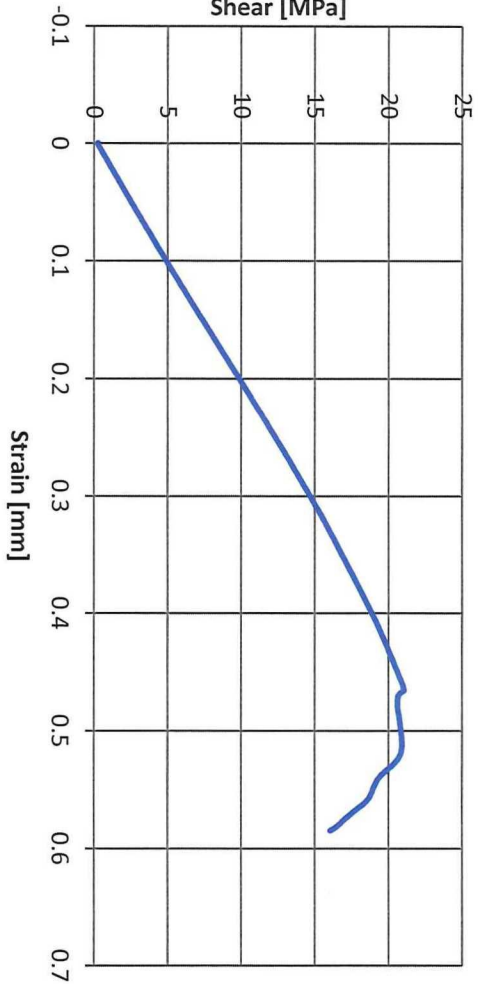
UW11122013-2-001



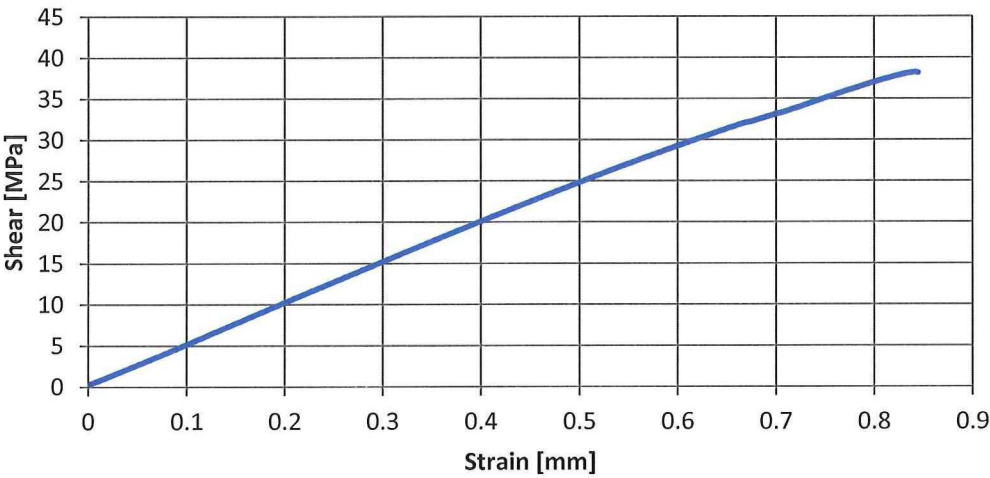
UW11122013-2-002



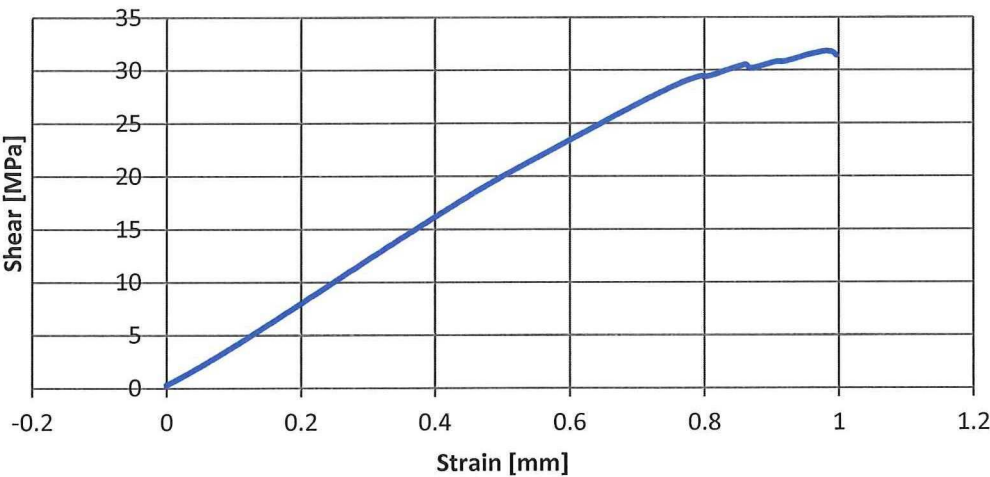
UW11122013-2-003



UW11122013-2-004



UW11122013-2-005



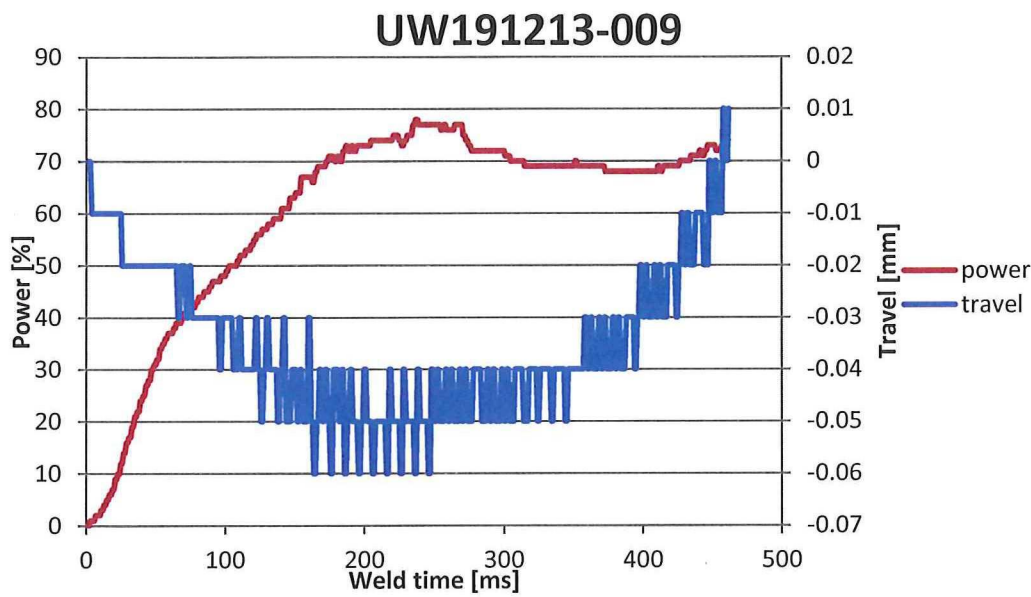
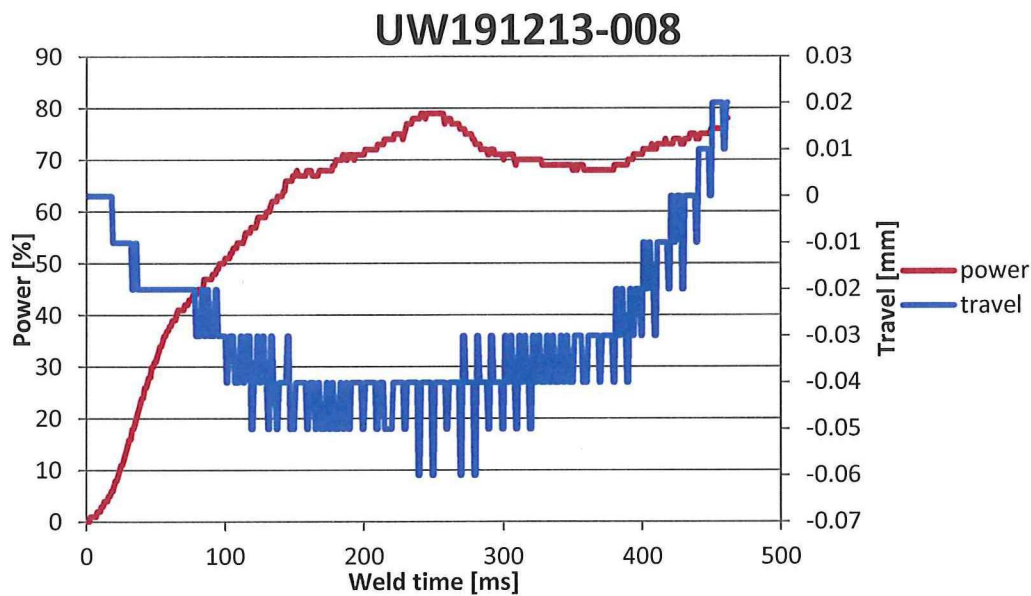


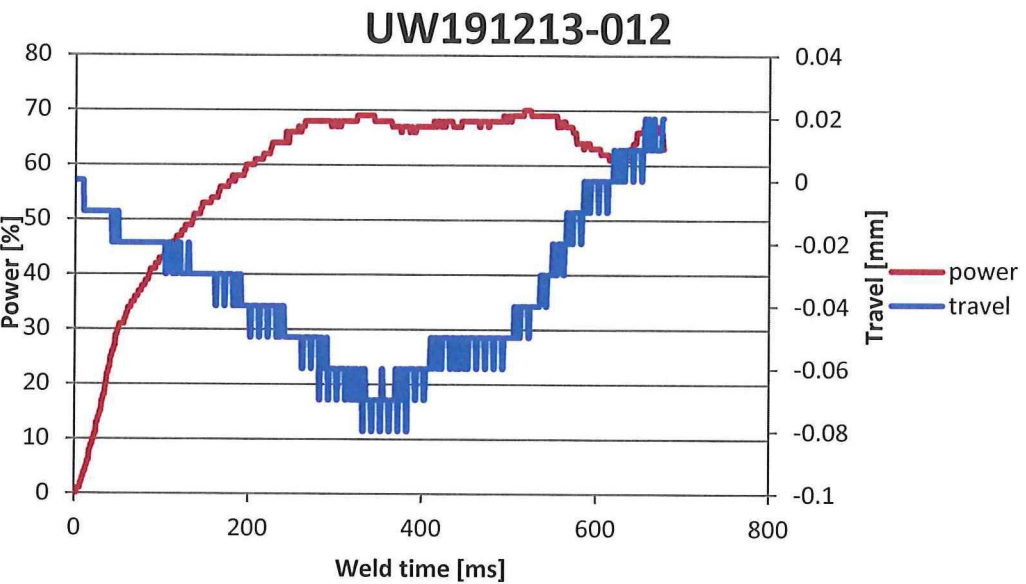
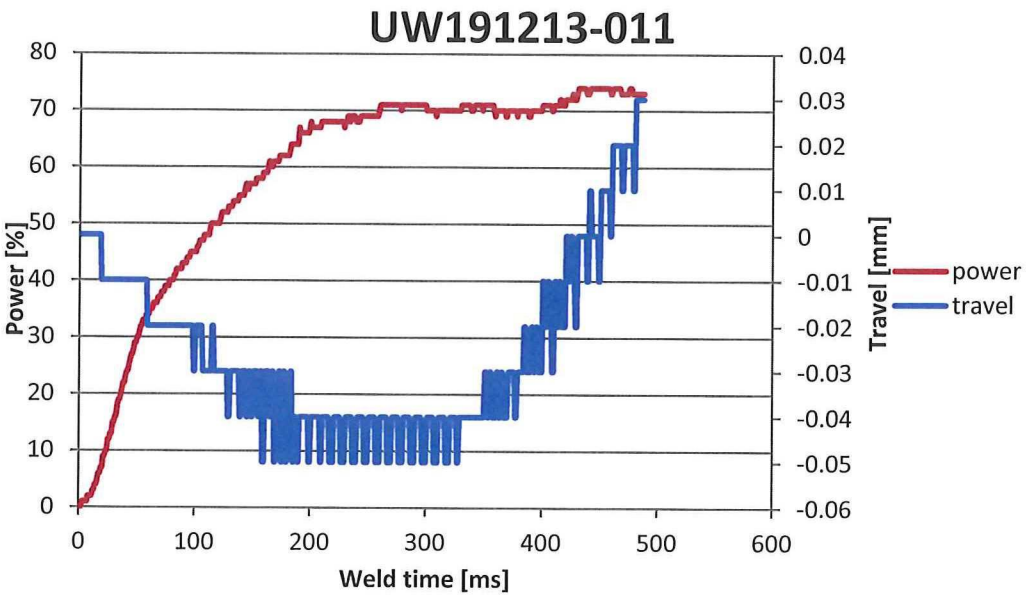
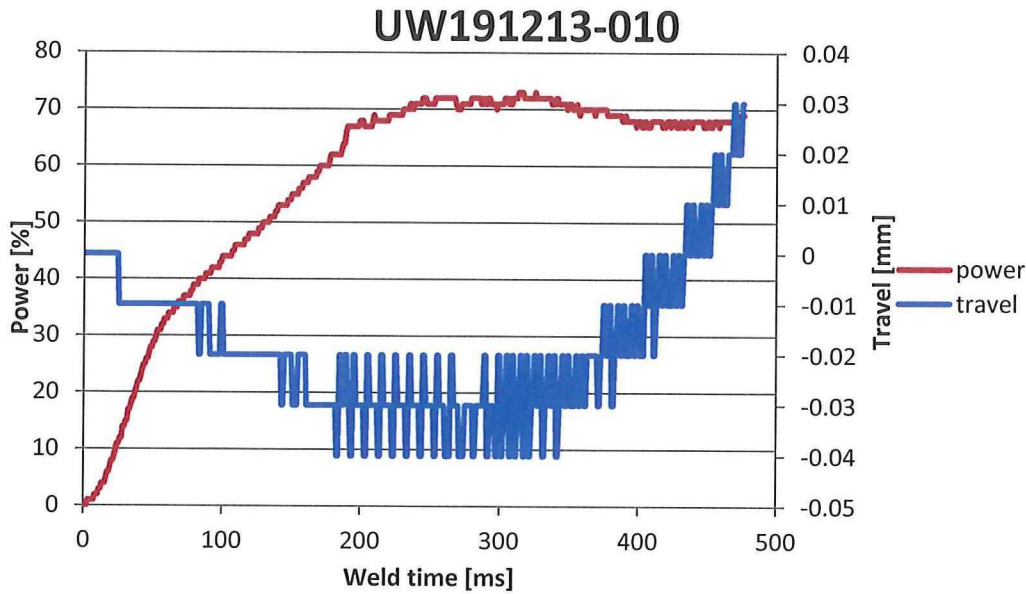


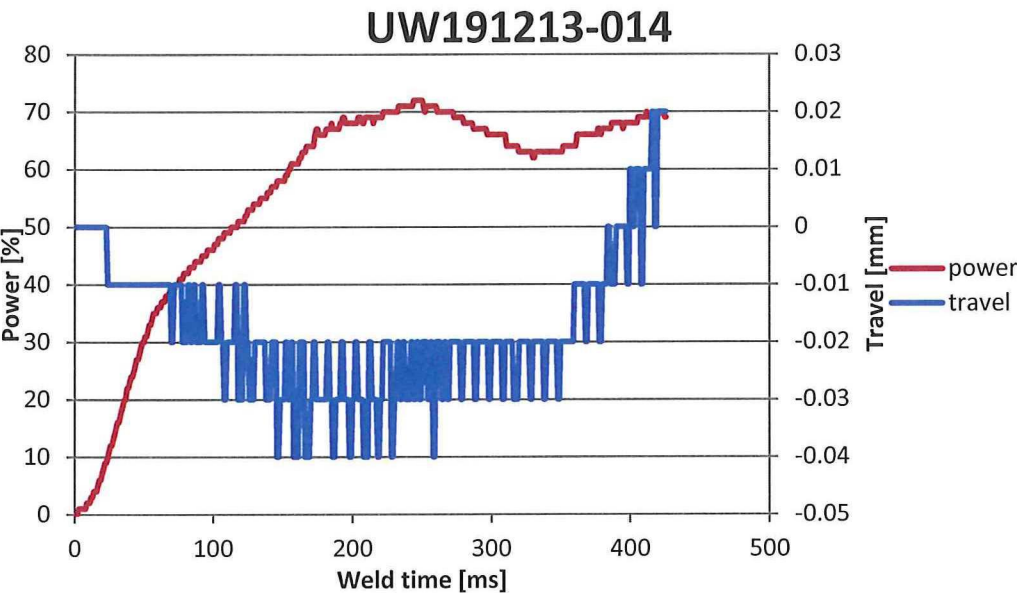
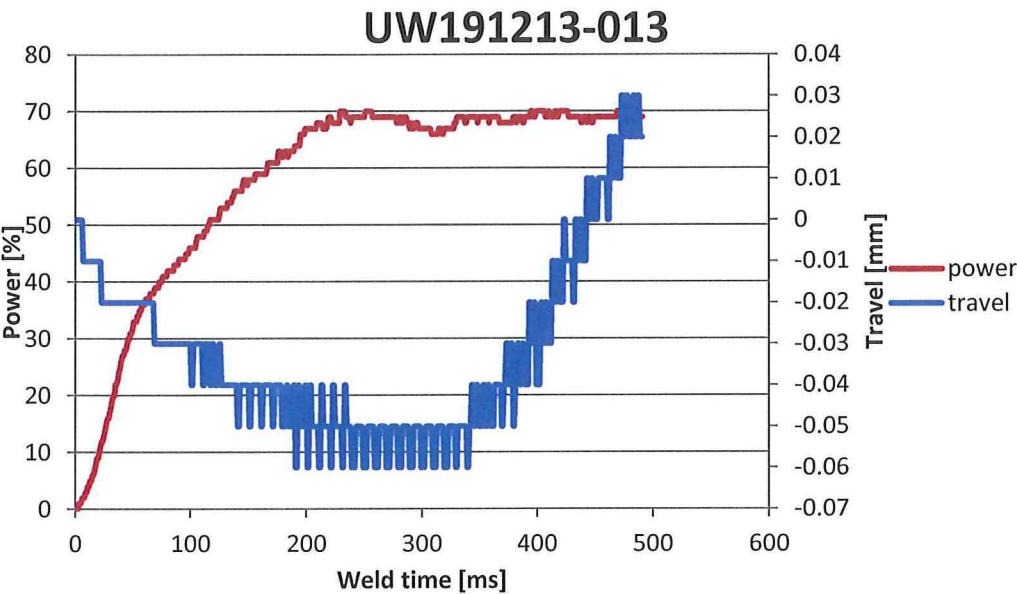
F. Welding and LSS Curves for 500 [N] Travel Controlled Energy Determination Welds and Energy Controlled Spot Welding of s Larger Overlap

Energy determination

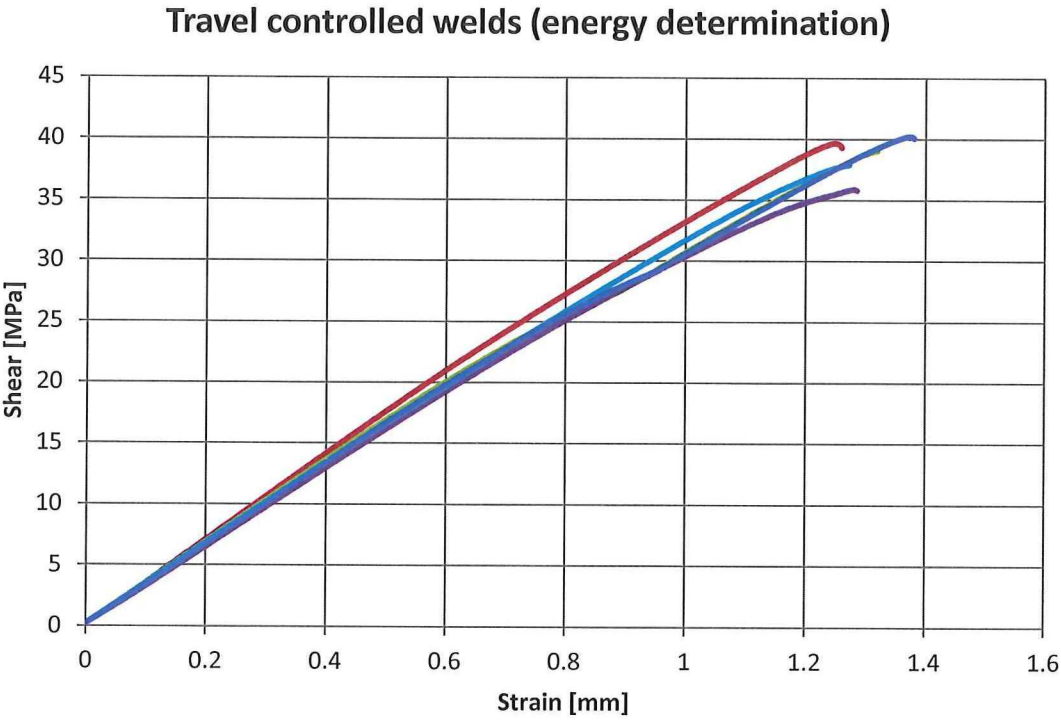
|                  |                            | I) Initial Phase    | II) Vibration Phase |                     |                            |                       | III) Solidification Phase |                   |
|------------------|----------------------------|---------------------|---------------------|---------------------|----------------------------|-----------------------|---------------------------|-------------------|
| Materials        | Sonotrode                  | Rise of Force [N/s] | Weld. Force [N]     | Rise of Force [N/s] | Amplitu de [μm] (set. [-]) | Controlling Parameter | Force                     | Holding Time [ms] |
| TT weave – weave | Rectangular 14.9 · 30 [mm] | 250                 | 500                 | 0                   | 84.6 (3)                   | Travel, opt.: 20 [%]  | 1000                      | 4000              |





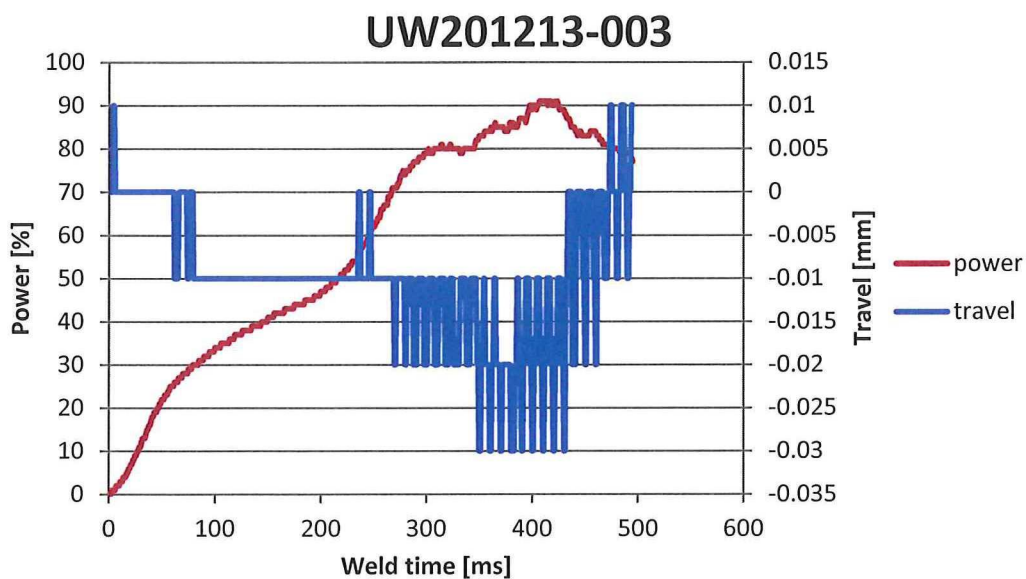
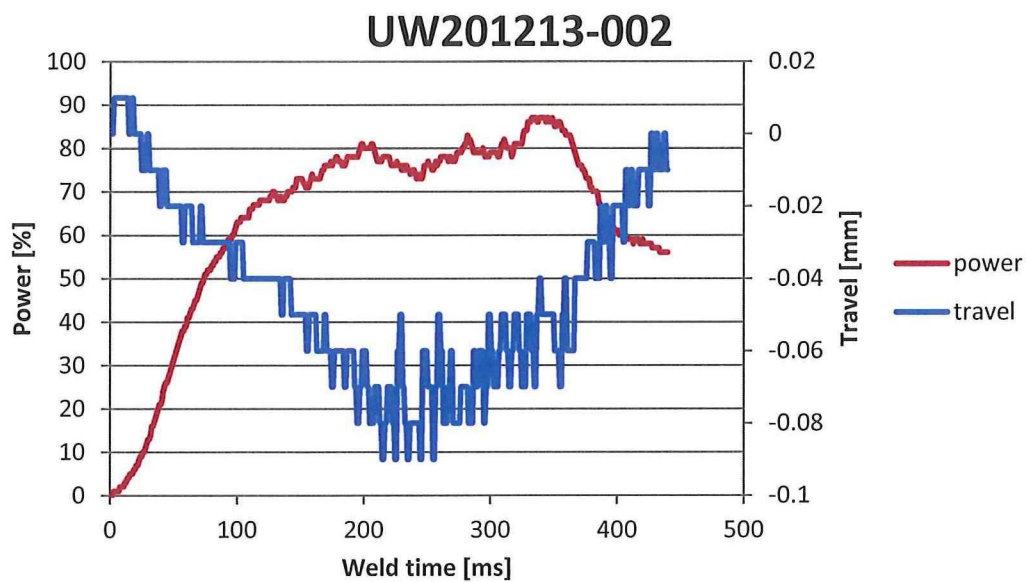
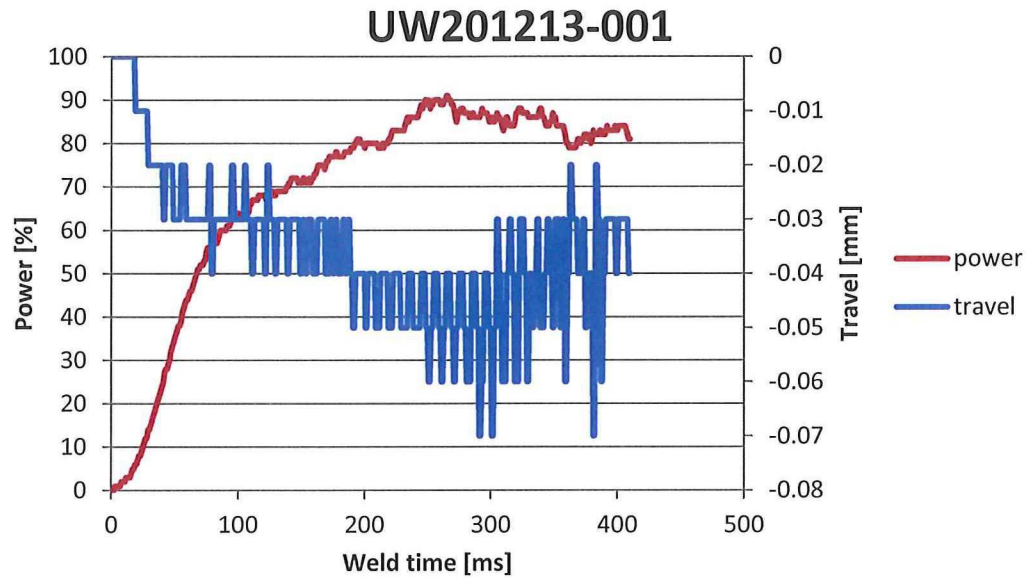


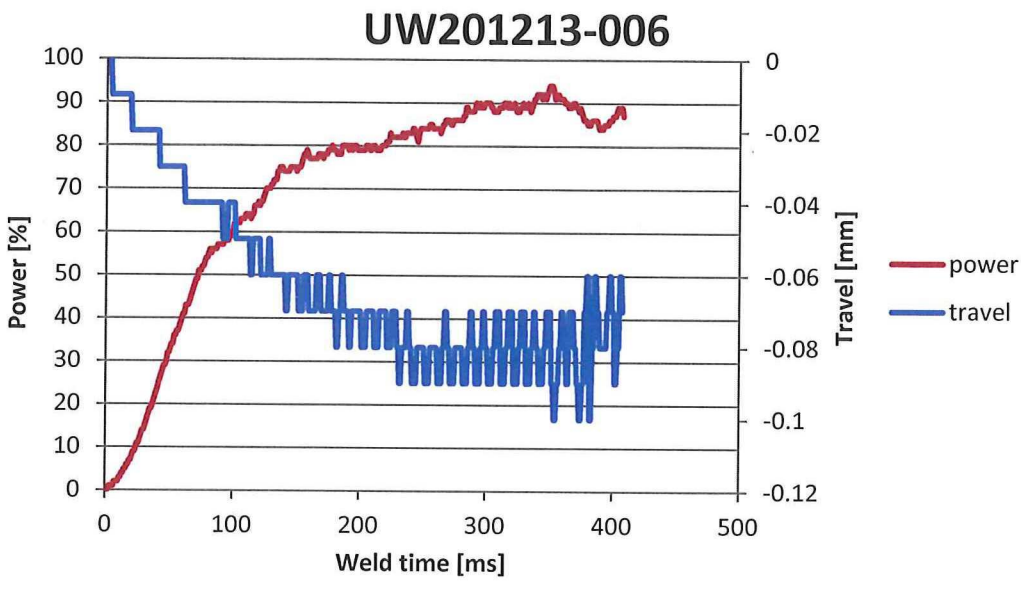
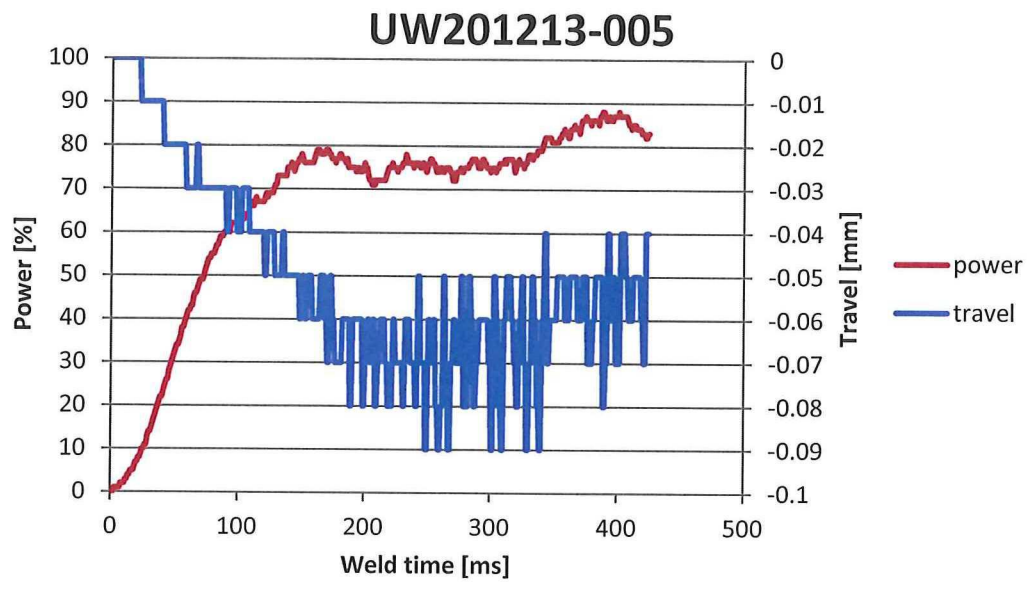
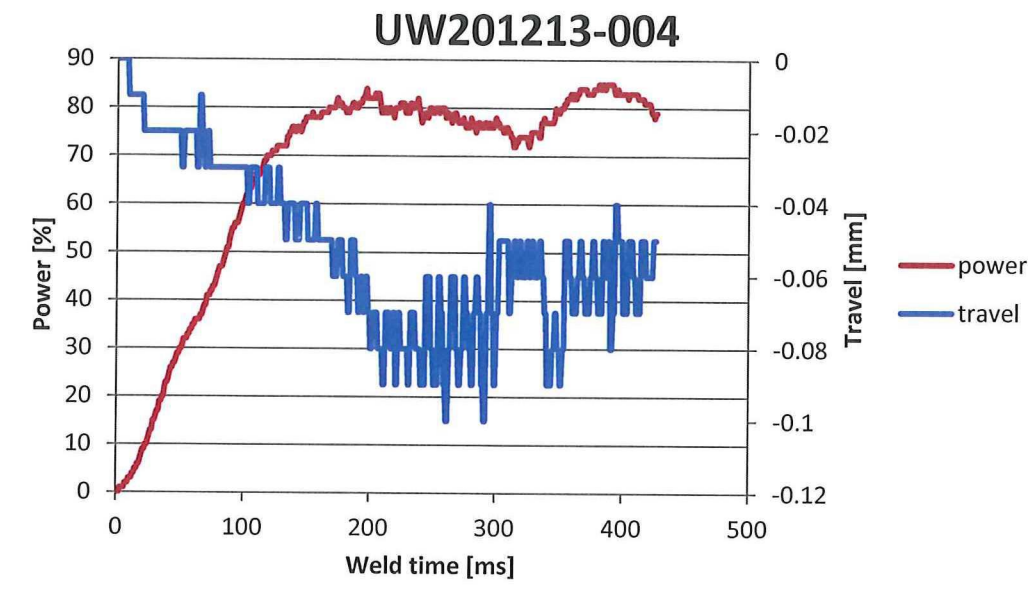




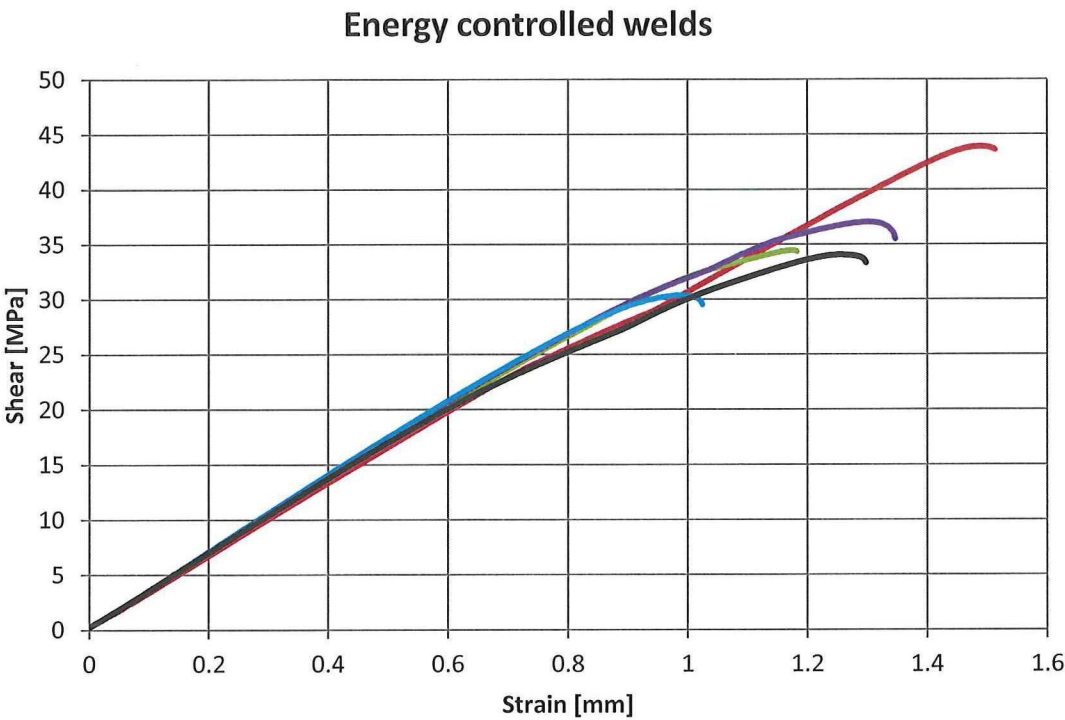
Zero travel

|                  |                            | I) Initial Phase    | II) Vibration Phase |                     |                            |                        | III) Solidification Phase |                   |
|------------------|----------------------------|---------------------|---------------------|---------------------|----------------------------|------------------------|---------------------------|-------------------|
| Materials        | Sonotrode                  | Rise of Force [N/s] | Weld. Force [N]     | Rise of Force [N/s] | Amplitu de [µm] (set. [-]) | Controlling Parameter  | Force                     | Holding Time [ms] |
| TT weave – weave | Rectangular 14.9 · 30 [mm] | 250                 | 500                 | 0                   | 84.6 (3)                   | Energy, opt.: 855 [Ws] | 1000                      | 4000              |





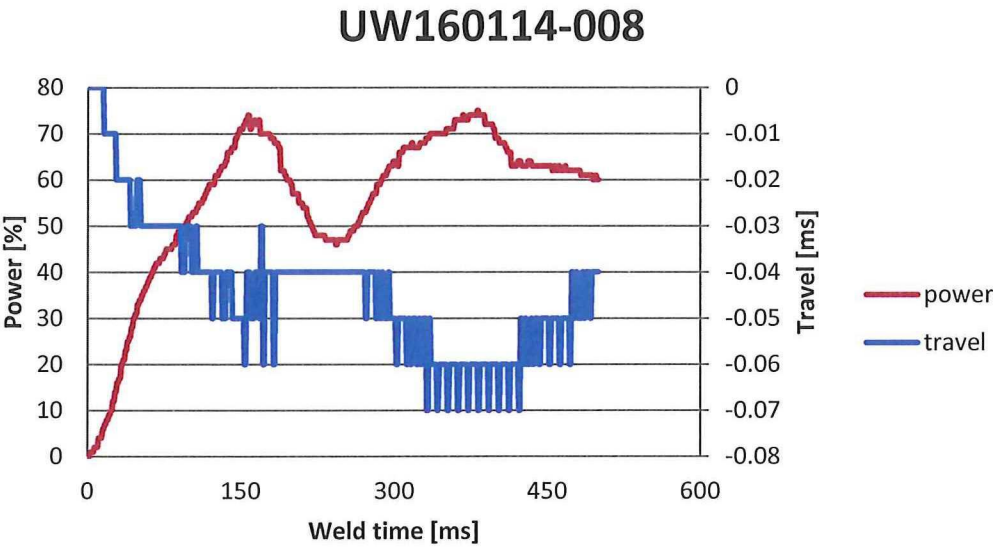
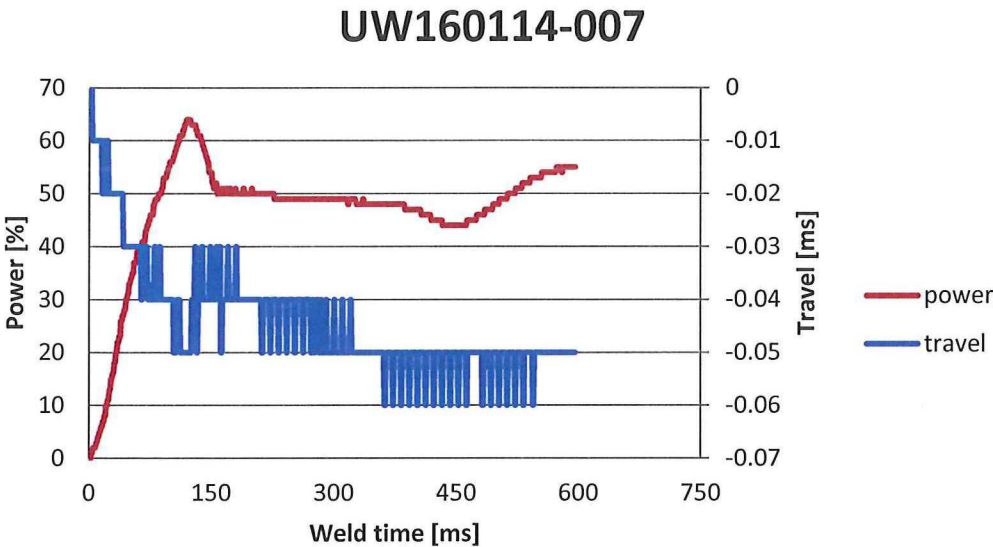






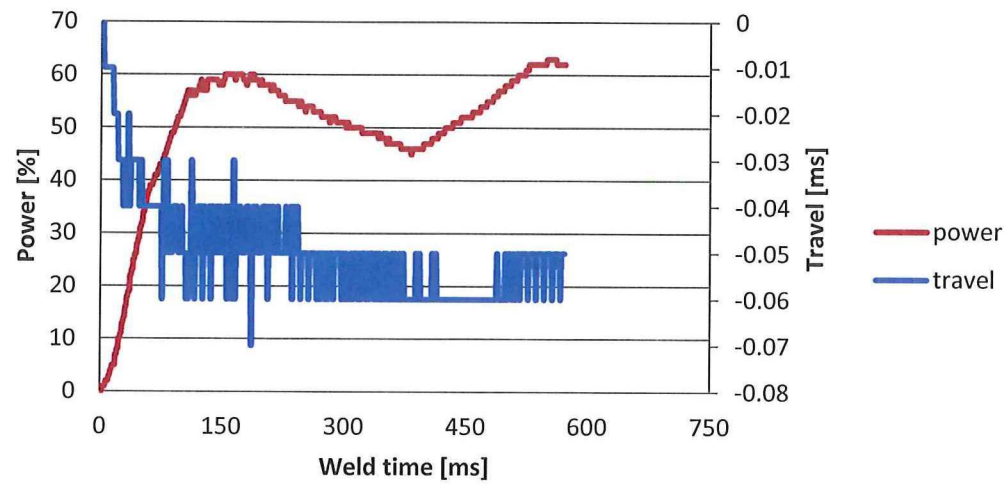
G. Welding and LSS Curves for 500 [N] Energy Controlled Spot Welds Using Dedicated Area Sized ED

|                  |                            | I) Initial Phase    | II) Vibration Phase |                     |                            |                        | III) Solidification Phase |                   |
|------------------|----------------------------|---------------------|---------------------|---------------------|----------------------------|------------------------|---------------------------|-------------------|
| Materials        | Sonotrode                  | Rise of Force [N/s] | Weld. Force [N]     | Rise of Force [N/s] | Amplitu de [μm] (set. [-]) | Controlling Parameter  | Force                     | Holding Time [ms] |
| TC weave – weave | Rectangular 14.9 · 30 [mm] | 250                 | 500                 | 0                   | 84.6 (3)                   | Energy, opt.: 855 [Ws] | 1000                      | 4000              |

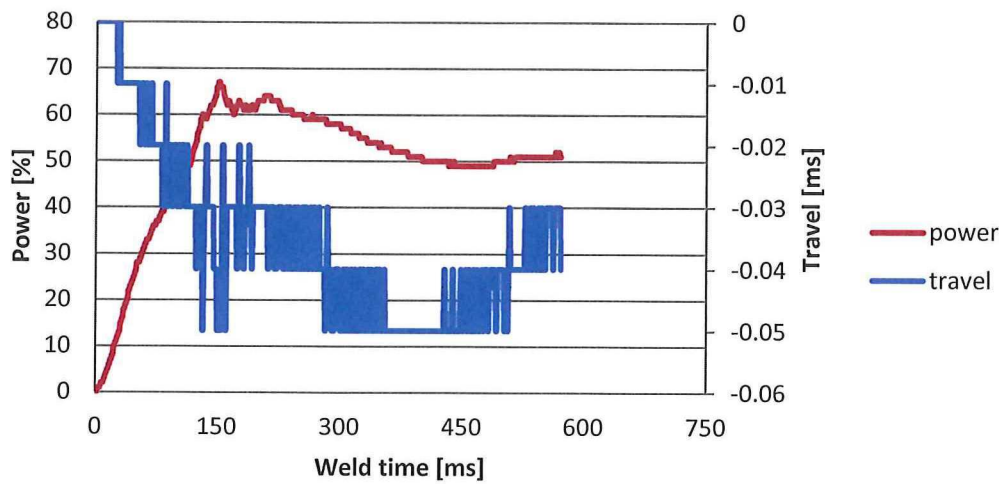


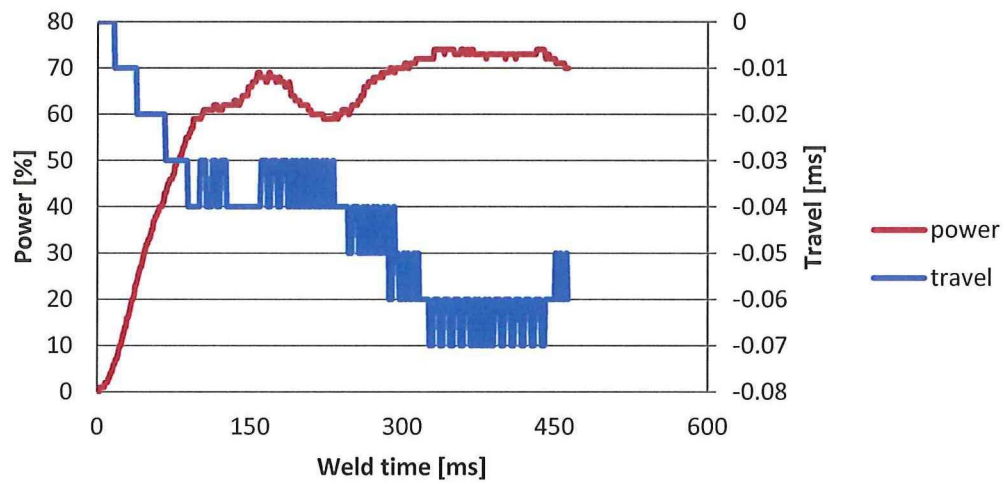
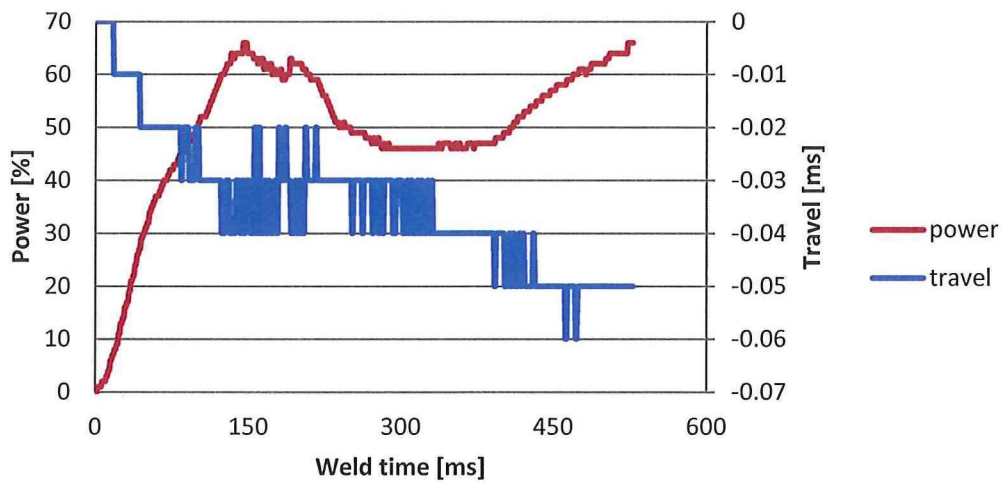


UW160114-009

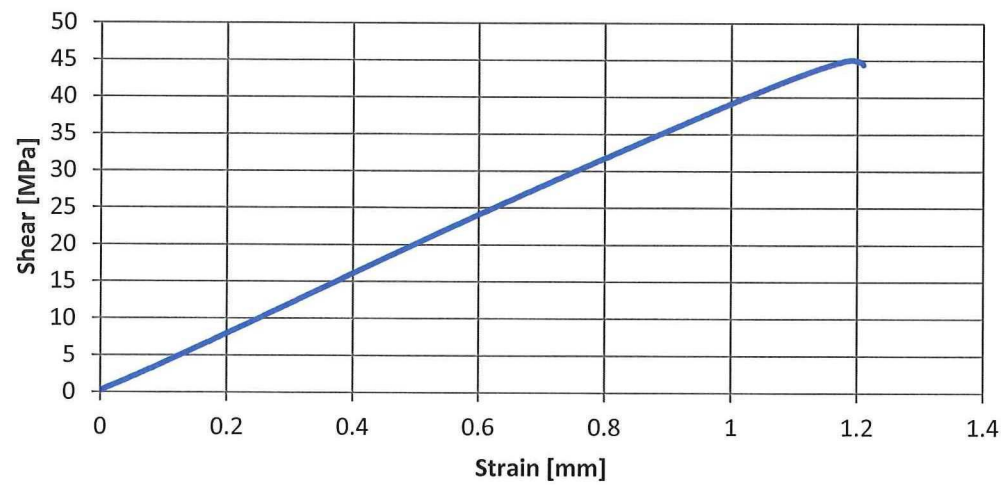


UW160114-010

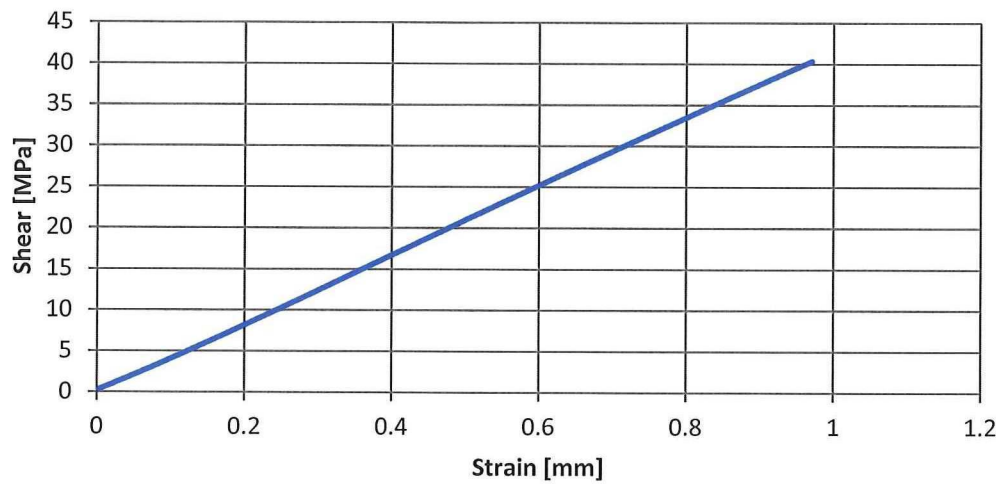


**UW160114-011****UW160114-012**

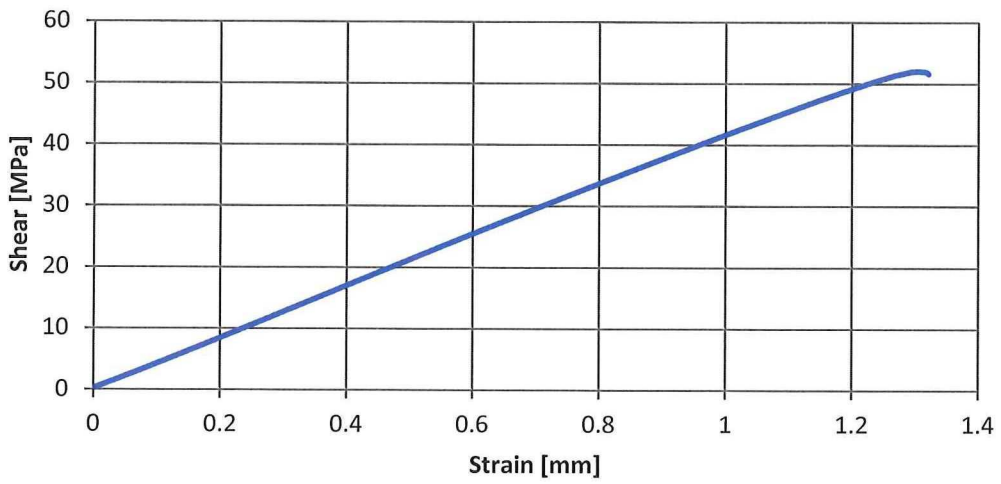
UW160114-007



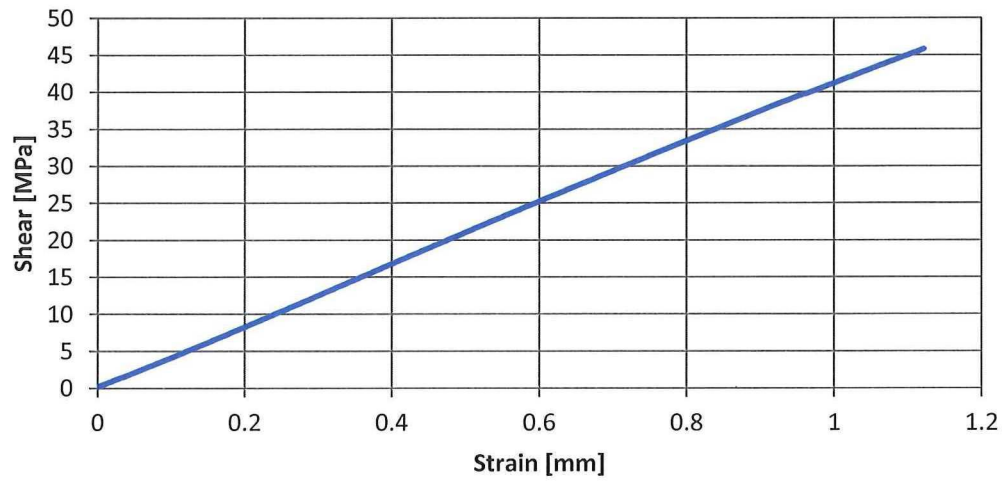
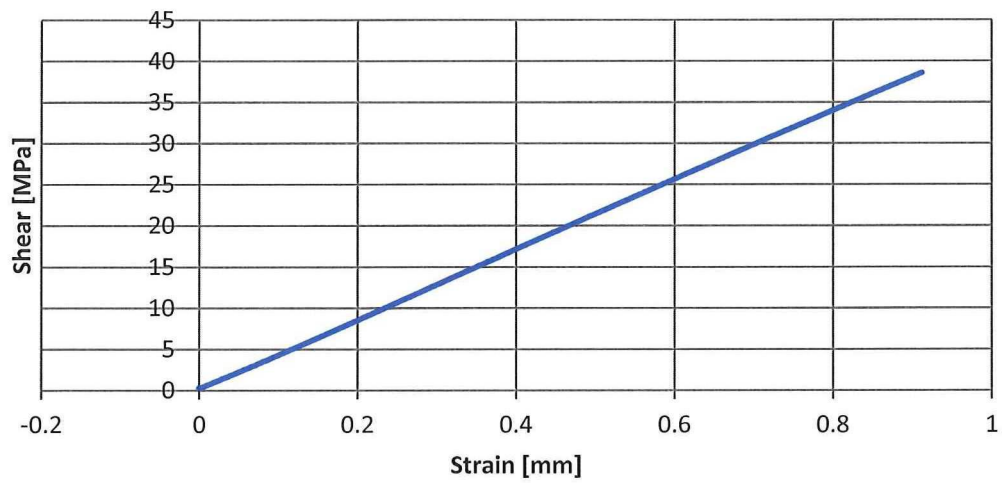
UW160114-008



UW160114-009



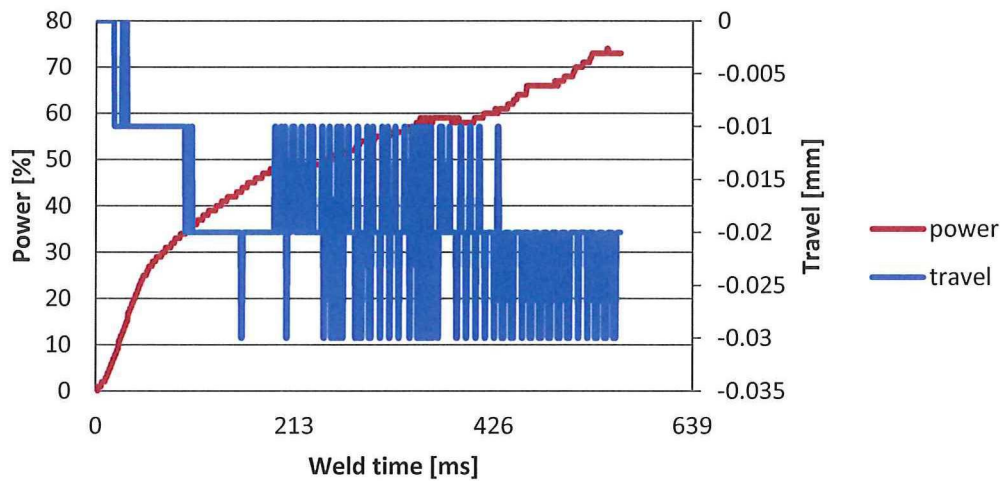


**UW160114-010****UW160114-011**

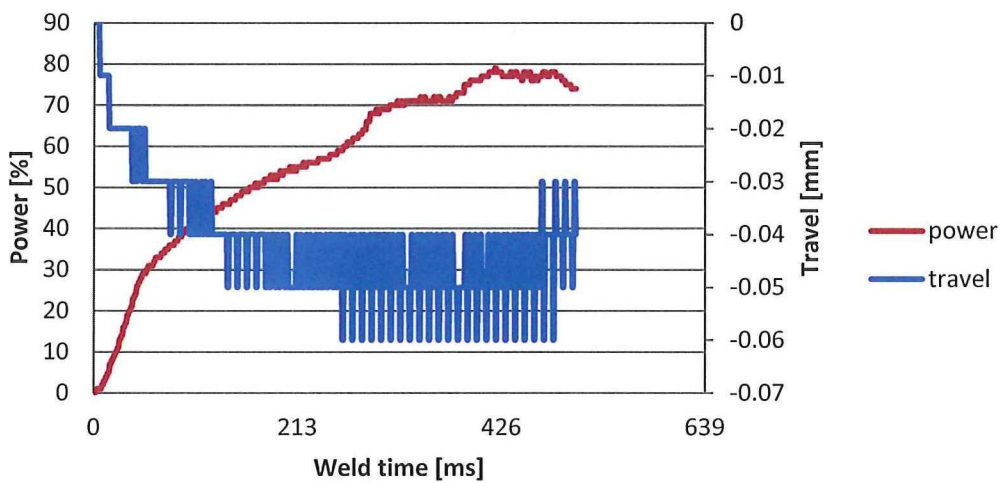


H. Welding and LSS Curves for 500 [N] Energy Controlled Spot Welds Using Dedicated Area Sized ED Welding Weave (90 [°] Ten Cate) – Chopped Material

UW280114-003

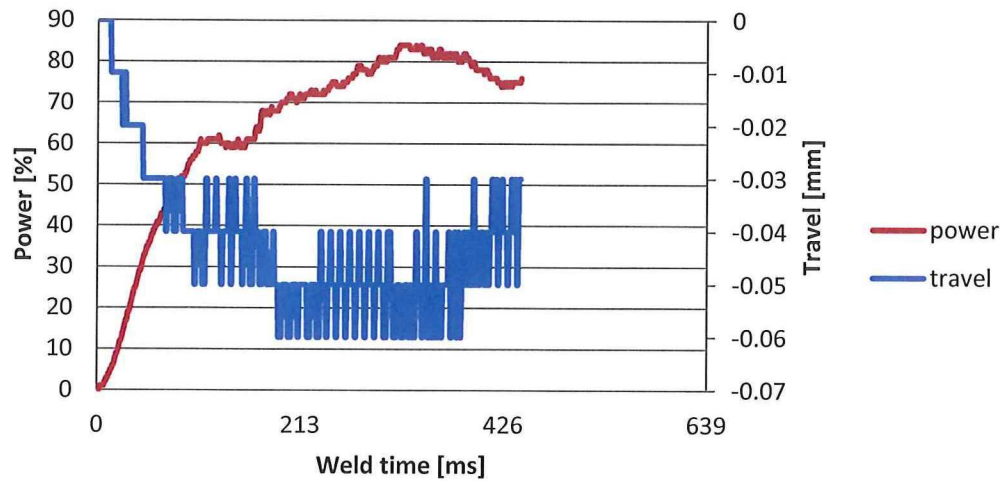


UW280114-004

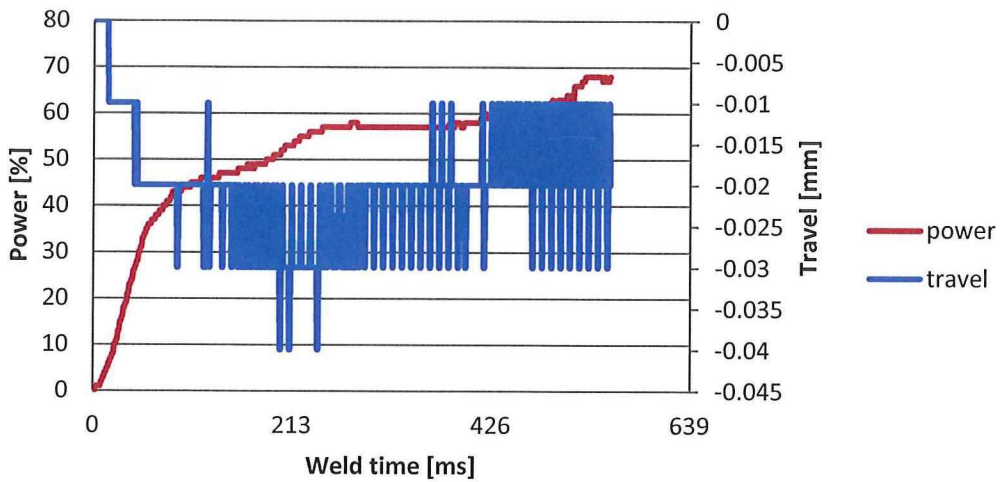




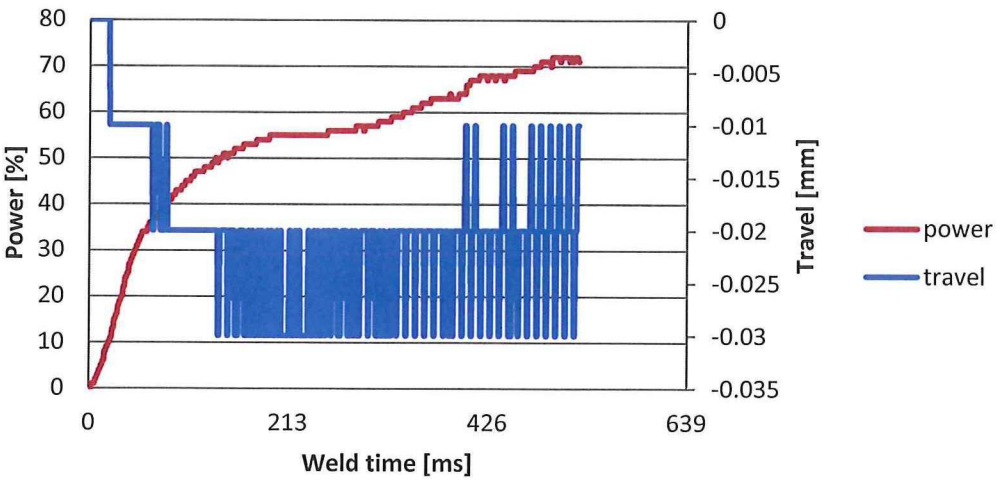
UW280114-005



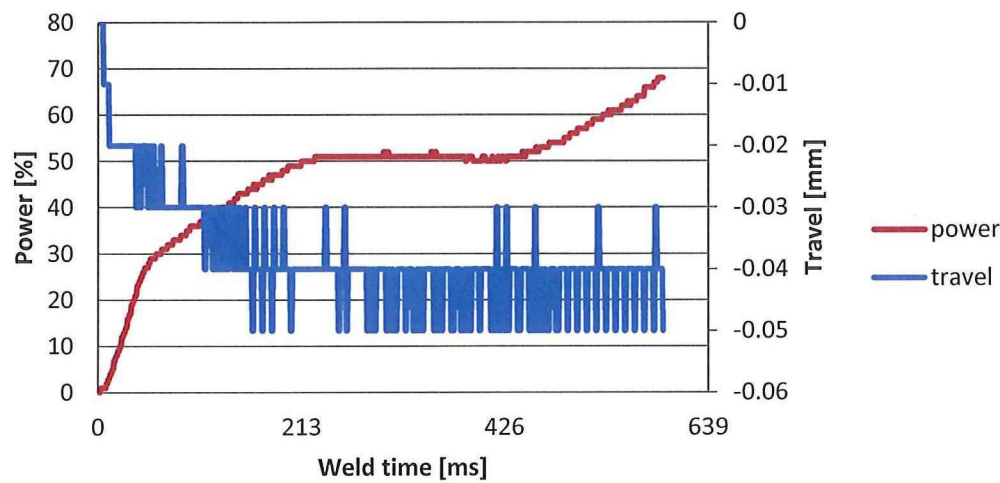
UW280114-006



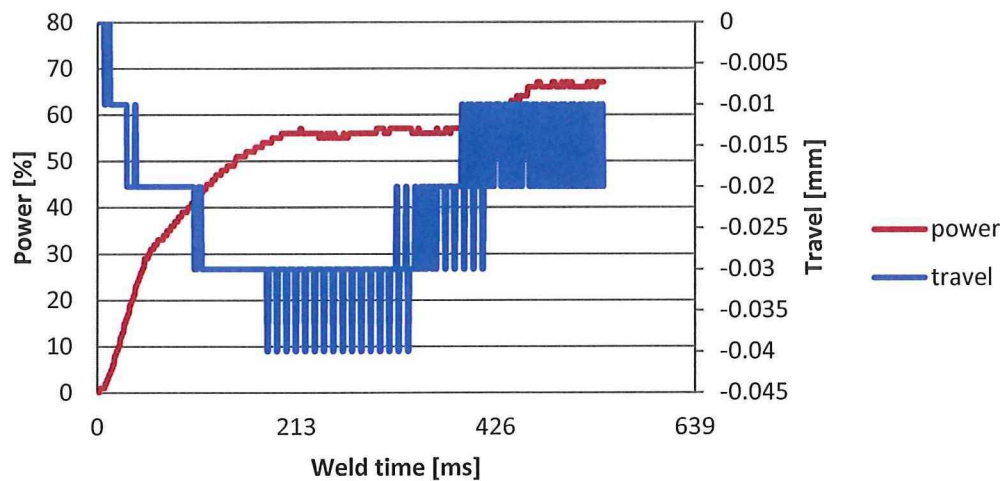
UW280114-007



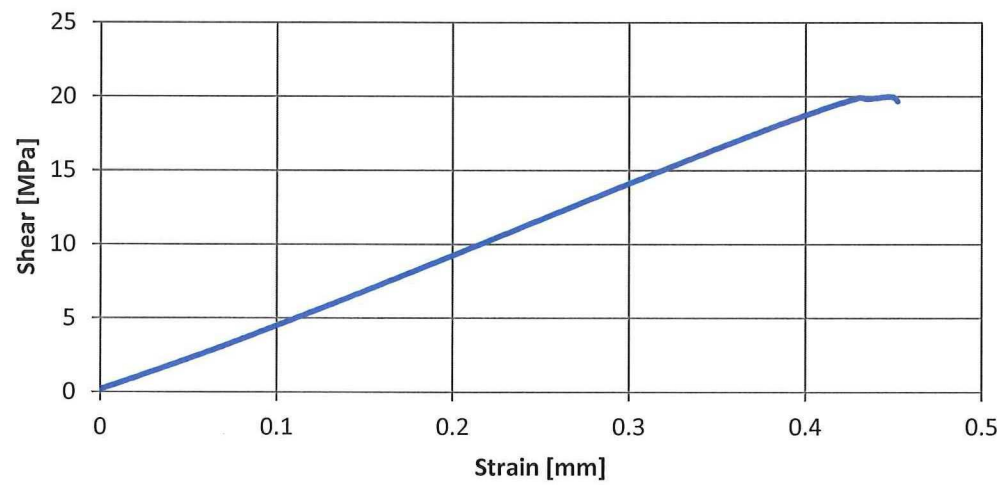
UW280114-008



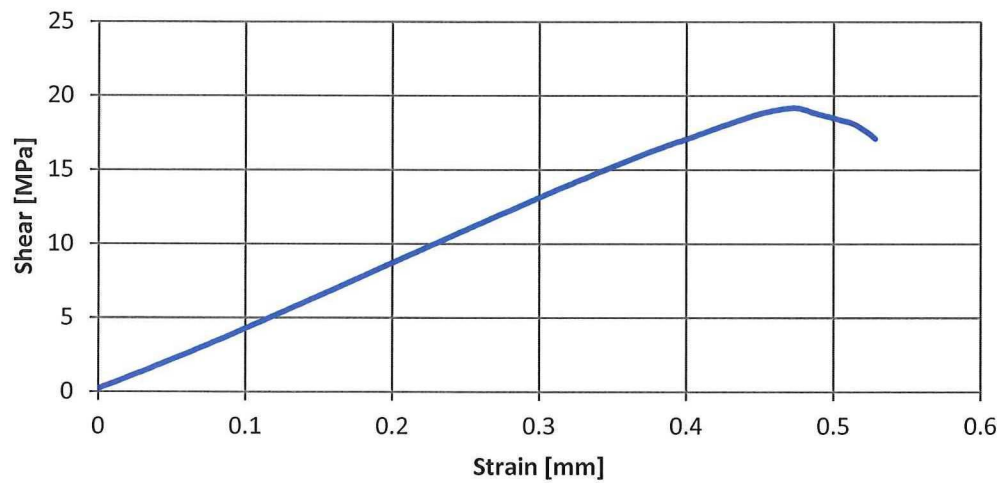
UW280114-009



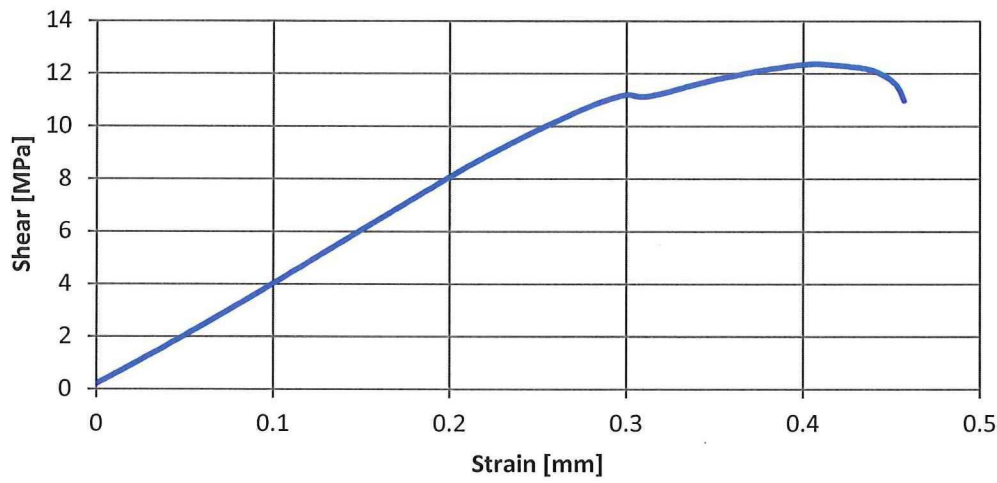
UW280114-003



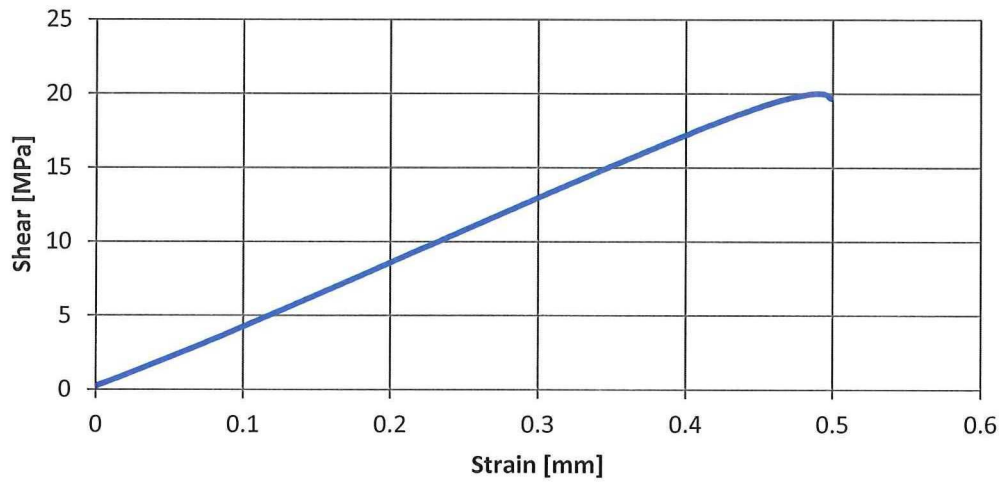
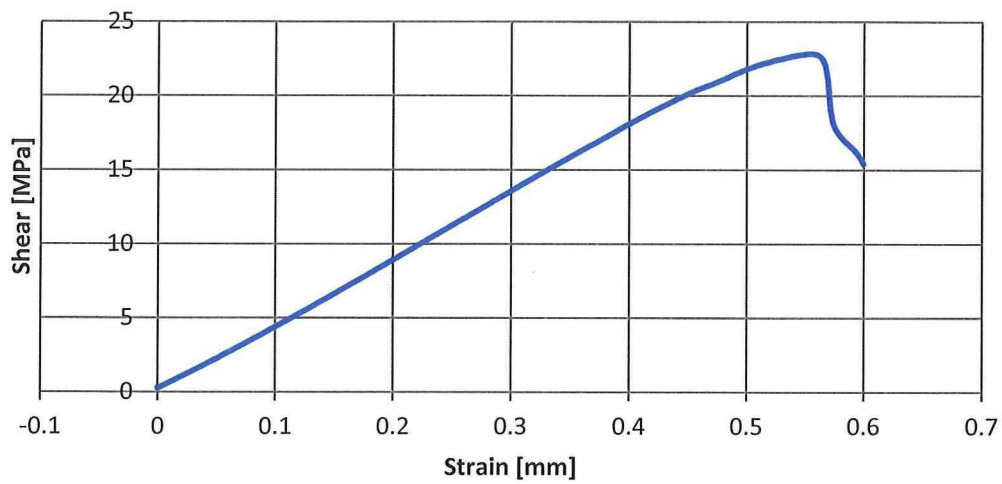
UW280114-004



UW280114-005





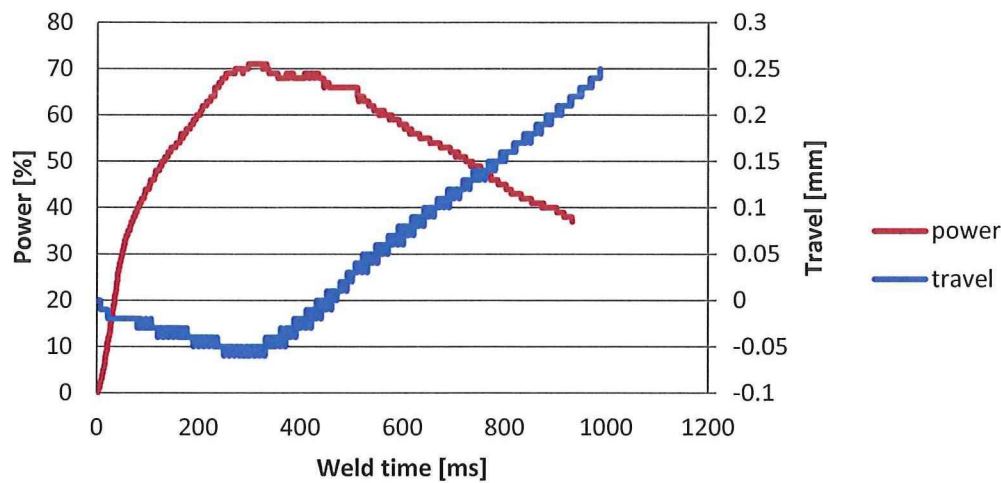
**UW280114-007****UW280114-008**



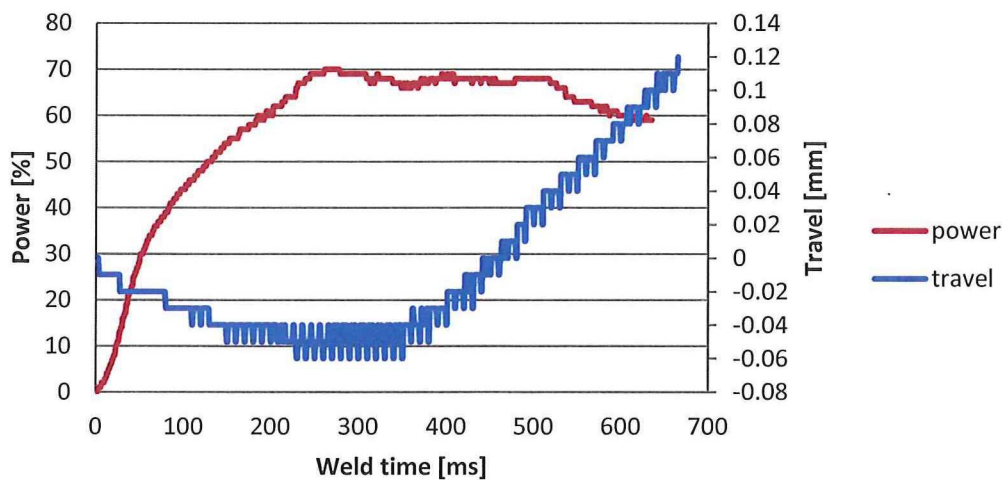
## I. Welding and LSS Curves for Pre-attached ED Welding

|                     |                               | I) Initial Phase    | II) Vibration Phase |                     |                           |                         | III) Solidification Phase |                   |
|---------------------|-------------------------------|---------------------|---------------------|---------------------|---------------------------|-------------------------|---------------------------|-------------------|
| Materials           | Sonotrode                     | Rise of Force [N/s] | Weld. Force [N]     | Rise of Force [N/s] | Amplitude [μm] (set. [-]) | Controlling Parameter   | Force                     | Holding Time [ms] |
| TC weave<br>– weave | Rectangular<br>14.9 · 30 [mm] | 250                 | 500                 | 0                   | 84.6 (3)                  | Travel, opt.:<br>20 [%] | 1000                      | 4000              |

### UW020214-005

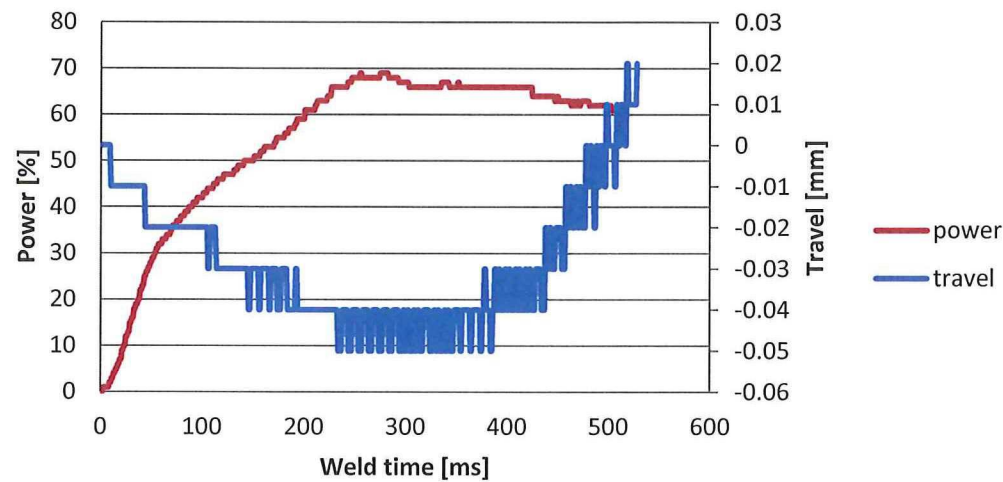


### UW020214-006

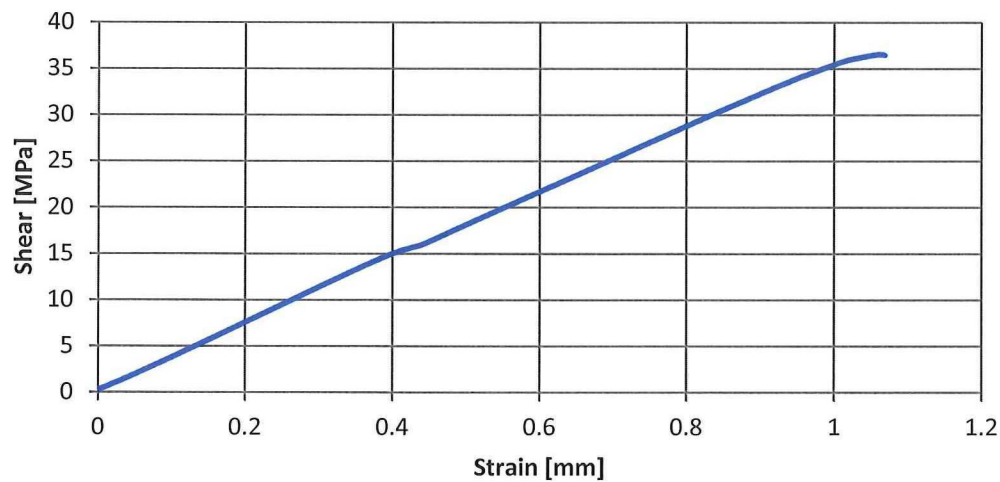




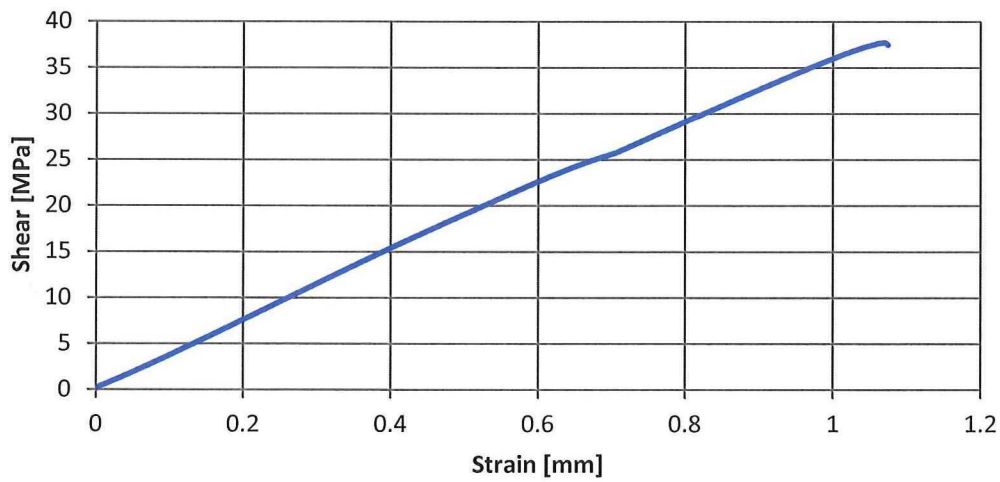
UW020214-007



UW02022014-004



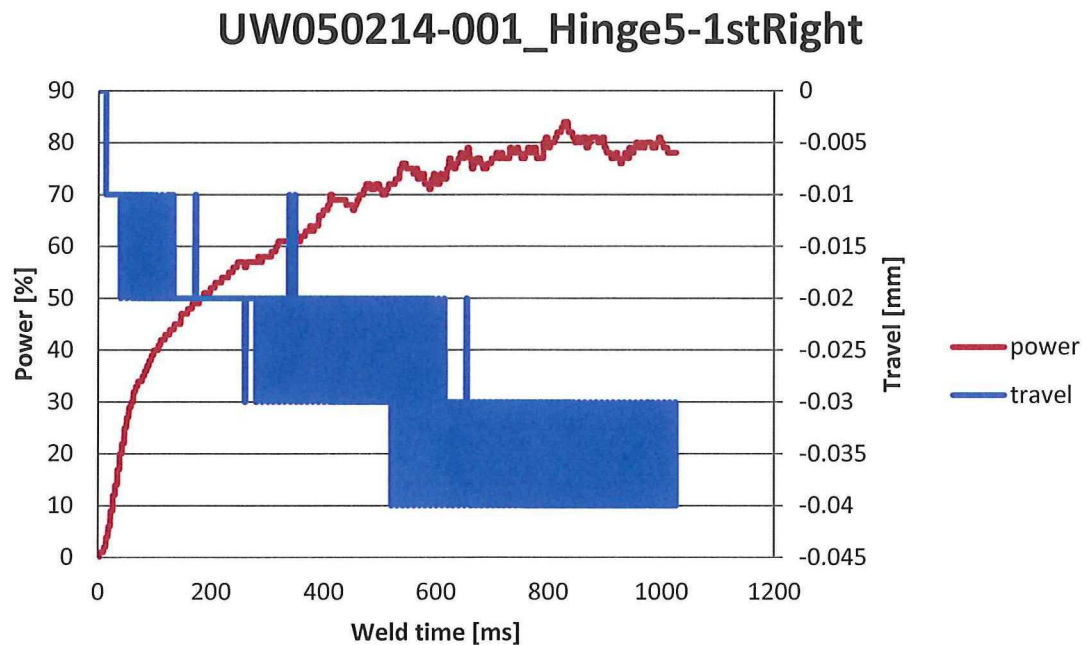
UW02022014-007



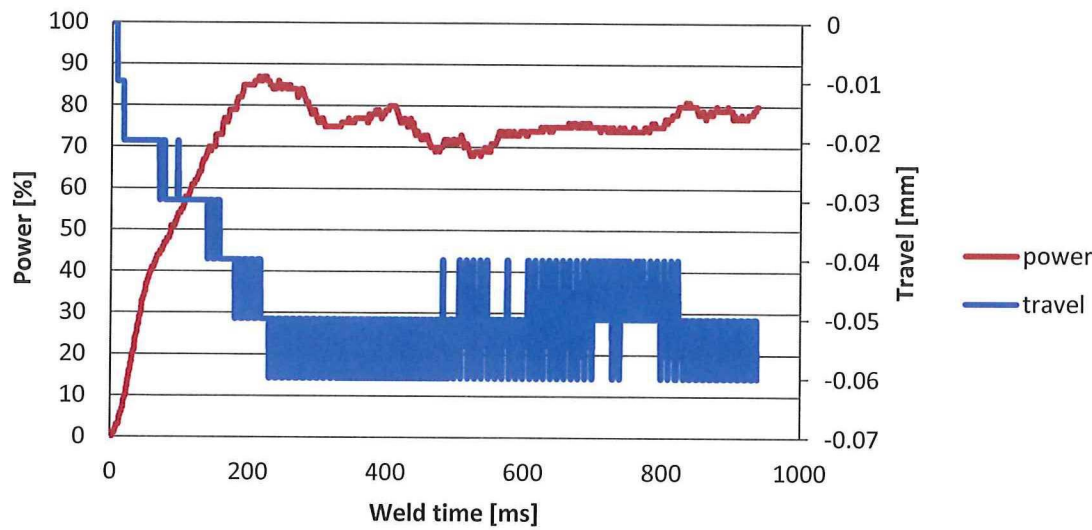
## J. Welding Curves for Hinge Welding

|                  |                            | I) Initial Phase    | II) Vibration Phase |                     |                           |                       | III) Solidification Phase |                   |
|------------------|----------------------------|---------------------|---------------------|---------------------|---------------------------|-----------------------|---------------------------|-------------------|
| Materials        | Sonotrode                  | Rise of Force [N/s] | Weld. Force [N]     | Rise of Force [N/s] | Amplitude [μm] (set. [-]) | Controlling Parameter | Force                     | Holding Time [ms] |
| TC weave – hinge | Rectangular 14.9 · 30 [mm] | 250                 | 500                 | 0                   | 84.6 (3)                  | Energy 2000 [Ws]      | 1000                      | 4000              |

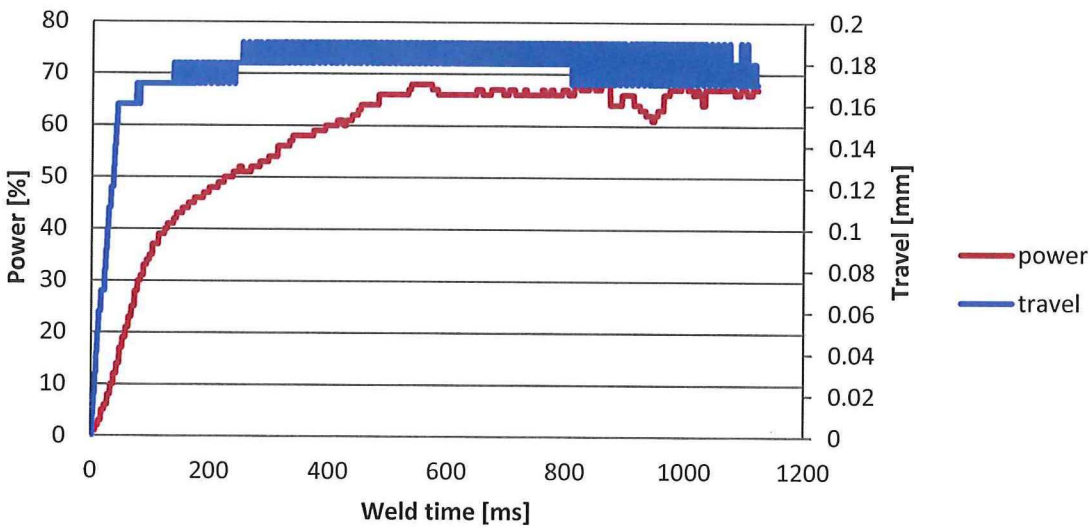
Note: Left and Right in the chart titles is as seen from the bottom of the hinge with the flange facing away (orientation of the hinge inside the jig)



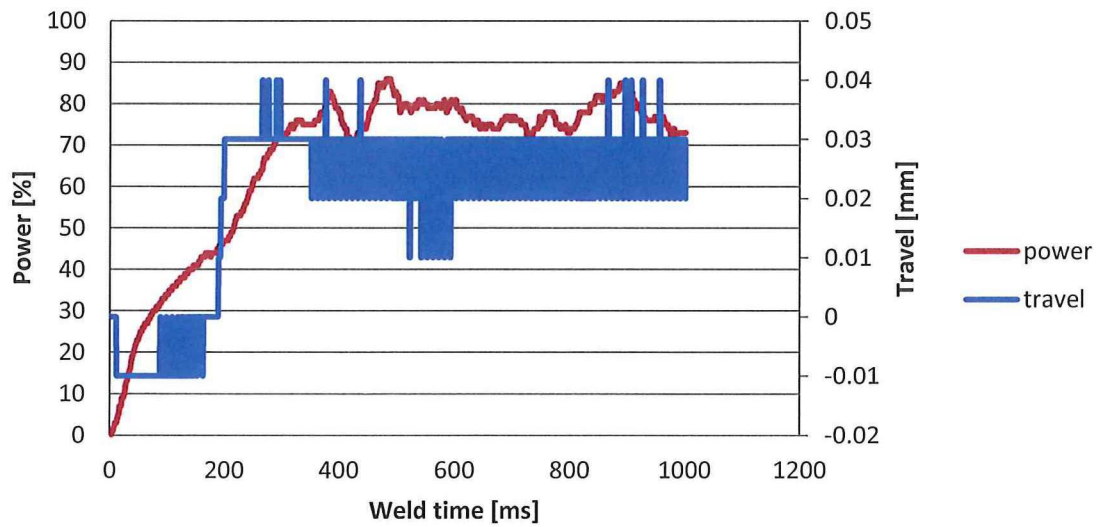
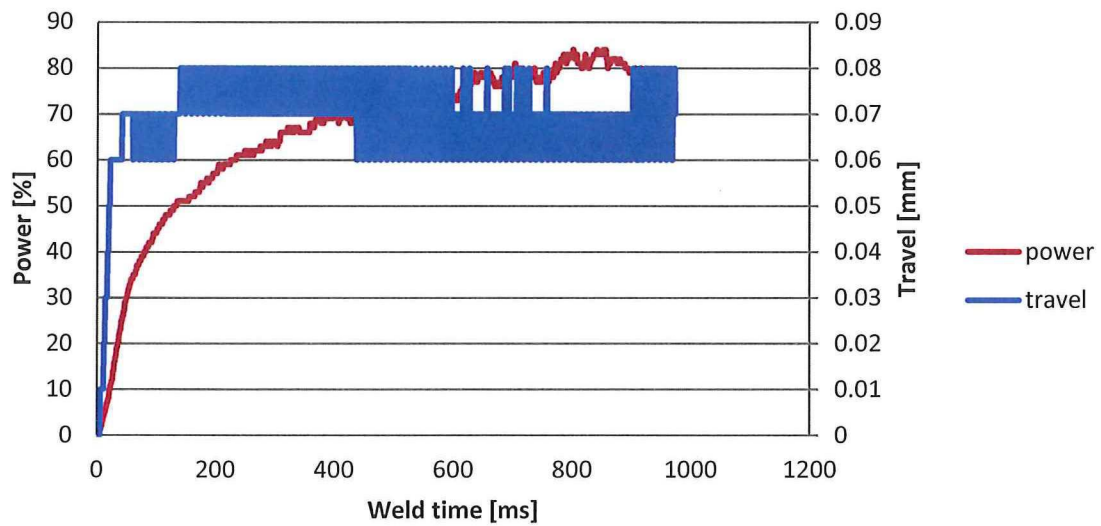
UW050214-002\_Hinge5-2ndLeft



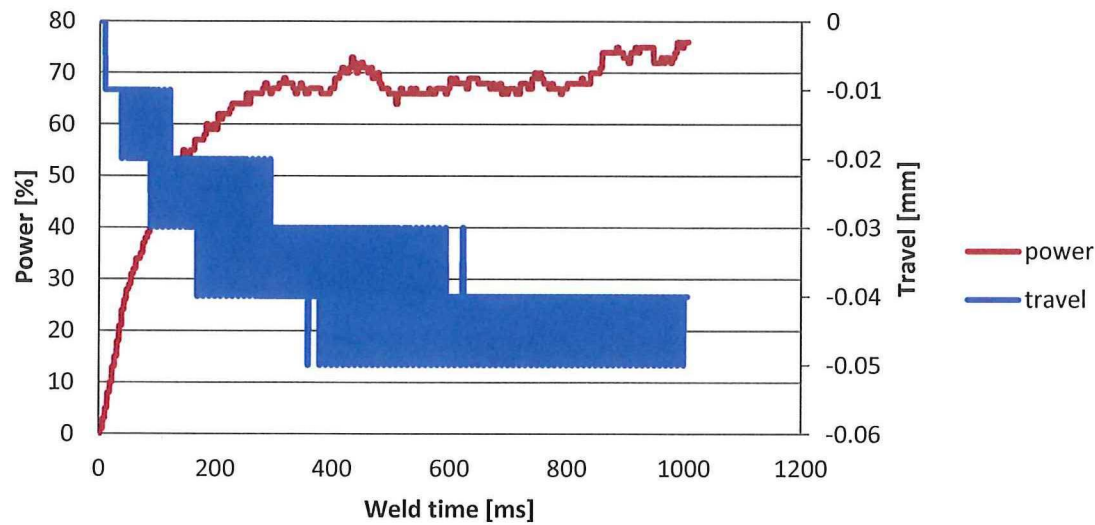
UW050214-003\_Hinge6-1stLeft



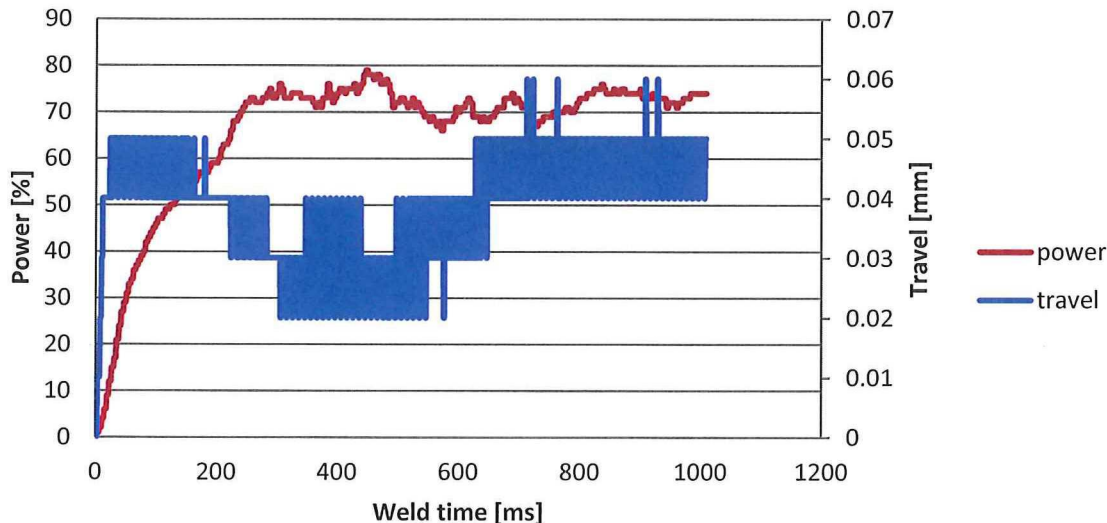


**UW050214-004\_Hinge6-2ndRight****UW050214-005\_Hinge7-1stRight**

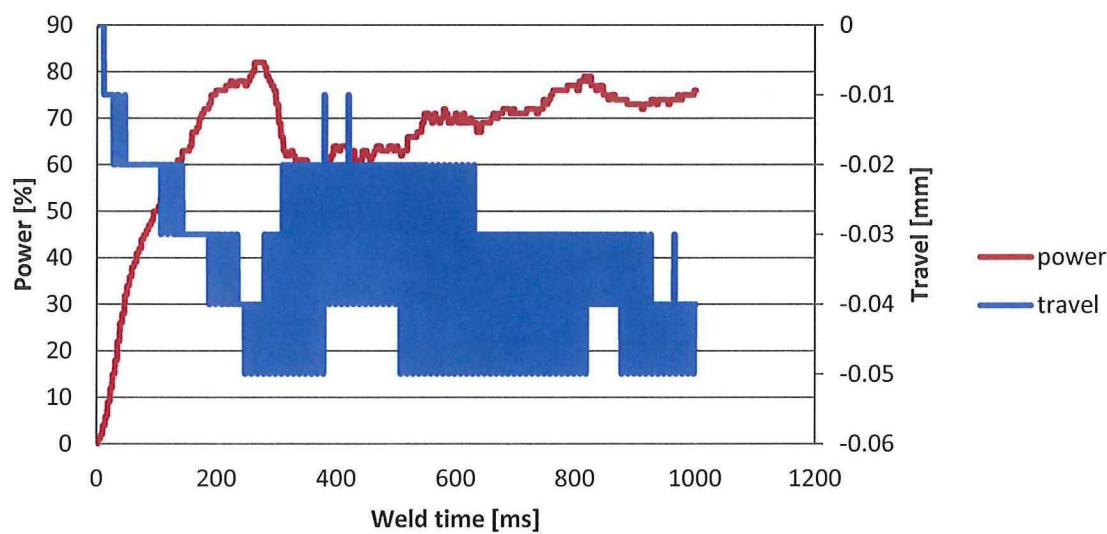
UW050214-006\_Hinge7-2ndLeft



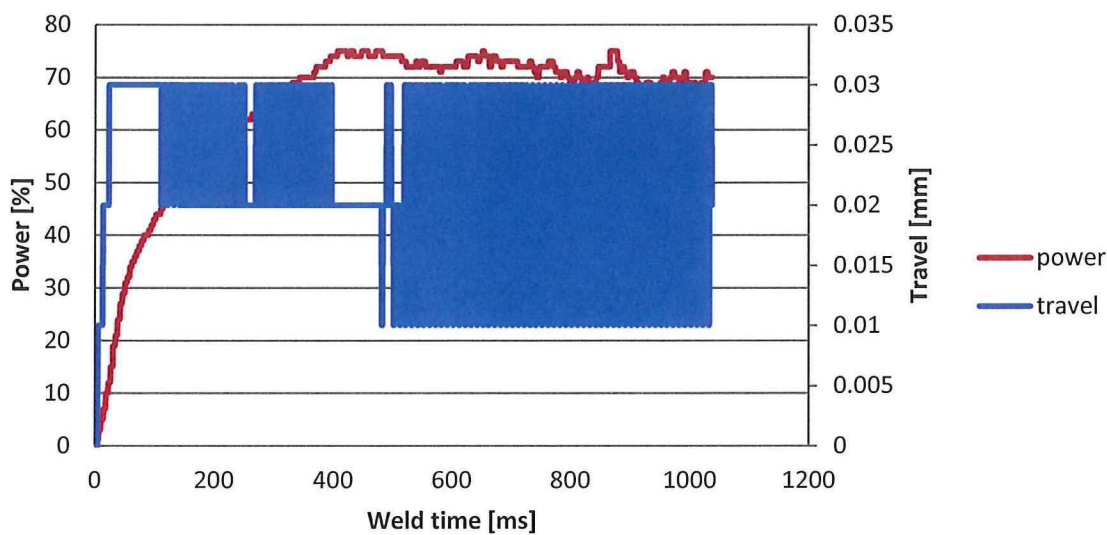
UW050214-007\_Hinge8-1stLeft



UW050214-008\_Hinge8-2ndRight

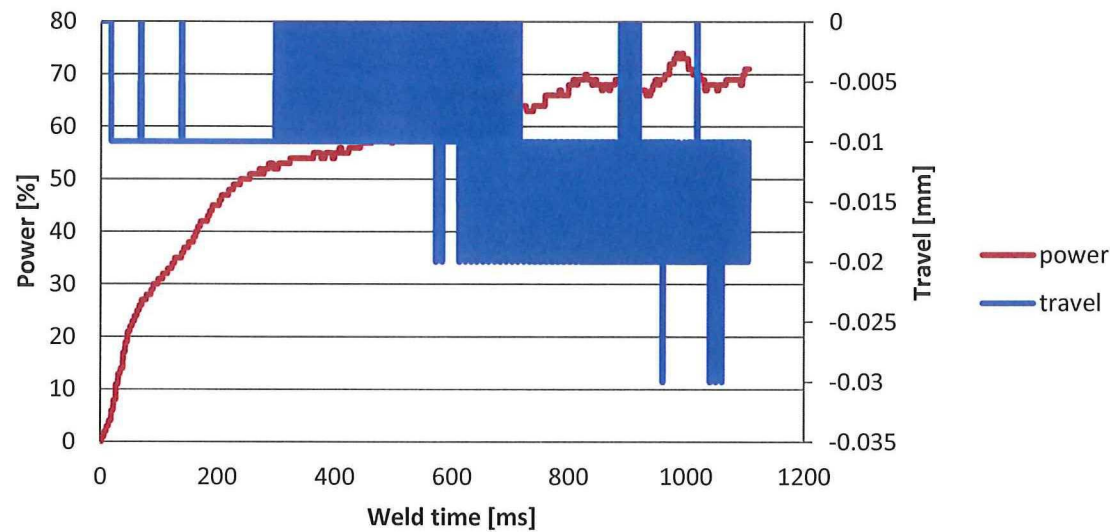


UW050214-009\_Hinge9-1stRight

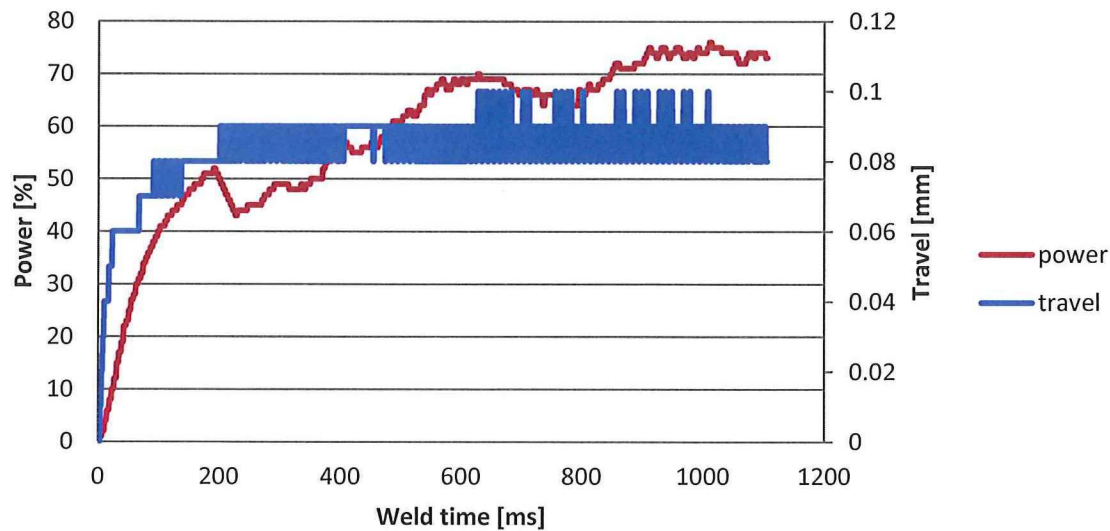




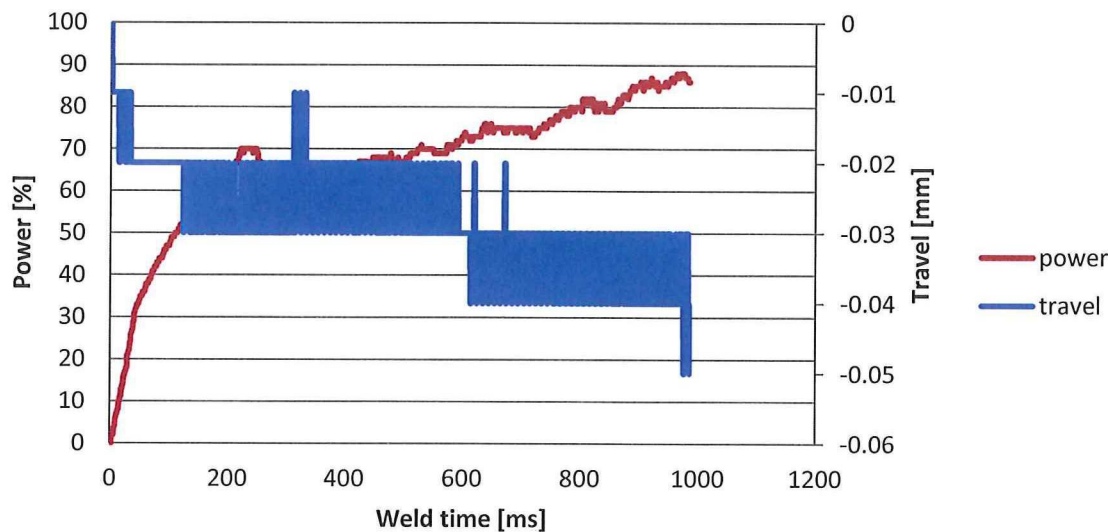
UW050214-010\_Hinge9-2ndLeft



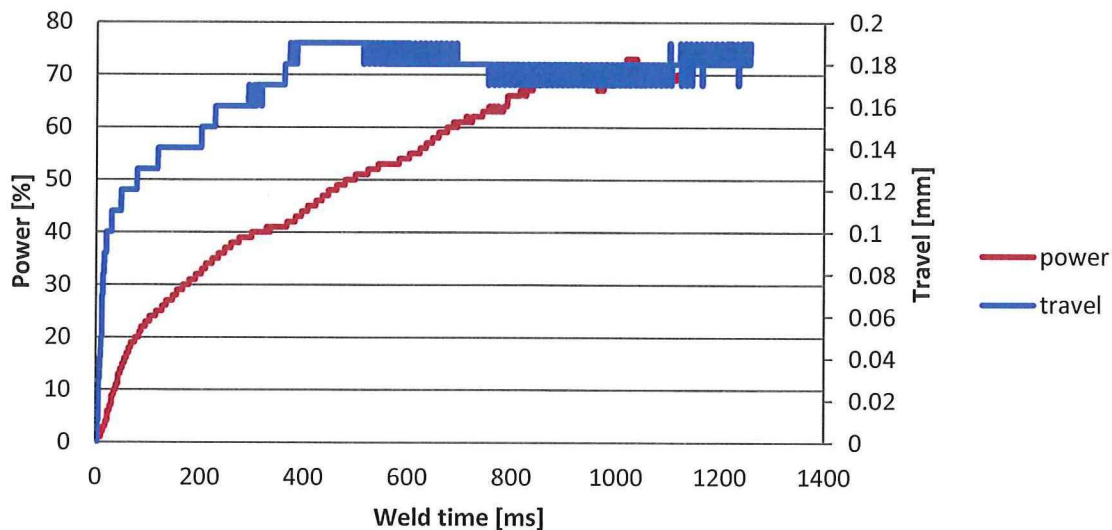
UW050214-011\_Hinge10-1stLeft



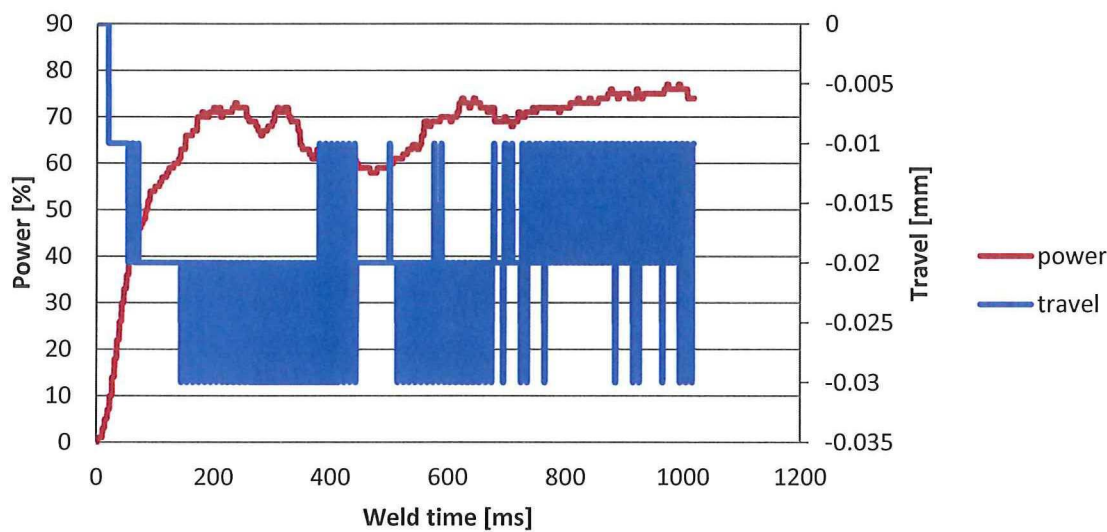
UW050214-012\_Hinge10-2ndRight



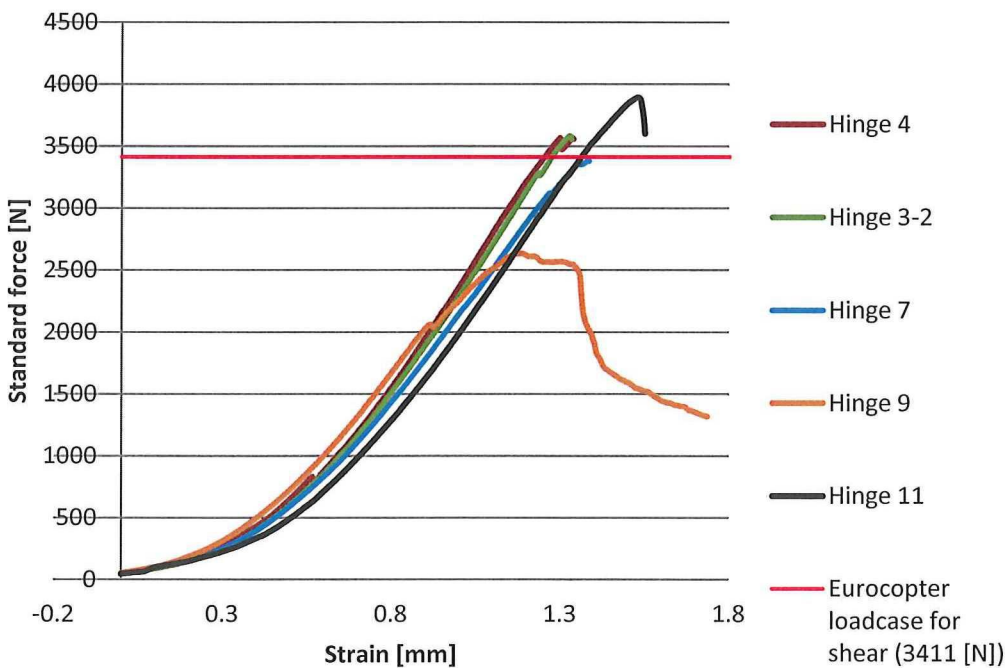
UW050214-013\_Hinge11-1stRight



UW050214-014\_Hinge11-2ndLeft



Strength tests results for welded hinges





|           |                                     | WELDING |         |                 |                             |               |            |      |         | Tension                         |                    |
|-----------|-------------------------------------|---------|---------|-----------------|-----------------------------|---------------|------------|------|---------|---------------------------------|--------------------|
|           | Tab name (sub-series - specimen ID) | ED      | Hinge t | Plate thickness | Welding on: Travel - Energy | Weld distance | Max. Power | Time | Energy  | F <sub>max</sub>                | F <sub>Break</sub> |
|           | [-]                                 | [-]     | [mm]    | [mm]            | [%] - [Ws]                  | [mm]          | [%]        | [ms] | [Ws]    | [N]                             | [N]                |
| Hinge 2   | UW040214-002_Hinge2-1stRight        | TenCate | 4.07    | 2.44            | 1400                        | 0.22          | 67         | 858  | 1401.67 | 1297.30969                      | 754.6151733        |
|           | UW040214-003_Hinge2-2ndLeft         | TenCate |         |                 | 1400                        | 0.07          | 73         | 896  | 1402.08 |                                 |                    |
| Hinge 3   | UW040214-004_Hinge3-1stLeft         | TenCate | 4.13    | 2.5             | 1600                        | 0.25          | 103        | 666  | 1601.45 |                                 |                    |
|           | UW040214-005_Hinge3-2ndRight        | TenCate |         |                 | 1600                        | 0.14          | 94         | 715  | 1600.09 |                                 |                    |
| Hinge 4   | UW040214-006_Hinge4-1stRight        | TenCate | 3.83    | 2.53            | 1800                        | 0.24          | 82         | 860  | 1801.49 | 3567.78931                      | 3556.164551        |
|           | UW040214-007_Hinge4-2ndLeft         | TenCate |         |                 | 1800                        | 0.07          | 91         | 857  | 1801.73 |                                 |                    |
| Hinge 3-2 | UW040214-008_Hinge3-2-1stLeft       | Tenax   | 4.13    | 2.5             | 2000                        | 0.17          | 79         | 997  | 2000.3  | 3581.33887                      | 3554.463623        |
|           | UW040214-009_Hinge3-2-2ndRight      | Tenax   |         |                 | 2000                        | 0.12          | 75         | 1117 | 2000.17 |                                 |                    |
|           |                                     |         |         |                 |                             |               |            |      |         |                                 |                    |
| Hinge 5   | UW050214-001_Hinge5-1stRight        | Tenax   | 4.03    | 2.45            | 2000                        | 0.1           | 84         | 1038 | 2002.06 | 3600*                           | N/A                |
|           | UW050214-002_Hinge5-2ndLeft         | Tenax   |         |                 | 2000                        | 0.07          | 87         | 949  | 2002.08 | *estimate, Zwick did not record |                    |
| Hinge 6   | UW050214-003_Hinge6-1stLeft         | Tenax   | 4.03    | 2.41            | 2000                        | 0.34          | 71         | 1136 | 2000.37 |                                 |                    |
|           | UW050214-004_Hinge6-2ndRight        | Tenax   |         |                 | 2000                        | 0.18          | 87         | 1016 | 2000.95 |                                 |                    |
| Hinge 7   | UW050214-005_Hinge7-1stRight        | Tenax   | 4.13    | 2.44            | 2000                        | 0.2           | 85         | 1017 | 2001.6  | 3382.30249                      | 3379.220215        |
|           | UW050214-006_Hinge7-2ndLeft         | Tenax   |         |                 | 2000                        | 0.09          | 76         | 1074 | 2000.03 |                                 |                    |
| Hinge 8   | UW050214-007_Hinge8-1stLeft         | Tenax   | 3.9     | 2.4             | 2000                        | 0.18          | 79         | 1025 | 2001.93 |                                 |                    |
|           | UW050214-008_Hinge8-2ndRight        | Tenax   |         |                 | 2000                        | 0.08          | 83         | 1026 | 2001.57 |                                 |                    |
| Hinge 9   | UW050214-009_Hinge9-1stRight        | Tenax   | 3.9     | 2.42            | 2000                        | 0.16          | 76         | 1049 | 2000.8  | 2635.00171                      | 1317.129639        |
|           | UW050214-010_Hinge9-2ndLeft         | Tenax   |         |                 | 2000                        | 0.11          | 74         | 1195 | 2001.97 |                                 |                    |
| Hinge 10  | UW050214-011_Hinge10-1stLeft        | Tenax   | 4.04    | 2.42            | 2000                        | 0.23          | 76         | 1149 | 2000.18 |                                 |                    |
|           | UW050214-012_Hinge10-2ndRight       | Tenax   |         |                 | 2000                        | 0.09          | 89         | 1017 | 2000.4  |                                 |                    |
| Hinge 11  | UW050214-013_Hinge11-1stRight       | Tenax   | 4.07    | 2.41            | 2000                        | 0.3           | 75         | 1271 | 2001.63 | 3892.8689                       | 3600.234619        |
|           | UW050214-014_Hinge11-2ndLeft        | Tenax   |         |                 | 2000                        | 0.11          | 77         | 1034 | 2000.41 |                                 |                    |



## Bibliography

- [1] (2013, May) Clean Sky Joint Technology Initiative (JTI). [Online]. <http://www.cleansky.eu>
- [2] P. K. Mallick, *Fiber-Reinforced Composites - Materials, Manufacturing and Design*. Dearborn, Michigan, United States of America: CRC Press Taylor & Francis Group, 2007.
- [3] I. Y. Chang and J. K. Lees, "Recent Developments in Thermoplastic Composites: A Reveiw of Matrix Systems and Processing Methods," *Journal of Thermoplastic Composite Materials*, vol. 1, pp. 277-296, Jul. 1988.
- [4] A. Yousefpour and e. al., "Fusion Bonding/Welding of Thermoplastic Composites," *Journal of Thermoplastic Composite Materials*, vol. 17, pp. 303-341, 2004.
- [5] I. F. Villegas, "High-Speed Spot Welding of Continuous Fibre Reinforce Thermoplastic Composites," Delft University of Technology, 2012.
- [6] C. Ageorges, L. Ye, and M. Hou, "Advances in Fusion Bonding Techniques for Joining Thermoplastic Matrix Composites: a Review," *Composites Part A: Applied Science and Manufacturing*, pp. 839-857, Oct. 2000.
- [7] H. M. Lu, A. Benatar, and F. G. He, "Sequential Ultrasonic Welding of PEEK/Graphite Composite Plates," in *Annual Technical Conference - ANTEC*, Montreal, Quebec, Canada, 1991, pp. 2523-2526.
- [8] Clean Sky Joint Technology Initiative. (2013, Oct.) WP A.5.1. Equipped Airframe demonstration preparation Demonstrator -F1. Powerpoint.
- [9] N. Eguémann and e. al., "Manufacturing and Recycling of Complex Composite Thermoplastic Parts for Aerospace Application," Fachhochschule Norwestschweiz, Institut für Kuststofftechnik, 2012.
- [10] J. William D. Callister, *Materials Science and Engineering an Introduction*. United States of America: John Wiley & Sons, Inc, 2007.
- [11] R. J. Young and P. A. Lovell, *Introduction to Polymers*, 3rd ed. Boca Raton, United States of America: CRC Press, 2011.
- [12] G. D. Limited. (2013) CES EduPack 2013 Version 12.2.13. TU Delft Software.
- [13] Matweb. (2014, Jan.) Matweb Material Property Data. [Online]. <http://www.matweb.com/>
- [14] F. C. Campbell, *Manufacturing Processes for Advanced Composites*. Oxford, United Kingdom: Elsevier, 2004.



- [15] I. M. Daniel and O. Ishai, *Engineering Mechanics of Composite Materials*. Oxford, New York: Oxford University Press Inc., 1994.
- [16] S. K. Mazumdar, *Composites Manufacturing: Materials, Products, and Process Engineering*. Boca Raton, United States of America: CRC Press, 2002.
- [17] S. Pimenta and S. T. Pinho, "Recycling Carbon Fibre Reinforced Polymers for Structural Applications: Technology Review and Market Outlook," *Waste Management*, no. 31, pp. 378-392, Oct. 2011.
- [18] M. Roux, N. Eguémann, L. Giger, and C. Dransfeld, "High performance thermoplastic composite processing and recycling: from cradle to cradle," University of Applied Sciences Northwestern Switzerland, Institute of Polymer Engineering Paper, 2013.
- [19] M. E. Otheguy and e. al., "Recycling of End-of-life Thermoplastic Composite Boats," *Plastic, Rubber and Composites*, vol. 38, no. 9/10, pp. 406-411, 2009.
- [20] I. F. Villegas, "Ultrasonic Welding of Advanced Thermoplastic Composites: An Investigation on Energy-Directing Surfaces," *Advances in Polymer Technology*, vol. 29, no. 2, pp. 112-121, 2010.
- [21] I. F. Villegas, M. Barroso-Romero, and H. E. N. Bersee, "Analysis of the Effect of the Welding Parameters in Ultrasonic Welding of CF/PEI Composites," Delft University of Technology, 2012.
- [22] I. F. Villegas, "In Situ Monitoring of Ultrasonic Welding of Thermoplastic Composites Through Power and Displacement Data," Delft University of Technology, 2012.
- [23] H. Potente, "Ultrasonic Welding - Principles & Theory," *Materials & Design*, vol. 5, pp. 228-234, Oct. 1984.
- [24] A. Benatar and T. G. Gutowski, "Ultrasonic Welding of PEEK Graphite APC-2 Composites," *Polymer Engineering and Science*, vol. 29, no. 23, pp. 1705-1721, Dec. 1989.
- [25] M. R. Rani and R. Rudramoorthy, "Computational modeling and experimental studies of the dynamic performance of ultrasonic horn profiles used in plastic welding," *Ultrasonics*, vol. 53, pp. 763-772, Nov. 2012.
- [26] Z. Zhang and e. al., "Study on Heating Process of Ultrasonic Welding for Thermoplastics," *Journal of Thermoplastic Composite Materials*, vol. 23, pp. 647-664, Sep. 2010.
- [27] A. Levy, I. Fernandez Villegas, and S. Le Corre, "Modeling of the heating phenomena in ultrasonic welding of thermoplastic composites," *Journal of Materials and Processing Technology*, 2014.
- [28] University of California, Berkeley . (2013, Jul.) FEAP. [Online].

<http://www.ce.berkeley.edu/projects/feap/>

- [29] N. Eguémann, *Chip Length Sample Production, Hinge Production and Loading Case*. Brugg, Oct. 2013, Meeting, Interview.
- [30] H. Shi, I. Fernandez Villegas, and H. E. N. Bersee, "Strength and Failure Modes in Resistance Welded Thermoplastic Composite Joints: Effect of Fibre-Matrix Adhesion and Fibre Orientation," *Composites: Part A*, vol. 55, pp. 1-10, 2013.
- [31] L. P. Giger, "PEEK/CF Chips Pre-Demonstrator: Eurocopter Door Hinge," FHNW Thesis, 2012.
- [32] A. Kwakernaak, "Adhesive Bonding, structures and stresses, Joining technology," AE4740 Lecture.
- [33] N. Eguémann, *Chip Length Short Fibre Lap Shear Sample Production*. Brugg, Oct. 2013, Meeting, Interview.
- [34] van Nobelen BV. (2014) van Nobelen Machine Fabriek Constructie Bedrijf. [Online]. <http://www.vannobelendelft.nl/home.html>

